Mitigation of crude oil fouling by the use of HiTRAN inserts

Phillips, Donald Z.

Award date:
2000

Awarding institution:
University of Bath

MITIGATION OF CRUDE OIL FOULING BY THE USE OF HiTRAN® INSERTS

submitted by Donald Z Phillips

for the degree of PhD of the University of Bath

1999

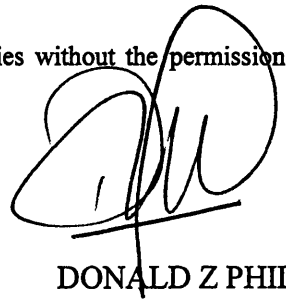

DONALD Z PHILLIPS

ProQuest LLC
789 East Eisenhower Parkway
P.O. Box 1346
Ann Arbor, MI 48106-1346

Abstract

Fouling of heat exchange equipment can be defined as the accumulation of material on the heat transfer surface in sufficient quantities to reduce the effectiveness of the exchanger. This study was initiated to quantify the benefits of HiTRAN® inserts with regard to fouling prevention and to establish a generic method for their confident implementation. The effect on fouling rates of the key process parameters such as initial surface temperature, flow-rate and insert presence and geometry have been studied using Maya crude oil flowing inside round tubes.

Experimental studies with bare tubes have shown that increases in velocity could either increase or decrease the initial fouling rate depending on whether the overall mechanism was controlled by mass transfer or kinetics. Over the range of velocities studied (0.5 m s^{-1} to 4.0 m s^{-1}) the apparent activation energy for the overall fouling process was found to vary between 26 kJ mol^{-1} and 149 kJ mol^{-1}, the value increasing with increasing velocity, indicating a strong influence by mass transfer phenomena.

Experimental studies with inserts have shown that under nominally identical operating conditions to bare tubes, fouling rates can either be increased or decreased by their presence, depending on whether the mechanism is mass transfer or kinetically controlled. At relatively low velocities (~ 0.5 m s^{-1}), where the fouling reaction was typically mass transfer controlled, the presence of inserts increased the fouling rate. At relatively high velocities (> 1.0 m s^{-1}), where the fouling reaction was typically kinetically controlled, the presence of inserts reduced fouling rates.

Studies with inserts have also revealed evidence of a critical insert density of 290 loops m^{-1}. Below this value variations in both density and loop wire diameter

significantly affected the fouling rate. Conversely, above the critical loop density, increasing both density and wire loop diameter appeared to have little effect.

Epstein's mathematical model has been adapted in an attempt to account for both bare tube and insert fouling rates with Maya crude. The model was evaluated using three different apparent activation energies, namely 26 kJ mol^{-1}, 77 kJ mol^{-1} and 149 kJ mol^{-1}.

Using the lowest apparent activation energy (26 kJ mol^{-1}) the model shows good agreement with the bare tube experimental data, predicting with reasonable accuracy the velocity at which the fouling process becomes kinetically controlled. To predict the effect of a HiTRAN® insert on fouling the appropriate friction factor for the insert was substituted in to the model. However, agreement between predicted fouling rates and experimental results was poor.

Replacing the average apparent activation energy with 77 kJ mol^{-1} the model did not predict the trends seen with the experimental data for bare tubes. Instead the model predicted a decrease in the fouling rate with increasing velocity. However, the trends predicted by the model for tubes containing inserts were in general agreement with those found experimentally. The predicted values of fouling resistance were found to be generally larger, with agreement improving as the velocity was increased. Increasing the apparent activation energy still further to 149 kJ mol^{-1} resulted in the prediction of fouling rate trends that were contrary to those observed experimentally.

Acknowledgements

The work in this thesis has been carried out at the Department of Chemical Engineering at the University of Bath between October 1995 and September 1998. During this period I have enjoyed the support and encouragement of a number of people, too numerous to mention. I would however, like to take this opportunity to thank a number of people who have contributed significantly to the project.

First and foremost I must thank Barry Crittenden and Stan Kolaczkowski at the University of Bath, for their support and guidance throughout the three years and for the opportunity to work in such an interesting field. Equally I thank the Engineering and Physical Sciences Research Council (EPSRC) and BP Oil Ltd., in particular Dave King, whose enthusiasm, support and regular input throughout the project was invaluable both to the project and myself.

Similarly I would like to thank Martin Gough and Ian Gibbard at Cal-Gavin for their expert guidance in the use of HiTRAN® inserts and enthusiasm that they have shown towards the project.

The technical support provided by Mac Forsyth and the technical support staff, in particular Merv Newnes and Elaine Odgers, for enabling me to modify and operate the experimental rig is greatly appreciated. Additionally, I would like to thank Dave M^{c}Lurgh and Abbie Gosling who probably know more about hydrocarbon fouling than they wanted to!

Finally I must also thank Don and Sandie Phillips and Gladys Barnes whose help, support and general guidance made my time a great deal easier for me than I probably deserved!

Contents

List of figures

List of tables

List of plates

Nomenclature

A_T	area of heat transfer	(m^2)
c'	constant in equation (2.10)	(W m^{-2} kg^{-1} s)
c''	constant in equation (2.12)	(kg^{-1} s K)
c	constant in equation (2.8)	(kg^{-1} s W m^{-2} K^{-1})
C_b	bulk concentration of precursor	(kg m^{-3})
C_{Pb}	concentration of precursor in bulk	(kg m^{-3})
C_{Pi}	concentration of precursor at interface	(kg m^{-3})
C_{fb}	concentration of foulant in bulk	(kg m^{-3})
C_{fi}	concentration of foulant at interface	(kg m^{-3})
$C_{b(5.26)}$	bulk concentration using equation (5.26)	(kg m^{-3})
$C_{b(5.27)}$	bulk concentration using equation (5.27)	(kg m^{-3})
C_P	specific heat capacity	(kJ kg^{-1} $°C^{-1}$)
C_s	surface concentration	(kg m^{-3})
D_f	diffusivity	(m^2 s^{-1})
D_a	diffusivity of asphaltene	(m^2 s^{-1})
d_i	internal tube diameter	(m)
d_O	external tube diameter	(m)
d_T	diameter at thermocouples	(m)
E	activation energy	(kJ mol^{-1})
E_A	apparent activation energy	(kJ $kmol^{-1}$)
F_T	temperature correction factor	
G	mass flow rate	(kg h^{-1})
h	heat transfer coefficient	(W m^{-2} K^{-1})
h_i	internal heat transfer coefficient	(W m^{-2} K^{-1})
h_O	external heat transfer coefficient	(W m^{-2} K^{-1})

j_h	heat transfer factor	
j_f	friction factor	
k'	mass constant	
k	thermal conductivity	($W\ m^{-1}\ K^{-1}$)
k_b	thermal conductivity of the bulk fluid	($W\ m^{-1}\ K^{-1}$)
k_c	thermal conductivity of coke	($W\ m^{-1}\ K^{-1}$)
k_f	thermal conductivity of foulant	($kW\ m^{-1}\ K^{-1}$)
k_{lf}	thermal conductivity of liquid in the film	($W\ m^{-1}\ K^{-1}$)
k_w	wall thermal conductivity	($W\ m^{-1}\ K^{-1}$)
K_f	mass transfer coefficient of foulant	($m\ h^{-1}$)
K_P	mass transfer coefficient of precursor	($m\ h^{-1}$)
k''	reactivity rate factor	($kg^{n-1}\ s^2\ m^{(3n-2)}$)
k_m	mass transfer coefficient	($m\ s^{-1}$)
k_r	chemical plus attachment rate constant	($m^{(3n-2)}\ kg^{-1(n-1)}\ s^{-1}$)
k_R	reaction rate constant	($m\ h^{-1}$)
L	distance between pressure tappings	(m)
L_S	test cell length	(m)
L_T	length of thermocouple in test cell	(m)
m	stoichiometric factor	
MW_a	molecular weight of asphaltene	
MW_{solv}	molecular weight of crude	
n	reaction order	
N_f	mass flux of foulant	($kg\ m^{-2}\ h^{-1}$)
N_P	mass flux of precursor	($kg\ m^{-2}\ h^{-1}$)
Q	duty	(W)
q	heat flux	($W\ m^{-2}$)

R	universal gas constant	(kJ kmol^{-1} K^{-1})
r_ϕ	mass flux ratio	
r_C	concentration ratio	
r_k	chemical plus attachment rate ratio	
Re	Reynolds number	
R_f^∞	asymptotic fouling resistance	(m^2 K W^{-1})
$R_{f(t)}$	fouling resistance at time "t"	(m^2 K W^{-1})
$R_{f(0)}^{\cdot}$	initial fouling rate	(m^2 K W^{-1} s^{-1} or h^{-1})
$R_{f(t)}^{\cdot}$	fouling rate at time "t"	(m^2 K W^{-1} s^{-1} or h^{-1})
R_{fi}	internal fouling resistance	(m^2 K W^{-1})
R_{fO}	external fouling	(m^2 K W^{-1})
R_w	resistance of the tube wall	(m^2 K W^{-1})
R_W	resistance of the tube wall	(m^2 K W^{-1})
Sc	Schmidt number	
SG_a	specific gravity of asphaltene	
t	time	(s or h)
T^*	transition temperature	(°C or K)
T_b	bulk fluid temperature	(°C or K)
T_{bi}	inlet bulk temperature	(°C or K)
T_{bo}	outlet bulk temperature	(°C or K)
T_f	temperature of fluid film	(°C or K)
T_T	thermocouple temperature	(°C or K)
T_w	tube wall temperature	(°C or K)
u_m	mean linear velocity	(m s^{-1})
u_c	friction velocity	(m s^{-1})
$(u_c)_0$	benchmark friction velocity	(m s^{-1})

U_O	overall heat transfer coefficient	(W m^{-2} K^{-1})
$U_{O(0)}$	overall heat transfer coefficient at time "0"	(W m^{-2} K^{-1})
$U_{O(t)}$	overall heat transfer coefficient at time "t"	(W m^{-2} K^{-1})
V_a	molar volume of asphaltene	(m^3 $kmol^{-1}$)
x_f	depth of foulant	(m)
$X_{o/c}$	oil to coke ratio	

Greek letters

ρ	density	(kg m^{-3})
ρ_f	density of foulant	(kg m^{-3})
ϕ	deposition flux	(kg m^2 s^{-1})
β	time constant	(h^{-1})
ψ	function of deposit structure	
ν	kinematic viscosity	(mm^2 s^{-1})
μ	viscosity	(Pa s)
μ_{solv}	viscosity of solvent	(Pa s)
μ_w	viscosity at wall temperature	(Pa s)
τ	wall shear stress	(N m^{-2})
ϕ_d	deposition rate at time "t"	(m^2 K W^{-1} h^{-1})
ΔP	pressure drop	(N m^{-2})
ϕ_r	removal rate at time "t"	(m^2 K W^{-1} h^{-1})
ϕ_{solv}	association factor of solvent	
ΔT	temperature difference	(°C or K)
ΔT_{lm}	log mean temperature difference	(°C or K)

1. Introduction

The purpose of this research project is to investigate the impact of process parameters and HiTRAN® inserts upon the fouling of hydrocarbon crude oils and to develop a fouling model to account for the results.

Fouling in heat exchangers can be broadly defined as the deposition and accumulation of material on a heat transfer surface. Fouling may occur in any system where equipment is used to transfer heat and may result in economic penalties which, due to reduced profit margins, may adversely affect the overall economic performance of the plant. Consequently, increased effort has been directed at the reduction in operating costs, the most quantifiable of which are costs incurred by fouling, estimated to be some US$4,413 M world wide in 1981 (Van Nostrand, Leach and Haluslka (1981)). Although these costs are somewhat dated, there is no indication that the total cost, or the relative impact of fouling has diminished, as increasingly competitive markets have further reduced operating and profit margins. As a result there is significant motivation towards understanding the factors affecting fouling, with the aim of minimising the impact that this phenomenon has on operational plant.

Fouling rates and asymptotic fouling resistances of hydrocarbon streams are influenced by chemical reaction rates (controlled by temperature) and the rate of mass transfer of the reactant from the bulk fluid to the reaction site (predominantly controlled by fluid flow-rate and turbulence). It follows therefore that changes in any of the parameters affecting temperature and mass transfer will also have an effect on fouling rates.

It is widely accepted in the petroleum industry that fouling rates and asymptotic fouling resistances can be minimised by increasing the fluid velocity, or by reducing the heat transfer surface temperature. Increasing the fluid velocity results in greater turbulence,

and therefore greater film heat transfer coefficients. Generally this also results in a reduction in the surface temperature for a fluid being heated. However, increases in velocity can also increase the rate of mass transfer of fouling precursors both to and from the heat transfer surface.

How fouling rates and asymptotic fouling resistances are affected by increased fluid turbulence and flow-rate therefore depends on the relative balance of mass transfer and chemical reaction effects. Increased turbulence within a tube and lower surface temperatures can also be achieved by using turbulence promoting devices such as mechanical inserts. Because of their relatively low cost, inserts are becoming increasingly favoured in the petroleum industry to reduce fouling rates, asymptotic fouling resistances and to intensify existing heat transfer equipment. HiTRAN® inserts manufactured by Cal-Gavin have been identified in numerous published papers as having particular potential to control fouling.

Due to the complex nature of fouling, the effect that placing an insert (such as HiTRAN®) into a heat exchange network may not always be predictable. Inserts increase both heat and mass transfer rates within tubes. Therefore careful consideration is required in the selection of an insert to mitigate fouling. Incorrect selection could lead to increased rather than decreased fouling rates and asymptotic resistances.

Before mitigation strategies can be implemented in industrial plant, confidence in the correct selection of an insert is essential. Consequently this project entitled "Mitigation of crude oil fouling by the use of HiTRAN® inserts" has been sponsored by British Petroleum Oil Limited (BP Oil Ltd.) and the Engineering and Physical Sciences Research Council (EPSRC) in order to quantify the benefit of the installation of HiTRAN® inserts into a hydrocarbon stream. The prime objectives of this project are:

1. to quantify the benefits of HiTRAN® inserts, with regard to fouling prevention;

2. to establish generic design data and a method for the confident implementation of HiTRAN® inserts.

To achieve these objectives it is necessary to study the effects of process variables such as surface temperature, flow-rate, heat flux and the installation of HiTRAN® inserts on fouling rates and asymptotic fouling resistances in carefully controlled experiments.

Using a pilot-scale recycle flow apparatus, it is possible to correlate initial fouling rates and asymptotic fouling resistances against carefully controlled process variables (such as surface temperature and flow velocity), as well as against the density and geometry of HiTRAN® inserts. The use of laboratory based test rigs enables a generic design method based on reaction engineering and film transport theories to be developed. This method can then be used to assist equipment designers and operators to determine optimum strategies for controlling crude oil fouling in heat exchangers.

In order to fulfil the project objectives, this thesis presents a review of the most relevant literature on hydrocarbon fouling, a description of the experimental apparatus and modifications made as part of the study, the results of experimental trials, the derivation and testing of a mathematical model, together with conclusions and recommendations for further study. The chapters are as follows:

2. Fouling in heat transfer equipment: this chapter presents a historical review of fouling, concentrating on the economic penalties, the effects of process parameters, together with fouling mitigation methods. Throughout this chapter the emphasis is on the fouling of heat transfer equipment from hydrocarbon streams.

3. Experimental apparatus, procedures and materials: this chapter presents a description of the hydrocarbon fouling rig at the University of Bath together with full details of the modifications made as part of this study. This chapter also includes details on the criteria used in the selection of the test fluid.

4. Results and discussion: this chapter presents the results of the fouling experiments conducted as part of this study. This chapter also details the equations used to assess and rationalise the raw experimental data.

5. Modelling hydrocarbon fouling: this chapter presents a historical review of fouling models, primarily concentrating on those which contribute to the model developed in this study.

6. Conclusions and recommendations: this chapter discusses the significance of the results of this fouling study in the context of the aims and objectives; recommendations arising from the study are also included.

7. References: this chapter lists the sources of data used in the thesis text.

This chapter has provided an initial introduction to hydrocarbon fouling, its mechanism and the influence of key process parameters, including the effect of HiTRAN® inserts. The project objectives and an outline of following chapters have also been included. Additionally, this chapter has introduced the financial impetus behind mitigating fouling, existing practices, current technologies and the obstacles to their implementation.

2. Fouling in heat transfer equipment

Fouling in heat exchangers can be broadly defined as the deposition and accumulation of material on the heat transfer surface, which can have a number of effects on performance (Bott (1990)):

1. formation of a barrier to heat transfer, thereby reducing the ability of the exchanger to transfer heat;

2. increased surface roughness, thereby increasing local heat transfer coefficient and pressure drop;

3. reduction of flow area, thereby increasing velocity and pressure drop.

Fouling mechanisms may be categorised into six main areas that describe the principal causes of the accumulation of deposit. These include salt formation, deposition of fine solid material, products of chemical reactions, products of corrosion, biological organism growth and crystallisation (Epstein (1981)). While fouling mechanisms may be classified into six separate categories, fouling often involves more than one such mechanism. For example, crystallisation and particulate fouling mechanisms may occur in the same process since crystals may form in the bulk solution to then be deposited as particles on the heat transfer surface. The category which best describes the overall fouling mechanism is dependent on the media and conditions encountered:

1. scaling: the precipitation of inverse solubility salts (such as $CaCO_3$, $CaSO_4$, $Ca(PO_4)_2$, $CaSiO_3$, $Ca(OH)_2$, $Mg(OH)_2$, $MgSiO_3$, Na_2SO_4, Li_2SO_4 and Li_2CO_3 in water) onto a superheated transfer surface. Though more severe under boiling conditions, scaling also occurs when hard water or aqueous solutions undergo sensible heating;

2. particulate fouling: the accumulation of particles suspended in a liquid onto a heat transfer surface. This includes gravitational settling of relatively large particles onto a horizontal heat transfer surface (Sedimentation Fouling), as well as deposition of colloidal particles by other mechanisms onto a heat transfer surface;

3. chemical reaction fouling: the formation of deposits through chemical reactions at the heat transfer surface (in which the surface material itself is not a reactant) or in the bulk fluid. Polymerisation, cracking and coking of hydrocarbons are prime examples;

4. corrosion fouling: the heat transfer surface itself reacts to produce corrosion products thereby fouling the surface, which may then foster the attachment of other potential fouling materials;

5. bio-fouling: biological organisms which attach themselves to the heat transfer surface, or generate slimes that then adhere to the heat transfer surface;

6. freezing fouling: the solidification of a pure liquid or constituents of a liquid solution on to the heat transfer surface.

Ultimately fouling in industrial equipment results in financial penalties which, due to reduced profit margins, have increased the significance of fouling on the economic performance of the process plant. The motivation to assess accurately the economic impact of fouling has not always been high, because of the belief that "heat exchanger fouling is usually allowed for at the design stage, therefore there is little point in measuring it if no changes or alterations can be made" (Pritchard (1988)).

The limited enthusiasm for evaluating fouling costs is made more acute by the fact that monitoring day to day fouling on industrial plants is often limited to the cumulative cost of burning extra fuel in fired exchangers and operating anti-fouling programmes. However, the true financial penalties of fouling are not limited to those incurred in plant operation, but are the result of costs incurred in the following six categories (Pritchard (1988)):

1. initial capital costs;
2. installation costs;
3. anti-fouling programme costs;
4. fuel costs;
5. maintenance costs;
6. costs of lost production.

The initial capital cost category covers the provision of heat transfer surface area additional to that calculated at the preliminary design stage. The additional area compensates for the predicted reduction in exchanger efficiency as fouling resistances develop. This can potentially increase capital costs by as much as 20% (Garrett-Price (1985)). A safety factor, in the region of 25%, is usually applied to give the total exchanger area (Pritchard (1988)). To minimise the effect of fouling on an exchanger, it may be fabricated from exotic materials, such as stainless steel or titanium, possibly adding a further 20% to its cost (Garrett-Price (1985)).

Installation costs are subsequently raised as the provision of the additional area just described adds weight and overall volume to the heat exchanger, increases the dead and

live weight load, provision for which has to be incorporated into the design of support equipment (Pritchard (1988)).

Anti-fouling programmes typically utilise the interaction of an added chemical with the fouling agent to keep the rate of fouling to an acceptable level. This often requires the installation of a separate system, thus incurring costs typically arising from storage, injection, monitoring and chemical metering equipment, as well as the purchase of anti-fouling chemicals (Pritchard (1988)). Anti-foulant chemical supplies, cleaning services and on-line and off-line cleaning equipment supplies, have been estimated to cost US$2,000 M per year (Rebello, Richlen and Childs (1988)). Cost savings arising from the use of an anti-fouling programme are not known with any degree of certainty.

The additional energy required due to reduced efficiency in fouled equipment means that the balance has to be provided externally using a primary or secondary fuel. Primary fuels are usually burnt in fired process heaters, customarily making up the energy not recovered in heat exchange units, whilst secondary fuels, such as electricity, compensate for any additional pressure drop incurred as a result of increased surface roughness or reduction of flow area.

Maintenance costs are those incurred through deposit removal during the preparation of exchanger equipment (e.g. pulling tube bundles), and through the provision of cleaning equipment (Pritchard (1988)).

Lost opportunity costs represent revenues forfeited due to the plant failing to produce products for release into the market place. These costs may also include lost opportunity caused by a fall in production during times of seasonal high demand (Pritchard (1988)).

Taking all the above areas into consideration, the total fouling costs in Britain and North America, for all industrial plants, amounted to approximately US$8,010 M in 1982. The costs are summarised in Table 2.1 (Rebello *et al* (1988)).

Table 2.1 Fouling-related expenses of British and American industries

Component cost	Annual Cost (US$ M)
America	
Capital and installation costs	1,280
Energy losses	3,500
Maintenance	2,000
Lost production	200
Total	***6,980***
Britain	
Capital and installation costs	190
Energy losses	480
Maintenance	170
Lost production	190
Total	***1,030***

Although these costs are somewhat dated, there is no indication that the order of magnitude nor the relative impact of fouling has diminished, as increasingly competitive markets have reduced operating and profit margins still further.

The substantial (and growing) financial penalties of fouling have prompted industry to investigate new technologies and ideas with the aim of mitigating fouling. Research has been identified as the most efficient method available to advance understanding of fouling mechanisms and the effects of process parameters on fouling rates and asymptotic fouling resistance values (Rebello *et al* (1988)). Research additionally

permits strategies and new technologies to be assessed in an environment where trials do not affect the daily operation of industrial plant. The need for fouling research however, has not been considered universal (Rebello *et al* (1988)). In plant areas where fouling does not limit exchanger performance, or could be effectively and economically controlled by chemical addition, it is not deemed problematic. In contrast, in critical processing areas where fouling dramatically affects plant performance or the addition of anti-foulant chemicals cannot effectively or economically control fouling, it is deemed to be a major concern (Rebello *et al* (1988)).

The contrast in perceived economic impact that fouling has on various items of heat exchange equipment has resulted in the prioritisation of research into areas where the problem has the greatest impact (Rebello *et al* (1988)).

In the petroleum industry alone some US$4,413 M has been attributed to fouling, of which the greatest single contribution is due to crude distillation units, accounting for 67%. These costs are summarised in Table 2.2 (Van Nostrand, Leach and Haluslka (1981)).

Table 2.2 Fouling-related expenses in non-communist countries (1981)

	Capacity 10^3 Bbl/SD	**Energy (US$ M)**	**Yield (US$ M)**	**Maintenance (US$ M)**	**Total (US$ M)**
Crude Distillation	62,000	632.4	2,312.6	21.7	2,966.7
Hydro-treating	21,500	255.6	243.7	11.9	511.2
Visbreaking	1,500	254.3	63.0	18.0	335.3
Reforming	8,400	359.3	235.2	5.0	599.7
Total		**1,501.8**	**2,854.5**	**56.6**	**4,412.9**

Based on the costs presented in Table 2.2, Rebello *et al* (1988) concluded that a high priority should be place on fouling in heat exchangers in the petroleum industries, principally crude distillation units where the costs were the greatest.

In order to maximise the limited resources available, Rebello *et al* (1988) suggested that research should concentrate on five key areas, regardless of the media or system encountered. These areas were:

1. quantitative studies of deposition and removal of foulants, promoting better understanding of transport rate phenomena, and deposition and attachment mechanisms;

2. the mechanisms of the induction period, allowing the possibility for its extension, thereby reducing overall the fouling rate;

3. the effects of exchanger geometry on the transport, deposition and detachment rates, so configurations can be designed to minimise fouling;

4. the effectiveness of on-line mitigation and cleaning techniques, to assess accurately the advantages of these technologies;

5. industrial process foulants and their effects on costs, so as to better predict the economic viability of future mitigation projects.

The financial incentives for reducing the costs that arise due to fouling in hydrocarbon systems, especially crude oil systems, are great. Furthermore, reducing the financial penalties engendered due to fouling, even by small percentages, can represent significant savings in costs, ultimately resulting in increased profits. This project aims therefore to study the process parameters affecting fouling from crude oil and the effectiveness of HiTRAN® inserts as a method of mitigating the problem.

2.1 Quantifying fouling

The high priority placed on shell and tube exchangers in crude oil distillation units (CDUs) is due to the pivotal role they play in the economic viability of oil refineries. CDUs have three principal areas, heat recovery and heating and fractionation.

Heat is recovered in the CDU using a series of shell and tube heat exchangers in series, generally called a "preheat train". The use of shell and tube heat exchangers in preheat trains is universal due to their relatively simple construction, simplicity and ease of cleaning once fouled.

The recovered heat significantly reduces the amount of additional energy that may be required to raise the crude oil to the required temperature to achieve the separation of the various components (gasoline, kerosene, fuel oil, etc.). Additional heat is added in furnaces, generally combusting primary fuels such as gas or fuel oil.

Fouling can occur in any system where equipment is used to transfer heat. However, the presence of a fouling deposit does not always measurably alter the effectiveness of the exchanger with regard to its capacity to transfer heat. To assess the effects that fouling has on heat transfer and heat transfer equipment a method that will measure and quantify fouling is essential. In this section a description of the key method used to calculate fouling resistances is given.

For a shell and tube heat exchanger the effectiveness is characterised by the overall heat transfer coefficient (U_O), defined as the ability of the exchanger to transfer heat (Q) across a given area (A_T), with a defined log mean temperature difference (ΔT_{lm}) and temperature correction factor (F_T). This is illustrated by equation (2.1). The use of F_T compensates for the effect that exchanger configuration (single-pass / multi-pass) has on

U_O. It therefore enables the same equation to be used regardless. Single-pass exchangers typically have a F_T value of 1.00, reducing as the number of passes increases.

$$U_O = \frac{Q}{A_T F_T \Delta T_{lm}} \tag{2.1}$$

The use of ΔT_{lm} permits a single figure to account for the mean temperature difference between the hot and cold streams regardless of configuration. Counter current exchanger operation results in a smaller average temperature difference. This is because the hot fluid can leave the exchanger at a lower temperature than the exit temperature of the cold fluid. For a given surface area (A_T) this results in higher values of U_O, maximising the heat recovery. Conversely, co-current exchanger operation results in a larger ΔT_{lm} due to the hot fluid never achieving a lower temperature than the exit temperature of the cold fluid. This does not allow for maximum heat recovery, resulting in lower values of U_O for a given surface area A_T.

The presence of a fouling layer increases the resistance to heat transfer, reducing the value of U_O and generally leading to a reduction in the exchanger's performance. However, in certain circumstances, normally for short periods of time, increases in U_O (shown schematically by a negative fouling resistance in Figure 2.1) are not uncommon. Consequently, the performance of the heat exchanger can be improved and the presence of the fouling layer appears to result in a negative fouling resistance.

For heat transfer equipment which transfers heat without combusting fuels, the fouling resistance is measured by studying the difference in the effectiveness of the heat exchanger, using the overall heat transfer coefficient at a given time "*t*" ($U_{O(t)}$) against a benchmark value ($U_{O(0)}$). The benchmark can be taken to be either U_O at start-up of the equipment or the theoretical design value. The overall fouling resistance at time "*t*" ($R_{f(t)}$) can then be calculated using equation (2.2):

$$R_{f(t)} = \frac{1}{U_{O(t)}} - \frac{1}{U_{O(0)}} \tag{2.2}$$

Evaluating fouling using U_O relies on the presence of sufficient deposit to affect the performance of the exchanger measurably. The method does not make allowances for changes in U_O that arise from variations in operating conditions and as such does not present a true picture of the magnitude of fouling. However, under stable operating conditions, this method provides a relatively good indication of the level of fouling in a shell and tube exchanger.

2.1.1 Use of time to categorise fouling responses

As time progresses, the fouling layer may build up to a level where the resistance to heat transfer results in an exchanger being shut down for cleaning. However, in some circumstances, once a certain period of time has elapsed, the fouling resistance may not increase any further, because it has tended to an asymptotic value.

In many circumstances before any change in exchanger performance is noted, an induction period is often seen, as illustrated in Figure 2.1. Induction periods are principally seen at start-up of the equipment and can continue for days or months, depending on the media and conditions.

Plotting fouling resistance against time can be a useful method to predict how the exchanger may perform in the future, thereby allowing exchanger operation and cleaning cycles to be optimised. Generally there are four types of fouling response, illustrated in Figure 2.1 and described below:

1. linear, where the fouling resistance increases at a constant rate;

2. falling rate, where the rate of change of fouling resistance falls with time;

3. asymptotic, where the net rate of change in fouling resistance falls to zero as the resistance tends to a maximum;

4. negative, where the performance of the exchanger is improved by the presence of the fouling layer.

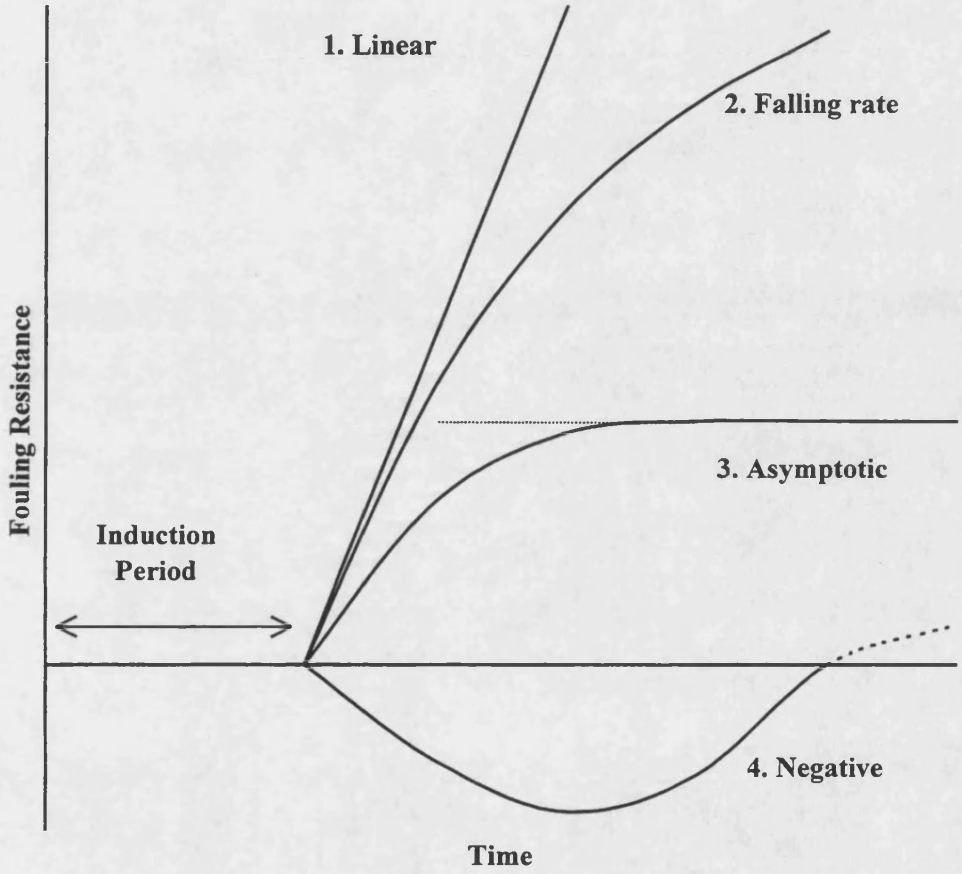

Figure 2.1 Use of time to classify fouling

These fouling responses may be combined to describe any fouling trend experienced; in general it is not possible to determine whether or not an initial linear fouling response will eventually become falling rate, or asymptotic, given a sufficiently long period of operation.

2.2 Mechanisms of crude oil fouling

The fouling of heat exchange equipment in hydrocarbon systems is due to the formation of insoluble products which accumulate on the heat transfer surface. The fluid

composition and conditions encountered in the exchanger are the key criteria in determining the predominant fouling mechanism (e.g. scaling, particulate, chemical reaction, etc.).

It is not possible to identify a single compound or mechanism responsible for fouling due to the complexity of crude oils and their mixtures. However, by studying fouling from relatively simple constituent hydrocarbon fractions it is possible to elucidate trends and dependencies on process parameters experienced in such complex fluids. The generalised mechanism of chemical reaction fouling is described by the following sequence of events (Epstein (1983)):

1. initiation: where chemical reactions occur to form insoluble material;
2. transport: where the foulant particles, or molecules, move from the bulk fluid to the heat transfer surface;
3. attachment: where the foulant bonds to the heat transfer surface;
4. removal: where the attached foulant is removed and re-entrained by the bulk fluid;
5. ageing: where the attached deposit is altered and forms a stronger attachment to the heat transfer surface.

This set of events is schematically shown in Figure 2.2 and described in greater detail in the following sections.

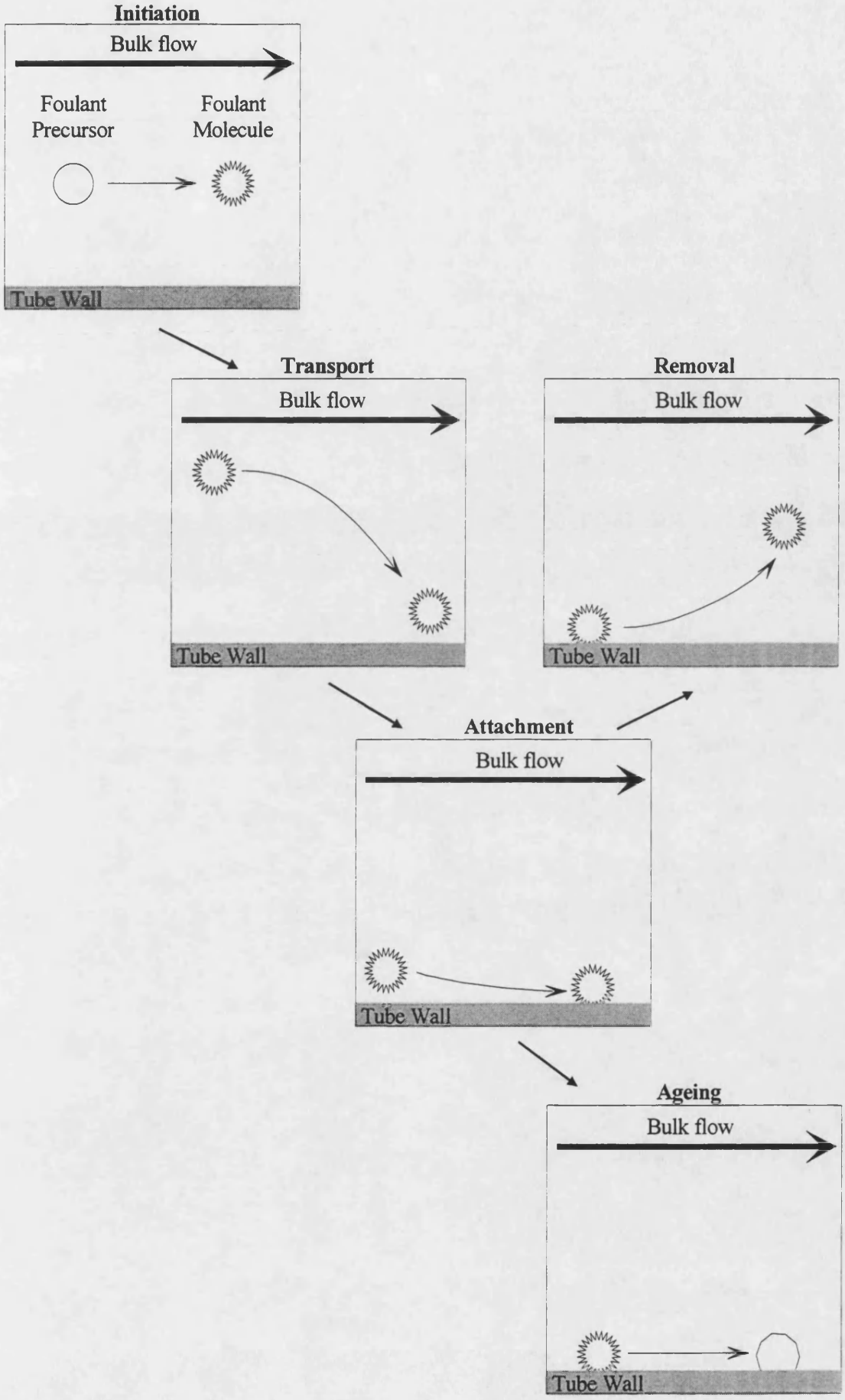

Figure 2.2 Sequence of events involved in fouling of hydrocarbon streams

2.2.1 Initiation

In hydrocarbon fouling, initiation is the term used to describe the formation of an insoluble material which may then be deposited on the tube surface. The overall chemical reaction mechanism is not fully understood but is thought to be one or more of the three component mechanisms (Crittenden (1988a)):

1. cracking and coking;
2. polymerisation;
3. autoxidation.

The mechanism predominantly responsible for the formation of fouling deposits will depend on the operating conditions, such as temperature, flow-rate, composition, etc. Crude oil is a complex fluid comprising a wide variety of compounds. It therefore follows that the overall chemical reaction mechanism may be a combination of all the above component mechanisms. The influence of the operating conditions on the above mechanisms is described in greater detail in the following text.

2.2.1.1 Cracking and coking

Cracking and coking reactions occur primarily at high temperature and in the gas phase. These mechanisms are therefore usually found in fired heaters, where tube wall temperatures can easily exceed 500 °C. The cracking and coking mechanism is a two stage process. The primary reactions comprise cracking and dehydrogenation, which occur rapidly at temperatures greater than 375 °C (650 K) (Fitzer, Mueller and Schaeffer (1971)). The secondary reactions involve the cyclisation of hydrocarbon chains to form aromatics followed by condensation to form high molecular weight polycyclic aromatic molecules. Cyclisation of aliphatic hydrocarbons occurs at a

temperature above 675 °C (950 K), whilst condensation occurs between 330 °C and 530 °C (600 K - 800 K). Although little is known of the secondary reactions, the Diels-Alder mechanism has been proposed. Cross-linking between polycyclic systems to form large molecules, which may then become insoluble and be deposited on the heat transfer surface, can occur *via* free radical pyrocondensation mechanisms (Crittenden (1988a)).

2.2.1.2 Polymerisation

In polymerisation reactions a single compound (monomer) reacts with itself (or a similar molecule) to form a large chain comprised of multiple units. There are three main steps in polymerisation fouling (Crittenden (1988a)):

1. radical formation and chain initiation, where free radicals are formed which then abstract hydrogen from an organic molecule to initiate the formation of an organic radical;

2. chain propagation, where the organic radical reacts with an organic molecule creating a larger free radical chain;

3. chain termination, where two radicals combine to produce products.

As fouling only occurs when insoluble material accumulates on the heat transfer surface, it will only be evident if the polymer is insoluble in the monomer or monomer solution (Crittenden (1988a)).

2.2.1.3 Autoxidation

At temperatures below 400 °C, such as in crude oil preheat exchanger trains, autoxidation has been identified as the key mechanism for fouling in liquid phase hydrocarbon streams being heated (Crittenden and Khater (1984); Zabarnick (1993); Wilson and Watkinson (1995 and 1996); Jones, Balster and Post (1995) and Panchal,

Halpern, Kuru and Miller (1997)). The autoxidation mechanism involves three main steps:

1. initiation;
2. propagation;
3. termination.

The autoxidation mechanism occurs *via* free radical reactions. Typically the mechanism involves the reaction of organic radicals with molecular oxygen and organic molecules (Crittenden (1988a)). The reaction can be initiated by a number of processes:

1. thermal breakdowns;
2. ultra violet (UV) radiation;
3. metallic ions;
4. chemical initiation.

The mechanism of autoxidation is summarised in the following simplified reaction scheme (Wilson *et al* (1996)):

Initiation	$X \rightarrow X^{\bullet}$
Propagation	$RH + X^{\bullet} \rightarrow R^{\bullet} + XH$
	$R^{\bullet} + O_2 \rightarrow ROO^{\bullet}$
	$ROO^{\bullet} + RH \rightarrow RO_2H + R^{\bullet}$
	$ROO^{\bullet} + RH \rightarrow ROOH^{\bullet}(\equiv R^{\bullet})$
Termination	$2\ ROO^{\bullet} \rightarrow$ Products
	$R^{\bullet} + R^{\bullet} \rightarrow$ Products
	$R^{\bullet} + ROO^{\bullet} \rightarrow$ Products

2.2.2 Transport

Fouling is only evident if there is transport and accumulation of material on the heat transfer surface. The method of foulant particle transport to the surface may be categorised into two main areas:

1. isothermal particle transport;

2. non-isothermal particle transport.

The individual mechanisms of transport vary and depend on the fluid, particle size, physical dimensions of the exchanger and the heating conditions.

2.2.2.1 Isothermal Particle Transport

Ignoring the effect gravity may have on the particles, it is considered that isothermal particle transport to the heat transfer surface is comprised of the following processes (Epstein (1988)):

1. diffusion: suspended colloidal particles move with the fluid and are carried to the heat transfer surface by Brownian motion of the fluid molecules, through the viscous (pseudo-laminar) sub-layer. This is an effective model to use on particles <1μm in diameter;

2. inertia: this regime assumes that the particles are large enough to attain a kinetic energy sufficient that it will not be completely dissipated in the viscous sub-layer. This energy may be imparted by the motion of the bulk fluid, the effect of turbulent eddies, or a combination of both. Impaction is a sub-group of inertial deposition.

2.2.2.2 *Non-Isothermal Particle Transport*

It is possible for flowing fluids undergoing heating at low Reynolds numbers to develop pronounced temperature gradients, leading to differences in physical properties between the fluid at the tube wall and the bulk. These differences can affect the deposition of particles on the tube surface, possibly giving rise to the following phenomena (Epstein (1988)):

1. thermophoresis: where convection currents are set up in the fluid, resulting in fine particles moving preferentially in the direction of the fluid currents. Therefore hot surfaces repel and cold surfaces attract particles;

2. thermoelectric: where an EMF is induced in a stream, which then imparts a charge on the tube surface. The charge may result in a preferential attraction of particles, possibly charged, as a consequence of reactions in the bulk liquid. This will only become significant if the charge is great enough or the particles are small enough.

Surface roughness is an important consideration regardless of the transport mechanism. An increase in roughness reduces the thickness of the viscous sub-layer and increases turbulence within the tube, possibly promoting particle transport.

2.2.3 Attachment, removal and ageing

Once the fouling material has been transported to the heat transfer surface, it may either be re-entrained into the bulk fluid or it may bond to the heat transfer surface. If the fouling deposits are weakly attached to the heat exchanger surface, they may be removed by the shear action of the fluid and entrained to the bulk.

Initial adhesion to the heat transfer surface is predominantly comprised of weak bonds such as van der Waals forces, depicted by Figure 2.3 (Hauser and Sommer (1990)).

These bonds are weak and easily broken by the shear action of the fluid. Re-entrainment of foulant particles deposited on the surface can affect the duration of the induction period, as insufficient fouling material accumulates on the heat transfer surface to affect the exchanger performance.

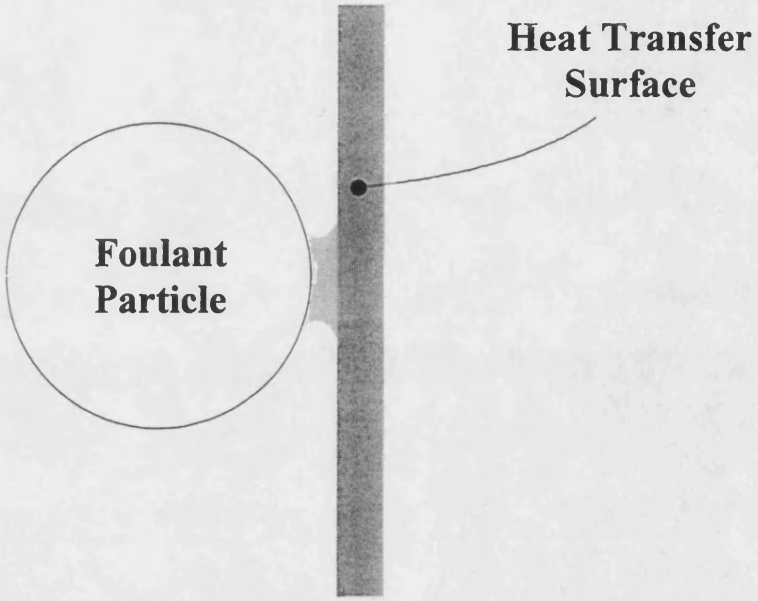

Figure 2.3 Schematic of van der Waals attraction

Particles exposed to raised temperatures at the heat transfer surface may undergo subsequent degradation reactions. The subsequent reactions may result in products which further adhere to the heat transfer surface, possibly forming material bridges, as illustrated by Figure 2.4 (Hauser *et al* (1990)). A fouling deposit attached by material bridges is more likely to remain on the heat transfer surface when exposed to the shear forces resulting from flowing fluids. This is especially true when compared with particles attached by weak bonds such as van der Waals forces.

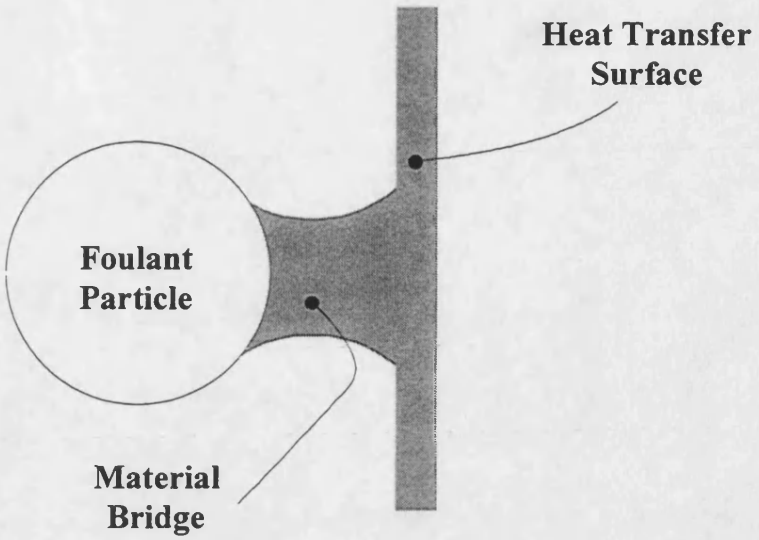

Figure 2.4 Schematic of material bridges

Subsequent thermal degradation of the material bridges results in the fouling deposit attaching to the heat transfer surface with strong chemical bonds, see Figure 2.5 (Hauser *et al* (1990)). The formation of strong chemical bonds between the surface and the foulant material explains why on-line cleaning methods can become ineffective over time.

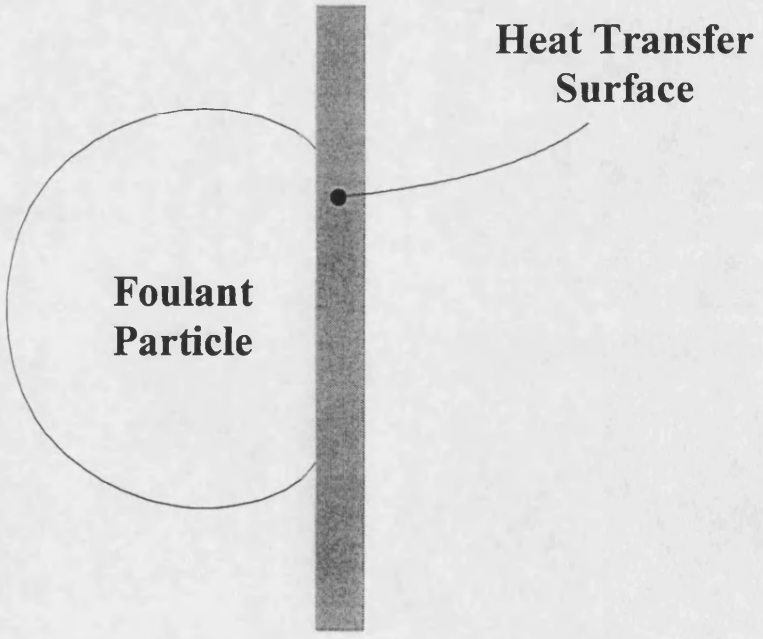

Figure 2.5 Schematic of chemical bonding

The accumulation of fouling layers does not always result in the shut-down of heat transfer equipment for cleaning. After a period of time, the insoluble material may be deposited and removed from the heat transfer surface at the same rate, resulting in zero

net accumulation. If there is no accumulation at the heat transfer surface an asymptotic fouling resistance results, as illustrated schematically in Figure 2.1.

The attachment and the removal of foulant particles at the heat transfer surface are key steps in the overall fouling process. Once on the heat transfer surface, the deposit may alter chemically or physically. The chemical or physical alterations may make the deposit easier or harder for the shear force to remove it. The thermal exposure times of the bulk fluid and deposits at the heat transfer surface have been identified as intrinsic to the determination of deposit morphology. Generally the greater the residence time at the heat transfer surface, the more tenacious the deposit (Jones, Balster and Post (1995)).

2.3 The effects of process parameters on hydrocarbon fouling

Due to the large number of constituent compounds in crude oil, it is impossible to predict with confidence which fouling mechanisms will be dominant in any particular case. However, a number of studies have been conducted into parameters affecting fouling rates and asymptotic fouling resistances. The key parameters apart from composition, are:

1. temperature;
2. flow-rate;
3. pressure and vaporisation.

Fouling rates and asymptotic fouling resistances of hydrocarbon streams are influenced by chemical reaction rates (controlled by temperature) and by the rate of mass transfer of the reactant from the bulk fluid to the reaction site (predominantly controlled by fluid flow-rate). Therefore, it follows that changes in any of the parameters affecting temperature and mass transfer will also have an effect on overall fouling rates. Pressure,

hence vaporisation, has a dramatic effect on the rate of chemical reaction and mass transfer. Vaporised fluid leaves the lower and side heat transfer surfaces and migrates to the upper surface of horizontal tubes. The movement of the vapour increases the fluid turbulence at all these locations. The increased turbulence increases the heat transfer rate, reducing the surface temperature, and increases the mass transfer rate. The effects of changes in the each of the above parameters will be described in the following sections.

2.3.1 Temperature

Due to the complexity of crude oils, the overall mechanism involved in the fouling is complex, often involving many component mechanisms. Therefore, a simple dependency on temperature cannot always be expected. A number of studies have shown that the fouling rate (particularly the initial rate) can be related to the surface temperature (T_w) by an activation energy (E) and the gas constant (R), following the Arrhenius relationship, illustrated by equation (2.3) (Taylor and Wallace (1968); Watkinson and Epstein (1969); Watkinson and Epstein (1970); Taylor (1974); Vranos, Marteney, and Knight (1981); Crittenden and Khater (1984); Crittenden, Hout and Alderman (1987); Crittenden, Kolaczkowski and Downey (1992); Crittenden, Kolaczkowski and Takemoto (1993); Jones and Balster (1994) and Wilson and Watkinson (1995)):

$$Overall Deposition\,(Fouling)\ Rate \propto e^{\left(\frac{-E}{RT_w}\right)} \qquad (2.3)$$

Simulating industrial situations in carefully controlled laboratory experiments allows for activation energies to be calculated. However, the Arrhenius equation is strictly used to account for chemical reaction rates alone and does not allow for the effect of mass transfer rates. Hydrocarbon fouling rates in heat exchangers are dependent on both mass

transfer and chemical reaction rates. It follows therefore that activation energies calculated in the laboratory may not be truly representative of the chemical reaction kinetics, but may include mass transfer effects. Apparent activation energies (E_A) therefore incorporate chemical reaction and mass transfer effects.

Apparent activation energies have been calculated for various hydrocarbon streams based on overall fouling rates. An apparent activation energy greater than 40 kJ mol^{-1} is indicative of a chemical reaction mechanism, whereas an apparent activation energy below 40 kJ mol^{-1} indicates that mass transfer mechanisms may make a major contribution. Table 2.3 (Crittenden *et al* (1993)) summarises values of the apparent activation energy for various hydrocarbon streams:

Table 2.3 Apparent activation energies of various fractions of petroleum products and hydrocarbon mixtures

Fluid	Apparent activation energy ($kJmol^{-1}$)	Temperature Range (°C)	Author
Pure n-Paraffin	40	93 - 260	Taylor *et al* (1968)
Sour Gas Oil	120	146 - 204	Watkinson *et al* (1969)
Liquid Jet Fuels	42	149 - 260	Vranos *et al* (1981)
Kerosene Vapour	70	350 - 630	Crittenden *et al* (1984)
Styrene Polym'n	39	22 - 98	Crittenden *et al* (1987)
Light Crude Oils	33	160 - 280	Crittenden *et al* (1992)
Heavy Crude Oils	21	160 - 280	Crittenden *et al* (1992)

A number of studies have found complex plots departing from equation (2.3) following the shape shown in Figure 2.6. The observed step change in deposition rate at temperature "T*" has been attributed to the transition from the liquid to gas phase of the test fluid, or a change in the overall fouling mechanism (Taylor (1974), Vranos *et al* (1981) and Crittenden *et al* (1984)).

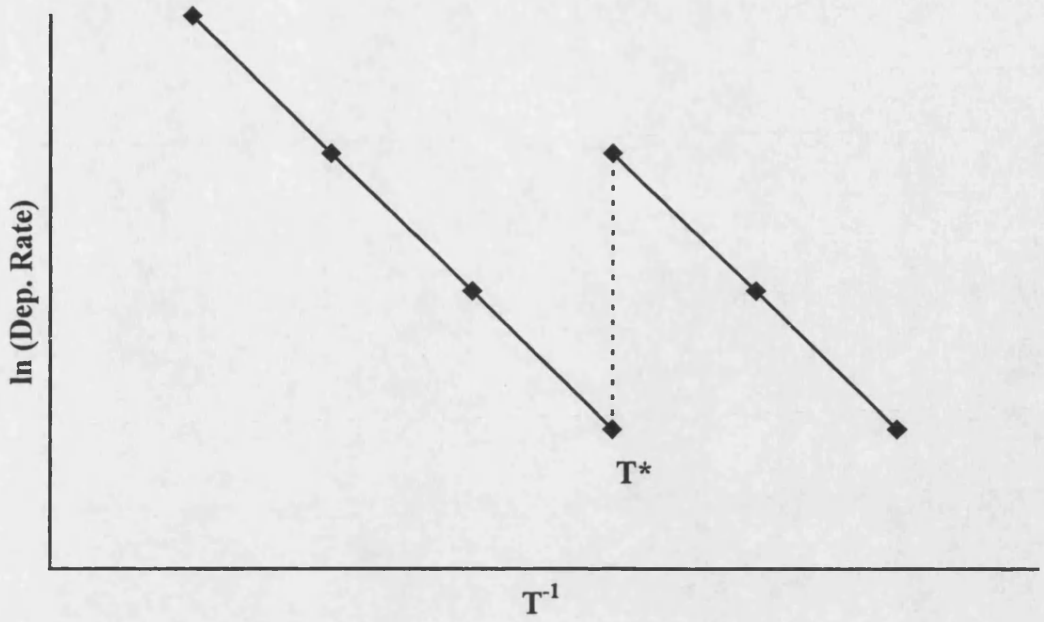

Figure 2.6 Arrhenius plot showing change in mechanism

2.3.2 Flow-rate

It is widely accepted in the petroleum industry that for fluids being heated fouling rates and asymptotic fouling resistances may be minimised through increasing the flow velocity in a heat transfer tube, or reducing the tube surface temperature. Higher flow-rates result in greater local heat transfer coefficients. Consequently, at nominally identical exchanger duties the surface temperature is reduced. However, increased flow-rates also affect the rate of mass transfer, increasing the transport of fouling particles both to and from the heat transfer surface. Deposit removal rates can be enhanced by the greater turbulence created using higher velocities.

Increased flow-rates also reduce the size of the boundary layer adjacent to the tube surface, resulting in a reduction in the volume of fluid exposed to temperatures greater than that of the bulk. This reduces the residence time and the length of time taken for the fouling particle (or fouling precursor) to reach the fluid surface (Nelson (1934)).

The effect that increasing flow-rate has on fouling rates and asymptotic fouling resistances depends on the relative balance of mass transfer and chemical reaction rates. A study on sour gas oils found that increased velocities reduced asymptotic fouling resistances (Watkinson *et al* (1969)). Previously, it was proposed that fouling resistances at any time *"t"*, ($R_{f(t)}$) could be related to the asymptotic fouling resistance (R_f^{∞}) by the use of a time constant (β) given by equation (2.4) (Kern and Seaton (1959)):

$$R_{f(t)} = R_f^{\infty}\left(1 - e^{-\beta t}\right) \tag{2.4}$$

Subsequently, it was found that at low heat fluxes, correlation between the results of equation (2.4) and the experimental data was very good (Watkinson *et al* (1969)). Furthermore, the equation parameters β and R_f^{∞} were found experimentally to have the following dependencies on the mass flow rate (G) (Watkinson *et al* (1969)):

$$R_f^{\infty} \propto G^{-2} \tag{2.5}$$

$$\beta \propto G \tag{2.6}$$

These dependencies show that for sour gas oils at least, asymptotic fouling resistances may be reduced by increasing the flow-rate (Watkinson *et al* (1969)). Based on this work, the initial fouling rate ($R^{\bullet}_{f(0)}$) was shown to be related to T_w and G by an apparent activation energy (E_A) and a pre-exponential factor (A), in an Arrhenius type relationship, as shown in equation (2.7) (Watkinson *et al* (1970)):

$$R^{\bullet}_{f(0)} = \mathrm{A}\frac{e^{\left(\frac{-E_A}{RT_w}\right)}}{\mathrm{G}^{1.07}} \tag{2.7}$$

Moreover, increases in flow-rate increase the individual film heat transfer coefficient (h), which is considered to be related to the mass flow-rate by a constant (c), illustrated in equation (2.8) (Crittenden, Hout and Alderman (1987)):

$$h = cG^{0.8} \tag{2.8}$$

The temperature of a tube wall in a heat exchanger is dependent on a number of parameters, notably the heat flux, the temperature difference between the hot and cold fluids and the film heat transfer coefficients inside and outside the tube. However, in electrically heated systems, the surface temperature (T_w) of the heat transfer surface may be related to the bulk temperature (T_b) by the heat flux (q) and the film heat transfer coefficient (h), as shown by equation (2.9) (Crittenden, Hout and Alderman (1987)):

$$T_w = T_b + \frac{q}{h} \tag{2.9}$$

By substituting equation (2.8) into equation (2.9), the effect of increasing mass flow-rate (G) on the tube wall temperature (T_w) may be described by equation (2.10) (Crittenden, Hout and Alderman (1987)):

$$T_w = T_b + \frac{q}{cG^{0.8}} \tag{2.10}$$

For a given heat flux and bulk temperature, equation (2.10) indicates that there are advantages to increasing the flow-rate of the fluid. This is due to the reduction in tube wall temperature, which results in lower reaction fouling rates (as indicated by the Arrhenius relationship).

Increasing the mass flow-rate whilst maintaining a constant outlet temperature from the heat exchanger results in a proportional increase in heat flux (q). In this case, flow-rate and heat flux can be related by a constant (c'), given by equation (2.11):

$$q = c'G \tag{2.11}$$

Substituting equation (2.11) into equation (2.10), T_w can be related to G and T_b by a constant (c''), as shown in equation (2.12) (Crittenden, Hout and Alderman (1987)):

$$T_w = T_b + c''G^{0.2} \tag{2.12}$$

In this case an increase in mass flow-rate results in an increase in tube wall temperature, which may cause an increased fouling rate.

A study that used a hydrocarbon fluid and maintained a constant heater outlet temperature found that increased fouling rates resulted from increased mass flow-rates (Smith (1969)). This was attributed to the increase in surface temperature illustrated by equation (2.12). Hydrocarbon fouling allegedly follows Arrhenius type dependencies on temperature. Hence it may be deduced that a higher surface temperature will result in an increase in reaction rate. However, increased fluid flow-rates also result in increased shear rates and mass transfer coefficients, thus affecting the removal of deposits from the tube surface and mass transfer both to and from the heat transfer surface of the reactive species.

At relatively low surface temperatures the rate of a chemical reaction may be low, to the extent that it may become the rate-limiting step. An increase in velocity will not increase the deposition rate, but might increase the removal rate by increasing fluid shear. Therefore, the overall fouling rate would be reduced (Crittenden, Hout and Alderman (1987) and Wilson, Lai and Watkinson (1995)). Where the increase in flow-

rate results in decreased fouling, control of the overall reaction rate is with the chemical reaction. This is termed "kinetic control".

At relatively high surface temperatures the rate of chemical reactions is high. Increasing the flow-rate under these circumstances will result in an increase in the rate of fouling; this is termed "mass transfer control" (Crittenden *et al* (1987) and Wilson, Lai and Watkinson (1995)).

The effect of flow-rate on the fouling rate therefore may depend on the relative balance of mass transfer and kinetic effects. This is shown in Figure 2.7 (adapted from Crittenden, Hout and Alderman (1987)) in which both mass transfer and chemical kinetic control were found for the polymerisation of styrene in kerosene.

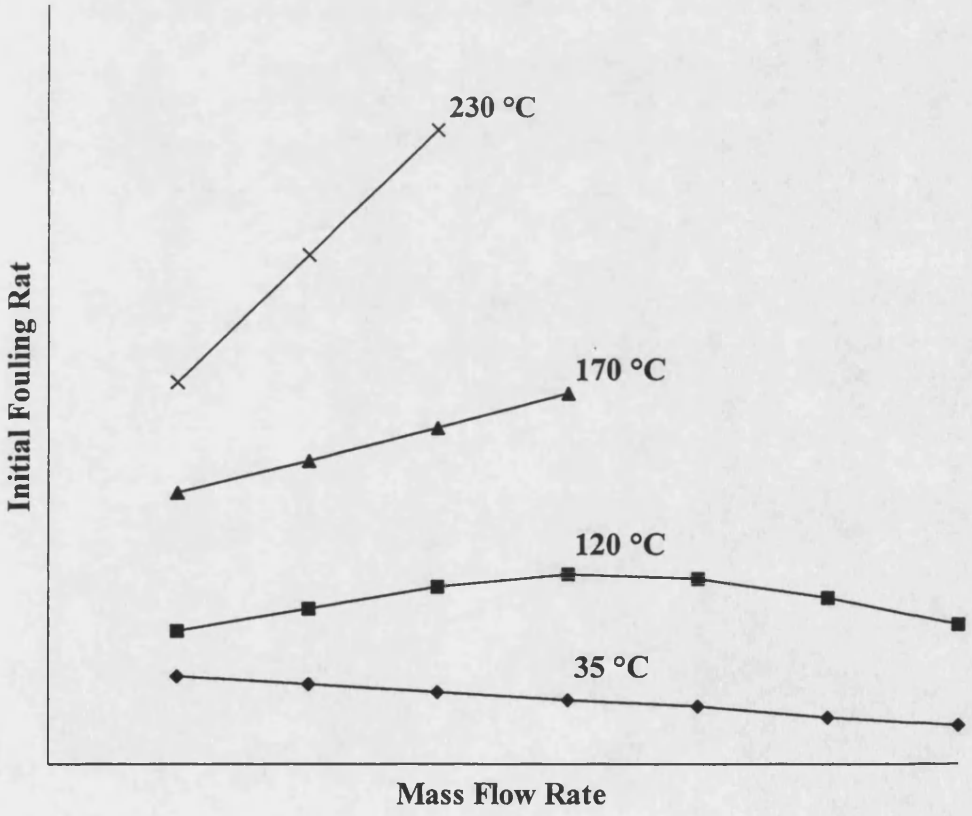

Figure 2.7 Effect of mass transfer on Initial Fouling Rate

At 35 °C the fouling rate is under kinetic control as the rate decreases with increasing velocity. At 120 °C the fouling rate is initially under mass transfer control as increased

velocity results in increased fouling rates. However, as flow-rate increases beyond the maximum there is a change from mass transfer control to kinetic control. At 170 °C and 230 °C increases in velocity result in raised fouling rates, illustrating mass transfer control.

It is clear therefore that the effect of flow-rate on fouling from hydrocarbons can be complex and dependent on the relative balance of mass transfer and chemical kinetic effects. Consequently, a number of important factors must be taken into account before choosing to increase the flow-rate in order to mitigate fouling (Crittenden (1988a)):

1. whether the fouling rate could be controlled completely or partially by the mass transfer of reactants or precursors to the hot heat transfer surface, as increasing velocity increases the mass transfer coefficient;

2. whether the laminar sub-layer is disturbed by the deposit roughness and if this is beneficial to heat transfer;

3. the effect of tube diameter, or other geometric factors;

4. the effect of changes in surface temperature that arise from changes in flow-rates.

2.3.3 Pressure and vaporisation

The boiling point of a liquid is defined as the temperature at which the pressure of the constituent vapour above the liquid is equal to the pressure in the surrounding environment. An increase in this pressure will therefore raise the temperature at which the liquid will vaporise. In equipment where the liquid is at or near its boiling point, the liquid will form bubbles of vapour on the heat transfer surface that remain there until

the bubble attains sufficient buoyancy to overcome the surface tension of the fluid and leave the surface. This process is termed "nucleate boiling" or "nucleation".

In many situations the nucleation of a fluid on a heat transfer surface increases the local heat transfer coefficient. At constant heat flux this variation in heat transfer coefficient may considerably alter the surface temperature. This in turn can dramatically affect the rate of liquid phase autoxidation reactions, which may affect the overall fouling rate. However, increases in system pressure also affect fouling rates by virtue of the fact that raised pressures improve the solubility of gases such as oxygen in fluids and suppress vaporisation, thereby promoting conditions favourable to liquid phase autoxidation reactions.

A fouling study using vaporising kerosene in a horizontal exchanger tube found that as the system pressure was increased, lower fouling rates were noted at bottom locations as the fluid bulk temperature increased (Crittenden *et al* (1984)). This appears to contradict the normally accepted dependency on the Arrhenius relationship (equation (2.3)). At the side and top locations, increases in fouling rate were noted as the bulk temperature increased (Crittenden *et al* (1984)). These findings were explained by the de-gassing of dissolved oxygen in the liquid phase to the gaseous phase as the bulk temperature increased and vaporisation occurred. The side and top locations, being in contact with both the gaseous and liquid phases, appeared to be essentially unaffected by the de-gassing (Crittenden *et al* (1984)).

2.4 The effects of composition on hydrocarbon fouling

Crude oils can be generically described by the ratio of relatively volatile products, such as kerosene, gasoline and gases (methane, ethane, propane and butane) to relatively non-volatile products such as diesel, heating oils and tar residues. Crude oils with a high ratio of volatile products are generally termed "light", whilst if the opposite is true they

are termed "heavy". The market value of crude oil is primarily based on the fraction that can be processed and sold at greatest profit, usually consisting of kerosene and gasoline. Light crude oils are normally more expensive than heavy crude oils because they require less processing to yield the valuable products such as kerosene and gasoline. However, some refinery operators process the relatively cheap heavy crudes, upgrading low value products, such as gas oil, to more valuable kerosene and gasoline products. The increased profit potential of upgrading cheaper oils can only be achieved by refineries that operate efficiently, minimising energy and material wastage. In these types of operation, the economic impact of fouling can be more acute.

Heavy crude oils generally have a greater proportion of components which promote fouling, such as asphaltenes, metallic ions, organic acids and sulphur compounds. The susceptibility to fouling of a hydrocarbon stream depends on its physical parameters, bulk composition and the concentration of reactive species, some of which may be present in trace quantities, e.g. sulphur and oxygen compounds, gases and metallic ions. The effects of these constituents are discussed in the following sections.

2.4.1 Sulphur compounds

Sulphur, in the form of sulphurous compounds such as thiols, sulphides, disulphides etc., may be present in quite high concentrations in some crude streams. A crude with a high concentration of sulphur containing compounds is usually termed "sour", whilst one with a low concentration is termed "sweet". For deoxygenated jet fuels the effect of sulphur compounds such as thiols, sulphides, disulphides and condensed thiophenes has been found, in general, to increase fouling rates. Increases in fouling rates were also found to be linked with increasing sulphur compound concentrations (Taylor (1976) and Jones and Balster (1995)).

2.4.2 Oxygen

Oxygen is present in all crude oils in the form of oxygenated compounds and molecular oxygen dissolved in transit or storage. The effects of the addition of oxygenated hydrocarbon molecules, such as peroxides, carboxylic acids, phenols, furans, alcohols, ketones and esters on the rates of fouling of deoxygenated jet fuel have been studied. It was found that some compounds, especially peroxides, increased the rates of fouling dramatically. The presence of some acids, ketones and esters either had a more moderate effect on the rate or no effect at all. It was also observed that cyclic compounds affected the rate of deposition less markedly than their aliphatic or aromatic equivalents (Taylor and Frankfield (1978) and Jones, Balster and Anderson (1992)).

2.4.3 Metallic ions

Metallic ions such as those of iron, chromium, vanadium, nickel and manganese are naturally present in trace quantities in most crude oils. A study on the effects of these on the rate of fouling in desulphurizer feedstock found that all of the studied ions affected the rate of fouling. The effects of these ions are summarised in Table 2.4 (Watkinson (1988)).

A more recent study has indicated that elucidating the role of ions, especially iron and sulphur, is critical to the understanding of fouling mechanisms in hydrocarbon systems. The formation of highly reactive iron and sulphur ionic species may be considered to be a crucial step in the initiation of fouling reactions, such as autoxidation and polymerisation, prior to the deposition of fouling material (Panchal, Halpern, Kuru and Miller (1997)).

The effect of iron on fouling rates is of particular interest as the concentration of this ion may be increased dramatically through the corrosive reactions of pipe-work. The rate of

corrosion in ferrous pipe work may be increased as a result of the presence of naphthenic acids present in acidic crude oils. However, preventative measures such as caustic injection, can be used to counter the acidity of the crude oil, thereby reducing the rate of corrosion.

Table 2.4 The effect of metallic ions on fouling in desulphurizer feedstock

	% Increase In Fouling ‡	
Metal† (1ppm)	**25% Coker 75% Straight Run Naphtha**	**100% Straight Run Naphtha**
Iron	47	17
Chromium	30	20
Vanadium	26	4
Nickel	11	51
Manganese	11	51

† - metal as oxide or oil soluble oleic or naphthenic acid salt
‡ - based on deposit ratings

Test conditions:

Temperature 315 °C Pressure 4.236 M Pa

2.4.4 Inert gases

The abundance of nitrogen in the atmosphere and its extensive use in refinery installations to blanket vessels results in quantities of N_2 dissolving in crude oil. It has been found that N_2 does not influence the fouling rates in crude oil streams, but does affect the point at which boiling occurs (Shalhi (1993)). Helium has also been found to affect only the point at which boiling occurs.

2.4.5 Role of resins and asphaltenes

A number of studies have shown that it is not the presence of asphaltenes, but rather their deposition, and hence their solubility, that is the most important factor in crude oil fouling (Lambourn and Durrieu (1983); Eaton and Lux (1984); Dickakian and Seay (1988) and Asomaning and Watkinson (1997)).

Asphaltenes can exhibit inverse-solubility characteristics. Hence a temperature rise may result in an increase in the insoluble asphaltene content in the bulk fluid. The role of asphaltenes in fouling can be summarised by the following set of sequential events (Dickakian *et al* (1988)):

1. the incompatibility between asphaltenes and the oil precipitates some of the asphaltenes;

2. the precipitated asphaltenes adhere to the hot heat transfer surface;

3. the asphaltenes then carbonise into infusible coke.

Step 3 produces an irreversible lowering of the heat transfer coefficient, which is unrecoverable without the use of off-line cleaning methods.

The role of resins in determining the rate of fouling is of secondary but nonetheless significant importance. This is due to the fact that the formation of asphaltenes is thought to occur *via* thermal degradation reactions of resins (Eaton *et al* (1984)).

2.5 The effects of fouling on exchanger design and operation

Reduced operating margins in refineries have resulted in greater demands on the operating plant to perform efficiently in order to reduce wastage of materials and energy and to minimise downtime. The design of a heat exchanger has therefore become

increasingly important, as the provision of additional heat transfer area (to allow for fouling) increases the capital cost of new equipment. The subsequent profitability of the operating plant may be reduced if equipment does not perform as designed due to the development of fouling resistances. The following section describes a number of the possible effects of fouling on the application of design allowances and the development of operational fouling resistances.

2.5.1 Design

Designing a heat exchanger is a process of trial and error, often requiring a number of iterations before an ideal solution in terms of cost and performance is achieved. The overall heat transfer coefficient (U_O) of an exchanger may be described as the result of heat transferred over the area supplied, as given in equation (2.1):

$$U_O = \frac{Q}{A_T F_T \Delta T_{lm}} \tag{2.1}$$

The overall heat transfer coefficient (U_O) may also be described as the reciprocal of the sum of individual resistances to heat transfer, as shown in equation (2.13) for a round tube:

$$\frac{1}{U_O} = \frac{1}{h_i}\left(\frac{d_O}{d_i}\right) + R_{fi}\left(\frac{d_O}{d_i}\right) + \frac{d_O \ln(d_O/d_i)}{2k_w} + \frac{1}{h_O} + R_{fO} \tag{2.13}$$

The individual resistances comprise the corresponding film resistances for the fluids on either side of the heat transfer surface, calculated from the heat transfer coefficients (h_i and h_o) together with fouling resistances (R_{fi} and R_{fO}), for inside and outside the tube (denoted by subscripts i and o respectively). The tube wall resistance may also be included, especially if the tube wall is thick. Here, the tube wall thermal conductivity is k_w. The five individual resistances are illustrated in Figure 2.8 for a tube side fluid being heated:

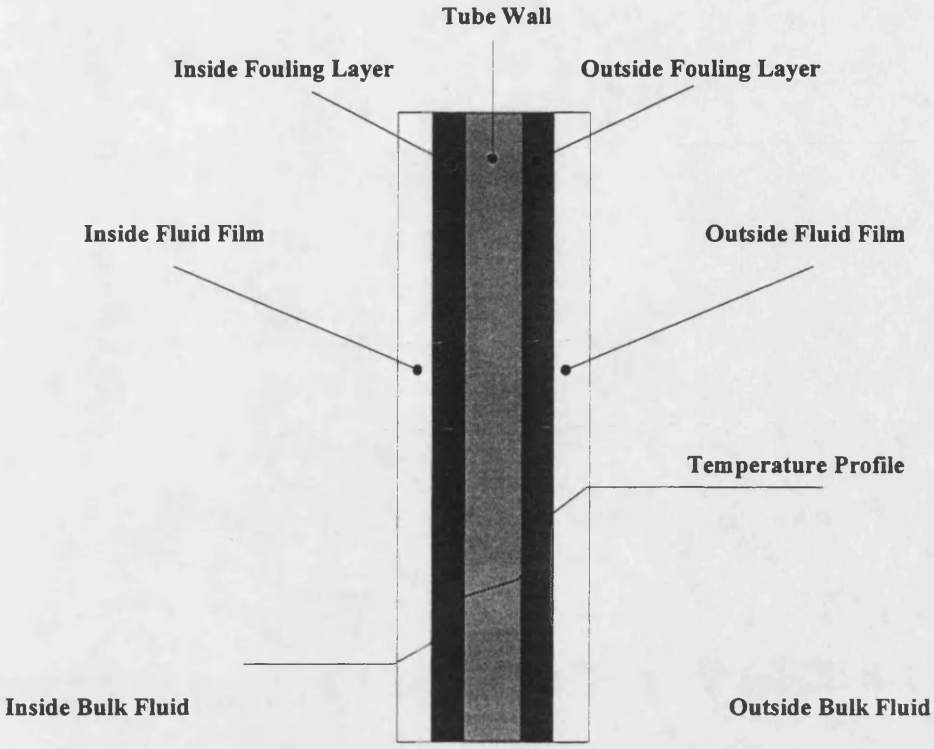

Figure 2.8 Film and fouling resistances either side of a tube wall

Compensation for fouling may be made at the design stage by increasing either the total exchanger area (A_T) or the log mean temperature difference (ΔT_{lm}), which can result in increased capital costs and / or running costs. In designing a heat exchanger a set of sequential steps is followed in order to size and optimise the design to achieve maximum economic and process performance. The variables altered to optimise the exchanger design are generally the heat exchange area (A_T), the tube length used and the number of passes. Altering the tube length and the number of passes affects the exchanger pressure drop, which requires careful consideration. The general design sequence followed is summarised below (Coulson, Richardson and Sinnott (1991)):

1. define the duty (Q);
2. collect physical property data (viscosity, density, etc.);
3. decide on type of exchanger;
4. select trial value for the overall heat transfer coefficient (U_O);

5. calculate the mean temperature difference (ΔT_{lm})

6. calculate area (A_T), using (equation (2.1));

7. decide on exchanger layout;

8. evaluate the individual coefficients (h_i, h_o etc.) for use in equation (2.13);

9. calculate U_O. If the value differs significantly from the estimated value, substitute the value calculated for the estimated value and return to step 6;

10. calculate pressure drop. If excessive, then return to steps 7 or 4 or 3 in order of preference;

11. optimise design, repeat steps 4 to 10 to determine the cheapest exchanger that will satisfy the duty, normally the one with the smallest area.

Clearly, the optimum design may depend critically on the choice of fouling resistances. The selection of a fouling allowance to be used in the design of a heat exchanger depends on the media and conditions encountered. For crude oil streams, a range of values are suggested by the Tubular Exchangers Manufacturers Association (TEMA), depending on the temperature, velocity and salinity of the crude. These are summarised in Table 2.5 (Chenoweth (1990)):

Table 2.5 Crude oil design fouling resistances recommended by TEMA (1978)

		Velocity (m s^{-1})		
	Temperature (°C)	**< 0.67**	**0.67 to 1.30**	**> 1.30**
Dry	**< 95**	5.28	3.52	3.52
	95 → 150	5.28	3.52	3.52
	150 → 260	7.12	5.28	3.52
	> 260	8.90	7.12	5.28
Salt	**< 95**	5.28	3.52	3.52
	95 → 150	8.90	7.12	7.12
	150 → 260	10.68	8.90	7.12
	> 260	12.46	10.68	8.90

Design fouling allowance x 10^4 (m^2 K W^{-1})

The increasing economic impact of fouling in operating plants has meant that the consideration of design allowances for fouling has become increasingly important. This is reflected in the commissioning of a report reviewing the Fouling Section of the 1978 sixth edition of the TEMA Standards. The report made the following general recommendations (Chenoweth (1990)):

1. an allowance should be provided for fouling through the use of individual fouling resistances for the two sides of the tube bundle;

2. the fouling resistance should reflect fouling alone and not uncertainties in the design of the heat exchanger, physical properties, temperatures or process requirements;

3. appropriate values of fouling resistances should be based on operating experiences where possible;

4. the purchaser, not the vendor, should supply the individual values of fouling resistances to be applied in exchanger design calculations, keeping US customary units but providing conversion factors to SI units;

5. the introduction of a new section entitled "Recommended Good Practices for Fouling" should be added to the next edition of the TEMA Standards;

6. the values currently in the fouling section of the TEMA Standards should be transferred across to the new edition;

7. the effects of corrosion and bio-fouling are complex and not well understood, and this should be represented by tabular data, not by a single Figure.

In addition to the general recommendations above, the report concluded that fouling allowances used in the design of exchangers for crude oil streams should be revised and the format updated. The revised, recommended fouling allowances are summarised in Table 2.6 (Chenoweth (1990)):

Table 2.6 Revised TEMA fouling resistance values

Temperature (°C)	Design fouling allowance $x\ 10^4$ ($m^2 K\ W^{-1}$)
< 120	3.52 to 7.04
120 to 180	5.28 to 7.04
180 to 230	7.04 to 8.80
> 230	8.80 to 10.56

Crude oil refiners have found that fouling allowances suggested by TEMA in designing heat exchangers are frequently exceeded, in some cases rapidly and by large margins (Lambourn *et al* (1983) and Crittenden *et al* (1992)). It follows that fouling values from

operational industrial heat exchange equipment could therefore be used to specify the design fouling resistance. This is particularly appropriate where exchangers of identical design are intended to replace existing equipment. However, the use of such data must be considered carefully as it may be inaccurate and misleading.

Fouling resistances generated from plant data are indicative of the operating conditions at that particular moment in time, and may not be representative of general operating conditions (Crittenden *et al* (1992)). Moreover, inaccuracy of industrial data could also lead to inappropriate fouling resistances being quoted. For example, errors of 1 °C in temperature and 1% in the flow-rate have been known to give rise to errors of 13% in the value of calculated fouling resistances (Crittenden *et al* (1992)). Therefore the use of fouling resistances calculated from plant data may not be wholly accurate.

It is not possible to say with certainty whether fouling resistances generated by plant data, using the process parameters at a specific time, will enable similar fouling resistances to be used for similar conditions but a different crude oil, as is suggested by the TEMA values. Furthermore, fouling resistances generated from plant data may be the result of inappropriate fouling resistances or excessive design allowances used at the design stage and therefore only an indication of the poor original design.

2.5.2 Operation

Once an exchanger has been designed and fabricated, and is in operation, the development of a fouling resistance will generally result in a reduction in U_O. Exchangers are an integral part of operating plants and perform one of two tasks in industry: either heat recovery from one stream to another, or temperature control.

Where networks of exchange equipment are used to recover heat, such as in crude oil preheat trains, the reduction of U_O due to fouling can result in a reduction in the

effectiveness of the exchanger network. Consequently, additional fuel consumption will be needed in fired heaters to make up the balance of heat that is un-recovered by the heat exchange network. To achieve the required furnace outlet temperature the development of a fouling resistance may therefore result in a reduction in the processing rate especially where the fired heater is at the limit of operation.

In situations where the exchange equipment is used to raise the temperature of one of the fluids to a set point, such as in reboilers, fouling increases the resistance to heat transfer, thereby resulting in an increase in the mean temperature difference (thermal driving force). This may become a problem if the fluid being heated is temperature-sensitive, as the increased tube surface temperature may lead to degradation of the fluid. With the exception of fired heaters, steam is used almost exclusively in heat exchangers to raise the temperature of the "cold" fluid to the required temperature. In these cases the mean temperature difference is increased by raising the steam pressure, which reduces its latent heat. As a result more steam needs to be condensed in order to transfer the required energy. This results in an increase in the energy demand on the boiler plant for two reasons:

1. to provide the additional mass of steam due to the reduced latent heat of the steam;

2. to raise the pressure of the steam to the required value.

Where exchange equipment is used to lower the temperature of one of the fluids to a set point, for example in pump around circuits, fouling may result in an increase in the exchanger outlet temperature of the hot fluid. Pump around circuits are used to control the separation of component fractions in distillation columns through returning relatively cool pump around fluid. This increases the temperature gradient over the column, resulting in a more effective separation of the constituent fractions. Therefore,

an increase in the temperature of the returning fluid in the pump around circuit may, in extreme cases, reduce the separation efficiency of the distillation column. This can cause the creation of products which fail to reach the required specification at the required production rates. In these situations the products are either re-processed, sold at a lesser rate, or a reduction in the refinery production rate is set up to enable the required product specifications to be maintained. In each of these scenarios the running costs are increased, reducing the profitability of the entire operation.

In certain circumstances, for short periods of time, an initial increase in U_O is sometimes observed (Figure 2.1). This may be attributed to increases in surface roughness when initial deposition causes roughening of the heat transfer surface, temporarily improving the film heat transfer coefficient. If the increase in heat transfer coefficient is greater than the increase in the resistance due to fouling (assuming the other values remain constant), then according to equation (2.13), U_O is increased. Consequently, the performance of the heat exchanger will be improved and this does not present a problem to plant operators.

2.6 Mitigating crude oil fouling

In general, profit margins arising from processing cheap, heavy crude oils can be greater than for light crude oils. Heavy crude oils are therefore becoming increasingly popular with refiners equipped with the appropriate technology. Heavy crude oils usually contain a significantly higher proportion of the classes of compounds which have been identified as having a significant role in fouling. This trend towards processing of heavy crude oils is leading to greater fouling problems in heat exchange equipment which may not originally have been designed to cope with the heavier material.

Due to the wide range of crude oils and hydrocarbon streams available, it is not possible to predict with confidence which measures need to be taken in order to best reduce the

effects of fouling in each particular case. Mitigation methods are varied and involve a number of technologies. However, it is widely accepted that raising the mass transfer coefficient and reducing the tube wall temperature through increasing flow-rate or turbulence in the tube are the simplest methods of reducing fouling rates and lowering asymptotic fouling resistances.

In the following sections a description of mitigation methods requiring no additional powered equipment and the use of preventative measures, either at the design stage or operational stage, will be given.

2.6.1 Exchanger configuration

Implementing mitigation measures at the design stage requires an understanding of the effect of process parameters on the fouling rate of the particular stream. In the petroleum industry it is generally believed that fouling rates and asymptotic fouling resistances may be reduced or eliminated by increasing the fluid flow-rate, resulting in reduced tube wall temperatures and increased shear removal of surface deposits.

Increased velocities may be achieved by reducing the flow area in a heat exchanger and can be achieved by utilising multi-pass configurations. However, allowance for additional pressure drop must be made. Certain exchangers are specifically designed to minimise fouling in service, such as spiral channel and cartridge exchangers. These are single flow channel devices in which the local velocity increases as a result of deposition reducing the area for fluid flow. The higher velocity (locally) increases the shear force of the fluid on the deposit. In such circumstances, the probability of deposit removal through the shear action of the fluid is increased.

In addition to alternative exchanger designs, auxiliary equipment may be fitted to remove deposits as they occur. These include self-cleaning systems which may use

circulating or fluidised solid systems, and / or surface scrapers. Fluidised bed heat exchangers have been found to reduce significantly fouling rates in particulate laden aqueous streams (Müller-Steinhagen and Jamialahmadi (1997)). Whilst fouling did occur, this study demonstrated that the lower rate resulted in longer run-times before the equipment was taken off-line for cleaning.

2.6.2 Operational considerations

As previously discussed, the composition of the crude oil and its constituents are as important in determining fouling rates and asymptotic fouling resistances as the temperature and flow-rate of the process stream (Lambourn *et al* (1983); Wilson and Vassiliadis (1997); Panchal *et al* (1997) and Crittenden, Kolaczkowski and Phillips (1997)).

Attention to good housekeeping and control of operational parameters affecting fouling therefore are important in avoiding the occurrence of conditions which promote fouling. These factors include, but are not limited to (Crittenden *et al* (1997)):

1. careful control of de-salter operations; controls should be optimised to eliminate salt and inorganic contents in the treated stream;

2. elimination of oxygen and air from process streams by purging, stripping, inert gas blanketing or floating roof storage tanks. The choice of technique depends on the nature of the feed; for example, its volatility;

3. reduction in slop oil recirculation since these materials tend to contain more oxygenated species, dissolved gases and cracked hydrocarbons;

4. reduction of the processing of unsaturated or cracked feed-stocks wherever possible;

5. elimination of particulate material from process streams; in particular sludge from storage tanks should be prevented from travelling through the de-salter and exchanger trains;

6. avoidance of mixing of fluids which aggravate the precipitation of fouling material; for example, those mixtures of crude oils which promote the precipitation of asphaltenes.

In operating a plant economically, following the guidelines above may not always be practical. It is accepted that some degree of fouling will always occur. However, there does exist a critical point beyond which the fouling resistance affects the economic performance of the plant. Operation of the plant can impact the level and rate of fouling in the exchangers. It has been shown that modelling heat exchange networks and optimising their operation to minimise fouling can provide significant cost benefits (Wilson *et al* (1997) and Müller-Steinhagen *et al* (1997)). Furthermore, optimising exchanger operation to minimise fouling results in longer runtimes, reducing the possibility of incurring costs arising from cleaning, maintenance and lost production.

2.6.3 Anti-foulant additives

Many proprietary anti-foulant chemicals are available to control hydrocarbon fouling, by interacting with the foulant, preventing either its formation or its adherence to the heat transfer surface. Chemicals are dosed into the process stream in low concentrations and are effective only if used within the range of process conditions specified for that particular formulation. A summary of the categories used to describe anti-foulant chemicals is shown in Table 2.7 (Crittenden *et al* (1997)):

Table 2.7 Function of anti-foulant chemicals

Property	Function
Dispersant	prevents particles from agglomerating and sticking to surfaces and causes disintegration and removal of deposits
Anti-corrosion	minimises growth of corrosion products and inhibits metal catalysis of organic polymerisation reactions
Metal co-ordination, chelation and sequestration	deactivates metal ions which catalyse free radical polymerisation reactions
Antioxidant / antipolymerant	destroys peroxides or reacts with free radicals to prevent autoxidation reactions
Detergent	similar to dispersant but polar and ionic in its action
Neutralisation	reacts via pH control to neutralise troublesome compounds

Laboratory trials are suggested prior to selection and implementation of an anti-foulant programme, to ensure that correct anti-foulant chemicals and dosages are chosen.

2.6.4 Intensification of heat transfer surfaces

The limited financial resources available to plant operators and designers, and the complex relationships between flow-rate, temperature and composition of the stream, have meant that combating fouling needs to be assessed both economically and technically. The challenge of mitigating fouling economically has been partially met by looking at upgrading rather than replacing existing equipment, resulting in improvements to existing exchanger performance at substantially reduced costs.

Upgrading may be achieved through the intensification of the tube surface, whereby the tube, either inside or outside, is altered in some way, with the main aim of increasing the heat transfer coefficient. Intensified surfaces can increase the effectiveness of an

exchanger by not only increasing the individual heat transfer coefficients but also by reducing fouling. In discussing intensification methods, it is first important to distinguish between augmentation and extension of plain surfaces. Augmentation is the situation in which the plain surface is added to, achieving increased heat transfer coefficients through the use of turbulators or inserts (Epstein (1983)). Extension is the provision of greater heat transfer area which may be achieved the use of fins or special tubes such as those of ribbed or knurled designs (Epstein (1983)).

Augmentation is a rapidly expanding area of business and there now exists a number of technologies for both shell and tube sides. Shell side intensification is limited to the use of tube extension, alternate tube designs and baffle alterations, such as the application of helical baffle geometry. Shell side technologies will not be discussed further in this thesis because crude oils tend to be passed inside tubes to facilitate cleaning when fouling occurs. For inside the tube there is a wide variety of augmentation methods available for specific tasks. Tube side enhancement can be divided into two categories (Bergles (1988)):

1. passive: those methods which do not require any external power, which include:

    - treated surfaces, roughened surfaces, extended surfaces, displaced enhancement devices, swirl flow, surface-tension devices and additives

2. active: those methods which require additional power to be applied, which include:

    - mechanical aids, surface vibration, fluid vibration, electrostatic fields

The technologies described above have been the subject of much heat transfer research and have been extensively developed for industrial use. However, only a small number

have been accepted as technology requiring further investigation for fouling purposes. These include, but are not necessarily limited to:

1. surface treatment;
2. enhanced tube design;
3. displaced enhancement devices (e.g. the HiTRAN® inserts).

2.6.4.1 *Treated surfaces*

The use of coatings on metal surfaces to assist the surface in performing a function is not new and has been utilised in many areas other than heavy industry. In industrial situations, materials such as Teflon® or glass are typically used. However, due to their high cost their use is limited to situations in which the process fluid requires their special material properties, such as in hydrofluoric acid service and the specialist chemicals industry. The selection of coatings able to withstand the process conditions required for long periods of operation may also prove difficult.

Treatment of the metal material itself reduces the likelihood of deterioration associated with surface coatings. Using particle accelerators to implant silicon ions into iron surfaces has been found to be effective in reducing fouling from an aqueous calcium sulphate solution under boiling conditions (Müller-Steinhagen and Zhao (1997)). Reducing fouling by surface treatment permits current design practices to be retained. Furthermore, the use of surface treatment maintains bare tube pressure drops. However, the high cost of surface treatment is likely to remain the single greatest obstacle to its widespread use.

2.6.4.2 Enhanced surfaces

In general, enhanced surfaces are those which are altered by tube design rather than by the fitting of inserts. The complex geometry of enhanced tubes, such as internally ribbed, knurled and Knudsen tubes, means that production costs are greater than for plain tubes. The complex geometry of enhanced tubes generally increases the turbulence, thereby increasing the heat transfer coefficient and the pressure drop. The significantly higher heat transfer coefficients achieved by using enhanced tubes (in comparison with bare tubes) have meant that in some circumstances it has been possible to reduce velocities so as to stay within the original bare tube pressure drop allowances, whilst still performing the required duty. This is principally achieved by re-engineering the flow configuration of the exchanger, typically reducing the number of passes. Currently, enhanced tubes are principally utilised on non-critical applications such as cooling water services due to the scepticism concerning their advantages (Bergles and Somerscales (1995); Watkinson (1990)). Consequently, their installation in critical operating areas, such as in crude oil pre-heat trains, has met with some resistance. This is primarily due to the belief that enhanced tubes will foul and their complex geometry will prevent effective cleaning. Studies have found that whilst enhanced surfaces do foul, they nonetheless out-perform bare tubes in similar service (Bergles (1988) and Watkinson (1990 and 1991)). It has not yet been possible to verify the possibility of cleaning enhanced tubes.

2.6.4.3 HiTRAN® inserts

Inserts are manufactured to fit inside tubes and designed to increase fluid turbulence, thereby increasing heat and mass transfer and pressure drop. Inserts are generally installed in existing exchangers as retrofits, making them a relatively economic option to increase the efficiency of the exchanger and possibly to reduce fouling. The relatively

simple procedure of retrofitting tube side devices to existing exchangers means that tube side inserts, such as twisted tapes, turbulators, moving springs and wire matrix devices, may have a greater range of application than the other augmentation techniques. However, as with enhanced tubes, significant re-engineering of existing heat exchange equipment may be required to keep within bare tube pressure drop limitations.

HiTRAN® inserts manufactured by Cal-Gavin have been used extensively in the petrochemical and oil refining industry to reduce fouling rates and lower asymptotic fouling resistances, as well as to intensify existing heat transfer equipment. This is due to the relatively low cost of fitting such a device. The HiTRAN® insert consists of a number of loops protruding from a central supporting spine, as shown in Plate 2.1; the number of loops per unit length determinines the insert density.

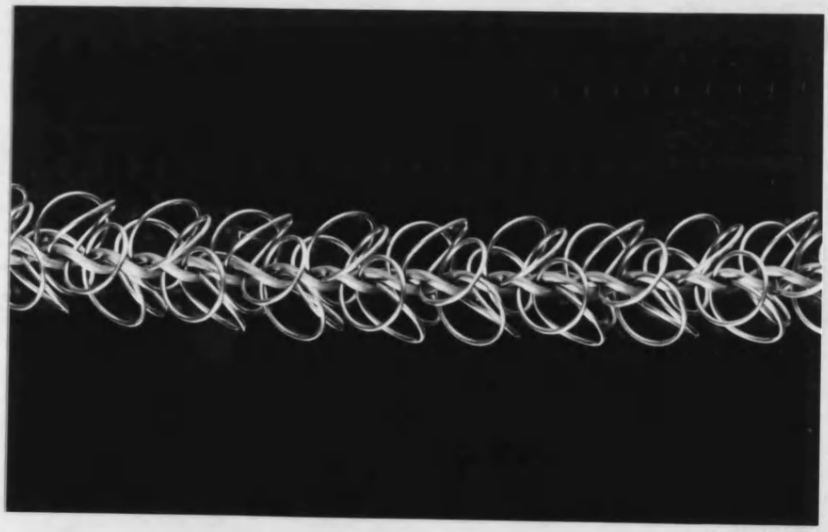

Plate 2.1 HiTRAN® insert

The HiTRAN® insert is constructed in such a way that the diameter is slightly oversized compared with the internal diameter of the tube. Once inserted into a tube the tips of each wire loop exert a force on the tube wall sufficient to counteract the drag force created by the flowing fluid that would otherwise move the insert downstream. Consequently, the insert is held in place. Only the tips of the loops come into contact with the tube surface, as shown in Figure 2.9:

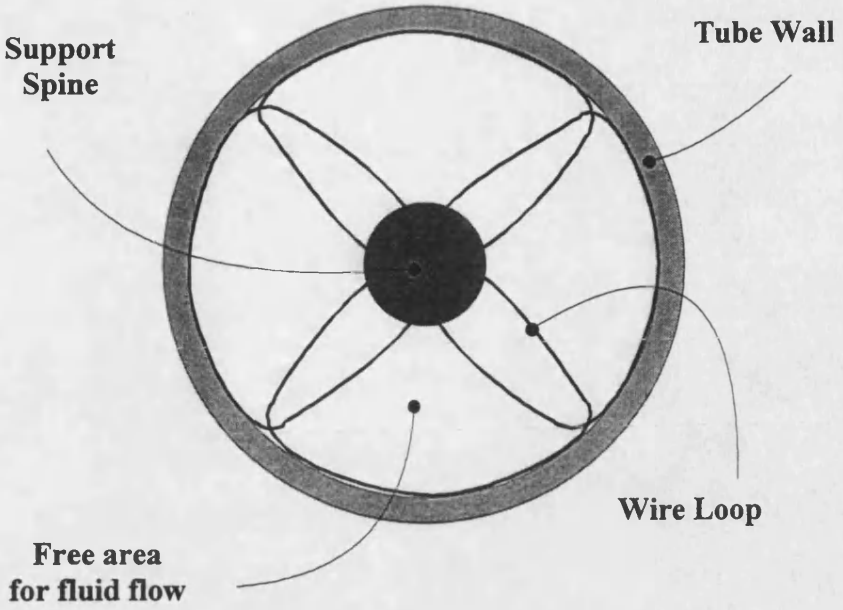

Figure 2.9 Cross section of a HiTRAN® insert in an exchanger tube

The insert is orientated in the tube such that the flow of the fluid is in the opposite direction to the rake of the loop, as illustrated in Figure 2.10:

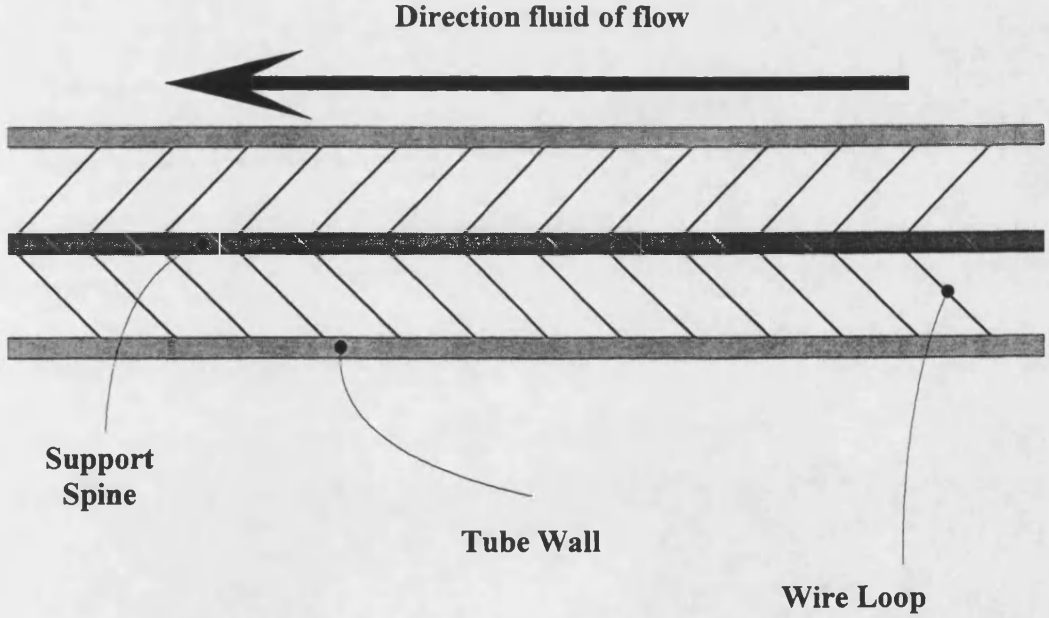

Figure 2.10 Longitudinal section of a HiTRAN® insert in an exchanger tube

Under nominally identical conditions, tubes containing HiTRAN® inserts experience more turbulent conditions in comparison with bare tubes. Therefore, tubes containing HiTRAN® inserts develop turbulent flow at lower Reynolds numbers than bare tubes, which are commonly accepted as developing turbulent flow at Reynolds numbers above 2,200.

The development of a fully turbulent regime at low Reynolds numbers means that no discontinuities in heat transfer factor between traditionally defined laminar and turbulent flow regimes are evident, as illustrated in Figure 2.11 (Gough and Terranova (1992)). It has been found that tubes fitted with HiTRAN® inserts experience heat transfer factors between two to ten times greater than those of bare tubes at nominally identical conditions. The increase depends on Reynolds number and insert density (Gough and Rogers (1987)).

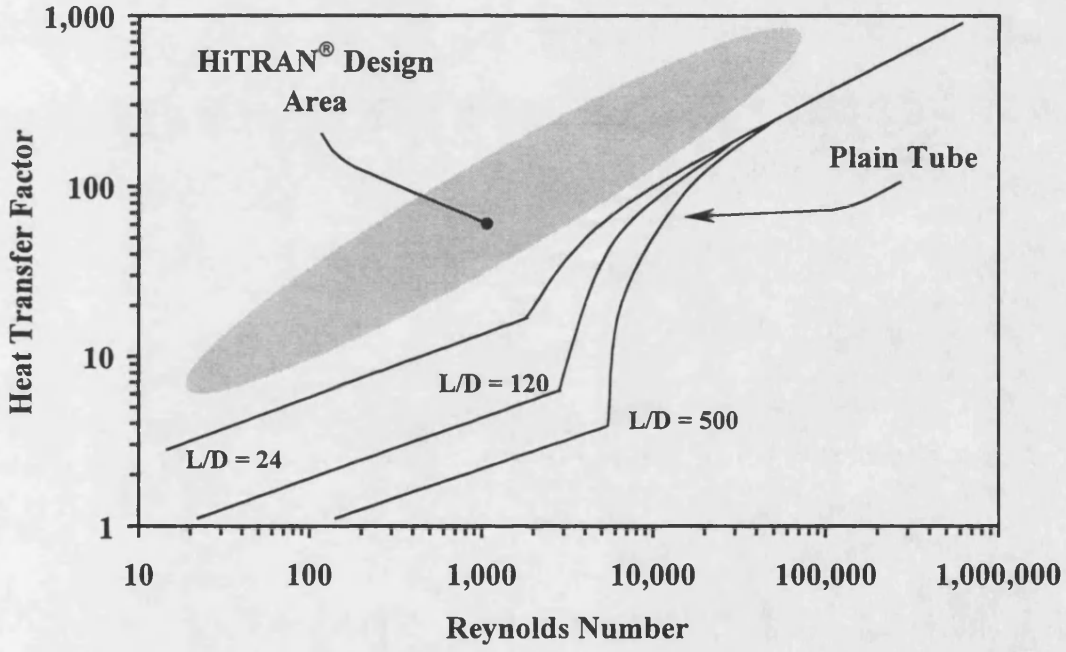

Figure 2.11 Graph showing the improvement of HiTRAN® inserts over plain tubes

The use of heat transfer factors (j_h) in exchanger design allows data to be correlated over a wide range of Reynolds numbers using a single set of equations. Kern reports that heat transfer factors can range from $x10^1$ (Re ~ 1 x 10^1) to $x10^3$ (Re ~ 1 x 10^6) in carbon steel heat exchanger tubing (Kern (1950)).

An increase in heat transfer factor represents a corresponding increase in heat transfer coefficient. Figure 2.11 suggests that even at low Reynolds numbers, the heat transfer coefficient may be greater for tubes fitted with HiTRAN® inserts than for bare tubes at a

higher velocity. However, under identical conditions, the added advantage of inserts comes at the cost of increased pressure drop. In comparison with bare tubes at nominally identical conditions, tubes fitted with inserts may experience pressure drops up to sixty times greater than for bare tubes. The increase depends on the density of the insert and the velocity of the fluid (Oliver and Aldington (1988)). Greater heat transfer coefficients may be experienced by tubes containing inserts at lower Reynolds numbers than by bare tubes. Consequently, it is possible to reduce fluid velocity whilst improving the performance of the exchanger. This allows original bare pressure drop limitations to be maintained (Gough and Rogers (1992)).

2.6.4.3.1 Fouling and HiTRAN® inserts

HiTRAN® inserts have been found not only to improve heat transfer rates but also to reduce fouling rates and asymptotic fouling resistances in hydrocarbon streams (Gough and Rogers (1987, 1992); Gough and Terranova (1992); Crittenden, Kolaczkowski, and Takemoto (1993); Polley, Nasr and Terranova (1994); Polley and Gibbard (1995); M°Mullan, Gough, Gibbard and Polley (1995); Thome (1992); Shalhi (1993) and Takemoto (1993)).

For a Light Arabian crude oil containing 10% dissolved waxy sludge, the reduction in fouling rates and asymptotic resistances for a given fluid velocity has been found to be a function of the density of the HiTRAN® insert (Crittenden *et al* (1993)). As the density of the HiTRAN® insert was increased it was found that the fouling rate was reduced, however, it was noted that the lowest insert density nonetheless provided substantial reductions in fouling rate compared with bare tubes at nominally identical conditions (Crittenden *et al* (1993)).

Due to the simplicity of the HiTRAN® insert design, existing exchangers may be retrofitted with minimal alteration to the physical layout. An industrial study on a tar oil

residue heater has found that by re-engineering the exchanger, HiTRAN® inserts could achieve significantly reduced fouling whilst maintaining bare tube pressure drop allowances (Gough *et al* (1987)). Originally the exchanger required shutdown for cleaning every eight weeks, due to the high level of fouling. After the inserts were installed, run-times were increased to 4½ years. Figure 2.12 (Gough *et al* (1987)) summarises these results; the insert was installed after point 3.

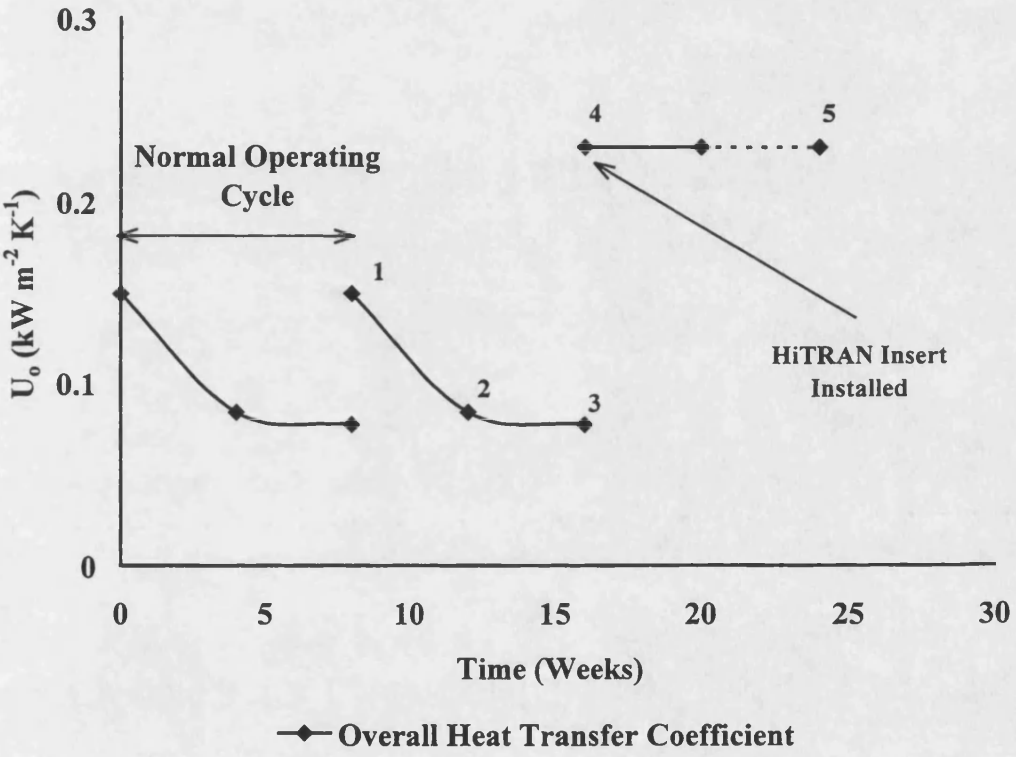

Figure 2.12 Tar heater oil performance results

Although greater pressure drops were allowed for, the overall system losses were not increased. This was achieved through a combination of the following (Gough *et al* (1987)):

1. a reduction in the number of passes in the exchanger, thereby increasing the fluid flow area, and resulting in a drop in velocity;

2. a reduction the fluid viscosity arising from increased bulk temperatures due to improved heat transfer.

The success or failure of a heat exchanger retrofit with inserts depends on the correct redesign and configuration of the physical layout of the existing exchanger. However, it has been found that the physical properties of the fluid may also be important factors in determining the relative benefit of inserts. The use of HiTRAN® inserts in exchangers that handle viscous fluids has been found to result in greater benefits than has their installation in exchangers with low viscosity fluids at nominally identical conditions (Polley *et al* (1994)). The benefits are summarised in Table 2.8 (Polley *et al* (1994)):

Table 2.8 Level of beneficial effect of inserts in different fluids

Fluid	Beneficial Effect
Water	Good, at Low Duty
Low Viscosity Organic	Low
Moderate Viscosity Organic	Good
High Viscosity Oils	High

Inserts are primarily used to upgrade or mitigate a fouling problem in existing exchangers. However, using inserts at the design stage can have additional benefits. Increased performance by enhanced heat transfer results in decreased size, lower approach temperatures and reduced capital costs (Gough *et al* (1987)). The ability of the HiTRAN® insert to reduce fouling may reduce the capital costs still further by permitting the designer to use a lower fouling allowance at the design stage.

Careful consideration is required however, when using HiTRAN® inserts in hydrocarbon streams, because installation of an insert results in increased mass transfer as well as increased heat transfer. In situations where large activation energies are experienced, or where the fouling rate is kinetically controlled, the reduction in the wall temperature resulting from increased heat transfer coefficients may be the most beneficial effect and the increase in mass transfer may not be as important. However,

where the overall fouling mechanism is controlled by mass transfer of foulant precursors to the heat transfer surface, the increase in mass transfer to the wall may have an effect that overrides that arising from the reduction in the wall temperature, thereby possibly leading to increased fouling rates (Watkinson (1991)).

2.7 *Fouling research*

There exists great impetus for research into hydrocarbon fouling due to the large financial penalties incurred by fouling. The gains to be made by reducing fouling, even by low levels, are significant. The complex mechanisms involved and their dependency on key parameters such as velocity and surface temperature mean that fundamental research into fouling needs to be conducted in the laboratory where accurate control over these parameters can be maintained. However, the practical problem of fouling means that it also needs to be studied industrially. Research conducted in parallel in the laboratory and in industrial situations is required, as the results of fundamental laboratory fouling studies conducted need to be applied to industrial situations.

2.7.1 Refinery research

Refinery operation is dictated by market forces. Thus the isolation and the study of key parameters affecting fouling are not practical, due to the numerous operational changes which can take place over the lengths of time required for appreciable fouling to occur. Moreover, a number of additional problems may also need to be overcome (Crittenden, Kolaczkowski and Downey (1992)):

1. the accuracy of plant data;

2. the inability to control the plant conditions to suit the experimental conditions desired by the researcher;

3. the lack of sensing equipment at critical locations.

These difficulties may combine to result in large errors in the calculation of fouling resistances. For example, errors of 1 °C in temperature and 1% in the flow-rate may give rise to an error of 13% in the calculation of fouling resistance (Crittenden *et al* (1992)).

Refinery based research is more realistic in its appraisal of the problem of fouling because it assesses fouling in terms of exchanger configuration and operation in real situations. As such, it is an important element in enabling engineers and operators to understand fouling completely. However, in industrial situations the lack of control over the individual parameters that affect fouling rates and resistances does not permit the development of a model that can be universally applied to assist in developing effective mitigation strategies.

2.7.2 Laboratory Based Research

Heat exchangers in industry often take a long period of time, weeks or perhaps months, to achieve appreciable levels of fouling, during which frequent alterations in operating conditions can occur due to demand. Acceptable rates of fouling can be achieved in the laboratory through conducting trials at reduced flow-rates and by recycling test fluids, while at the same time maintaining temperatures, feedstocks and construction materials as would be encountered in industry. However, upon achieving results in an acceptable period of time in the laboratory (typically 100 hrs), deposits have been found to have a higher organic content compared with those formed using similar fluids, temperatures and velocities (Crittenden (1988b)).

Unlike studies on refineries, the fluid subjected to fouling experimentation in the laboratory may be recycled in order to reduce the amount of inventory required. On the

one hand, the use of single pass systems can incur safety and space penalties, most notably due to the large quantities of crude oil that would be required. On the other hand the recirculation of a test fluid can raise questions regarding the effects of possible depletion or accumulation of fouling precursors in the bulk fluid. Consequently, the results generated after a number of runs with a recycle fluid may be called in to question. Experimental work with crude oil has shown that recirculation of feedstocks has little, if any, effect on the chemical composition of the sample (Takemoto (1993)). However, degassing of the fluid must be expected as the experimental sequence progresses (Takemoto (1993)).

It is accepted that fouling is a complex problem and that it is dependent on the fluid and conditions encountered. The vast array of mechanisms involved complicates the application of laboratory results to an industrial situation (Schreier and Fryer (1995)). However, trends based on results generated in the laboratory are found to agree to a large extent with plant data and may be considered applicable (Crittenden (1988b)). The use of data from both industrial and laboratory sources therefore may be required in order to enable a practical solution and a reliable predictive model to be developed.

2.8 Synopsis

Hydrocarbon fouling of shell and tube heat exchanges has occurred since they were first used and its effects on exchanger effectiveness monitored. The reduction of profit margins in refining operations has resulted in greater focus on reducing, or eliminating fouling due to its significant cost. Consequently, a number of studies into the effects of the key fouling mechanisms and those process parameters influencing fouling rates have enjoyed significant support.

These studies have found that crude oil fouling comprises a combination of mechanisms, principally liquid phase autoxidation reactions and physical deposition.

Fouling rates have been found to exhibit an Arrhenius type dependency on surface temperature. However, whether the fouling rate is increased or decreased with changes in velocity is dependent on the relative balance of mass transfer and chemical kinetic effects. Alternate studies have found that the presence of compounds containing sulphur, oxygen and metallic ions can also have significant effects on fouling rates in hydrocarbon streams.

It is expected that any shell and tube heat exchanger in crude oil service will undergo fouling at some point in its operational lifetime. To compensate for this, an additional allowance can be made at the design stage, possibly resulting in higher overall costs to the purchaser. However, using an excessive fouling allowance can result in an over-sized exchanger that fouls due to areas of poor distribution. Consequently, the designer must take care when selecting an appropriate fouling allowance.

Alternate exchanger designs have also been considered, principally those which increase the shear removal of deposits by locally increasing velocity. Self cleaning systems can be fitted to existing shell and tube heat exchange equipment, to remove surface deposits as they accumulate on the tube surface.

For operational shell and tube heat exchangers fouling effects can be minimised by the addition of chemicals which inhibit the formation of fouling deposits, or their adhesion to the tube surface. The specific anti-foulant formulation used is dependent on the nature of the foulant and prevailing conditions.

The impetus to reduce fouling from hydrocarbons has extended to the development of technologies such as augmented tubes, such as Knudsen, internally ribbed, etc., treated tubes and mechanical devices such as HiTRAN® inserts. Whilst all of these devices have been shown to reduce fouling when compared with bare tubes, significant interest has been shown in the HiTRAN® insert. This is primarily due to its design flexibility,

ease of installation and relatively low cost in comparison with other options such as those mentioned above.

The installation of HiTRAN® inserts in conjunction with exchanger re-engineering has been found to mitigate fouling in shell and tube heat exchange equipment in existing in tar oil residue service. The modifications to the exchanger enabled extended runtimes and original pressure losses to be maintained. Laboratory based crude oil fouling research has shown HiTRAN® inserts to be effective in the reduction of fouling from crude oil.

The significant financial benefits arising from mitigating the effects of fouling have resulted in crude oil refining companies investing in extended fouling trials using HiTRAN® inserts. These have ranged from studying the fundamentals of the fouling mechanism in laboratory pilot scale experiments, to the study of fouling in practical situations on operational plant. The complexity of the fouling mechanism and its practical implications has resulted in the need for both types of research to be conducted and their results compared.

3. Experimental apparatus, procedures and materials

In order to achieve appreciable levels of fouling in industrial heat exchangers, long periods of time (typically several months) are often necessary. During these periods the demands of the market will result in frequent operational changes. Consequently, in industrial systems it is difficult to determine the influence on fouling of individual process parameters such as surface temperature, flow-rate and crude type.

With the aim of overcoming this limitation, a recycle flow rig was designed and commissioned at the University of Bath by Shalhi (1993). Shalhi evaluated the rig extensively, primarily using a heat transfer fluid. Takemoto (1993) then used the rig to investigate the fouling of a hydrocarbon fluid (Arabian Light and 10% waxy deposit).

The hydrocarbon fouling recycle flow rig comprises four main sections:

1. recycle flow loop;
2. test section(s);
3. pressure control system;
4. pressure relief system.

In this chapter a description of the hydrocarbon fouling test facility is provided together with full details of the modifications made as part of the study described in this thesis. For convenience, the main sections are described in the order given above. In addition, a summary of the test fluid used in this study is given. This includes the criteria used in the selection of the test fluid.

3.1 The hydrocarbon fouling recycle rig

As previously mentioned in Chapter 2, the known parameters affecting fouling are time, surface temperature, composition of the crude, pressure and vaporisation, flow-rate and insert presence and geometry.

The rig allows comparison of the rate of fouling in two parallel test sections. This enables the influence of independently adjustable variables such as surface temperature, flow-rate, insert presence and insert geometry to be investigated by altering one parameter being studied at a time between the two test sections.

The effect of time as a specific variable was not investigated. Furthermore, the composition of the crude was set at the beginning of the experimental series and was not a variable in this study.

As explained previously, fouling from hydrocarbons is most likely the product of liquid phase autoxidation reactions which, overall, follow an Arrhenius type rate dependency. Nucleation of the fluid on the heat transfer surface can affect the heat transfer coefficient. At constant heat flux this variation in heat transfer coefficient may alter the surface temperature, which in turn can dramatically affect the reaction rate and consequently the fouling rate.

Nucleation does not allow the scientific study of fouling rates as a function of one parameter (such as surface temperature, flow-rate and insert presence or geometry). Hence nucleation was suppressed and the effects of pressure and nucleation were therefore excluded from this study.

3.1.1 Recycle flow loop

A schematic of the recycle flow loop is provided in Figure 3.1. The main items in the loop are the hydrocarbon reservoir (0.105 m^3), a centrifugal pump (Worthington Simpson Ltd. 40/20 CMR 125) and a variable speed drive (Danfloss VLT 101). The liquid flow rates to the two parallel test sections are individually monitored with the use of KDG 9300 series flow meters (FI1 and FI2 for test sections 1 and 2 respectively).

The bulk of the test fluid is contained in the hydrocarbon reservoir. The fluid is continuously circulated around the recycle flow loop and through the test sections, using the hydrocarbon pump. The flow to each test section is controlled through a combination of valve position (VL1 or VL2 for test section 1 and 2 respectively) and pump speed.

The test fluid is heated to the required bulk fluid temperature by the 2 kW heating element located in the hydrocarbon reservoir, and by a bypass heater comprised of two 1 kW "K-Ring" heaters (Watlow Ltd.) situated in the test section bypass line.

Each test section is nominally identical and consists of a heated portion and individual instrumentation for the measurement of temperature and pressure drop. A test section is shown in Plate 3.1.

At the end of each fouling run the test sections are removed for inspection, deposit removal and cleaning. If inserts are used in an experimental run they are added prior to assembly and sealing.

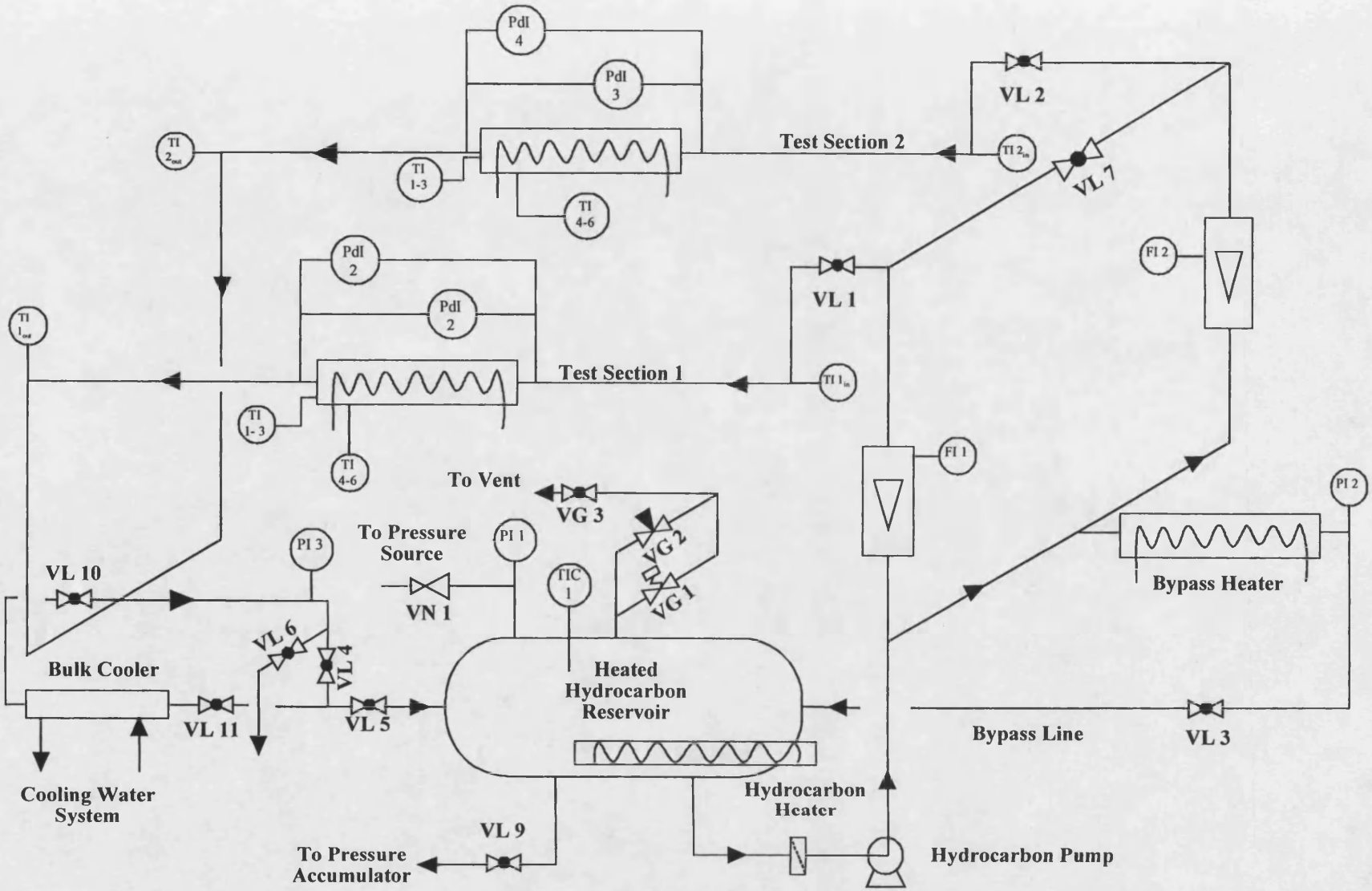

Figure 3.1 Schematic of the hydrocarbon flow loop

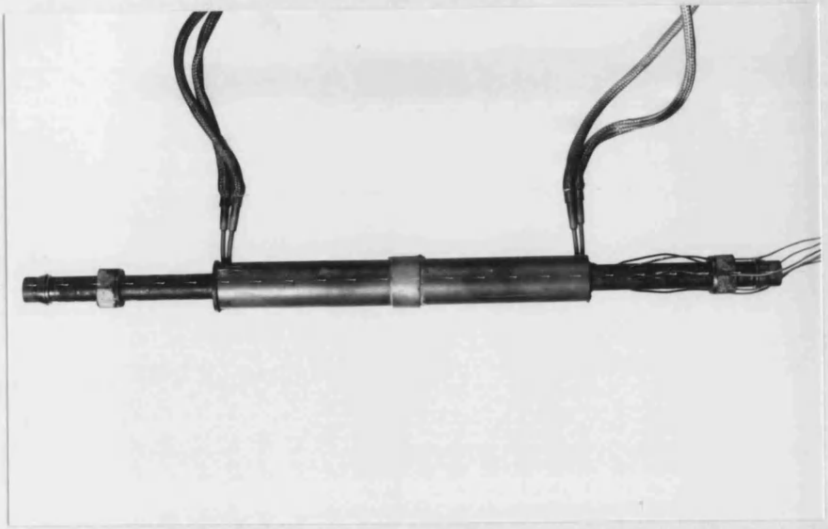

Plate 3.1 Test cell

3.1.2 Modifications to the recycle flow loop

As part of this project a number of modifications were made to the original test facility. These modifications were required in order to improve reliability, widen the operating range and reduce the turn-around time between runs. The modifications made to the rig are circled and highlighted by the solid lines in Figure 3.2. The modifications are now described.

3.1.2.1 Bulk Cooler

In order to improve the control of the bulk fluid temperature during experimental runs and to increase the rate of fluid cooling during the shutdown period, a cooler was added downstream of the test sections at the location shown in Figure 3.2. The cooler is a simple double pipe exchanger.

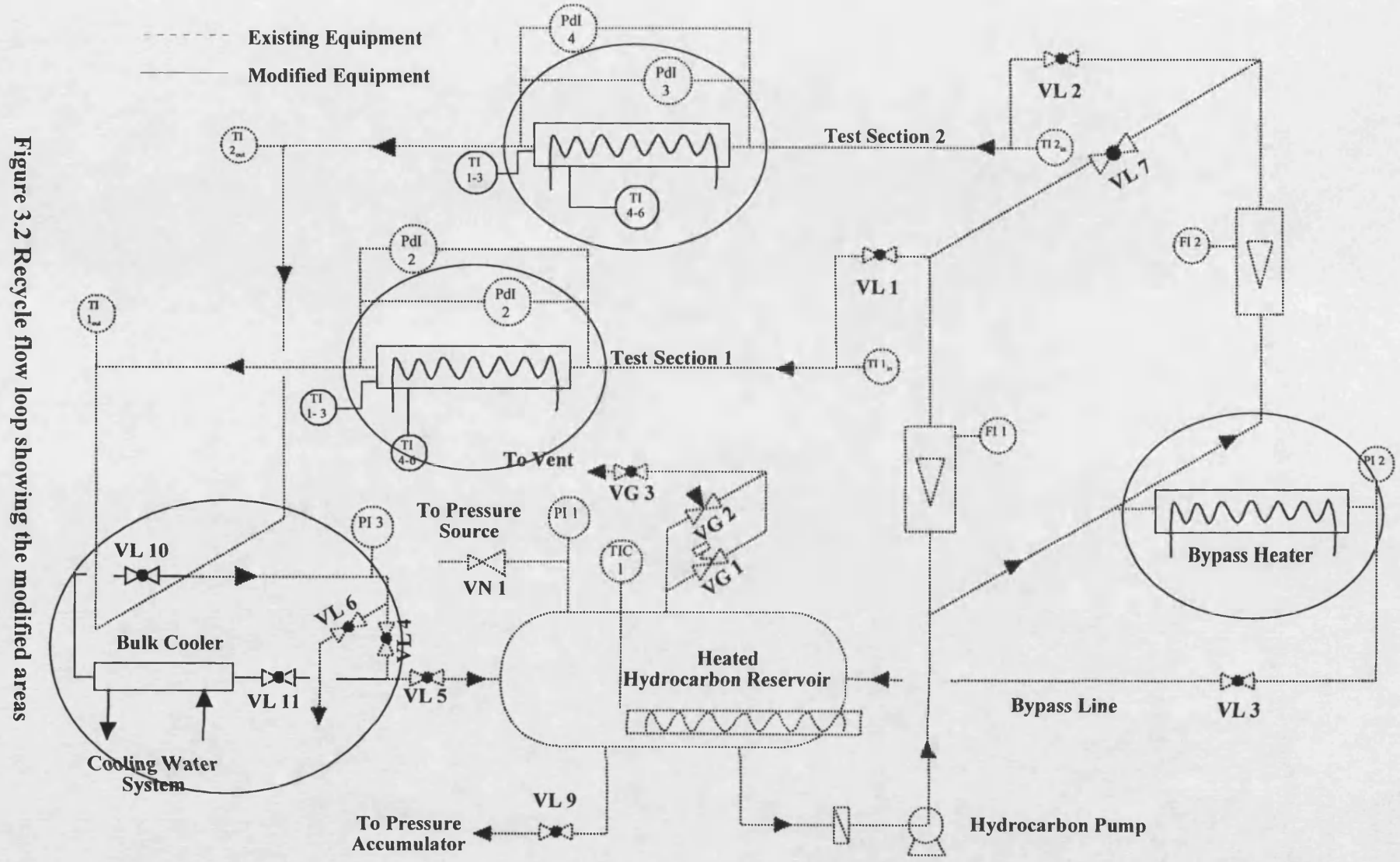

Figure 3.2 Recycle flow loop showing the modified areas

The internal tube has an outside diameter of 1" nominal (standard on the rig), while the annulus is formed using 2" nominal outside diameter tubing. The cooling water stubs were welded on to opposite ends of the outer tube and the annulus sealed using layered welds in order to form a watertight jacket around the inner tube.

The Department of Chemical Engineering's cooling water system was used as the source of the coolant in the annular space. The installation of the bulk cooler reduced the shut-down time of the test facility from 5 hrs to 2 hrs.

3.1.2.2 Bypass heater

In order to reduce the time required to heat the bulk fluid in the test rig and to minimise the use of the two test sections during the start-up phase, a heater was added to the bypass line at the location shown in Figure 3.2. The bypass heater was constructed from two 1 kW "K-Ring" heater units (Watlow Ltd.) and assembled in the same manner as the test sections. The design is described further in section 3.1.5.1.

3.1.3 Test sections

The test sections are constructed from standard tubing conforming to A179 specification. Each tube has a bore of 14.83 mm, an outer diameter of 19.05 mm and an overall length of 560 mm. A surface roughness measurement is provided in Appendix A.

Heat is provided by external electrical heaters, which are in good thermal contact with the outer surface of the test section tubing. The length of the heated section is 270 mm. Electrical power to the two test sections is independently controlled by Variac regulators and monitored by two multi-meters (Tabor Electronics Ltd. UDW 4501), one for each test section.

3.1.4 Modification to the test section design

The original design used by Takemoto (1993) utilised 10 individual cable heaters wound into a grooved steel collar that was sweated onto the test section tubing. The resulting heaters, however, were fragile and susceptible to damage.

The present study required repeated handling of the test sections for inspection, deposit removal and cleaning. This repeated handling increased the probability of breaking one or more of the cable heaters. Due to this high risk of damage, it became necessary to improve the design of the heater.

In addition, sweating the collar on to the test section tubing may not have been the best method of providing intimate contact between the two. The improved design also aimed to eliminate the potential problem of creating an additional resistance to heat transfer.

3.1.5 Revised Design

The design of each test section was revised to enable the operating range, reliability and robustness to be improved. The revised test section design was based on a modified "K-Ring" heater supplied by Watlow Ltd. A "K-Ring" heater is shown in Plate 3.2.

Initial trials utilising a prototype were conducted to ensure that the design was effective and reliable, and to identify possible construction problems.

3.1.5.1 The "K-Ring" heater

In the "K-Ring" heater, the heating elements are housed in a rigid tube. Brass forms the inner surface to which the elements are attached, while a stainless steel sheath protects them from the environment. Stainless steel is also used to re-enforce the heater / cable interface. All of these design features increase the robustness of the unit, thereby

allowing the repeated handling and dismantling of each fouling test section without damage.

The revised design was able to supply a maximum heat flux of 282 kW m^{-2}, which was an improvement in comparison with the 140 kW m^{-2} previously attainable by Takemoto. This increase in maximum attainable heat flux permitted a greater range of velocities to be studied for any given surface temperature in both bare tube and insert experiments.

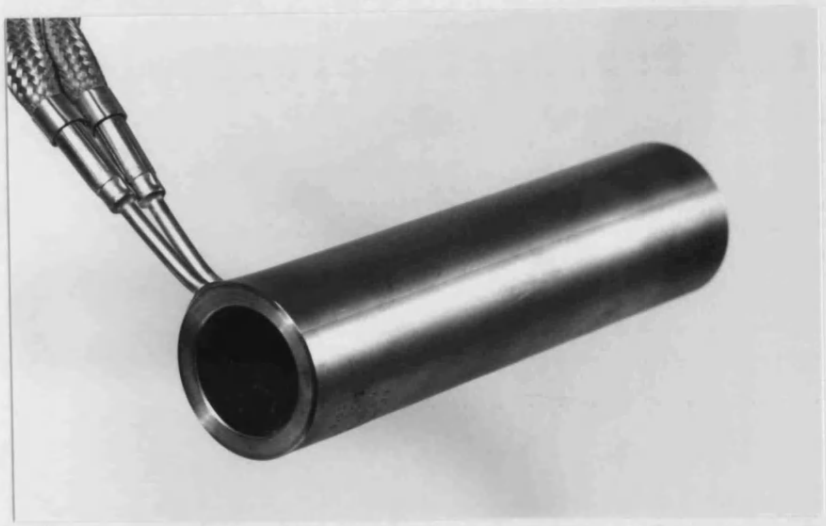

Plate 3.2 "K-Ring" heater

3.1.5.2 Test section construction

Initial trials were conducted to assess whether good thermal contact could be obtained by filling the annular void with a molten metal. It was proposed that the heaters would melt the metal *in situ*. This would have the added advantage of allowing the molten metal to flow through the entire annulus. The test piece consisted of a larger brass tube (with the same finish as the "K-Ring" heater) fitted around a sample of the test section tubing.

Metal or alloy wire was used in order to fill the void as it could be inserted directly into the annulus. The wire was wound around the test section tubing, which was then placed inside the larger tube with the annulus sealed with an end retaining cap.

Heat was then applied to melt the metal or alloy. Additional material was added as required to ensure that the void was filled completely. This trial was conducted in order to assess the possible effects occurring as the liquid metal cooled, solidified and contracted.

The results are shown in Plate 3.3. Visual inspection of these trials showed that excellent contact was achieved by filling the void in this manner. Zinc was chosen as the metal to be used as it has a high thermal conductivity (116 W m^{-1} K^{-1}). Furthermore, it has a melting point of 419 °C, which is significantly lower than the 760 °C maximum recommended operating temperature of the heater units. This allows the use of the heater to melt the zinc into the void, thus forming the best possible contact between heater and test section tubing.

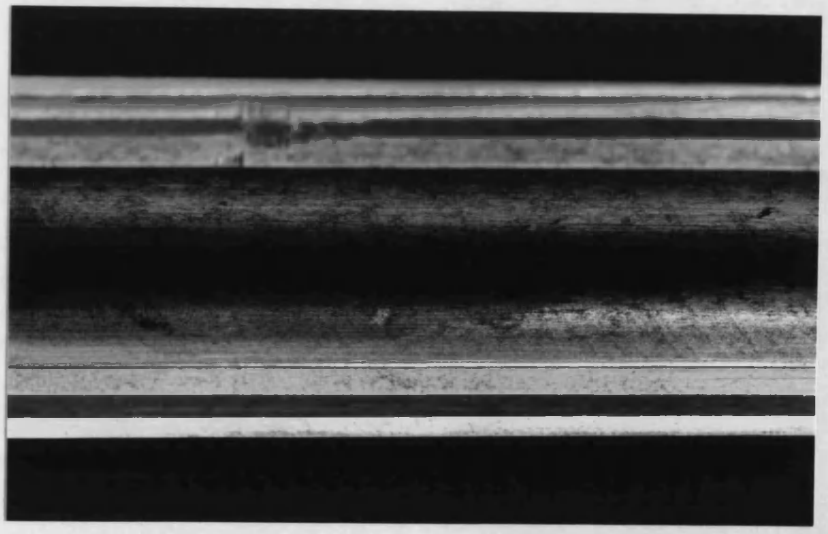

Plate 3.3 Results of trials on the effectiveness of a molten metal filled void

To allow the free flow of zinc in the annulus, the internal diameter of the heater tube was larger than the external diameter of the test section tubing. This reduced the possible effects of capillary action. The construction and evaluation of a prototype heater confirmed the suitability of the design to perform the task required.

To obtain a heated length of 270 mm, two "K-Ring" heaters were connected together using a jointing ring. The ring was constructed in such a way that its internal diameter was identical to the internal diameter of the heater units. As with the prototype, the end was sealed using an end-retaining cap and the void filled with the use of molten zinc. Schematics of the improved test sections are given in Figure 3.3 and Figure 3.4.

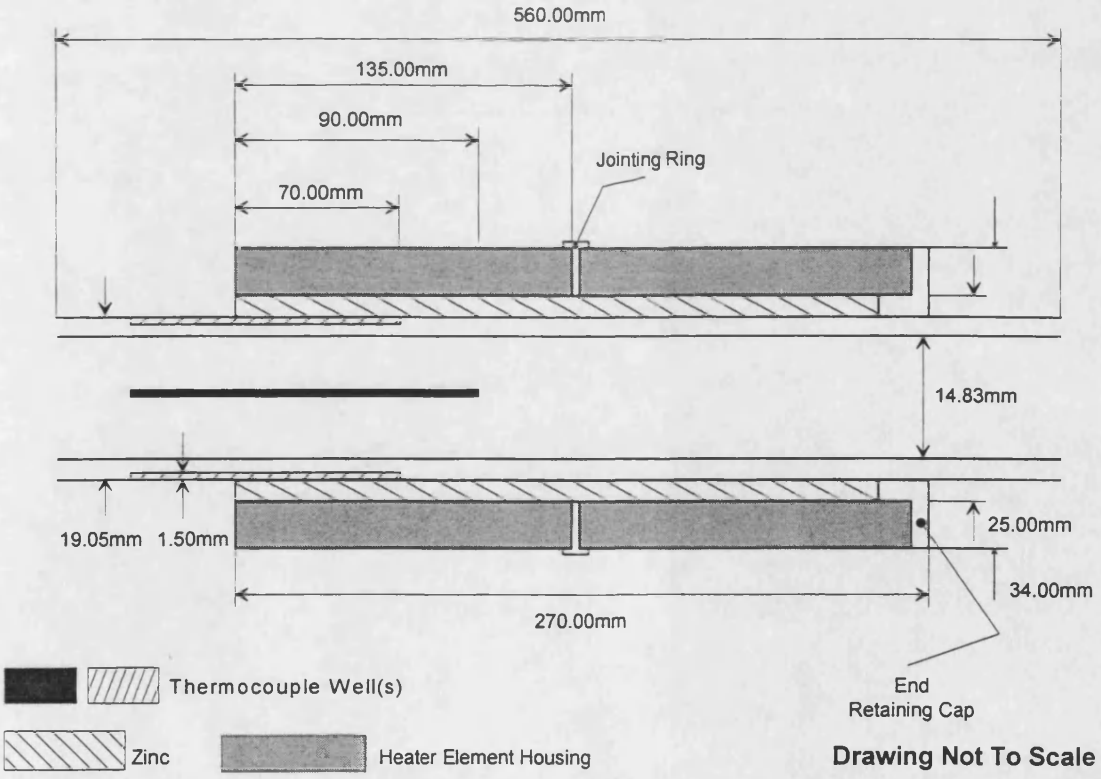

Figure 3.3 Heater attachment and longitudinal placement of thermocouples

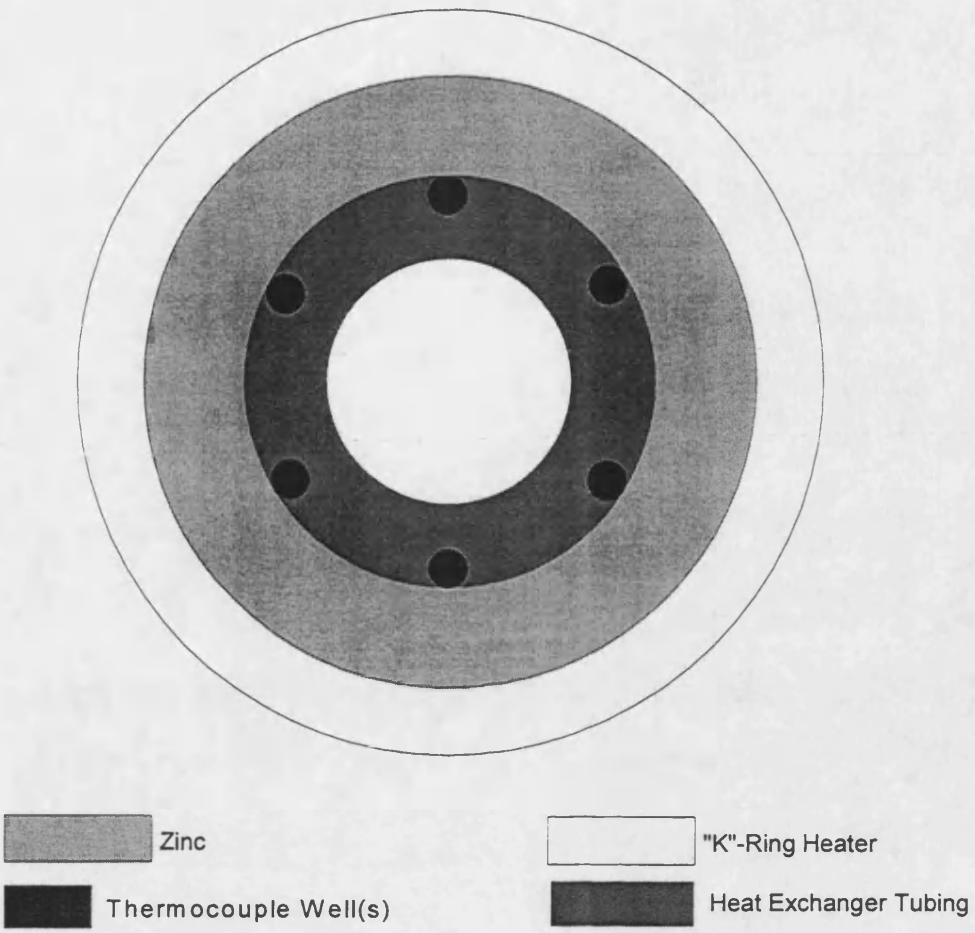

Figure 3.4 Heater attachment and circumferential placement of thermocouples

3.1.5.3 Thermocouple Location

To elucidate the variation of heat transfer and fouling rates, thermocouples were located in grooves on the heat exchanger tubing at two axial positions, 20 mm apart. To permit the study of circumferential variation in fouling rates each axial position had three equally spaced thermocouples at 120° separation. Schematics of the locations of the thermocouples are given in Figure 3.3 and Figure 3.4. A summary of the original test sections, as used by Takemoto (1993), and the revised design of the test sections is given in Table 3.1 for comparative purposes.

Table 3.1 Summary and comparison of the alternate designs for the test rig

	Previous	Current
Tube		
Internal Diameter	14.83 mm	14.83 mm
External Diameter	19.05mm	19.05 mm
Length	560 mm	560 mm
Material	A179 Carbon Steel	A179 Carbon Steel
Heater		
Type	Wound Cable	"K-Ring" Series
Heated Test Section Length	262 mm	270 mm (2 x 135 mm)
Max. Heat Flux	140 kW m^{-2}	282 kW m^{-2}
Attachment	Wound To Collar	Molten Metal Filled
Thermocouple		
Size	1.5 mm	1.5 mm
Number of Thermocouples	4	6
Circumferential Separation	23.45 mm	16.05 mm
Type	K	K
Miscellaneous		
Pressure Drop Tappings	580 mm	580 mm

3.1.5.4 Evaluating the design using the Wilson Plot method

The construction quality of the test section was quantified by utilising the Wilson Plot method. This determines the resistance to heat transfer (R_w) between the thermocouples and the inner surface of the tube wall.

The values of R_w, heat flux (q), the thermocouple temperature (T_T) and the inner surface temperature of the tube wall (T_S) are related by equation (3.1). This means that for a low

value of R_w (dependent on heat flux) the temperature difference between the thermocouple and the inner wall of the tube is also low.

$$T_s = T_T - R_w q \tag{3.1}$$

The use of the Wilson plot enables R_w to be derived graphically by plotting the reciprocal of the overall heat transfer coefficient (U_o^{-1}) against the variation in mean linear velocity to the power -0.8 ($u_m^{-0.8}$). For a constant heat flux, a straight-line relationship should be obtained, as illustrated by equation (3.2).

$$\frac{1}{U_o} = m\frac{1}{u_m^{0.8}} + R_w \tag{3.2}$$

In this plot the gradient *"m"* is a function of the fluid while the intercept is equal to R_w. A non-fouling heat transfer fluid (Santotherm SP 50) was used in order to eliminate any possible contribution of fouling to the overall resistance to heat transfer as the Wilson Plot experiments were conducted.

A development of the Wilson Plot method may be found in Appendix A. Wilson Plots for the average results from test sections 1 and 2 are given Figure 3.5.

As no heat is generated between the thermocouples and the inner surface of the tube wall, the small negative values calculated for the intercept may be considered to be due to experimental errors. Effectively, therefore, the thermal resistance between the thermocouples and the inner surface of the tube is virtually zero, as desired.

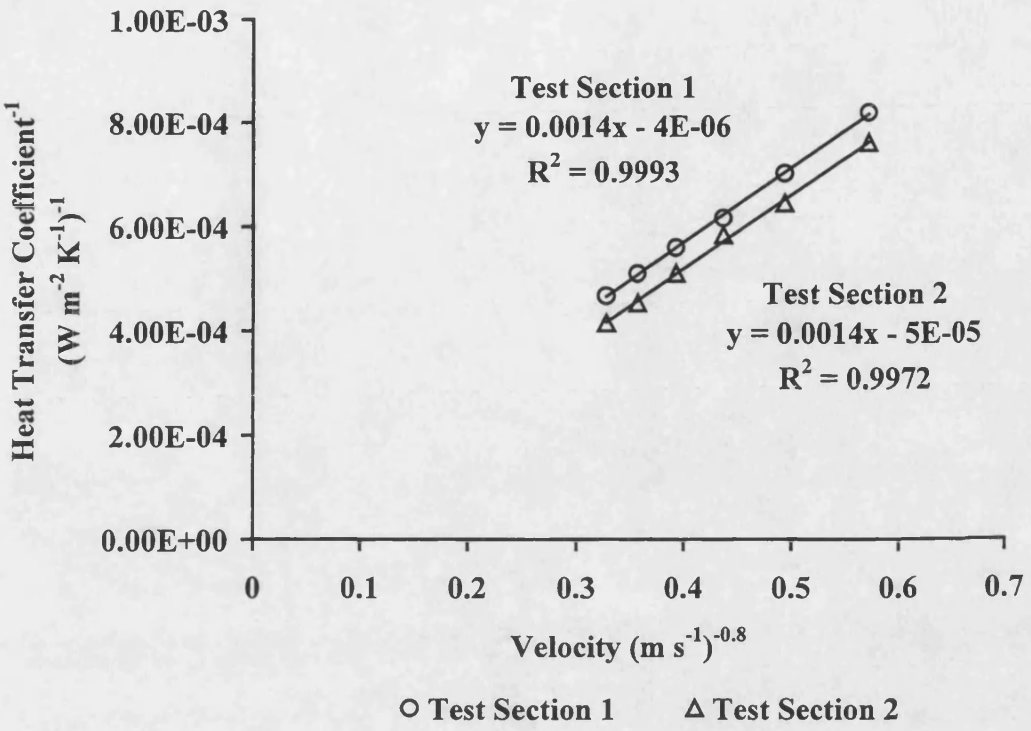

Figure 3.5 Wilson Plots of test sections 1 and 2

Both test sections exhibited excellent thermal contact with negligible resistance to heat transfer over the range of heat fluxes studied. The results are summarised in Table 3.2.

Table 3.2 Summary of wall resistance values for the test sections

	Thermocouple Number	R_W Value (m^2 K W^{-1})
Test Cell 1	1 - 3	0.0000
	4 - 6	0.0000
	Average	**0.0000**
Test Cell 2	1 - 3	0.0000
	4 - 6	0.0000
	Average	**0.0000**

At the range of heat fluxes studied, the negligible resistance to heat transfer results in a zero temperature difference between the thermocouples and the inner walls for both test sections (equation 3.1).

3.1.6 Length of insert

For this study the length of the insert was increased from 300 mm (used by Takemoto (1993)) to 560 mm. This minimised possible end effects arising from the flow entering the insert matrix. The increased length also increased the pressure drop, thereby reducing the proportion of error which was experienced in the pressure difference gauges at low pressure drops.

3.1.7 Pressure control system

As highlighted in section 2.7, fouling from hydrocarbons is most likely the product of liquid phase autoxidation reactions which exhibit an Arrhenius type dependency on temperature. Nucleation of fluid on a heat transfer surface may affect the local heat transfer coefficient. At constant heat flux any variation in heat transfer coefficient may alter the surface temperature considerably. This in turn may dramatically affect the reaction rate, consequently changing the fouling rate in the experiment.

Vaporisation in the test sections does not allow the study single phase fouling rates. Consequently, maintenance of a constant and adequate pressure is essential to prevent vaporisation during each experiment. A schematic of the pressure control system used to prevent nucleation during the normal operation, start-up and shut-down phases is given in Figure 3.6.

The system incorporates a movable piston which separates nitrogen gas from the crude oil. Free movement of the piston and the use of valves VG4 and VG5 allow the bulk pressure to remain constant as the test fluid expands or contracts, in accordance with bulk fluid temperature fluctuations. The operation of the pressure control system is described in section 3.2.3.

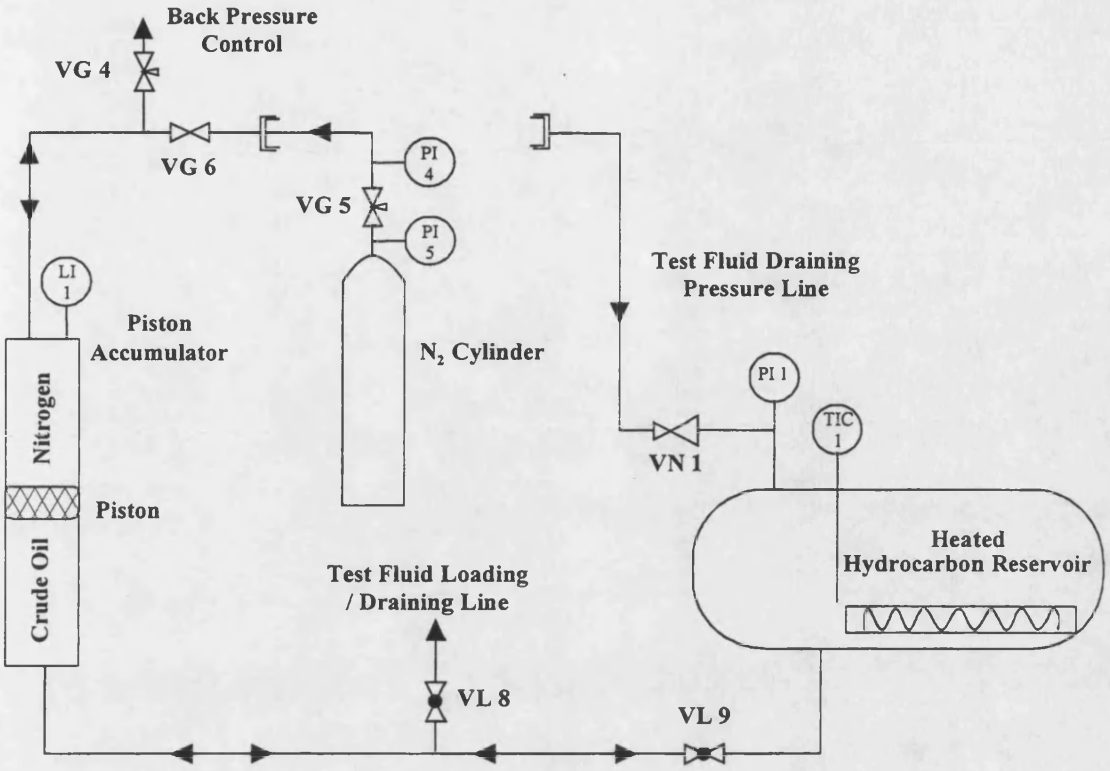

Figure 3.6 Schematic of pressure control system

3.1.8 Pressure relief system

The pressure relief system was located on the hydrocarbon reservoir and set at 20 bar. This is 25% above normal operating pressure. A schematic of the pressure relief system is given in Figure 3.7.

In the event of over-pressure, fluid is discharged *via* the pressure relief valve (VG1). The fluid is then cooled in the relief line cooler and any volatile organic vapours are condensed. The liquid and condensed vapours are then trapped in the condensate pot. The remaining vapours are discharged to the atmosphere outside the laboratory environment *via* a flame trap.

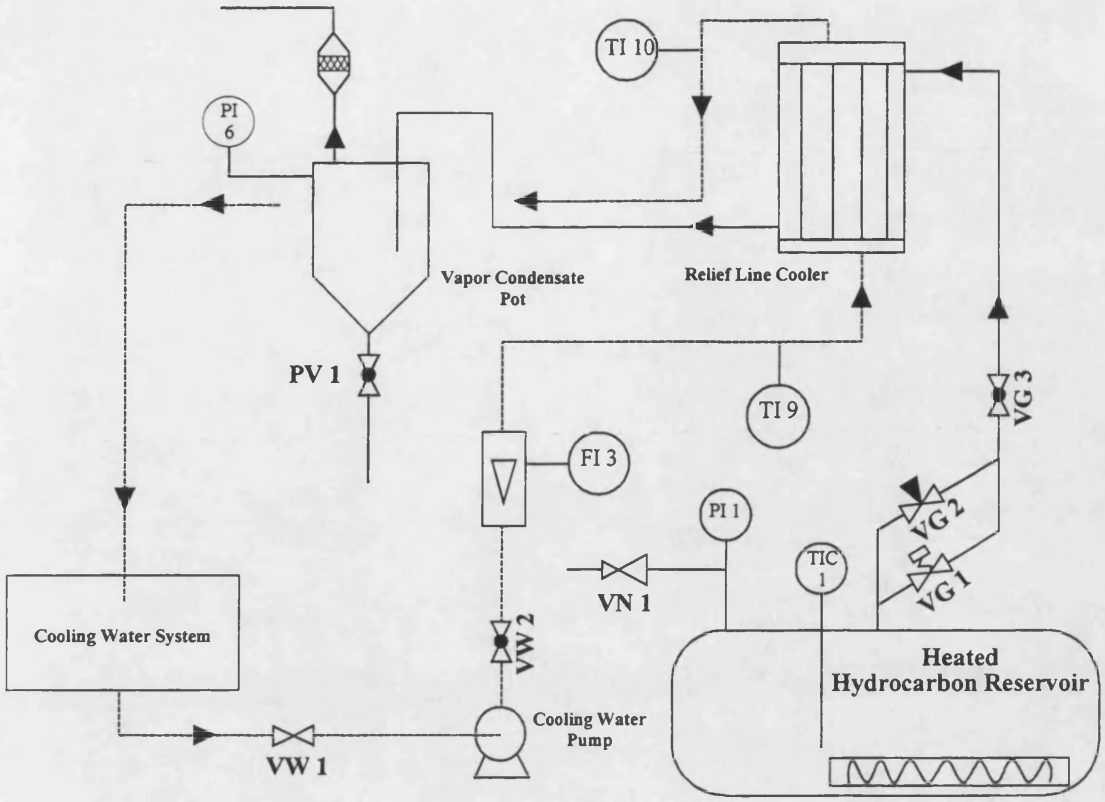

Figure 3.7 Flow schematic of the pressure relief system

3.2 General operating procedure

In this section a description of the basic operating procedure of the hydrocarbon fouling test facility is given. The key considerations are: control of the bulk fluid temperature, flow-rate, and system pressure.

3.2.1 Flow-rate control

The effect of flow-rate on fouling rates and resistances is well documented and has been discussed in section 2.7. The setting and accurate control of flow-rates are therefore essential to any study of hydrocarbon fouling.

Test section flow-rates were set and controlled by a combination of pump speed and valve position. The pump speed was controlled by the use of the Danfloss variable speed drive, while the flow through each test section was controlled by valve VL1 (test

section 1) or valve VL2 (test section 2). By controlling the flow-rate in this manner, possible variations in the pump output on heat transfer were reduced to a minimum.

3.2.2 Temperature control

At a given, constant heat flux, a variation in bulk temperature results in changes in the surface temperature (equation 3.1). This in turn may affect the rate of the fouling reaction. Therefore, accurate control of the bulk temperature of the fluid is essential to the investigation of changes in temperature due to fouling.

A constant bulk fluid temperature (normally 150 °C) was maintained in each experiment by the temperature controller (Severn Science Type 810). The temperature controller regulates power to the 2 kW reservoir heater.

To assist the reservoir heater during the warm-up phase and to reduce the warm-up time, a bypass heater was added as part of this study (see 3.1.2.2). The power to the bypass heater was set to prevent the element temperature from rising above 200 °C (in order to suppress fouling). During the final stages of the warm-up phase (~125 °C to 150 °C) the test section heaters were used to assist the reservoir and bypass heaters and to warm-up the test section heaters.

Because of heat loss to the surroundings, certain combinations of flow-rate and test section surface temperature could have resulted in a decrease in bulk fluid temperature which could not be compensated for by the bulk heater alone. In these situations the bypass heater was used, in addition to the reservoir heater, to control the fluid bulk temperature.

Adjustments were made to the power output of the bypass heater by controlling the electricity supply voltage using a transformer. The power to the bypass heater was determined by observing the bulk fluid temperature given by the temperature controller.

Certain combinations of flow-rate and test section surface temperature resulted in an increase in bulk fluid temperature, which could not be compensated for by the natural heat loss from the fluid to the atmosphere through the exposed pipe-work. In these cases the bulk cooler was used to control the bulk fluid temperature.

In order to maintain a constant bulk fluid temperature, a portion of the returning test fluid was removed from the main return line and cooled below the set point. The mixing of the cooled portion with the remainder of the bulk fluid resulted in no significant temperature deviation from the desired value.

The cooling could be increased if necessary by passing more test fluid through the bulk cooler. This movement of flow was achieved using a combination of valves VL4, VL10 and VL11.

3.2.3 Pressure control

The system pressure was set (normally at 15 bar) and maintained by regulator valve (VG5) at the nitrogen source. Pressure increases due to the expansion of the test fluid during heating or over-pressure were controlled by the let down valve (VG4). The combination of VG4 and VG5 facilitated avoidance of excessive pressure fluctuations around the set point during an experiment.

3.3 Test fluid

In previous research on the hydrocarbon recycle fouling rig, Takemoto (1993) completed experimental runs of approximately 100 hours duration using Arabian Light oil to which was added +10% waxy deposit. This meant that turn-around times were typically in the region of two weeks per run. Due to constraints on the experimentation schedule, a reduction in the run time was required.

Takemoto (1993) also reported the possible presence of nucleate boiling in some experimental runs. To eliminate nucleate boiling (and hence its effect on fouling) a relatively low bubble pressure (below 15 bar) was required when operating at surface temperatures close to the maximum operating surface temperature of the test sections (400 °C).

3.3.1 Selection

The rate of fouling on various crude oils was evaluated during trials using a Jet Fuel Thermal Oxidation Test (JFTOT) rig, conducted by Andrew Gilmore at BP Oil Ltd. They were all completed at an outlet temperature of 315 °C and a flow-rate of 250 ml h^{-1}. The crude oils evaluated in this manner were:

1. Forties;
2. Foinaven;
3. Maya;
4. Arabian Light (+10% waxy deposit).

The Arabian Light (+10% waxy deposit) was the test fluid used in the previous hydrocarbon fouling study by Takemoto (1993). It was added to the trial as a benchmark to indicate how other crude oils may respond in the recycle flow loop.

Foinaven did not foul in the JFTOT trials and was not acceptable for the current research.

The fouling tests on the JFTOT rig found that both Forties and Maya crudes fouled at approximately the same rate. However, after consultation with BP Oil Ltd, Maya was selected as the test fluid for the fouling project due to the low percentage of "light end"

(C_1 to C_5) components. The physical data of Maya crude are summarised in Appendix B.

3.3.2 Physical properties of the test fluid

The Maya crude was classified and its physical properties derived by the use of the American Petroleum Institute (API) Technical Data Book. Relevant sections from the API Technical Data Book and a Gas Chromatograph of the oil can be found in Appendix B.

The Watson K value of 11.72 was derived from the API 11A4.1 standard chart, given in Appendix B.

Specific heat capacity (C_P) was calculated from the bulk temperature of the fluid (T_b) using the API 7D2.2 method. Further details are provided in Appendix B. For fluid temperatures below 400 °C, specific heat capacity is given by the following equation:

$$C_P = 0.127 + 6.62 \times 10^{-3} T_b + 3.09 \times 10^{-6} T_b^2 \qquad (3.3)$$

Thermal conductivity (k) was calculated from T_b using API 12A3.1 (provided in Appendix B). For undefined hydrocarbon mixtures up to 34.5 bar, thermal conductivity is given by:

$$k = 0.1337 - \left(1.420 \times 10^{-4}\right) T_b \qquad (3.4)$$

Using equation 3.4, average errors of 10% can be expected.

The bulk density of the crude oil (ρ) was predicted using T_b *via* equation (3.5), derived from a least squares fit of assay data obtained from BP Oil Ltd. The plot of this data is given in Appendix B. Film fluid densities were calculated by substituting T_f instead of T_b.

$$\rho = 934.28 - 0.567T_b \tag{3.5}$$

The kinematic viscosity of the crude oil (ν) is predicted using T_b *via* equation (3.6), derived from a least squares fit of assay data obtained from BP Oil Ltd. The plot of this data is given in Appendix B.

$$\upsilon = 365.37e^{(-0.0368T_b)} \tag{3.6}$$

The dynamic viscosity (μ) may be calculated using equation (3.7):

$$\upsilon = \frac{\mu}{\rho} \times 10^6 \tag{3.7}$$

3.4 Synopsis

As part of this study a number of modifications were made to the hydrocarbon fouling rig. These modifications are described in greater detail in the text, but can be summarised by dividing them into two categories:

1. modifications made to the fouling rig generally;

2. modifications made to the test section in particular.

To increase the control of the experimental conditions a bulk cooler and bypass heater were added to the rig flow circuit. The bulk cooler was added in order to control bulk fluid temperature and increase the rate of fluid cooling during the shut down period. The bypass heater was added to reduce the length of time required to heat the bulk fluid and to minimise the use of the test section heaters during the warm-up period.

The test sections were modified as part of this study in order to improve operating range and reliability. Heat was supplied to the test sections using cylindrical Watlow K-Ring heaters surrounding the test section tubing. The inner diameter of the K-Ring heater was

larger in diameter than that of the outer surface of the tubing. A filler material was used to transfer heat from the heaters to the test section tubing. Zinc was used to fill the space created by the difference in the respective diameters, in order to provide good thermal contact. In addition to the modifications made to the heaters, the thermocouples were located in grooves 1.5 mm deep on the tube surface. It was found that the improved heating method and thermocouple placement resulted in negligible difference between the measured thermocouple temperature and the predicted inner surface temperature, using equation (3.1).

In order to reduce the run times from 100 hrs, a crude oil that exhibited a high rate of fouling was desirable. Preliminary trials using a JFTOT rig were completed and the results compared against a benchmark of Arabian Light plus 10% waxy sludge. The Arabian light (+10% waxy sludge) was used in the previous trials at the University of Bath (Takemoto (1993)). A number of crude oils were compared to the benchmark. Maya crude was selected because of its relatively high fouling rate. Following selection of the crude oil the physical properties of the crude were also derived.

4. Experimental results

This chapter presents the results of the fouling experiments conducted with Maya crude oil using either bare tubes or tubes containing HiTRAN® inserts. The various equations used to reduce the experimental data are also presented in this chapter. The surface temperatures and velocities used in this study were typical of the range of tube wall temperatures and velocities normally found in heat exchange equipment in crude oil heat exchangers, namely 0.5 m s^{-1} to 4.0 m s^{-1} and 250°C to 280°C (Coulson, Richardson and Sinnott (1993)). For each experiment, two graphs were produced; one showing the variation in U_O and the other the variation in fouling resistance, both against elapsed time. In total 65 runs were completed representing a sizeable volume of data. Therefore, only a summary of the data is presented in the following text. The raw experimental data with analysis is stored on six "3½" floppy discs. The discs may be found in disc holders at the back of this thesis.

4.1 Data analysis

4.1.1 Equations

This section presents the equations used to assess the experimental data obtained from the test runs. Calculation of the overall heat transfer coefficient (U_O) was based on the electrical power to the test section (Q), the theoretical efficiency of the heater (η), the heat transfer area at the separation between geometrically opposed thermocouples (A_T) and the temperature difference (ΔT), as described by equation (4.1):

$$U_O = \frac{Q\eta}{A_T \Delta T} \tag{4.1}$$

The heat flux (q) may be used to replace Q, η and A_T, and the temperature difference (ΔT) is that between the wall (T_w) and the bulk fluid (T_b), as described by equation (4.2):

$$U_O = \frac{q}{(T_w - T_b)} \tag{4.2}$$

Shalhi (1993) found η primarily to be a function of external surface temperature, the area of the outermost layer of insulation, and the ambient conditions. Following the results of his work η was calculated to be 98%. The dimensions of the insulation and external surface temperature in this study were found to be comparable with those noted in the previous study (Shalhi (1993)). Therefore a comparable theoretical heater efficiency of 98% was also assumed.

The bulk temperature (T_b) at any point along the length of the tube was calculated by assuming nominally constant physical properties between the inlet and outlet bulk fluid temperatures (T_{bi} and T_{bo}, respectively). A linear temperature gradient between the inlet and outlet locations was therefore assumed. Significant heat input was only applied over the length of the heaters within the test section (270 mm). The linear temperature gradient allows the bulk temperature at the thermocouple locations to be estimated by the displacement length of the thermocouple in the test section (L_T = 70 mm or 90 mm) as a fraction of the overall test section length (L_S = 270 mm). This is illustrated by equation (4.3):

$$T_b = T_{bi} + \frac{L_S - L_T}{L_S}(T_{bo} - T_{bi}) \tag{4.3}$$

The fouling resistance of the deposit at any time "*t*" ($R_{f(t)}$) may be calculated from the difference in U_O at the beginning of the experiment ($U_{O(0)}$) and at the chosen time "*t*" ($U_{O(t)}$), as described by equation (4.4):

$$R_{f(t)} = \frac{1}{U_{O(t)}} - \frac{1}{U_{O(0)}} \tag{4.4}$$

It is possible to use this equation because the heat flux was maintained constant. In many of the experiments the fouling resistance increased linearly throughout the duration of the run. In these circumstances the fouling rate was constant and equal to the initial value. However, in some runs the fouling rate reduced as the experiment progressed. In these situations the initial fouling rate was taken to be the fouling rate up to the point at which the fouling rate began to vary noticeably.

At time *t=0*, when the tube is clean and free of surface deposits, the internal heat transfer coefficient (h_i) was calculated from U_O and R_w. Differences in area between that at the thermocouple diameter (d_T) and that at internal diameter (d_i), where U_O and h_i are measured respectively (see Figure 3.3), was allowed for, by using equation (4.5):

$$\frac{1}{h_i} = \left(\frac{1}{U_O} - R_W\right)\frac{d_i}{d_T} \tag{4.5}$$

Significant resistance to heat transfer may be generated by the tube wall material and by poor contact between the heat source and the outer surface of the tube wall. This can result in differences in temperature measured by the thermocouple (T_T) and the true temperature of the inner wall (T_w). The difference between the two temperatures is a function of heat flux (q) and the resistance to heat transfer (R_w) calculated by the Wilson plot method, *via* equation (3.1):

$$T_w = T_T - R_w q \tag{3.1}$$

However, the thermocouples were located in grooves on the outside surface of the heat exchanger tubing. This was found to result in a negligible wall resistance (R_w) throughout the range of heat fluxes used in the Wilson plot. Therefore, the temperature difference between the thermocouple reading and the wall over the range of heat fluxes studied was considered to be negligible (as calculated by equation (3.1)).

The hydrodynamic performance of the insert was assessed by the use of the friction factor (j_f). The friction factor was calculated from the pressure drop (ΔP), the distance between pressure drop tappings (L_P), the tube internal diameter (d_i), the mean fluid velocity (u_m), the density of the fluid (ρ) and a viscosity correction factor based upon the viscosity at the temperatures in the bulk and at the tube wall (μ and μ_w respectively):

$$j_f = \frac{\Delta P d_i}{4 L \rho_f u_m^2 \left(\frac{\mu}{\mu_w}\right)^{-m}} \tag{4.6}$$

The viscosity correction factor is dependent on the Reynolds number of the stream; the power term (m) is 0.25 at Re < 2,100 and 0.14 at Re > 2,100 (Coulson, Richardson and Sinnott (1993)).

Comparison of the thermal performance between the inserts and the bare tubes was possible using the heat transfer factor (j_h). The heat transfer factor is related to the heat transfer coefficient (h), the density of the fluid (ρ), the mean fluid velocity (u_m), and the specific heat of the fluid (C_P) by the Stanton number (St) (equation (4.7)), and the diameter of the tube (d_i) and the thermal conductivity of the fluid (k) by the Nusselt number (Nu) (equation (4.8)):

$$St = \frac{h_i}{\rho u_m C_P} \tag{4.7}$$

$$Nu = \frac{h_i d_i}{k} \tag{4.8}$$

The relationship between heat transfer factor, Stanton number and Nusselt number is defined by equation (4.9):

$$j_h = St.Nu^{0.67}\left(\frac{\mu}{\mu_w}\right)^{-z} \tag{4.9}$$

A viscosity correction factor based upon the viscosity in the bulk and the wall (μ and μ_w respectively) is also applied, the power term (z) being 0.14 in all cases (Coulson, Richardson and Sinnott (1993)).

4.2 *Experiments with bare tubes*

As described previously, fouling of heat exchange equipment in hydrocarbon systems is due to the formation of insoluble products accumulating on the heat transfer surface in sufficient quantity to affect the exchanger performance. The type of fluid and conditions encountered in the exchanger are the key criteria in determining whether the fouling rate is either mass transfer or chemical reaction controlled. By studying the trends and effects of the key process parameters on fouling rates in bare tubes, a model can be developed to predict initial fouling rates. Modelling bare tube experimental data enables a better understanding of the relative balance of mass transfer and kinetic effects that control the fouling rate in hydrocarbon systems. Understanding the controlling factors in the overall fouling process is an essential prerequisite for enabling the prediction of the effect that placing an insert into a hydrocarbon stream will have. This section therefore presents the results of the experiments conducted with bare tubes in the hydrocarbon fouling rig.

4.2.1 Experimental conditions

The temperatures and velocities used in this study were comparable with those used in heat exchange equipment in crude preheat trains. The experimental parameters studied are summarised in Table 4.1. A tick in the table indicates that an experiment was carried out for the given combination of initial (clean) inside surface temperature and linear velocity.

Table 4.1 Summary of bare tube experimental parameters

Velocity	Reynolds	Temperature (°C)			
($m\ s^{-1}$)	Number	250	265	270	280
0.5	3,600	✓	×	×	✓
0.8	5,800	✓	×	×	✓
1.0	7,300	✓	✓	✓	✓
1.5	11,000	✓	✓	✓	✓
2.0	14,500	✓	✓	✓	✓
3.0	21,800	✓	✓	✓	✓
3.6	26,200	✓	✓	✓	✓
4.0	29,000	✓	✓	✓	✓

The velocity range used in the study corresponds to Reynolds numbers associated with the transition and the turbulent flow regimes. The ranges of experimental variables used compares well with the ranges of velocities and Reynolds numbers found in industrial shell and tube heat exchange equipment (Coulson, Richardson and Sinnott (1991)). The run schedule for the bare tube experiments is given by Table 4.2 to Table 4.5:

Table 4.2 Summary of bare tube experimentation conditions - 1

Run	Test Section	Velocity ($m\ s^{-1}$)	Initial Surface Temperature (°C)
1	1	2.0	250
	2	2.0	250
2	1	2.0	250
	2	2.0	250
3	1	2.0	250
	2	2.0	250
4	1	1.0	250
	2	2.0	250
5	1	2.0	250
	2	0.5	250
6	1	0.5	250
	2	2.0	250
7	1	2.0	250
	2	0.5	250
8	1	0.8	250
	2	2.0	250
9	1	3.0	250
	2	2.0	250
10	1	1.0	250
	2	2.0	250
11	1	2.0	300
	2	3.0	300

Note: Bulk temperature: 150 °C

Pressure: 15 bar

Table 4.3 Summary of bare tube experimentation conditions - 2

Run	Test Section	Velocity ($m\ s^{-1}$)	Initial Surface Temperature
12	1	2.0	200
	2	0.4	200
13	1	2.0	225
	2	0.5	225
14	1	3.0	280
	2	2.0	280
15	1	0.5	230
	2	2.0	230
16	1	1.0	280
	2	2.0	280
17	1	1.5	280
	2	2.0	280
18	1	3.6	280
	2	2.0	280
19	1	0.8	280
	2	2.0	280
20	1	2.0	280
	2	1.5	280
21	1	1.0	265
	2	2.0	265
22	1	3.0	265
	2	2.0	265

Note: Bulk temperature: 150 °C

Pressure: 15 bar

Table 4.4 Summary of bare tube experimentation conditions - 3

Run	Test Section	Velocity ($m\ s^{-1}$)	Initial Surface Temperature
23	1	1.5	265
	2	2.0	265
24	1	2.0	265
	2	1.0	265
25	1	1.5	265
	2	2.0	265
26	1	3.6	280
	2	2.0	280
27	1	2.0	280
	2	2.0	280
28	1	3.0	270
	2	2.0	270
29	1	1.0	270
	2	2.0	270
30	1	1.5	270
	2	2.0	270
31	1	3.0	225
	2	2.0	225
32	1	3.6	250
	2	2.0	250
33	1	3.6	265
	2	2.0	265

Note: Bulk temperature: 150 °C

Pressure: 15 bar

Table 4.5 Summary of bare tube experimentation conditions - 4

Run	Test Section	Velocity ($m\ s^{-1}$)	Initial Surface Temperature
34	1	3.6	270
	2	2.0	270
62	1	4.0	280
	2	-	-
64	1	4.0	265
	2	-	-
65	1	4.0	250
	2	-	-

Note: Bulk temperature: 150 °C

Pressure: 15 bar

4.2.2 Preliminary runs

Preliminary runs were conducted to verify the suitability of the new design of test section for comparative fouling experimentation. Runs 1, 2 and 3 were conducted under nominally identical initial conditions of clean surface temperature (250 °C), bulk temperature (150 °C), fluid velocity (2.0 $m\ s^{-1}$) and system pressure (15 bar). The bulk temperature was selected based on the design specification of the rig, whilst the surface temperature for the initial set of fouling experiments was chosen to be 250 °C, as this was the maximum surface temperature achievable in previous studies using the recycle flow loop (Shalhi (1993) and Takemoto (1993)). Inserts were not in place in either test section for any of the three preliminary runs.

The results for runs 1, 2 and 3 can be found in Figure 4.1. The fouling resistance in run 1 is seen to increase and tend towards an asymptote, whereas in runs 2 and 3 the fouling

resistance increased linearly throughout the entire duration of the experiment. In each of the three runs the agreement between the two test sections was excellent. The results from runs 2 and 3 were also comparable and both exhibited linear fouling characteristics. The poor comparison between run 1 and runs 2 and 3 is attributed (with evidence) to tube conditioning. All runs showed good reproducibility between the test sections in the same run, indicating that the parallel flow rig is a good tool for comparative study.

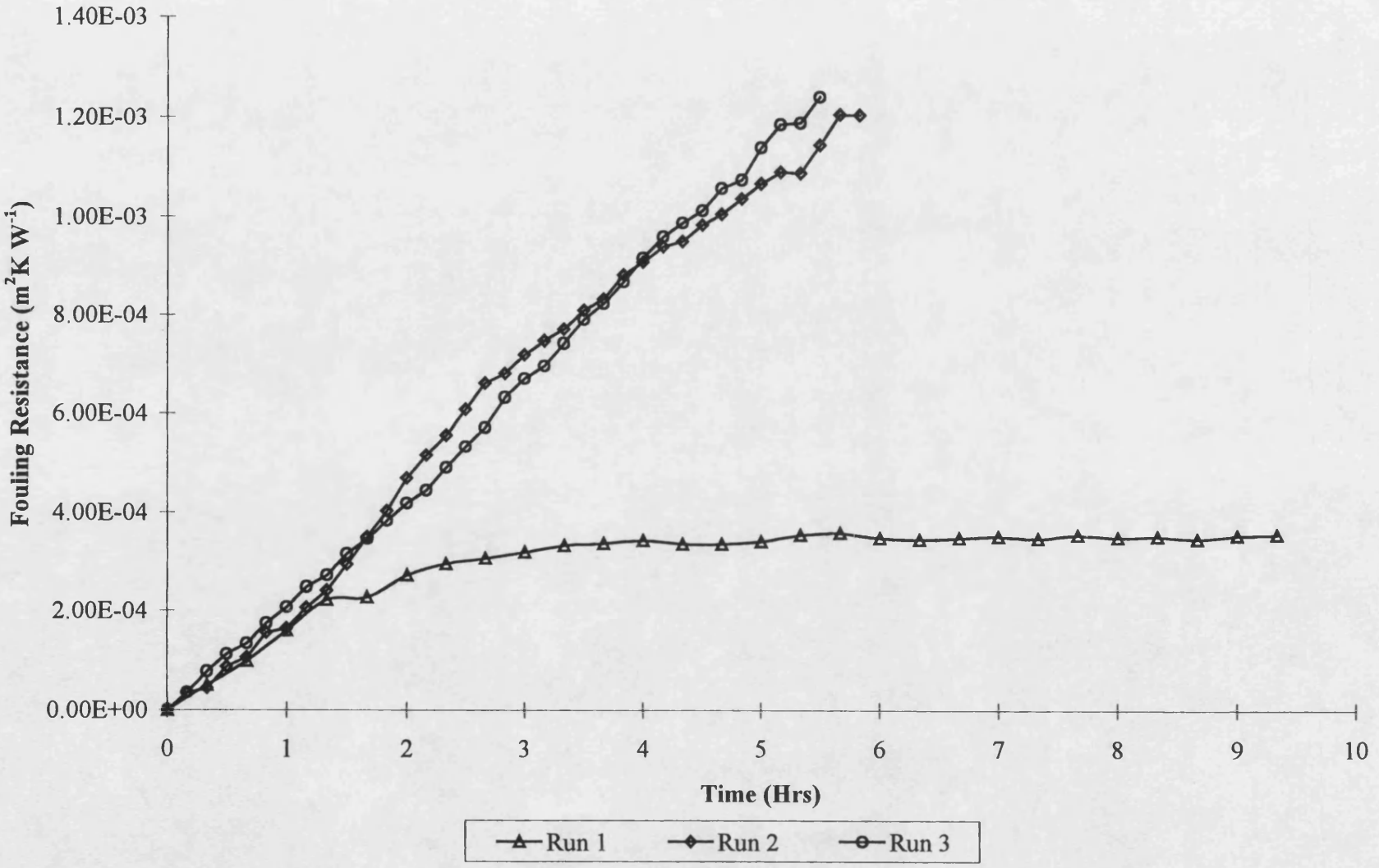

Figure 4.1 Graph showing the results of Runs 1, 2 and 3

4.2.3 The effect of velocity at 250 °C

Runs 4 to 10 together with 32 and 65 were conducted under nominally identical initial conditions, namely a clean surface temperature of 250 °C, a bulk temperature of 150 °C and a system pressure of 15 bar. The experimental conditions are summarised in Table 4.6.

Table 4.6 Summary of experimentation conditions at 250 °C

Run	Test Section	Velocity ($m\ s^{-1}$)
4	1	1.0
	2	2.0
5	1	2.0
	2	0.5
6	1	0.5
	2	2.0
7	1	2.0
	2	1.5
8	1	0.8
	2	2.0
9	1	3.0
	2	2.0
10	1	1.0
	2	2.0
32	1	3.6
	2	2.0
65	1	4.0
	2	-

In runs 4 to 10 and 32, the fluid velocity in one of the test sections was varied from run to run, whilst in the other test section a 2.0 m s^{-1} benchmark velocity was maintained. A benchmark velocity was not used in run 65 due to a previous heater failure.

It was found that the fouling resistance increased linearly with time in all runs. The fouling rate was therefore calculated using data collected over the entire duration of the runs. It was noted that there was a difference in the fouling rate from run to run in the test section operated with the 2.0 m s^{-1} benchmark velocity. Therefore, it was considered that the results using different velocities are better compared on a normalised basis; i.e. the fouling rate for each velocity is divided by the fouling rate at the 2.0 m s^{-1} benchmark velocity in the same run. The average and normalised fouling rates against velocity are summarised in Table 4.7 and shown in Figure 4.2 and Figure 4.3 respectively.

Table 4.7 Results of bare tube fouling runs at 250 °C

	Velocity		Fouling Rate	
Run	**Linear (ms^{-1})**	**Normalised**	**Average x 10^4 (m^2 K W^{-1} h^{-1})**	**Average Normalised**
5 & 6	0.4	0.20	0.563	0.37
8	0.8	0.40	1.740	0.63
4 & 10	1.0	0.50	2.020	0.89
7	1.5	0.75	2.060	0.99
Various	2.0	1.00	2.150	1.00
9	3.0	1.50	1.590	0.81
33	3.6	1.80	1.180	0.55
65	4.0	2.00	0.19	0.09

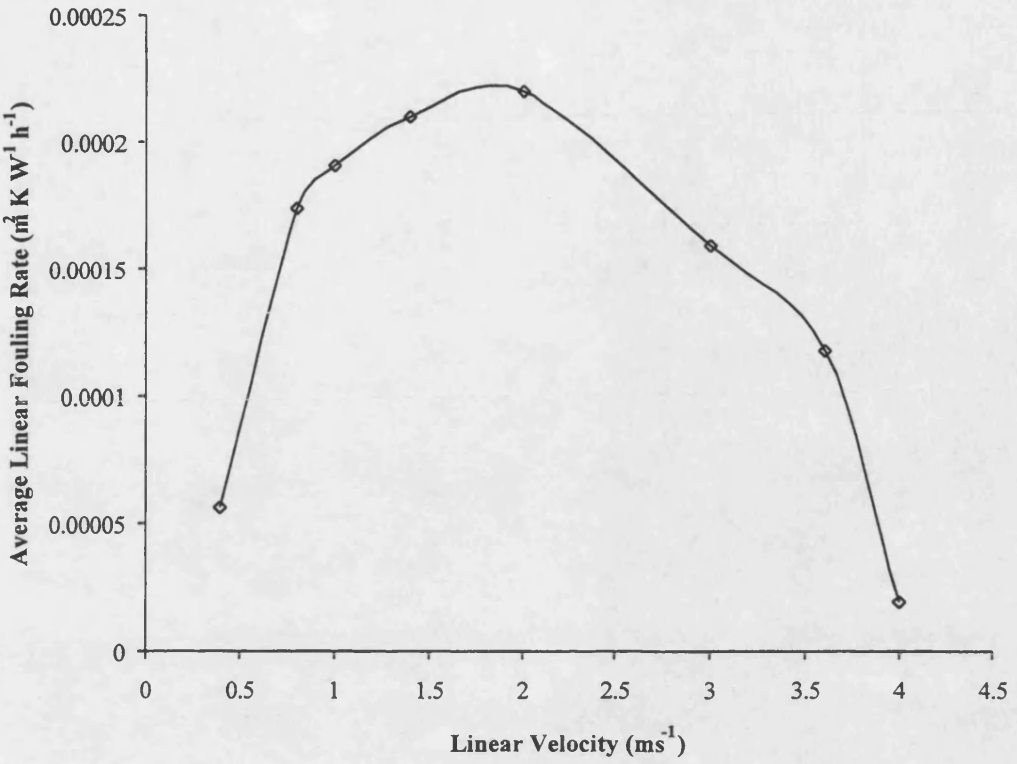

Figure 4.2 Average fouling rate against velocity at 250 °C

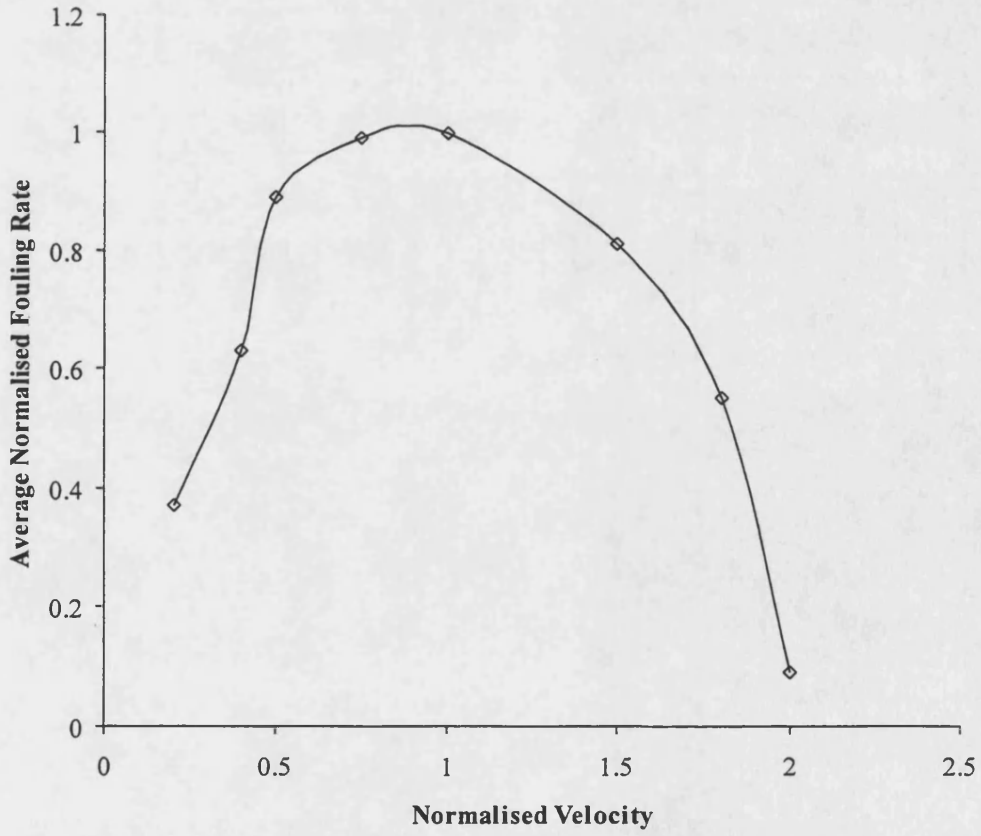

Figure 4.3 Normalised fouling rate against normalised velocity at 250 °C

The results show that for an initial clean surface temperature of 250 °C the normalised fouling rate increases with increasing velocity until approximately 2.0 m s^{-1}, beyond which the fouling rate then decreases with velocity. At this surface temperature the fouling rate is possibly being controlled by the rate of mass transfer up to approximately 2.0 m s^{-1}. At velocities greater than 2.0 m s^{-1}, the fouling rate is possibly being controlled by the kinetics of the fouling reactions. Encouragingly, the results for the average and normalised fouling rates (Figure 4.2 and Figure 4.3) show the same general trends and therefore offer good comparability.

4.2.4 The effect of velocity at 265 °C

Runs 21 to 25 together with 33 and 64 were conducted under nominally identical initial conditions, namely a clean surface temperature of 250 °C, a bulk temperature of 150 °C and a system pressure of 15 bar. The experimental conditions are summarised in Table 4.8. In runs 21 to 25 and 33 the fluid velocity in one of the test sections was varied from run to run, whilst in the other test section the 2.0 m s^{-1} benchmark velocity was maintained. A benchmark velocity was not used in run 64 due to a previous heater failure.

It was found that the fouling resistance increased linearly with time in all the cases studied. Therefore the fouling rate was calculated from data obtained over the entire duration of the runs. Again, it was noted that there was a difference in fouling rate from run to run at the 2.0 m s^{-1} benchmark velocity and so the data were normalised again as described previously. The average and normalised fouling rates against velocity are summarised in Table 4.9 and shown in Figure 4.4 and Figure 4.5 respectively.

Table 4.8 Summary of experimentation conditions at 265 °C

Run	Test Section	Velocity ($m\ s^{-1}$)
21	1	1.0
	2	2.0
22	1	3.0
	2	2.0
23	1	1.5
	2	2.0
24	1	2.0
	2	1.0
25	1	1.5
	2	2.0
33	1	3.6
	2	2.0
64	1	4.0
	2	-

Table 4.9 Results of bare tube fouling runs at 265 °C

Run	Velocity		Fouling Rate	
	Linear (ms^{-1})	Normalised	Average x 10^4 (m^2 K W^{-1} h^{-1})	Average Normalised
21 & 24	1.0	0.50	2.00	0.82
23 & 25	1.5	0.75	2.23	0.92
Various	2.0	1.00	2.42	1.00
22	3.0	1.50	3.14	1.04
33	3.6	1.80	2.71	0.90
64	4.0	2.00	0.51	0.21

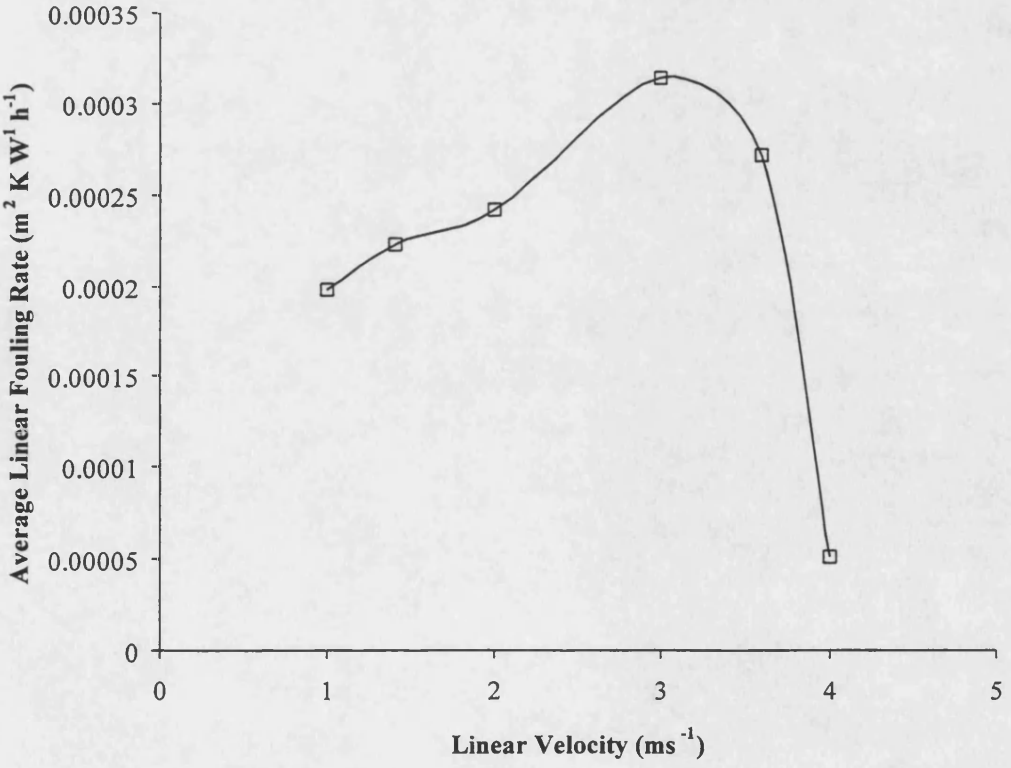

Figure 4.4 Average fouling rate against velocity at 265 °C

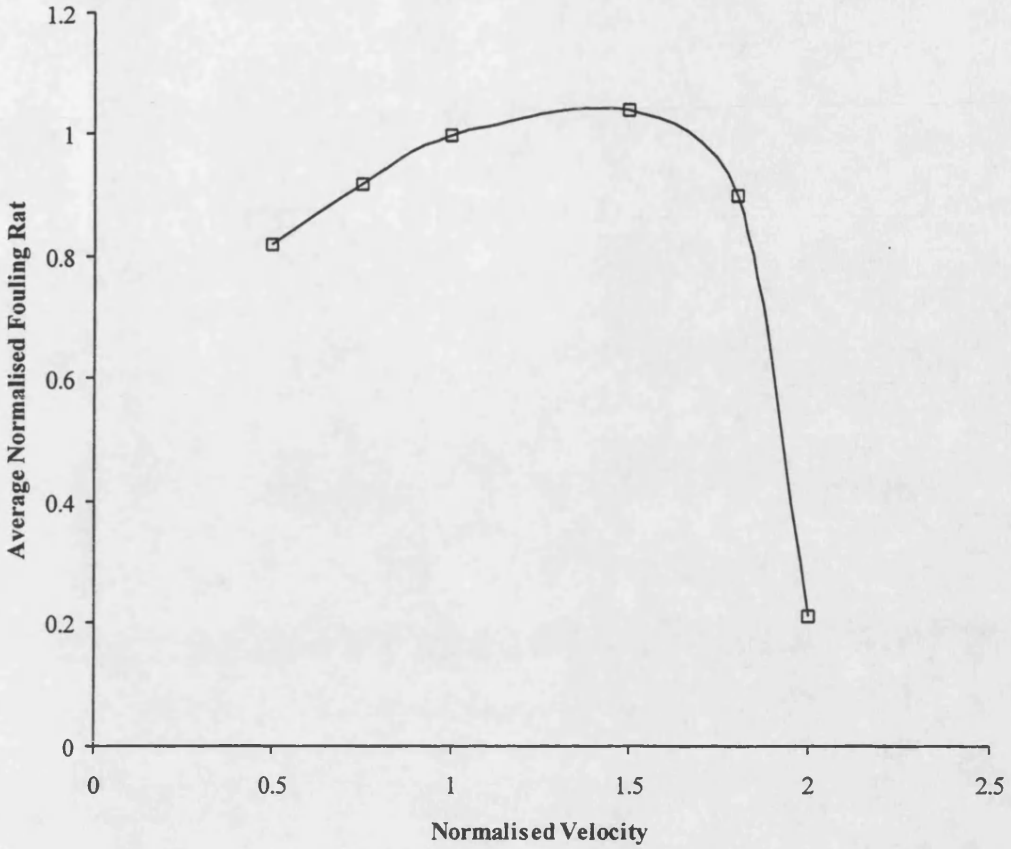

Figure 4.5 Normalised fouling rate against normalised velocity at 265 °C

These results show that at the higher surface temperature of 265 °C the peak in fouling rate occurs at a higher velocity of about 3.2 m s^{-1}. Additionally, the peak value at 265 °C is higher than at 250 °C.

4.2.5 The effect of velocity at 270 °C

Runs 28 to 30 together with 34 and 63 were conducted under nominally identical initial conditions, namely a clean surface temperature of 270 °C, a bulk temperature of 150 °C and a system pressure of 15 bar. The experimental conditions are summarised in Table 4.10. In runs 28 to 30, and 34 the fluid velocity in one of the test sections was varied from run to run, whilst in the other test section a 2.0 m s^{-1} benchmark velocity was maintained. A benchmark velocity was not used in run 63 due to heater failure.

Table 4.10 Summary of experimentation conditions at 270 °C

Run	Test Section	Velocity ($m\ s^{-1}$)
28	1	3.0
	2	2.0
29	1	1.0
	2	2.0
30	1	1.5
	2	2.0
34	1	3.6
	2	2.0
63	1	4.0
	2	-

The fouling resistance increased linearly with time in all runs. The average and normalised fouling rates against velocity are summarised in Table 4.11 and shown in Figure 4.6 and Figure 4.7.

Table 4.11 Results of bare tube fouling runs at 270 °C

	Velocity		Fouling Rate	
Run	Linear (ms^{-1})	Normalised	Average $x\ 10^4$ ($m^2\ K\ W^{-1}\ h^{-1}$)	Average Normalised
29	1.0	0.50	2.55	0.75
30	1.5	0.75	2.98	0.87
Various	2.0	1.00	3.42	1.00
28	3.0	1.50	3.72	1.09
34	3.6	1.80	3.72	1.09
63	4.0	2.00	2.37	0.69

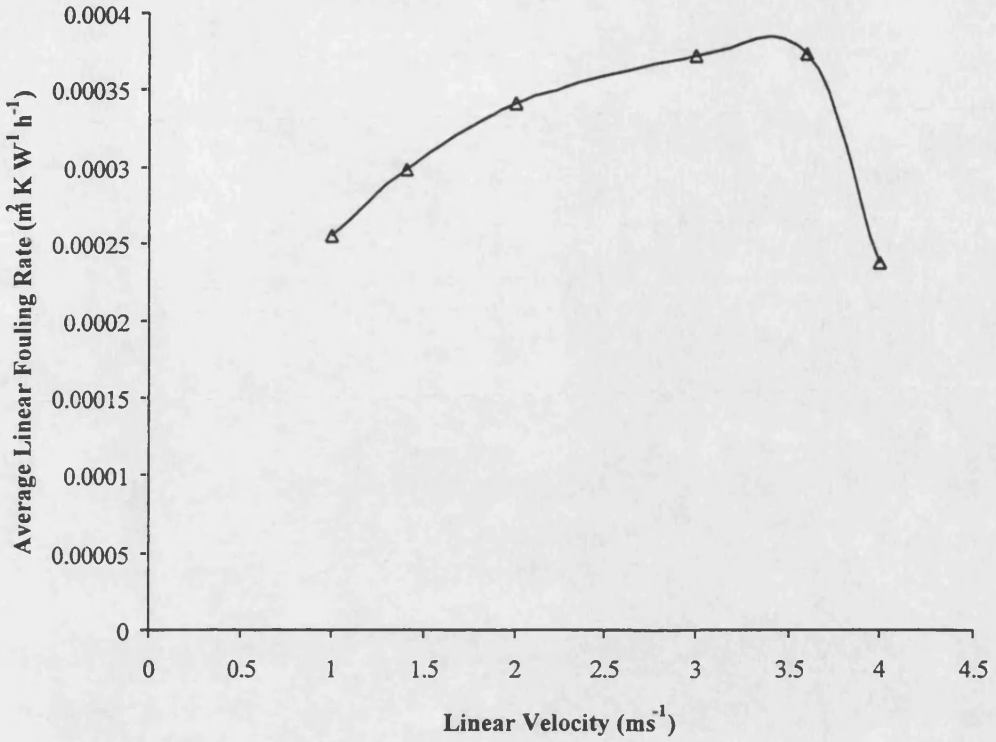

Figure 4.6 Average fouling rate against velocity at 270 °C

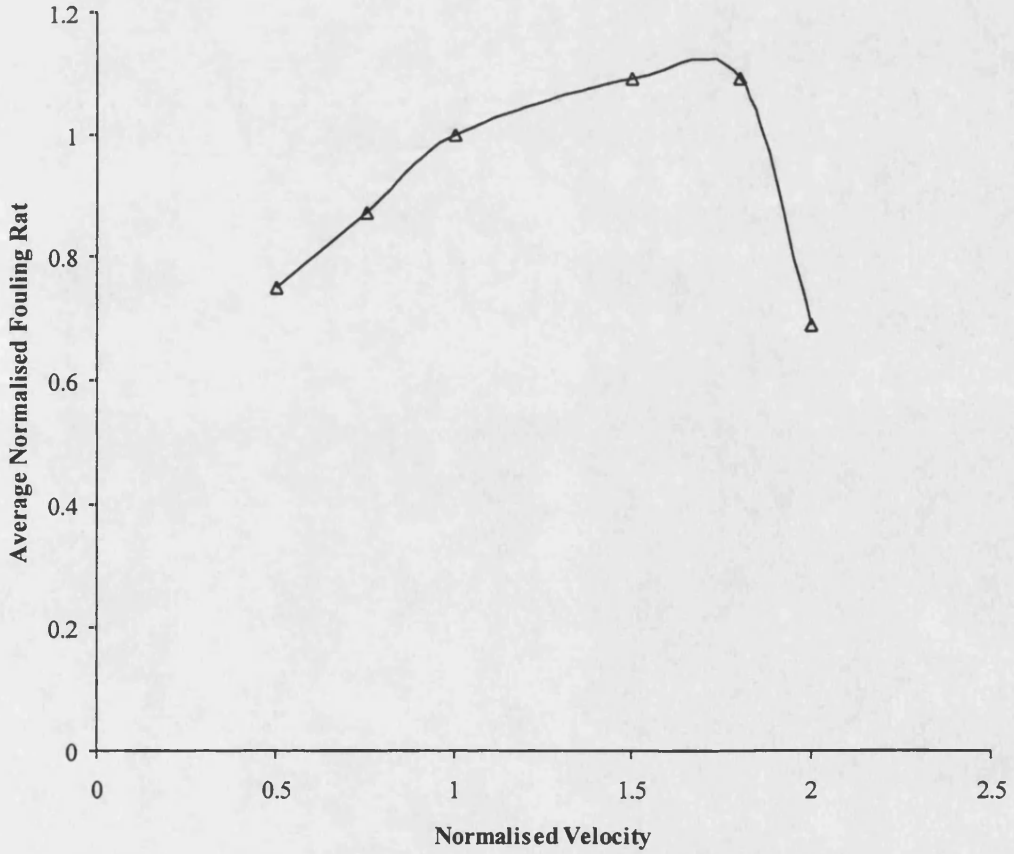

Figure 4.7 Normalised fouling rate against normalised velocity at 270 °C

Again, the peak fouling rate and velocity at which the peak occurs, have both increased with the increase in clean surface temperature

4.2.6 The effect of velocity at 280 °C

Runs 14, 16 to 20 together with 26, 27 and 62 were conducted under nominally identical initial conditions, namely a clean surface temperature of 280 °C, a bulk temperature of 150 °C and a system pressure of 15 bar. The experimental conditions are summarised in Table 4.12.

It was found that the fouling resistance increased linearly with time in all runs. The average and normalised fouling rates against velocity are summarised in Table 4.13 and shown in Figure 4.6 and Figure 4.7.

Table 4.12 Summary of experimentation conditions at 280 °C

Run	Test Section	Velocity ($m\ s^{-1}$)
14	1	2.0
	2	0.5
16	1	1.0
	2	2.0
17	1	1.5
	2	2.0
18	1	2.0
	2	0.5
19	1	0.8
	2	2.0
20	1	2.0
	2	1.5
26	1	3.6
	2	2.0
27	1	2.0
	2	2.0
62	1	4.0
	2	-

Table 4.13 Results of bare tube fouling runs at 280 °C

	Velocity		Fouling Rate	
Run	**Linear (ms^{-1})**	**Normalised**	**Average x 10^4 (m^2 K W^{-1} h^{-1})**	**Average Normalised**
14 & 18	*0.4*	*0.20*	*10.40*	*2.58*
19	*0.8*	*0.40*	*5.33*	*1.79*
17	1.0	0.50	2.68	0.59
20	1.5	0.75	3.26	0.72
Various	2.0	1.00	4.53	1.00
16	3.0	1.50	7.51	1.66
26	3.6	1.80	7.30	1.61
62	4.0	2.00	4.04	0.89

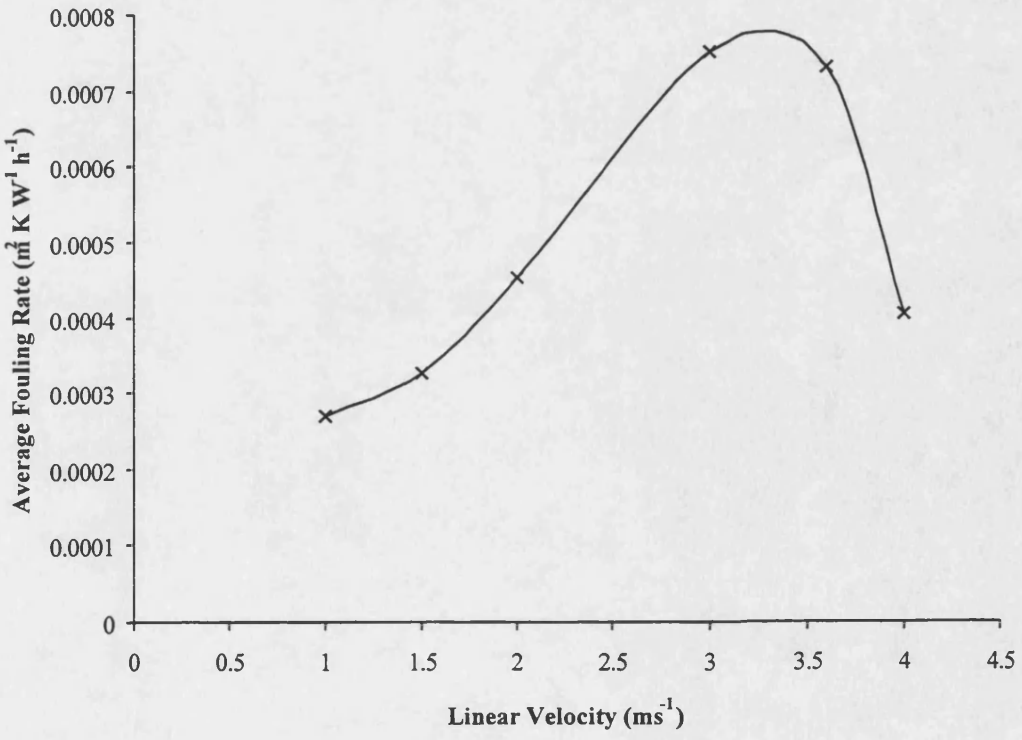

Figure 4.8 Average fouling rate against velocity at 280 °C

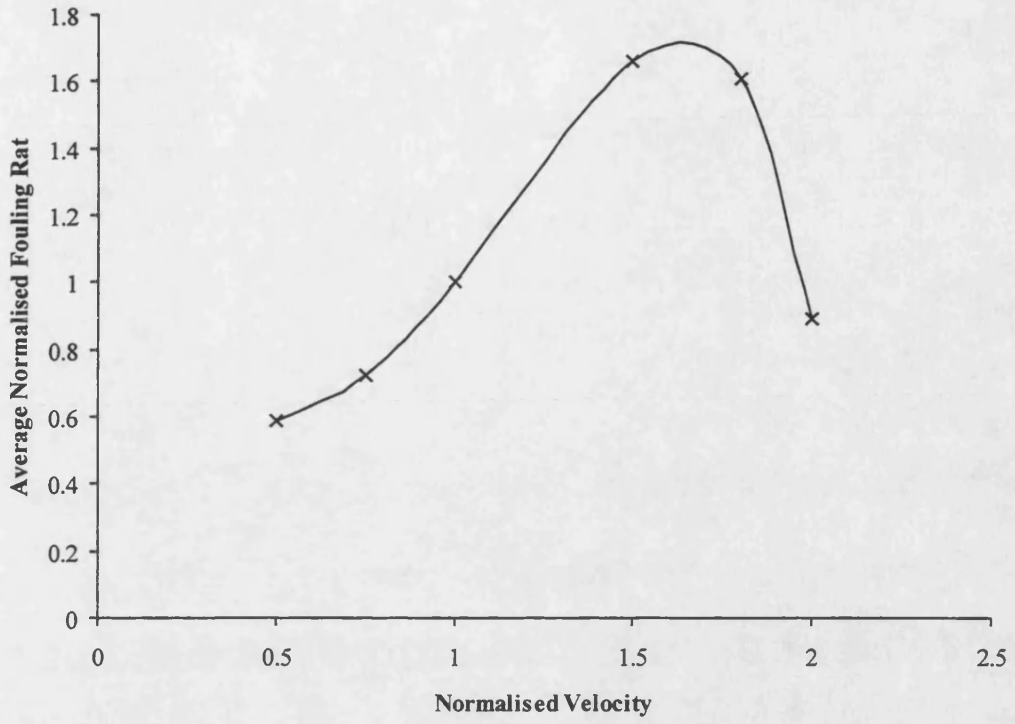

Figure 4.9 Normalised fouling rate against normalised velocity at 280 °C

The results (shown italicised in Table 4.12) with the lower velocities, 0.4 m s^{-1} and 0.8 m s^{-1} need to be considered with care. At these low velocities the control of temperature by alteration of the heat flux to reach the required surface temperature was not possible with the equipment available. Omitting these two low velocity data points, the velocity at which the peak fouling rate occurs was approximately 3.5 m s^{-1}, beyond which the fouling rate decreased.

4.2.7 Comparison of fouling at 250 °C, 265 °C, 270 °C and 280 °C

In order to compare the values at the different temperatures, all the values were normalised to the value at 2.0 m s^{-1} and 250 °C. The data are summarised in Table 4.14 and Figure 4.10. The normalised fouling rates against normalised linear velocity for all temperatures are summarised in Table 4.15 and plotted in Figure 4.11.

Table 4.14 Summary of fouling rates at temperatures studied

Velocity (ms^{-1})	Average Linear Fouling Rate ($m^2 K W^{-1} h^{-1}$) $x 10^4$			
	250 °C	*265 °C*	*270 °C*	*280 °C*
0.4	0.563	-	-	*10.40*
0.8	1.74	-	-	*5.33*
1.0	2.02	2.00	2.55	2.68
1.5	2.06	2.23	2.98	3.26
2.0	2.15	2.42	3.42	4.53
3.0	1.59	3.14	3.72	7.51
3.6	1.18	2.71	3.72	7.30
4.0	0.19	0.51	2.37	4.04

Table 4.15 Summary of normalised fouling rates at temperatures studied

Velocity (ms^{-1})	Normalised Velocity	Average Normalised Fouling Rate			
		250 °C	*265 °C*	*270 °C*	*280 °C*
0.4	0.20	0.37	-	-	*4.83*
0.8	0.40	0.63	-	-	*2.47*
1.0	0.50	0.89	0.93	1.18	1.24
1.5	0.75	0.99	1.03	1.38	1.51
2.0	1.00	1.00	1.12	1.59	2.10
3.0	1.50	0.81	1.46	1.73	3.49
3.6	1.80	0.55	1.26	1.73	3.39
4.0	2.00	0.09	0.24	1.10	1.88

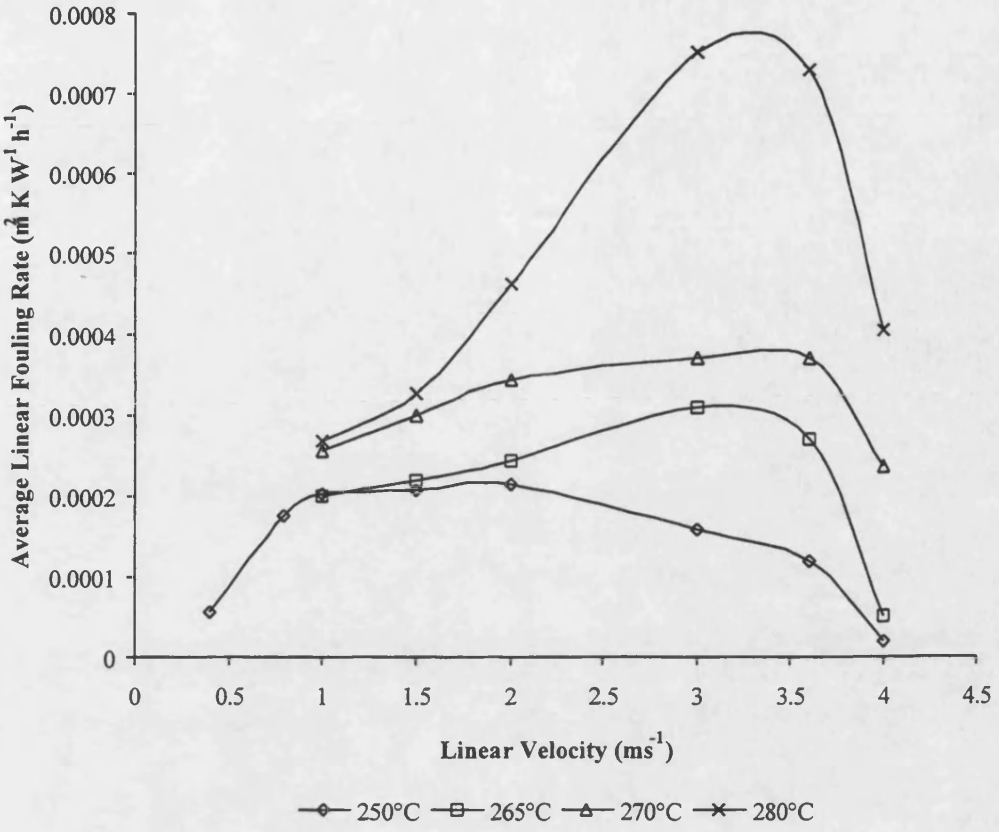

Figure 4.10 Summary of fouling rates at temperatures studied

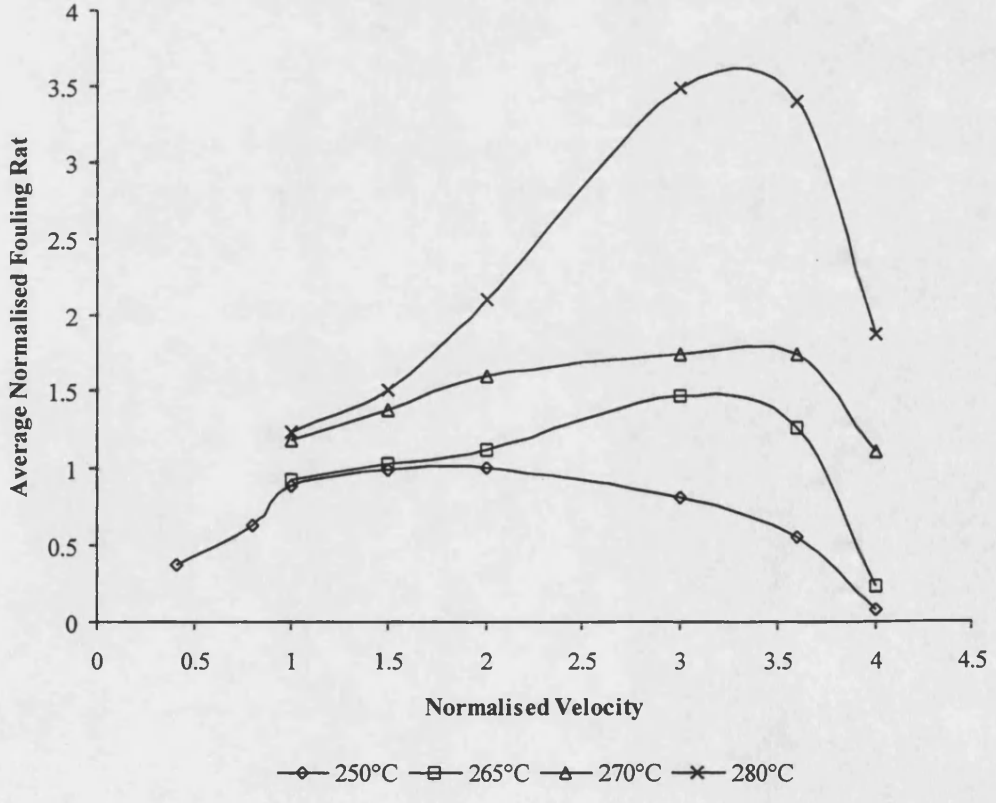

Figure 4.11 Summary of normalised fouling rates at temperatures studied

The results confirm that for a given velocity the fouling rate increases with temperature. For all initial surface temperatures an increase in the fouling rate with velocity is seen up to a maximum value, beyond which the fouling rate decreases with increasing velocity. In general, the velocity increases with increasing temperature. This might be expected as the relative balance between mass transfer control and kinetic control is expected to shift towards mass transfer as the temperature increases.

4.2.8 Threshold fouling temperature

Runs 11 to 15 and 31 were conducted with nominally identical conditions of bulk temperature (150 °C) and system pressure (15 bar). The clean surface temperatures and velocities were varied in each run, the 2.0 m s^{-1} benchmark velocity in one of the test sections being retained. The conditions and results of these runs are summarised in Table 4.16; no inserts were in place in either test section for the runs conducted in this section.

At an initial surface temperature of 300 °C and velocities of 2.0 m s^{-1} and 3.0 m s^{-1} (Run 11) the fouling rate was too great for the initial conditions of the experiment to be considered stable as it was not possible to control the temperature accurately. Fouling had increased the surface temperature to the 400 °C cut off limit after only 15 minutes.

No fouling was observed, or was too low to be measured, for initial surface temperatures below 225 °C, even at 0.5 m s^{-1}, the lowest velocity used in the study (Runs 12 and 13).

At 230 °C it was found there was fouling at 0.5 m s^{-1} but not at 2.0 m s^{-1}. This is most likely due to the combination of high mass transfer rates and low chemical kinetic rates at the higher velocity. This is indicative of the kinetic control expected at relatively low surface temperatures.

Table 4.16 Summary of experimentation conditions for threshold temperatures

Run	Test Section	Initial Surface Temperature (°C)	Velocity ($m\ s^{-1}$)	Linear Fouling Rate $x\ 10^{-4}$ ($m^2\ K\ kW^{-1}\ h^{-1}$)
11	1	300	2.0	very high
	2	300	3.0	very high
12	1	200	2.0	no fouling noted
	2	200	0.5	no fouling noted
13	1	225	2.0	no fouling noted
	2	225	0.5	no fouling noted
14	1	280	2.0	6.59
	2	280	0.5	6.64
15	1	230	0.5	1.90
	2	230	2.0	no fouling noted
31	1	200 → fouling	3.0	Fouling noted at 250 °C
	2	200 → fouling	2.0	Fouling noted at 240 °C

Note: Bulk pressure - 15 bar

Bulk temperature - 150 °C

For run 31 the velocities were set at 3.0 m s^{-1} and 2.0 m s^{-1} for test sections 1 and 2 respectively. The power supplied to the test sections was adjusted to give initial surface temperatures of 200 °C. Both test sections were studied for 30 minutes, during which no fouling was noted. The power to both test sections was then increased by 200 W and studied for a further period of 30 minutes. This pattern continued until fouling was evident in the test section studied. The results of this experiment (run 31) are shown in Figure 4.12 and Figure 4.13 for 2.0 m s^{-1} and 3.0 m s^{-1} respectively.

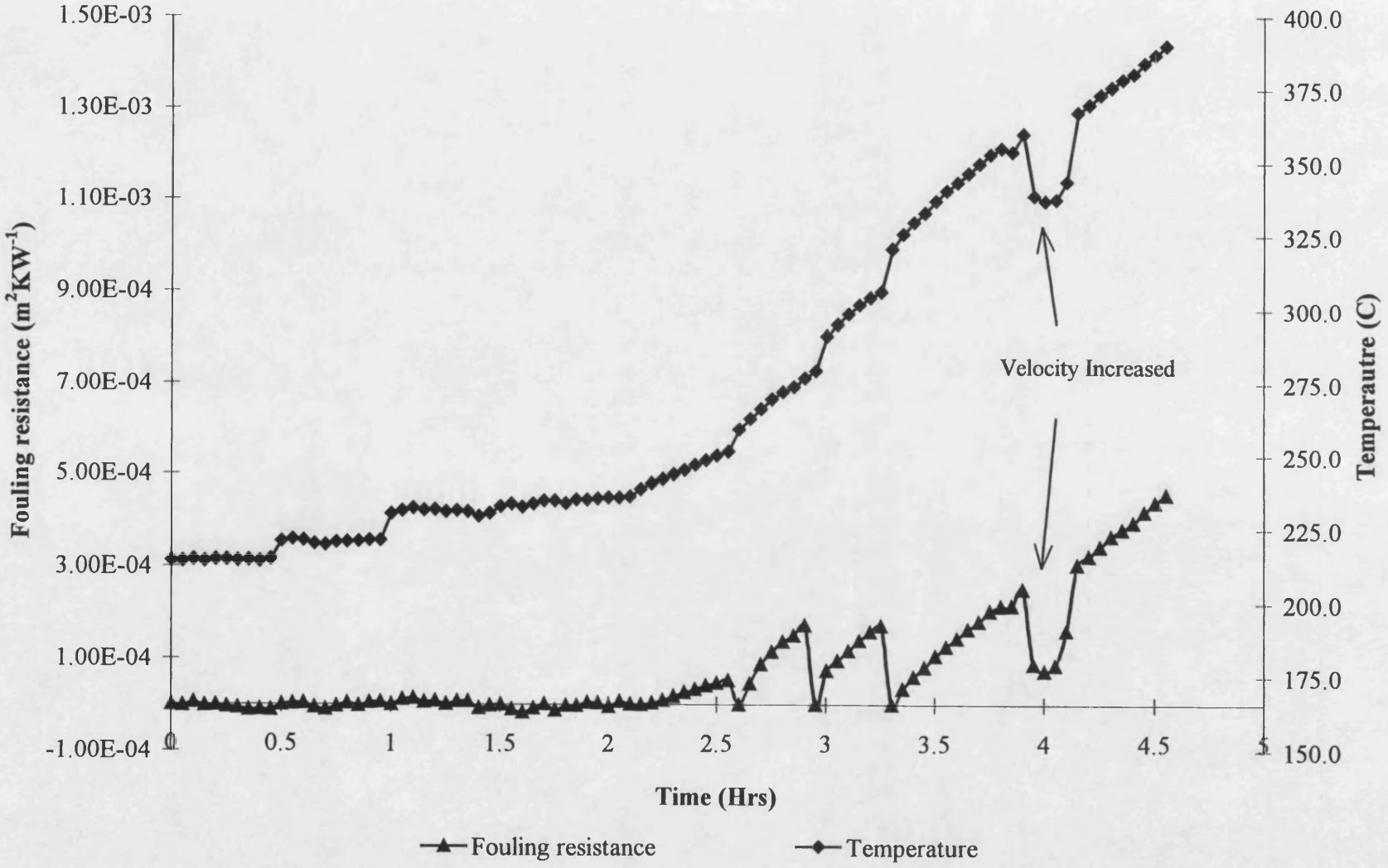

Figure 4.12 Chart showing the threshold fouling temperature at 2.0 m s^{-1}

Figure 4.13 Chart showing the threshold fouling temperature at 3.0 m s^{-1}

These results show that at 2.0 m s^{-1} the threshold fouling temperature seems to be approximately 240 °C, whilst at 3.0 m s^{-1} it seems to be approximately 250 °C. These results suggest that as the velocity is increased the threshold fouling temperature is also increased.

The results of the runs described so far indicate that the fouling rate is dependent on the relative balance of mass transfer and chemical kinetic effects. As the velocity increases the rate of mass transfer both to and from the heat transfer surface is also increased. It follows that the temperature at which the rate of chemical reaction is sufficient to enable deposits to form and adhere to the tube surface is also increased.

In order to gauge the adhesion of the deposit to the tube surface, the velocity in one of the test sections during run 31 was increased temporarily. Before the velocity was increased a period of time was allowed for the deposit to accumulate on the tube surface. The velocity in test section 2 was increased from 2.0 m s^{-1} to 3.0 m s^{-1} for a short period and returned to the original velocity. As is evident from Figure 4.12, the increase in velocity appeared to have little effect on either the fouling resistance or the fouling rate once the velocity was returned to the original value. This would indicate that at 2.0 m s^{-1} (with a surface temperature of approximately 250°C) the fouling deposits were adhering strongly to the tube surface.

4.2.9 Variation in circumferential and axial fouling rates

In order to monitor the variation of heat transfer and fouling rates along the tube length, six thermocouples per test section were arranged in two groups of three, separated axially by 20 mm as shown in Figure 3.3 and Figure 3.4. Within each of the two groups the three thermocouples were separated circumferentially by 120°.

It was found that there were no significant variations in fouling rate between the circumferential and axial thermocouple locations. This is not unexpected due to the small temperature difference between the two axial positions. However, the marked effect that temperature has on the fouling rate might have suggested even slight axial differences in temperature would have resulted in differences in fouling rate. The sensitivity and accuracy of the sensing equipment would need to be increased in order to allow small changes in temperature to be registered.

4.2.10 Apparent activation energy of the fouling process

The results of this study so far have suggested that fouling rates of Maya crude oil are the result of a balance between chemical reaction rates, affected strongly by temperature, and mass transfer rates, predominantly affected by fluid flow-rates. Hence, evaluation of a true activation energy for the fouling reaction, independent of the mass transfer, is not possible. An apparent activation energy, which includes a mass transfer contribution may be determined however. Apparent activation energies below 40 kJ $kmol^{-1}$ would indicate that the fouling rate is predominantly controlled by mechanisms other than chemical kinetics. Above 40 kJ $kmol^{-1}$ the key controlling step is that of the rate of chemical reaction of the fouling species. The apparent activation energy was calculated by plotting the logarithm of the fouling rate against the reciprocal of the initial absolute surface temperature in Kelvin (T_w^{-1}). The apparent activation energy was found by multiplying the slope of the semi-log plot by the universal gas constant (R), 0.008314 kJ mol^{-1}. The pre-exponential factor (A) was given by the intercept.

Only those velocities which were used at all the initial surface temperatures were chosen for the plots to calculate the activation energy namely 1.0 m s^{-1}, 1.5 m s^{-1}, 2.0 m s^{-1}, 3.0 m s^{-1} and 3.6 m s^{-1}. The plots are shown in Figure 4.14, Figure 4.15, Figure 4.16, Figure 4.17 and Figure 4.18 respectively.

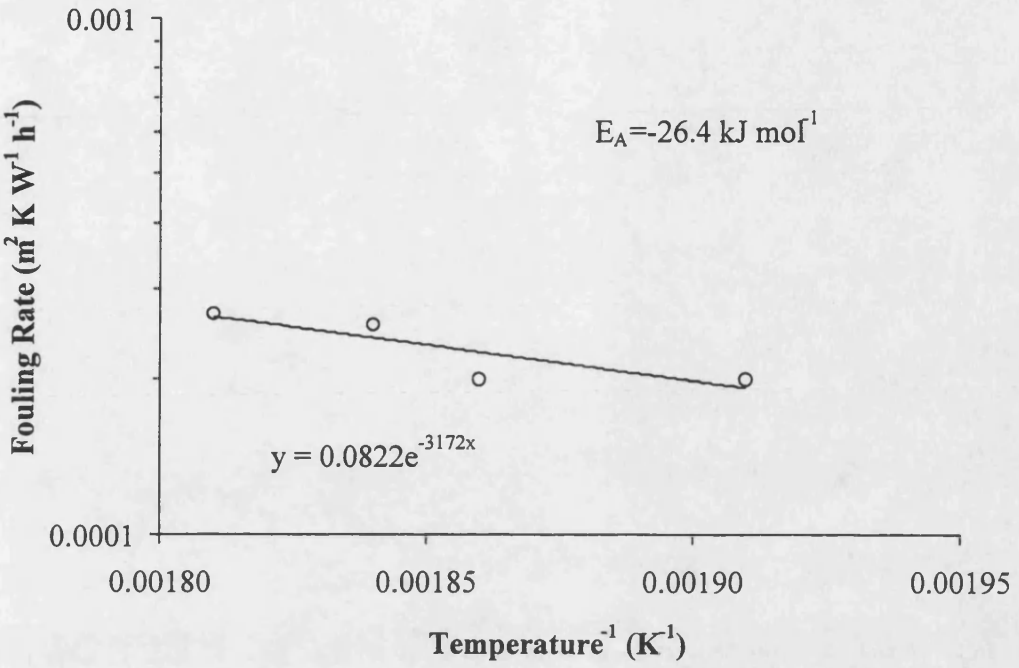

Figure 4.14 Arrhenius plot at 1.0 m s^{-1}

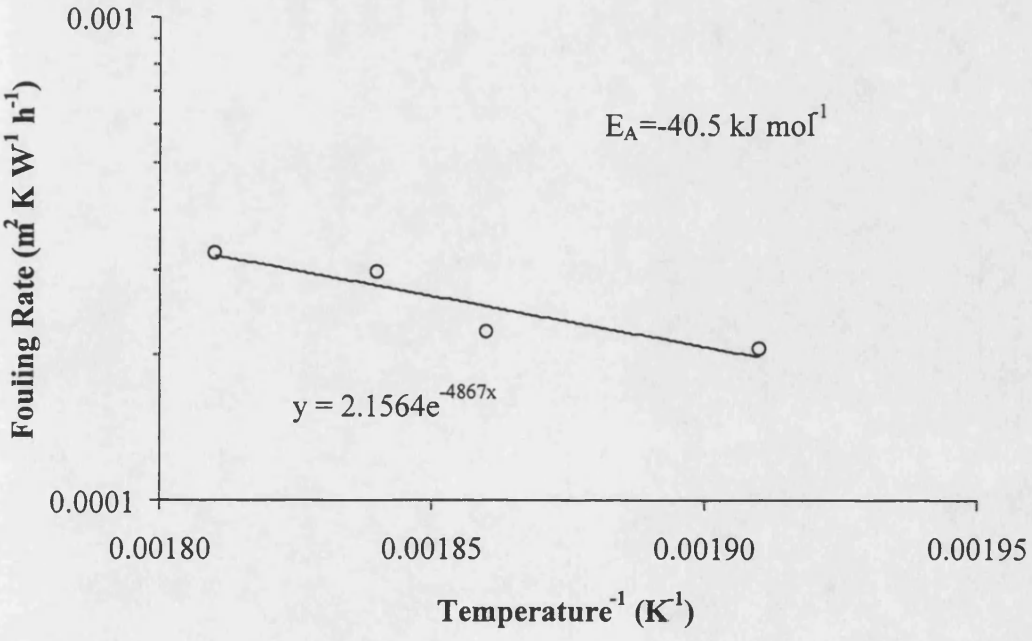

Figure 4.15 Arrhenius plot at 1.5 m s^{-1}

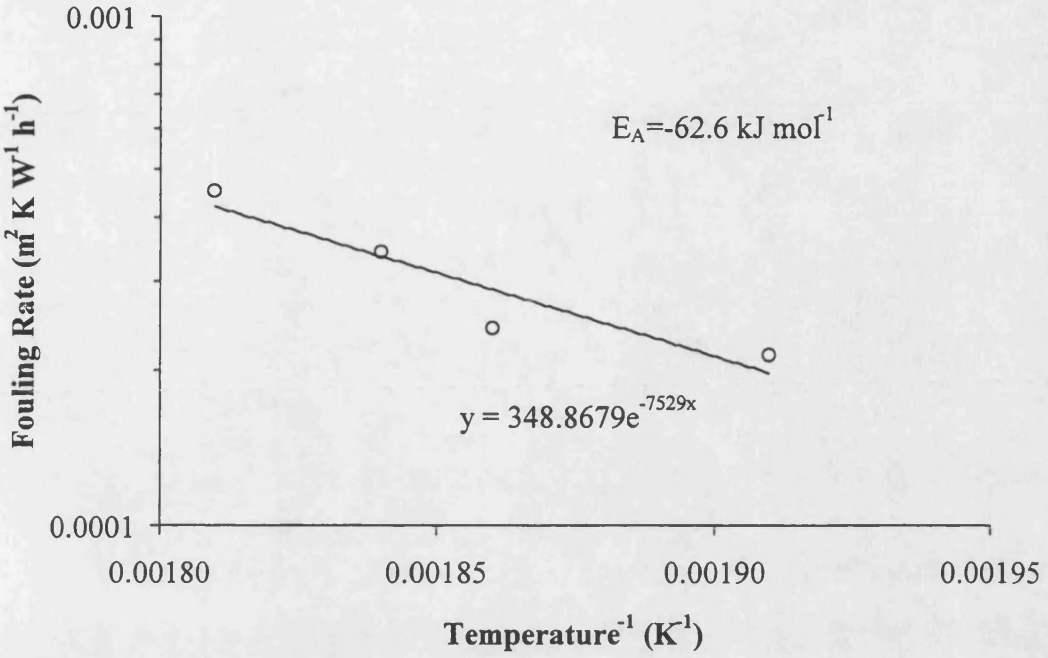

Figure 4.16 Arrhenius plot at 2.0 m s^{-1}

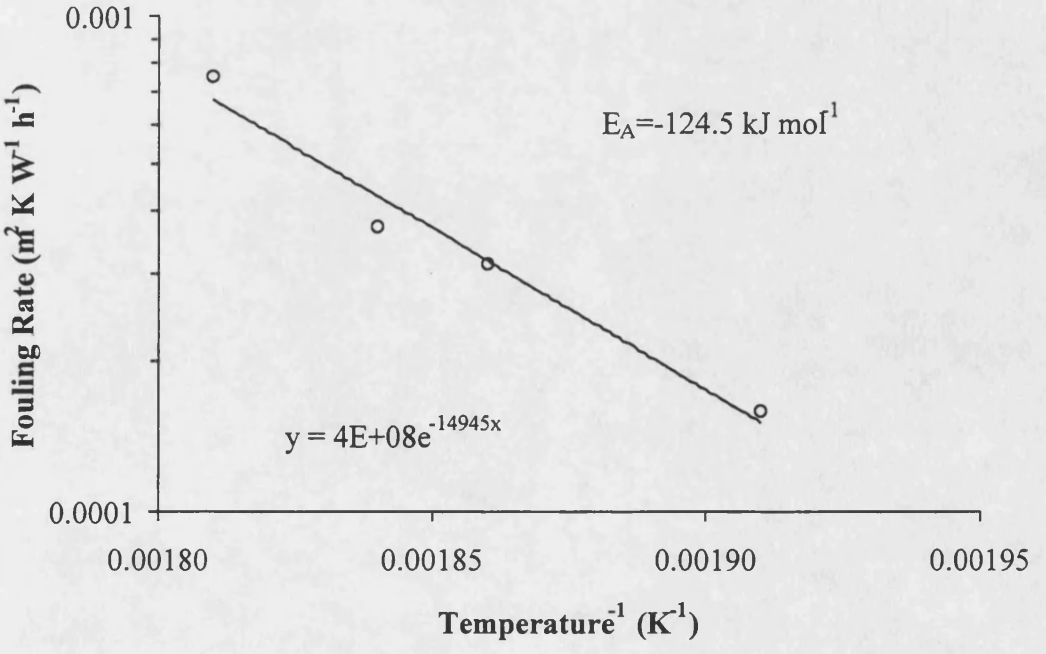

Figure 4.17 Arrhenius plot at 3.0 m s^{-1}

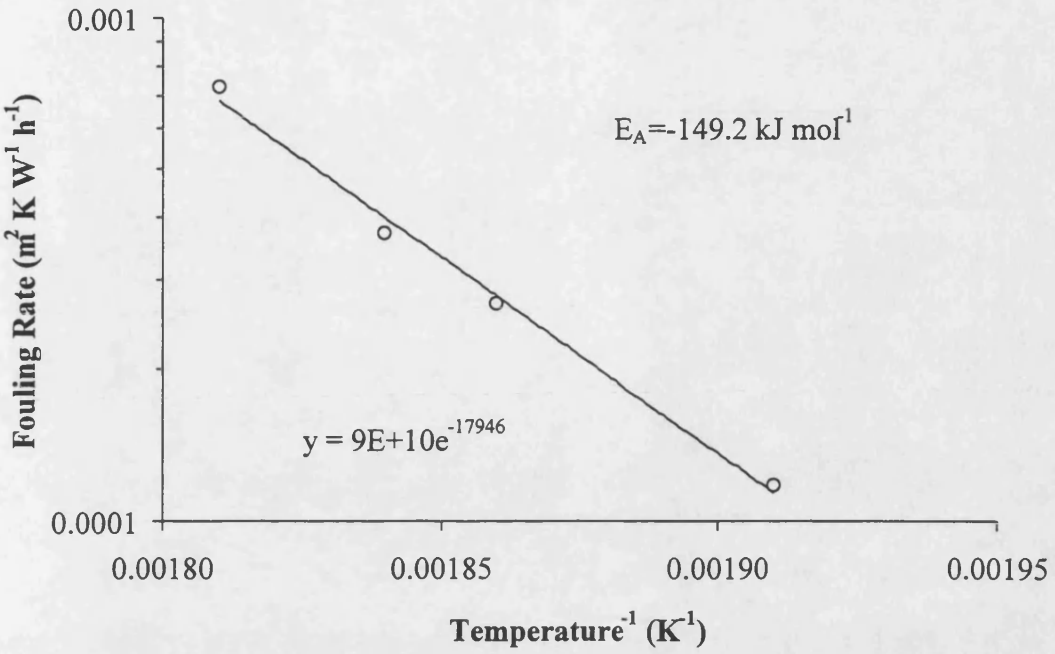

Figure 4.18 Arrhenius plot at 3.6 m s^{-1}

The apparent activation energies for the fouling reaction of Maya crude derived from shown in Figure 4.14 to Figure 4.18 are summarised in Table 4.17.

Table 4.17 Summary of apparent activation energy for Maya crude

Velocity (m s^{-1})	Apparent pre-exponential factor	Apparent activation energy (kJ mol^{-1})
1.0	0.082	26.4
1.5	2.156	40.5
2.0	348.860	62.6
3.0	1.000×10^{8}	124.5
3.6	9.000×10^{10}	149.2
Average	1.80×10^{10}	77.5

These results show that the apparent activation energy increases with increasing velocity, indicating a strong influence of mass transfer on the fouling mechanism. Figure 4.19 shows that the variation in activation energy with velocity seems to be almost linear at least over the range of velocities studied (1.0 to 4.0 ms^{-1}).

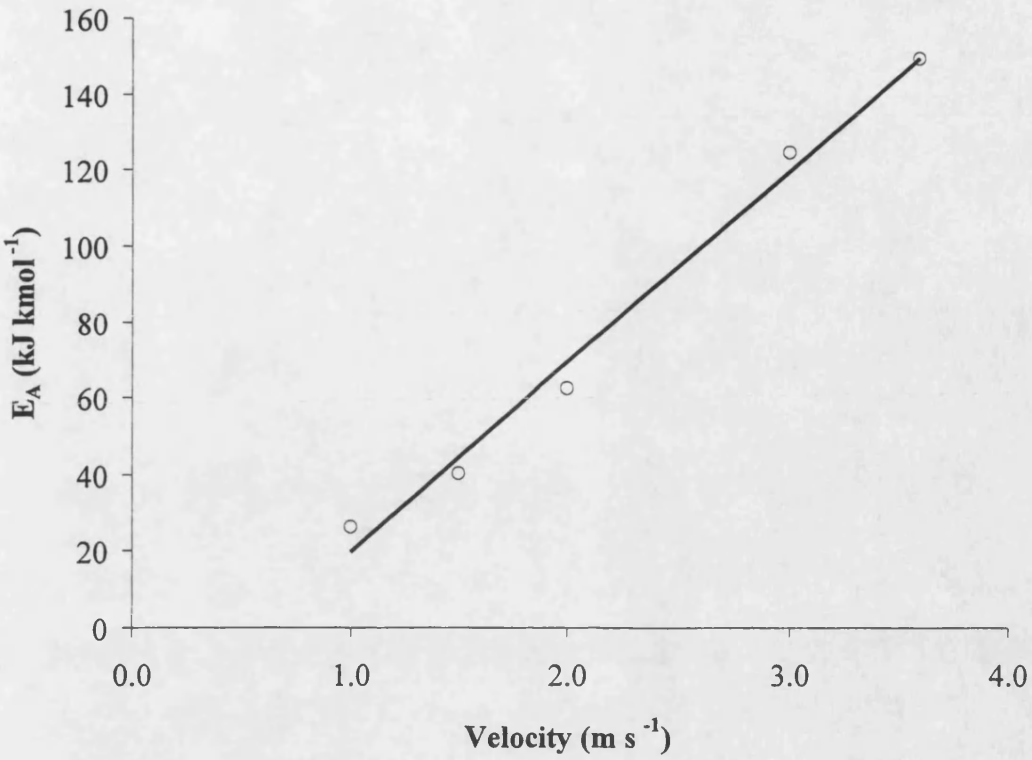

Figure 4.19 The effect of velocity on apparent activation energy

Where mass transfer affects activation energies, it ought to be possible to increase the velocity to a point beyond which further increases in velocity do not significantly affect the activation energy, that is to the point at which the overall process becomes kinetically controlled. In such a situation as velocity increases the activation energy would tend to a maximum, thereby allowing the activation energy of the chemical reaction to be estimated independent of the mass transfer effects. As is evident from Figure 4.19, however, the apparent activation energy seems to increase linearly with velocity over the range studied. Therefore the prediction of an activation energy independent of mass transfer effects is not possible to achieve in the rig at Bath because it is not possible to achieve sufficiently high velocities.

4.2.11 Friction factor

The use of friction factors (j_f) to assess the pressure drop in a length of pipe enables an identical set of equations to be used in smooth or rough pipes, for a wide range of

Reynolds numbers. At low Reynolds numbers (Re < 2,200) the boundary layer is relatively large and the pressure drop is a function of Reynolds number only. At higher Reynolds numbers (2,200 < Re < 100,000) the boundary layer is reduced to a point where pressure drop is a function of both Reynolds number and surface roughness (Coulson, Richardson, Backhurst and Harker (1993)). In general, the friction factor ranges from 0.8 (Re ~ 1 x 10^1) to 0.001 (Re ~ 1 x 10^6) in commercially available carbon steel heat exchanger tubing (Coulson, Richardson and Sinnott (1991)).

For this study values of j_f were calculated using equation (4.6). The pressure drop measurements are summarised in Appendix C. Values of j_f were correlated with Reynolds number (Re) using an exponential least mean squares fit of the data, and the results are shown Figure 4.20. It was found that the best fit of the data was achieved by fitting two curves, one equation (4.10) for Re below about 10,000, and the other (4.11) for Re above 10,000:

$$j_f = 0.1002e^{-0.0001\mathrm{Re}} \tag{4.10}$$

$$j_f = 0.0189e^{-0.000002\mathrm{Re}} \tag{4.11}$$

The discontinuity in j_f has been reported to occur at Re ~1,000 to 3,000 and at a friction factor of approximately 0.01 (Coulson, Richardson and Sinnott (1991)). For the current crude oil study, the experiments with bare tubes have shown that the discontinuity in j_f occurs at a Reynolds number of approximately Re ~10,000 and a j_f of 0.01. The difference in Reynolds number between this study and the literature may be explained by the fact that the crude oil may not have become fully turbulent until Re ≅ 10,000, whereas for fluids used elsewhere, full turbulence may have occurred at Re ≅ 2,200.

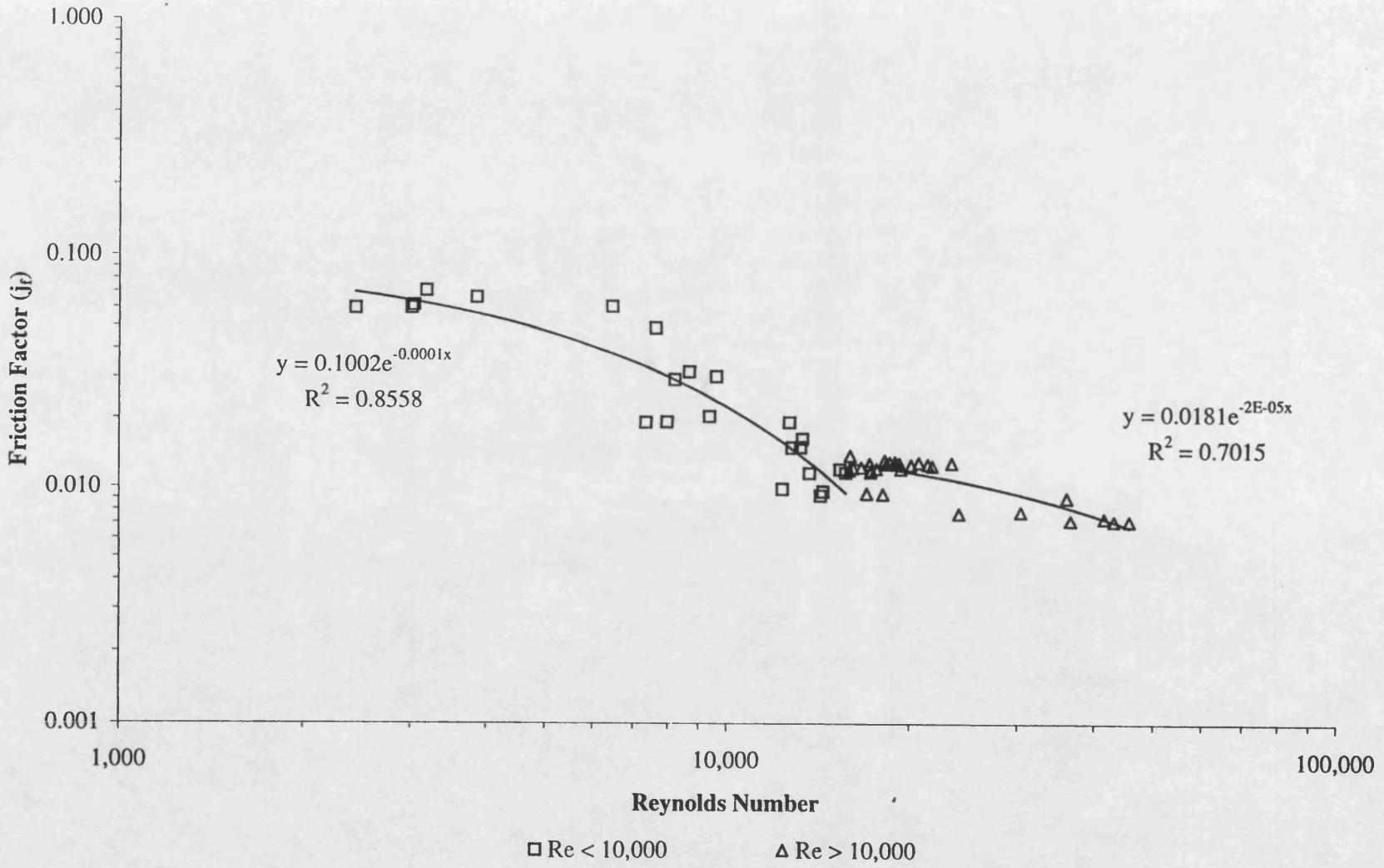

Figure 4.20 Variation in friction factor with Reynolds number in bare tubes

Additionally, the fouling deposits may perhaps have also affected the flow regime. However, the instrumentation available on the rig was not sufficient to elucidate this speculation.

4.2.12 Heat transfer factor

The use of heat transfer factors (j_h) in exchanger design allows data to be correlated over a wide range of Reynolds numbers using a single set of equations. In general, heat transfer factors range from 0.1 ($Re \sim 1 \times 10^1$) to 0.01 ($Re \sim 1 \times 10^6$) in carbon steel heat exchanger tubing (Coulson, Richardson and Sinnott (1991)). For this present research values of j_h were calculated using equation (4.9). The heat transfer factor was correlated with Reynolds number (Re) and a curve based on an exponential least mean squares fit of the data is shown in Figure 4.21. The heat transfer factor (j_h) is correlated with the Reynolds number (Re) by equation (4.12):

$$j_h = 0.1625\,\mathrm{Re}^{-0.4096} \tag{4.12}$$

The results from the bare tube study are comparable with the values quoted in the literature. No discontinuity is noted as Reynolds number is increased, as was observed for the friction factor. This might be expected since the experiments conducted were above the Reynolds number at which the discontinuity has been reported for bare tubes ($Re \sim 2{,}000$) (Coulson, Richardson and Sinnott (1991)).

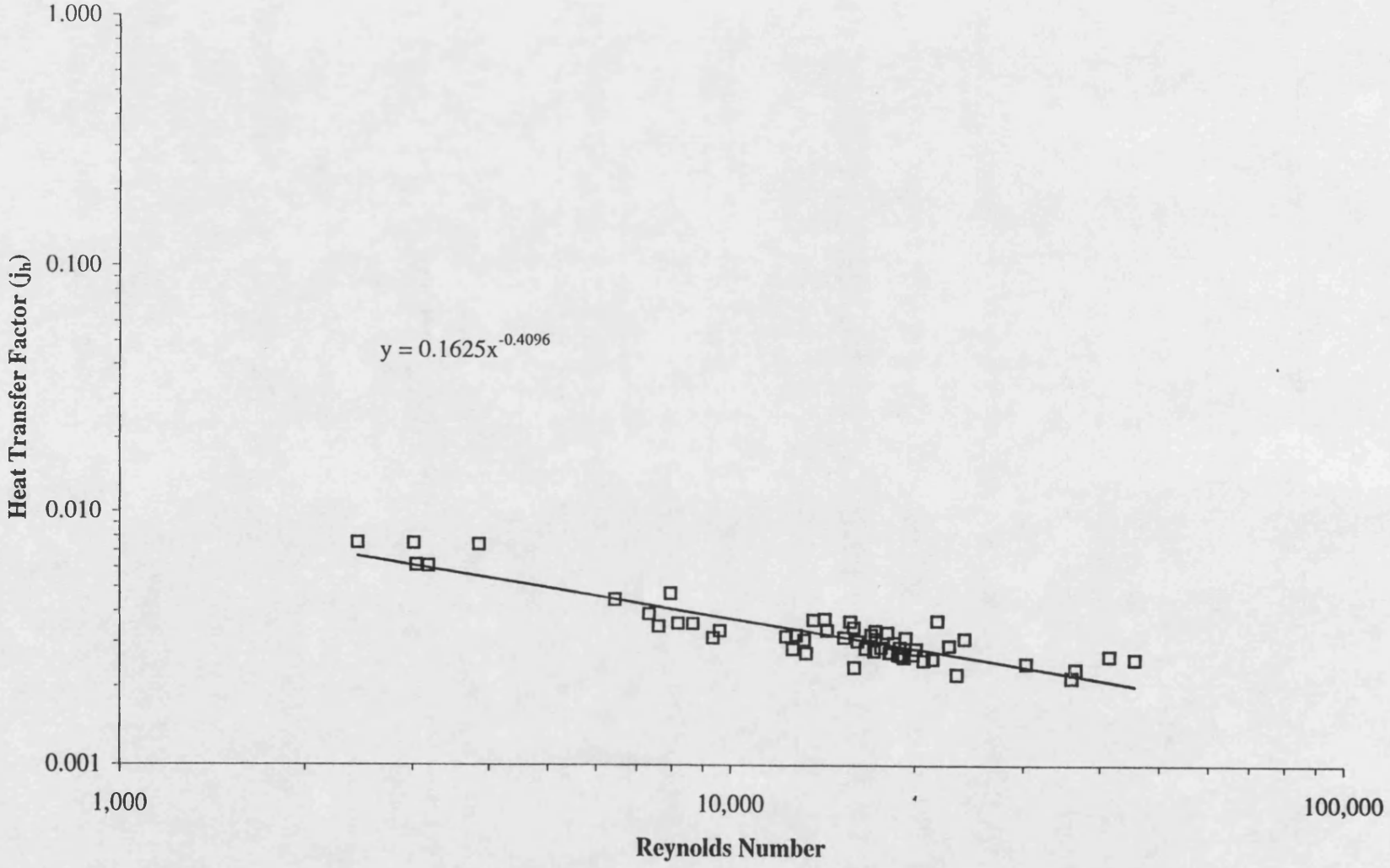

Figure 4.21 Variation in heat transfer factor with Reynolds number in bare tubes

4.2.13 Comparison of friction factor discontinuity and fouling rate

Increased heat and mass transfer coefficients result from increasing the turbulence of the fluid within a tube. In industrial heat exchange equipment this generally results in a reduction in the tube wall temperature. In circumstances where fouling rates are kinetically controlled the fouling rate would be reduced. However, increased turbulence also increases mass transfer rates. Where fouling rates are mass transfer controlled, an increase in turbulence can result in the possibility of increased fouling rates. This is particularly important where surface temperatures are maintained constant as the velocity is increased, as has been practised in this study.

Analysis of friction factor data has found that fully developed turbulent flow may not have been established until Re ≅ 10,000 in this study, as opposed to Re ≅ 2,200 for other studies quoted in the literature. In this study, a Reynolds number of 10,000 corresponds to a velocity of approximately 2.0 m s^{-1}, that is the benchmark velocity. As can be seen from Figure 4.22 Maya crude oil fouling rates become kinetically controlled at Reynolds numbers somewhat higher than the experimentally based suggestion that the transition to full turbulence occurs at Re ≅ 10,000.

This might suggest that the flow regime in the tubes in the range of Reynolds numbers studied does not significantly affect the mechanism of fouling in Maya crude oil. However, it should be remembered that the rig is primarily designed to observe fouling phenomena and not the structure of fluid flow. As such therefore, care must be exercised in interpreting these results. It is believed that the discontinuity in j_f as Re is increased is not a significant factor when interpreting the heat transfer and fouling results.

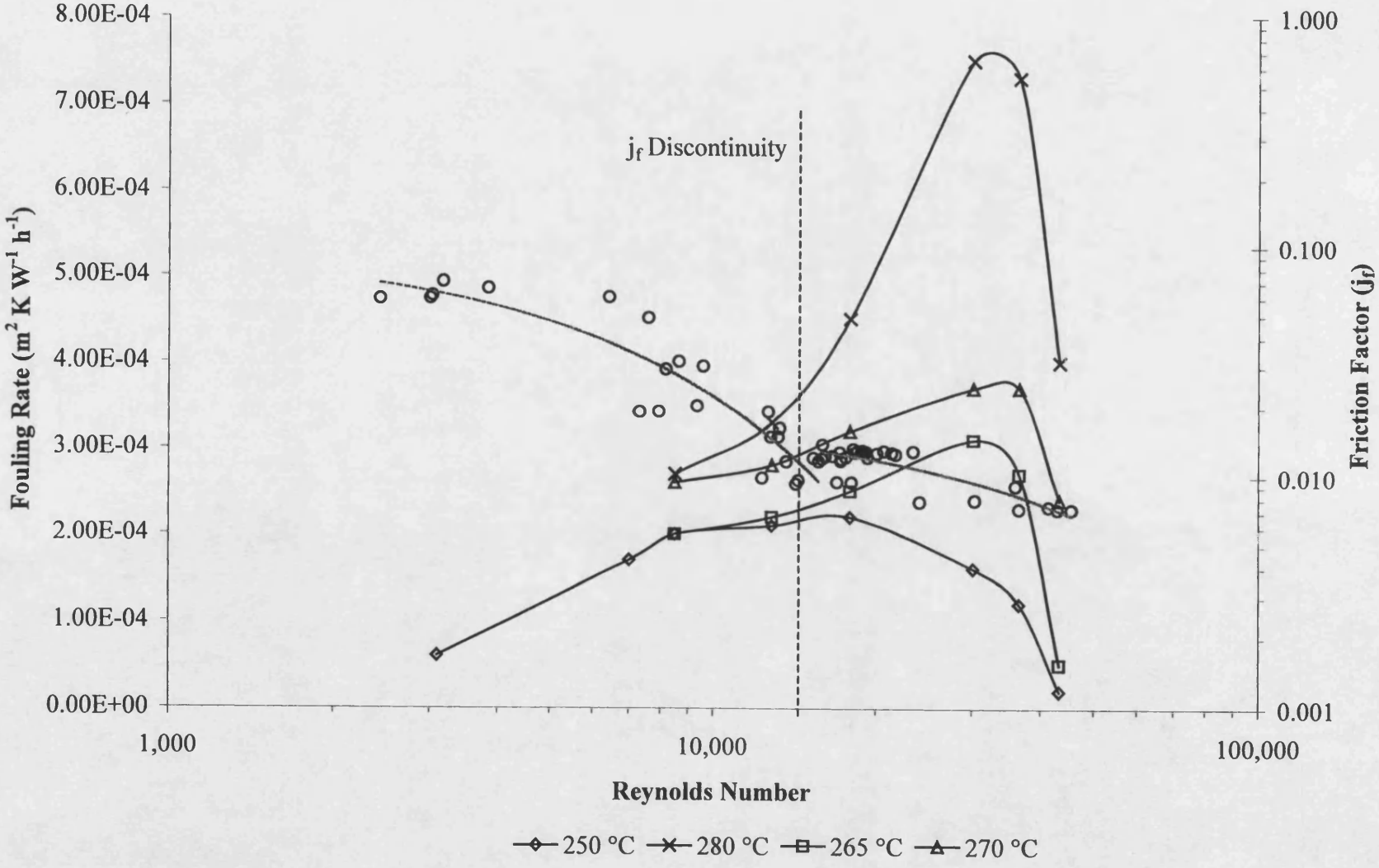

Figure 4.22 Comparison of friction factor discontinuity and fouling rates

4.2.14 Testing the parallel flow rig as a comparative tool

The parallel flow rig at the University of Bath was evaluated in previous studies using comparative assessments of fouling behaviour (Takemoto (1993)). He developed a film based model to account for the initial fouling rate in both a bare tube and a tube fitted with an insert. It was proposed that the initial fouling rate ($R^{\bullet}_{f(0)}$) was a function of the heat transfer coefficient (h_i), mean velocity (u_m), temperature at position "y" (T_y), activation energy (E), a dimensionless distance (y), a pre-exponential factor (A) and the universal gas constant (R), as illustrated by equation (4.13):

$$R^{\bullet}_{f(0)} = \frac{A}{h_i u_m} \int_0^1 \frac{1}{y} e^{\left(-\frac{E}{RT_y}\right)} \qquad (4.13)$$

By comparing fouling rates in the same run and maintaining nominally identical bulk and surface temperatures, the variation in the initial fouling rate ($R^{\bullet}_{f(0)}$) in alternate test sections (denoted by subscripts 1 and 2) could be related to the internal heat transfer coefficient (h_i) and the velocity (u) by equation (4.14) (Takemoto (1993)):

$$\frac{\left(R^{\bullet}_{f(0)}\right)_1}{\left(R^{\bullet}_{f(0)}\right)_2} \times \frac{h_{i2} u_{12}}{h_{i1} u_1} = 1 \qquad (4.14)$$

This relationship was tested on two different crude oils at clean initial surface temperatures ranging from 197°C to 239°C and at velocities ranging between 0.5 m s^{-1} and 1.1 m s^{-1}, both with and without inserts of varying density. Takemoto found that the experimental data fitted equation (4.14) well.

If this model developed for light Arabian crude by Takemoto is applicable to Maya crude then the product of fouling ratio and inverse of the heat transfer and velocity ratio should be equal to one. The correlation for Maya crude oil is shown in Figure 4.23.

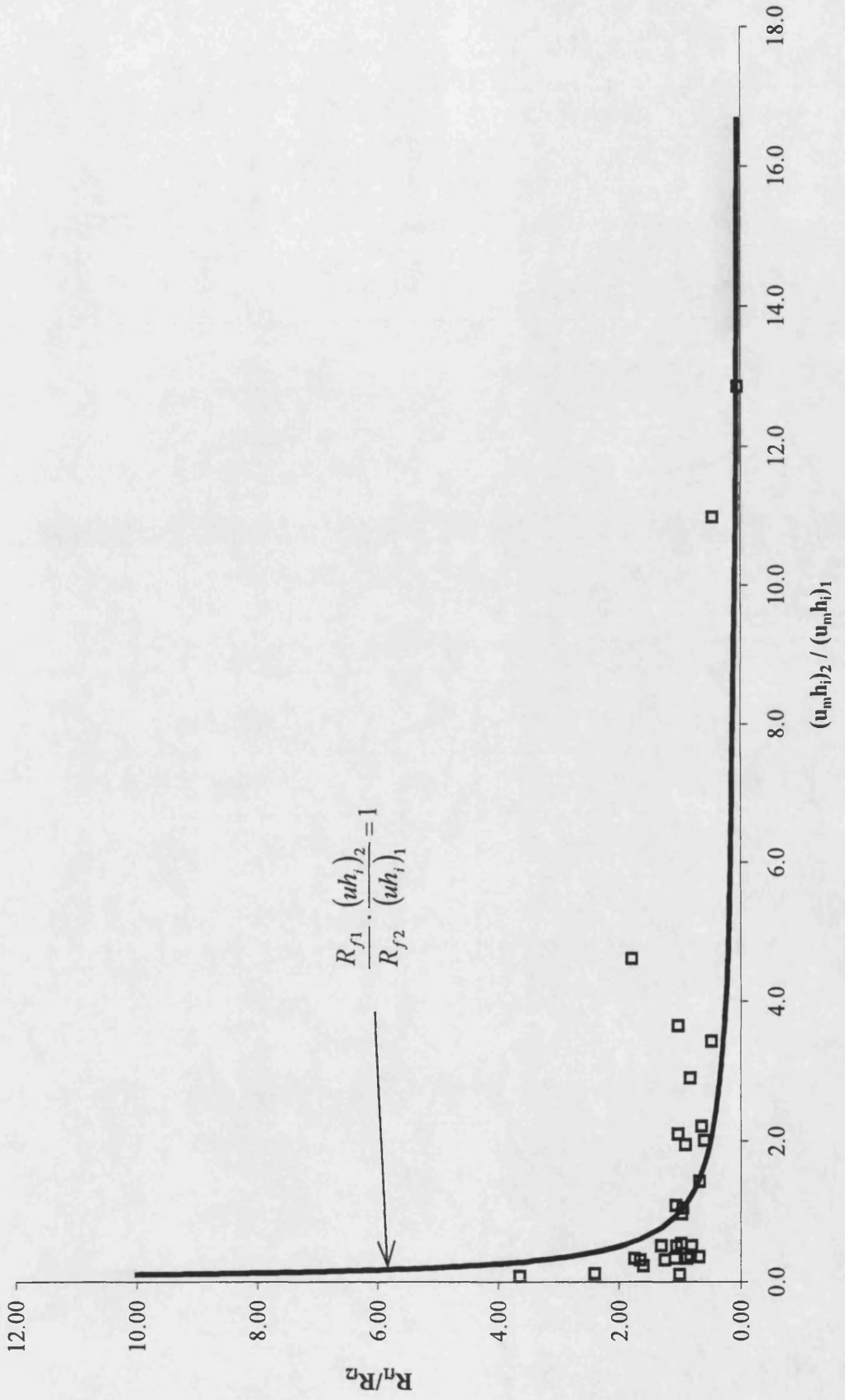

Figure 4.23 Effectiveness of the hydrocarbon fouling rig as a comparative tool

As seen in Figure 4.23 the experimental data agrees well with that predicted by equation (4.14). This indicates that the hydrocarbon fouling rig at the University of Bath is a good tool for the comparative study of hydrocarbon fouling.

4.2.15 Deposit analysis

As explained previously, asphaltenes and resins are particularly relevant due to the role that they may play in determining fouling rates in crude oil streams. Asphaltenes exhibit inverse-solubility characteristics. Hence temperature increases can result in increased insoluble asphaltene content in hotter regions of the fluid especially those nearer the tube surface. The role of resins in determining the rate of fouling is of secondary, but still significant, importance. This is because of the possibility that the formation of asphaltenes may occur by the thermal degradation reactions of resins.

The large number of compounds in the resin and asphaltene classes prevents the identification of any single compound or compounds as being specifically responsible for fouling. Therefore, the total amount of each class was considered to be an important matter for study and no attempt was made to identify and quantify individual compounds.

For the purpose of this study the selective solubility of each class (asphaltene and resin) in specific solvents was used to indicate the quantity of each class in the deposit. The resin and free oil content is the fraction that is soluble in n-heptane (Crittenden *et al* (1992)). The asphaltene content is the fraction of the sample that is soluble in toluene after solvent extraction by n-pentane (ASTM† D 893 - 92).

It was considered that the use of n-heptane in place of n-pentane would make little difference, if any, to the analysis. The coke content is defined as the amount of the

toluene insoluble fraction that is lost on ignition at 820 K (Crittenden *et al* (1992)). The remainder of the deposit, classified as ash, could then be subjected to elemental analysis.

The ASTM standard test method (ASTM D 893 - 92) specifies the use of glassware to dissolve the various fractions, with transfer of insoluble material for weighing by repeated washing. Soxhlet extraction requires no transfer of the insoluble materials for drying and weighing and was therefore considered to be superior to the standard method (ASTM D 893 - 92) in this respect.

Soxhlet extraction is based around the use of Cellulose extraction thimbles which allow the organic solution to pass through its walls freely whilst retaining the insoluble contents. Following Soxhlet extraction the samples were then placed in an oven at 105 °C to remove the remaining solvent from the cellulose thimble and deposit sample.

4.2.16 Sample collection

The collection of the sample was considered to be an important step in making representative analyses of the deposits. However, as deposit analysis was not the main focus of the project, a trade off between care in the recovery of the sample and time available had to be made.

Once the rig was cooled and dismantled, residual oil on the tube surface was allowed to drain from the test section by standing it vertically. Once a period of time had elapsed a visual inspection of the test section was conducted in order to identify whether the deposition of fouling material had occurred in the heated portion only, or over the entire length of the test section. After visual inspection, the fouling deposits were collected by repeated insertion and removal of a HiTRAN® insert which removed any remaining

---

† American Society of Testing and Materials

surface deposits. The HiTRAN® insert was used because the wire matrix retained very little fouling deposit once removed from the tube. It also permitted the collection of strongly adhered deposits immediately next to the tube surface. All of the deposits removed from the test section were stored in collection jars for subsequent analysis.

From Run 8 onwards, the bulk cooler, described previously, was used to reduce the shutdown time of the test facility from 5 hrs to 2 hrs. However, the continuous re-circulation of the test fluid at high velocity (> 4.0 m s^{-1}) through the test section might have resulted in the removal of a significant quantity of weakly adhered foulant from the surface of the test section tubing during the cooling down phase. As a consequence, after Run 8, insufficient amounts of deposit were collected for analysis due to the greater amount of free oil from the tube sides included in the sample.

4.2.16.1 Results of the deposit analysis

Visual inspection of the test sections revealed that notable accumulation of foulant material had occurred only in the heated portions of test sections. The deposits removed from the heated section were found to be soft and appeared to have a high free oil content. This was to be expected as the removal of the deposit unavoidably involved scraping the entire length of the test section which had a layer of oil on the surface even after standing to drain. The results of the analyses for resin and free oil, asphaltenes and coke contents are summarised in Table 4.18:

Table 4.18 Results of deposit analysis

Run	Test section	Velocity ($m\ s^{-1}$)	Content (%) Resin and free oil	Asphaltenes	Coke
2	1	2.0	85.20	13.70	1.10
	2	2.0	76.80	21.70	1.50
3	1	2.0	78.00	21.00	1.10
	2	2.0	71.40	26.90	1.80
4	1	1.0	82.60	16.30	1.10
	2	2.0	78.10	20.60	1.30
5	1	2.0	85.90	13.40	0.70
	2	0.4	78.20	20.70	1.10
6	1	0.4	76.90	22.00	1.10
	2	2.0	81.80	16.70	1.60
7	1	2.0	79.60	19.00	1.40
	2	1.5	81.30	17.60	1.10
8	1	0.8	85.80	13.00	1.30
	2	2.0	89.30	9.90	0.80
		Average	80.78	18.04	1.21

The results show no discernible trend between experimental conditions and asphaltene content. The asphaltene content of the Maya crude was approximately 10% whilst the average deposit asphaltene content was approximately 18%, an increase of approximately 8% in the deposit. This may be indicative of formation of further quantities of asphaltenes by the thermal degradation of resins, or the concentration of the existing asphaltenes on the heat transfer surface, or a combination of both.

The resin and free oil content of the samples was higher than would be expected. This was almost certainly due to the presence of significant quantities of free oil removed from the sides of the tube that was unavoidably included when removing the deposit for analysis. However, these results are in general agreement with Takemoto (1993), who also found an unexpectedly high resin and free oil content.

The high organic content in these samples compared with industrial samples can be attributed to the recovery methods. In industrial plant, circulation of a lighter petroleum fraction followed by steaming of the equipment is not uncommon (Crittenden et al (1992)). The use of fluids to flush the exchanger would most likely remove a significant amount of the free oil, light hydrocarbons and weakly adhered deposits from the tube surface. These actions result in a resin and free oil content of approximately 50%. As such these deposit analyses must be interpreted with caution.

4.3 Experimentation with tubes fitted with inserts

HiTRAN® inserts manufactured by Cal-Gavin have been extensively used in the refining industry to reduce fouling rates, reduce asymptotic fouling resistances and intensify existing heat transfer equipment. This is due to a number of reasons that centre around ease of installation, flexibility and relatively low cost. The HiTRAN® insert consists of a number of loops protruding from a central supporting spine, the density being determined by the number of loops per unit length.

In order to study the effects of both loop wire diameter and insert density on fouling rates, HiTRAN® inserts with different insert densities and loop wire diameters were used. In all cases the support spine was 1.22 mm in diameter. The densities and wire diameters used in this study are summarised in Table 4.19:

Table 4.19 Densities and wire diameters of HiTRAN® inserts

Name	Density (Loops m^{-1})	Loop wire diameter (mm)
Very Low Density Insert (VLDI)	~200	0.38 & 0.63
Low Density Insert (LDI)	~290	0.38 & 0.63
Medium Density Insert (MDI)	~420	0.38 & 0.63

In the text that follows, the insert will be annotated by the density followed by the wire diameter used in the support spine and loop. For example, a low density insert with a support spine diameter of 1.22 mm and a loop wire diameter of 0.63 mm will be referred to as "LDI (1.22; 0.63)".

Although higher insert densities of 650 loops m^{-1} were supplied by the manufacturer, the maximum power output of 4 kW from the electrical heaters in the test rig was insufficient to attain a surface temperature of 250 °C with a flow velocity of 2.0 m s^{-1}. Furthermore, the flow meters were not suitable for measuring the low volumetric flow-rates required to achieve suitable velocities to conduct useful studies of these high density inserts. Therefore, only VLDI, LDI and MDI inserts were studied. To assess the impact of the insert matrix on HiTRAN® performance, an insert with a matrix covering only part of the total length was used. This is identified by "Int." in the following sections.

The ranges of velocities and surface temperatures used during the insert study were approximately the same as those that occur in industrial shell and tube heat exchange equipment fitted with inserts (Crittenden *et al* (1992)). They are summarised in Table 4.20 to Table 4.24. A cross in the table indicates this run was not carried out. All velocities with inserts present are superficial, i.e. empty tube, velocities.

Table 4.20 Summary of VLDI (1.22; 0.63 & 0.38) experimental conditions

Velocity ($m\ s^{-1}$)	Reynolds Number	Temperature (250°C)	
		(1.22; 0.38)	(1.22; 0.63)
1.5	13,000	5	3
2.0	18,000	3	3

Table 4.21 Summary of LDI (1.22; 0.63 & 0.38) experimental conditions at 250 °C

Velocity ($m\ s^{-1}$)	Reynolds Number	Temperature (250°C)		
		Int.[§] (1.22; 0.38)	(1.22; 0.38)	(1.22; 0.63)
0.5	3,000	5	5	3
1.0	8,500	5	5	3
1.5	13,000	5	3	3
2.0	18,000	3	3	3

[§] Int. Signifies an intermittent insert with insert matrix covering only part of the insert length.

Table 4.22 Summary of MDI (1.22; 0.63 & 0.38) experimental conditions at 250 °C

Velocity ($m\ s^{-1}$)	Reynolds Number	(1.22; 0.38)	(1.22; 0.63)
0.5	3,000	3	3
1.0	8,500	3	3
1.5	13,000	3	3
2.0	18,000	3	3

Table 4.23 Summary of MDI (1.22; 0.63 & 0.38) experimental conditions at 265 °C

Velocity ($m\ s^{-1}$)	Reynolds Number	(1.22; 0.38)	(1.22; 0.63)
0.5	3,000	3	5
1.0	8,500	3	5
1.5	13,000	3	5
2.0	18,000	5	5

Table 4.24 Summary of MDI (1.22; 0.63 & 0.38) experimental conditions at 270 °C

Velocity ($m\ s^{-1}$)	Reynolds Number	(1.22; 0.38)	(1.22; 0.63)
0.5	3,000	3	5
1.0	8,500	5	5
1.5	13,000	5	5
2.0	18,000	5	5

4.3.1 The effect of very low density inserts (VLDI) on fouling rates

The lowest insert density (VLDI) was approximately 200 loops per metre. This insert was representative of the minimum practicable density, and is generally not available commercially. In comparison with bare tubes, tubes containing VLDI required greater power to attain nominally identical initial surface temperature. This is to be expected as the insert increases the internal heat transfer coefficient. The higher density LDI inserts were used as a benchmark. Table 4.20 summarises the conditions of the VLDI test study. The experimental results of the VLDI runs conducted at 250 °C are summarised in Table 4.25 and shown in Figure 4.24. Bare tube experimental data are included for comparison.

Table 4.25 Summary of experimentation conditions for VLDI runs

Run	Test Section	Insert	Velocity ($m\ s^{-1}$)	Linear Fouling Rate $x\ 10^5$ ($m^2\ K\ W^{-1}\ h^{-1}$)
41	1	VLDI (1.22; 0.38)	2.0	25.90
	2	LDI (1.22; 0.63)	2.0	18.00
45	1	VLDI (1.22; 0.63)	2.0	2.81
	2	LDI (1.22; 0.63)	2.0	2.20
48	1	VLDI (1.22; 0.63)	1.5	14.90
	2	LDI (1.22; 0.38)	1.5	3.42

Note: Bulk pressure - 15 bar

Bulk temperature - 150 °C

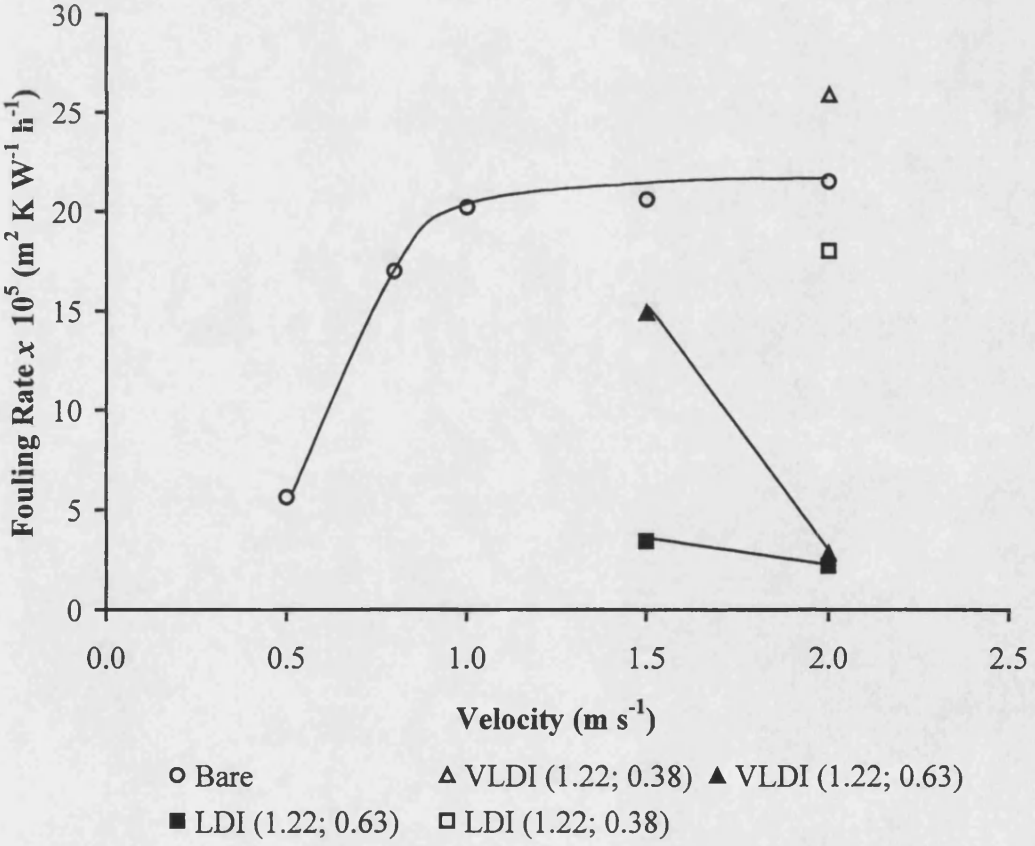

Figure 4.24 Fouling rate against velocity for VLDI at 250 °C

These results show that the VLDI (1.22; 0.38) seems to have little affect on the fouling rate compared with the bare tube case and with the tube containing the benchmark LDI (1.22; 0.38) at nominally identical conditions (2.0 m s^{-1} and 250 °C). Whilst the insert fouling rate was greater than the average bare tube fouling rate, it was within the range of experimental values found with bare tubes. Using a higher loop wire diameter (0.63 mm) under nominally identical conditions, the VLDI (1.22; 0.63) was found to be as effective at reducing the fouling rate at 2.0 m s^{-1} as the higher density LDI with the same loop wire diameter (0.63 mm).

The difference in fouling rates between the VLDI (1.22; 0.38) and VLDI (1.22; 0.63) can be attributed to a higher loop wire diameter creating a relatively more turbulent flow regime with the VLDI (1.22; 0.63), thereby promoting greater shear removal of surface deposits.

Experiments conducted at the same initial surface temperature of 250 °C but at a lower velocity (1.5 m s^{-1}) reveal that the fouling rate was increased from the values for 2.0 m s^{-1} for both the VLDI (1.22; 0.63) and the benchmark LDI (1.22; 0.63). However, the increase in fouling rate for the VLDI (1.22; 0.63) was much greater than that for the benchmark LDI (1.22; 0.63). The differences in fouling rate between the two insert densities with a fluid velocity of 1.5 m s^{-1} can be attributed to the relatively more turbulent regime with more loops in the higher density LDI (1.22; 0.63) promoting a greater shear removal of surface deposits.

The greater difference in fouling rates for a velocity of 1.5 m s^{-1} reducing to zero at 2.0 m s^{-1} might be indicative of a critical velocity, above which a variation in insert density has little effect.

The effect of velocity on fouling rates using the VLDI (1.22; 0.63 & 0.38) at higher temperatures was not studied due firstly to its relatively poor performance in comparison with the LDI and secondly the limited time available.

4.3.2 The effect of low density inserts (LDI) on fouling rates

The low density inserts, labelled LDI, had a loop density of approximately 290 loops per metre. In comparison with bare tubes, tubes containing LDI inserts required greater power to attain nominally identical initial surface temperatures. This is to be expected as inserts increase the internal heat transfer coefficient.

Averaging the results of experiments conducted at nominally identical conditions, the fouling rates for the low density inserts at the two loop wire diameters and configurations are summarised in Table 4.26 and Table 4.27 and shown in Figure 4.25. Bare tube experimental data are included for comparison.

Table 4.26 Summary of experimentation conditions for LDI runs

Run	Test Section	Insert	Velocity ($m\ s^{-1}$)	Linear Fouling Rate $x\ 10^5$ ($m^2\ K\ W^{-1}\ h^{-1}$)
36	1	Bare	2.0	20.10
	2	LDI (1.22; 0.63)	2.0	0.44
37	1	Bare	2.0	17.80
	2	LDI (1.22; 0.63)	2.0	2.63
38	1	MDI (1.22; 0.63)	2.0	1.21
	2	LDI (1.22; 0.63)	2.0	1.76
40	1	LDI (1.22; 0.38)	2.0	3.11
	2	LDI (1.22; 0.63)	2.0	14.70

Note: Bulk pressure - 15 bar

Bulk temperature - 150 °C

Table 4.27 Summary of experimentation conditions for LDI runs

Run	Test Section	Insert	Velocity ($m\ s^{-1}$)	Linear Fouling Rate $x\ 10^5$ ($m^2\ K\ W^{-1}\ h^{-1}$)
41	1	VLDI (1.22; 0.38)	2.0	25.90
	2	LDI (1.22; 0.38)	2.0	18.00
42	1	LDI (1.22; 0.63)	2.0	2.55
	2	MDI (1.22; 0.38)	2.0	1.58
43	1	LDI (1.22; 0.63)	1.0	25.50
	2	Bare	1.0	48.70
45	1	VLDI (1.22; 0.63)	2.0	2.81
	2	LDI (1.22; 0.63)	2.0	9.10
46	1	LDI‡ (1.22; 0.38)	2.0	18.20
	2	LDI (1.22; 0.38)	2.0	7.10
48	1	VLDI (1.22; 0.63)	1.5	14.90
	2	LDI (1.22; 0.38)	1.5	3.42
49	1	LDI (1.22; 0.63)	1.0	17.10
	2	-	-	
50	1	LDI (1.22; 0.63)	0.5	23.60
	2	-	-	

Note: ‡ interrupted

Bulk pressure - 15 bar

Bulk temperature - 150 °C

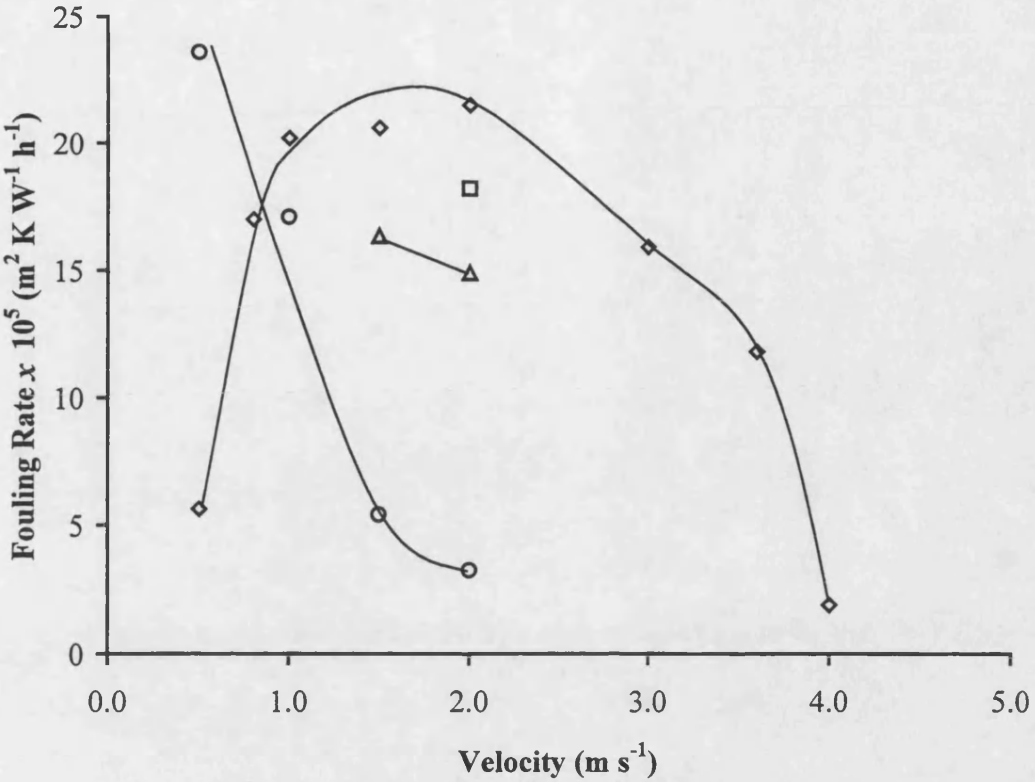

Figure 4.25 Fouling rate against velocity for LDI at 250 °C

In runs with the LDI (1.22; 0.63) it was found that the fouling rate reduced markedly as the velocity was increased. At the lowest velocity (0.5 m s^{-1}) the LDI (1.22; 0.63) fouling rate was comparable with that found for bare tubes at the benchmark of 2.0 m s^{-1}. With bare tubes operated above 2.0 m s^{-1} the fouling rate was found to decrease markedly with increasing velocity, indicating kinetic control. The decrease in fouling rate experienced with LDI (1.22; 0.63) as velocity increased from 0.5 m s^{-1} would be expected if the fouling rate were kinetically controlled.

For LDI (1.22; 0.38) it was also found that the fouling rate was decreased with increasing velocity. However, the smaller wire diameter of LDI (1.22; 0.38) did not provide such a large reduction in fouling rate as occurred with the LDI (1.22; 0.63). This can be attributed to the greater turbulence created by the higher (0.63 mm) loop wire diameter. Higher loop wire diameters protrude further into the bulk fluid, creating

a greater disturbance to the fluid flow. This increases the turbulence in the tube, thereby promoting greater mass transfer. Since the fouling rate reduces with increasing velocity, it is suggested that the attachment process is affected by velocity, perhaps in the manner suggested by Epstein (1983).

In order to assess further the effect of the insert matrix on HiTRAN® performance the interrupted LDI (1.22; 0.38) had an insert matrix only on the first half it length (280mm) compared with 560 mm for the normal insert. This meant that the matrix terminated 20 mm before the first set of thermocouples in the test section, as illustrated in Figure 4.26.

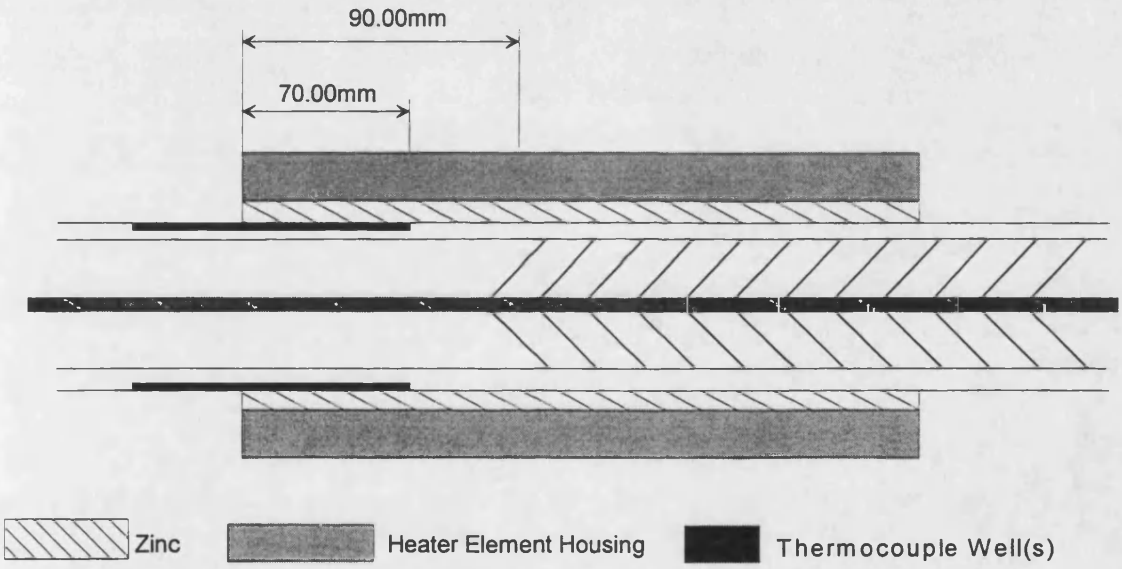

Figure 4.26 Interrupted LDI

As seen in Figure 4.25 the fouling rate for the interrupted LDI (1.22; 0.38) was found to be lower than for the bare tube at nominally identical conditions. However, the fouling rate of the interrupted LDI (1.22; 0.38) was found to be greater than for the nominally identical non-interrupted LDI (1.22; 0.38). This can be explained by the reformation of the boundary layer after the fluid has exited the interrupted insert matrix. This experiment demonstrates that whilst an interrupted insert can have a beneficial effect on the fouling rate, the maximum fouling reduction benefit is gained within the matrix itself.

The effect of velocity on fouling rates using the non-interrupted and interrupted LDI (1.22; 0.38) were not studied further due to their poorer performance in comparison with LDI (1.22; 0.63).

4.3.3 The effect of medium density inserts (MDI) on fouling rates

The highest density used in the research, labelled MDI, is representative of the average density supplied to industry by the manufacturer. In comparison with bare tubes, tubes containing MDI inserts again required greater power to attain nominally identical initial surface temperatures. As with the previous inserts, two wire loop diameters were studied; a low loop wire diameter (0.38 mm) and a high loop wire diameter (0.63 mm). The effect on the fouling rate with the higher diameter was studied only at 250 °C. The low wire diameter (0.38 mm) was studied in greater detail with runs being conducted at 250 °C, 265 °C and 270 °C. Due to limitations on the power output of the test sections only one velocity (0.5 m s^{-1}) was studied at the highest temperature of 270 °C. The power limitation also prevented the study of MDI (1.22; 0.38) at 280 °C.

The results for the medium density inserts at the two alternate loop wire diameters and an initial surface temperature of 250 °C are shown in Table 4.28 and Figure 4.27. The results of trials conducted at 265 °C with MDI (1.22; 0.38) are shown in Table 4.29 and Figure 4.28, and the single result for MDI (1.22; 0.38) at 270 °C is shown in Table 4.30 and Figure 4.29. Bare tube results are shown for comparison.

Table 4.28 Summary of experimentation conditions for MDI runs at 250 °C

Run	Test Section	Insert	Velocity ($m\ s^{-1}$)	Linear Fouling Rate $x\ 10^5$ ($m^2\ K\ W^{-1}\ h^{-1}$)
35	1	Bare	2.0	18.60
	2	MDI (1.22; 0.63)	2.0	2.22
38	1	MDI (1.22; 0.63)	2.0	1.21
	2	LDI (1.22; 0.63)	2.0	1.76
42	1	LDI (1.22; 0.63)	2.0	2.55
	2	MDI (1.22; 0.38)	2.0	1.58
44	1	MDI (1.22; 0.38)	2.0	1.75
	2	MDI (1.22; 0.38)	1.0	9.10
51	1	MDI (1.22; 0.38)	1.5	6.92
	2	-	-	-
52	1	MDI (1.22; 0.38)	1.0	16.10
	2	-	-	-
53	1	MDI (1.22; 0.38)	0.5	24.80
	2	-	-	-
54	1	MDI (1.22; 0.63)	1.0	16.90
	2	-	-	-
55	1	MDI (1.22; 0.63)	0.5	22.40
	2	-	-	-
56	1	MDI (1.22; 0.63)	1.5	1.11
	2	-	-	-

Note: Bulk pressure - 15 bar

Bulk temperature - 150 °C

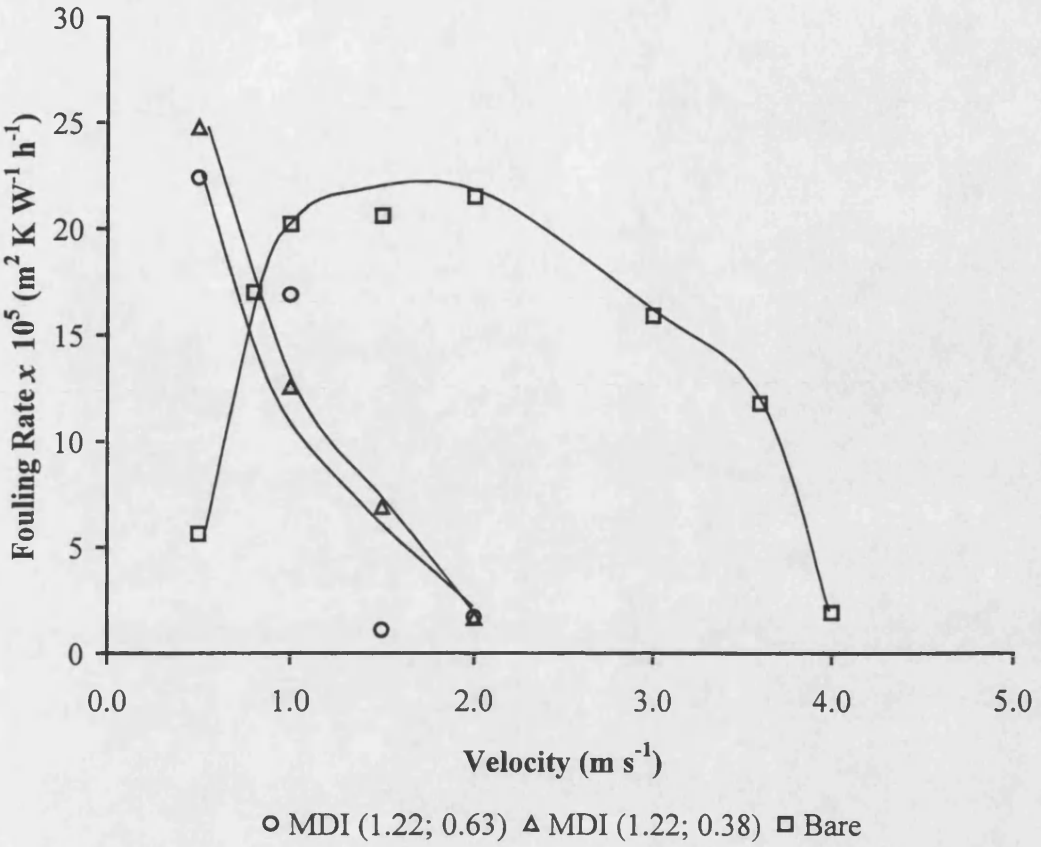

Figure 4.27 Fouling rate against velocity for MDI at 250 °C

Table 4.29 Summary of experimentation conditions for MDI runs at 265 °C

Run	Test Section	Insert	Velocity ($m\ s^{-1}$)	Linear Fouling Rate $x\ 10^5$ ($m^2\ K\ W^{-1}\ h^{-1}$)
57	1	MDI (1.22; 0.38)	1.0	26.70
	2	-	-	-
58	1	MDI (1.22; 0.38)	0.5	34.80
	2	-	-	-
59	1	MDI (1.22; 0.38)	1.5	16.70
	2	-	-	-

Note: Bulk pressure - 15 bar

Bulk temperature - 150 °C

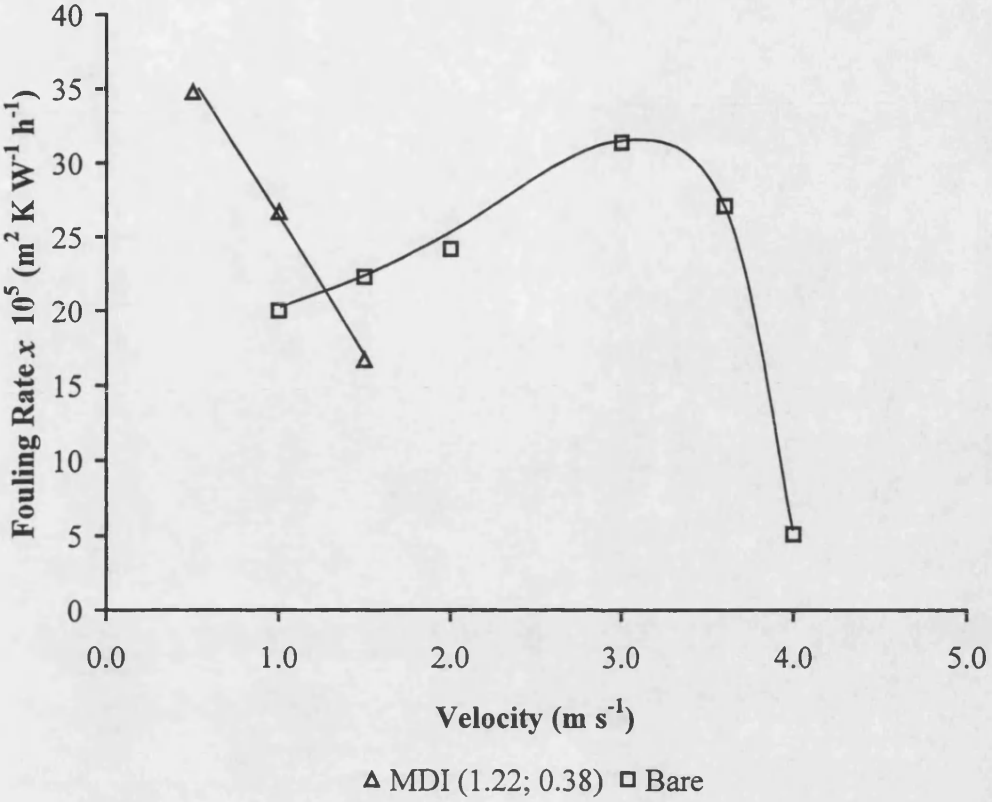

Figure 4.28 Fouling rate against velocity for MDI (1.22; 0.38) at 265 °C

Table 4.30 Summary of experimentation conditions for MDI runs at 270 °C

Run	Test Section	Insert	Velocity ($m\ s^{-1}$)	Linear Fouling Rate $x\ 10^{-5}$ ($m^2\ K\ W^{-1}\ h^{-1}$)
60	1	MDI (1.22; 0.38)	0.5	64.3
	2	-	-	-
61	1	MDI (1.22; 0.38)	1.0	Not enough power
	2	-	-	-

Note: Bulk pressure - 15 bar

Bulk temperature - 150 °C

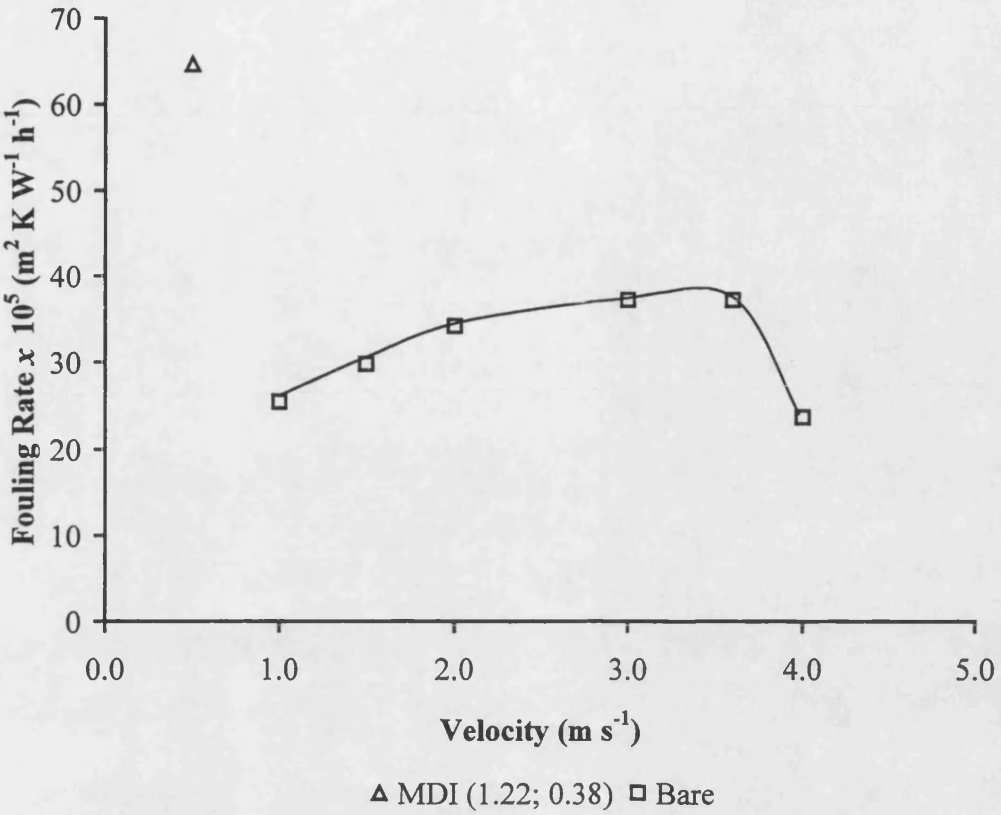

Figure 4.29 Fouling rate against velocity for MDI (1.22; 0.38) at 270 °C

In runs with MDI (1.22; 0.38) and MDI (1.22; 0.63) at 250 °C it can be seen from Figure 4.27 that increases in velocity towards 2.0 m s^{-1} resulted in decreased fouling rates. At the lowest velocity used (0.5 m s^{-1}) the fouling rates were comparable with those found with bare tubes at the higher velocity 2.0 m s^{-1}. In experiments conducted with bare tubes the fouling rate was found to decrease with increasing velocity beyond 2.0 m s^{-1}, indicating kinetic control. The decrease in the MDI fouling rates as velocity was increased from 0.5 m s^{-1} was therefore anticipated. Both inserts performed similarly, indicating that at this density (420 loops m^{-1}) the variation in wire diameter does not have a significant effect on the fouling rate.

In runs with MDI (1.22; 0.38) at 265 °C, Figure 4.28shows that increases in velocity up to 1.5 m s^{-1} resulted in reduced fouling rates. At the lowest velocity (0.5 m s^{-1}) the fouling rate was comparable to that found in bare tubes at 3.0 m s^{-1}. In experiments conducted with bare tubes the fouling rate was found to decrease with increasing

velocity beyond 3.0 m s^{-1}, indicating kinetic control at the higher velocities. Therefore the decrease in fouling rate experienced with MDI (1.22; 0.38) as the velocity increased from 0.5 m s^{-1} was to be expected.

Only one trial with MDI (1.22; 0.38) was completed at 0.5ms^{-1} because of power limitations in the test section. It was found that the fouling rate at 0.5ms^{-1} was greater for tubes containing the MDI (1.22; 0.38) than bare tubes. Indeed the fouling rate was greater than the maximum fouling rate experienced by bare tubes. Due to time constraints, duplicate experiments were not possible. Therefore, it was not possible to draw any formative conclusions from this single result. However, the higher fouling rate experienced by the tube containing the MDI (1.22; 0.38) when compared to bare tubes is in agreement with previous experiments.

These results demonstrate that inserts can reduce fouling at velocities greater than 1.5m s^{-1}, regardless of their density or loop diameter. Their use must be considered carefully however. It must be remembered that plant operators rarely operate their equipment at constant tube surface temperatures, as much greater power would required to maintain constant surface temperatures. At constant heat flux the presence of inserts could result in lower surface temperatures even at lower velocities, thereby reducing the overall fouling rate by reducing reaction rates.

4.3.4 Pressure drop and friction factor

Pressure drop in tubes is dependent on a number of criteria, predominantly fluid velocity, viscosity and the complexity of the flow channel. Installing inserts increases the complexity of the flow channel by creating a more tortuous route for the fluid to flow through. In comparison with bare tubes at identical velocities, the increased complexity of the flow channel in the insert matrix creates increased turbulence,

resulting in greater pressure drops. This can be limiting factor when assessing the relative benefits of installing an insert.

Under nominally identical operating conditions, tubes fitted with inserts were found to experience pressure drops between 5 and 17 times higher than those for bare tubes. It was also found that the pressure drop did not vary measurably throughout the duration of the experiment as fouling occurred. The pressure drops are summarised in Appendix C and shown in Figure 4.30.

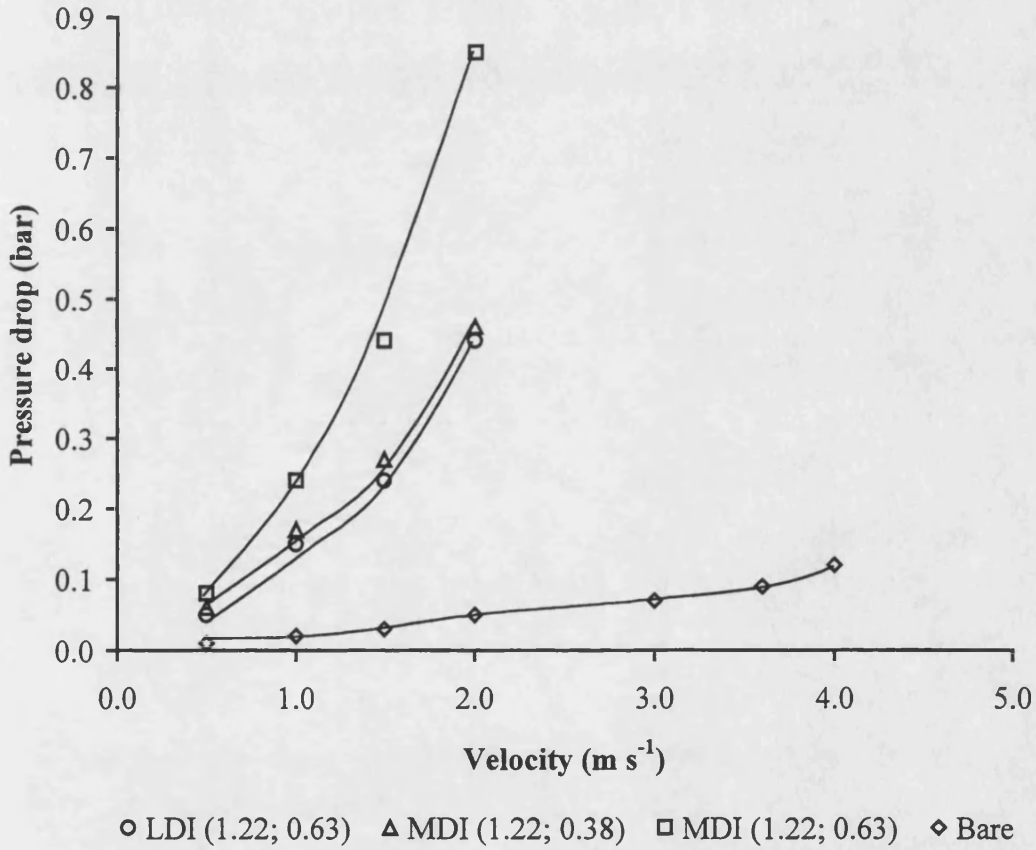

Figure 4.30 Variation in pressure drop with velocity

Friction factors are a function of velocity, physical properties of the fluid and the nature of the tube surface. Under nominally identical operating conditions the friction factor can vary by an order of magnitude, depending on the perceived surface roughness. The surface roughness can be considered to be representative of the average deviation from a mean of the surface topography. Surface roughness is quantified by the ratio of the

average height of the roughness to the tube diameter. For a given tube diameter the greater the height of the interruption, the rougher the tube is perceived to be.

Using equation (4.6) values of j_f were derived from experimental data taken during the fouling experiments. The values of j_f were then correlated against Reynolds number (Re), and are shown in Figure 4.31 and Figure 4.32. Equations based on the best least mean squares fit of the data for the inserts LDI (1.22; 0.63), MDI (1.22; 0.38) and MDI (1.22; 0.63) are given by equations (4.15), (4.16) and (4.17) respectively:

$$j_f = 2.5525\,\mathrm{Re}^{-0.3232} \tag{4.15}$$

$$j_f = 5.9642\,\mathrm{Re}^{-0.4061} \tag{4.16}$$

$$j_f = 1.0406\,\mathrm{Re}^{-0.1680} \tag{4.17}$$

Friction factor values for LDI (1.22; 0.63), MDI (1.22; 0.38) and MDI (1.22; 0.63) were found to be approximately ten times the values experienced in the bare tube operating under nominally identical conditions. MDI (1.22; 0.63) was found to exhibit the greatest increase in friction factor, followed by the MDI (1.22; 0.38) and then LDI (1.22; 0.63).

HiTRAN® inserts are held in place by spring action of the wire loops on the tube surface. The loop on the tube surface can be considered to have increased the surface roughness. Consequently the resulting increases in friction factor for a given velocity were expected.

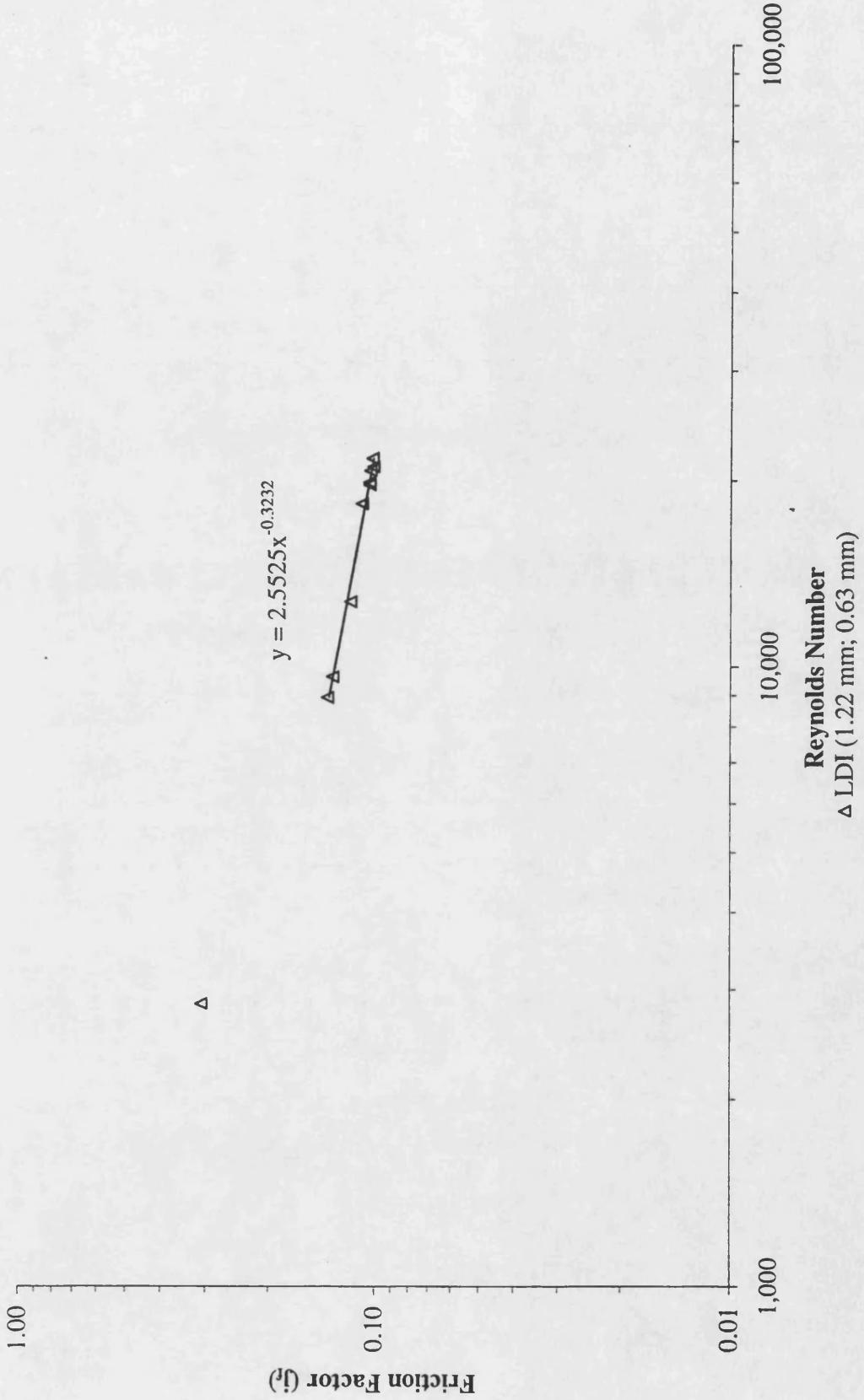

Figure 4.31 Variation in friction factor with Reynolds number for LDI

Figure 4.32 Variation in friction factor with Reynolds number for MDI

With all the inserts, a discontinuity in j_f at a Reynolds number of approximately 8,000 can be seen. This is at a slightly lower Re compared with the experimental results for the bare tubes, in which the discontinuity occurred at a Reynolds number of approximately 10,000. This is indicative of inserts establishing a turbulent flow regime at somewhat lower Reynolds numbers compared with bare tubes.

4.3.5 Heat transfer factor

Values of j_h were calculated using equation (4.9), using data from heat transfer measurements taken during the fouling experiments. These values were then correlated with Reynolds number (Re), the plots being shown in Figure 4.33 and Figure 4.34. Equations based on the best least mean squares fit of the data for inserts LDI (1.22; 0.63), MDI (1.22; 0.38) and MDI (1.22; 0.63) are given by equations (4.18), (4.19) and (4.20) respectively:

$$j_f = 0.2485\,\mathrm{Re}^{-0.3549} \tag{4.18}$$

$$j_f = 0.51486\,\mathrm{Re}^{-0.4337} \tag{4.19}$$

$$j_f = 0.7486\,\mathrm{Re}^{-0.4653} \tag{4.20}$$

All the inserts were found to have higher heat transfer factors in comparison with values derived from experimental data for bare tubes under nominally identical operating conditions. MDI (1.22; 0.63) was found to exhibit the greatest increase in heat transfer factor, followed by MDI (1.22; 0.38) and then LDI (1.22; 0.63). This is to be expected as the higher the insert density and loop wire diameter the greater the turbulence. No discontinuity was noted in the j_h - Re plots.

Figure 4.33 Variation in heat transfer factor with Reynolds number for LDI

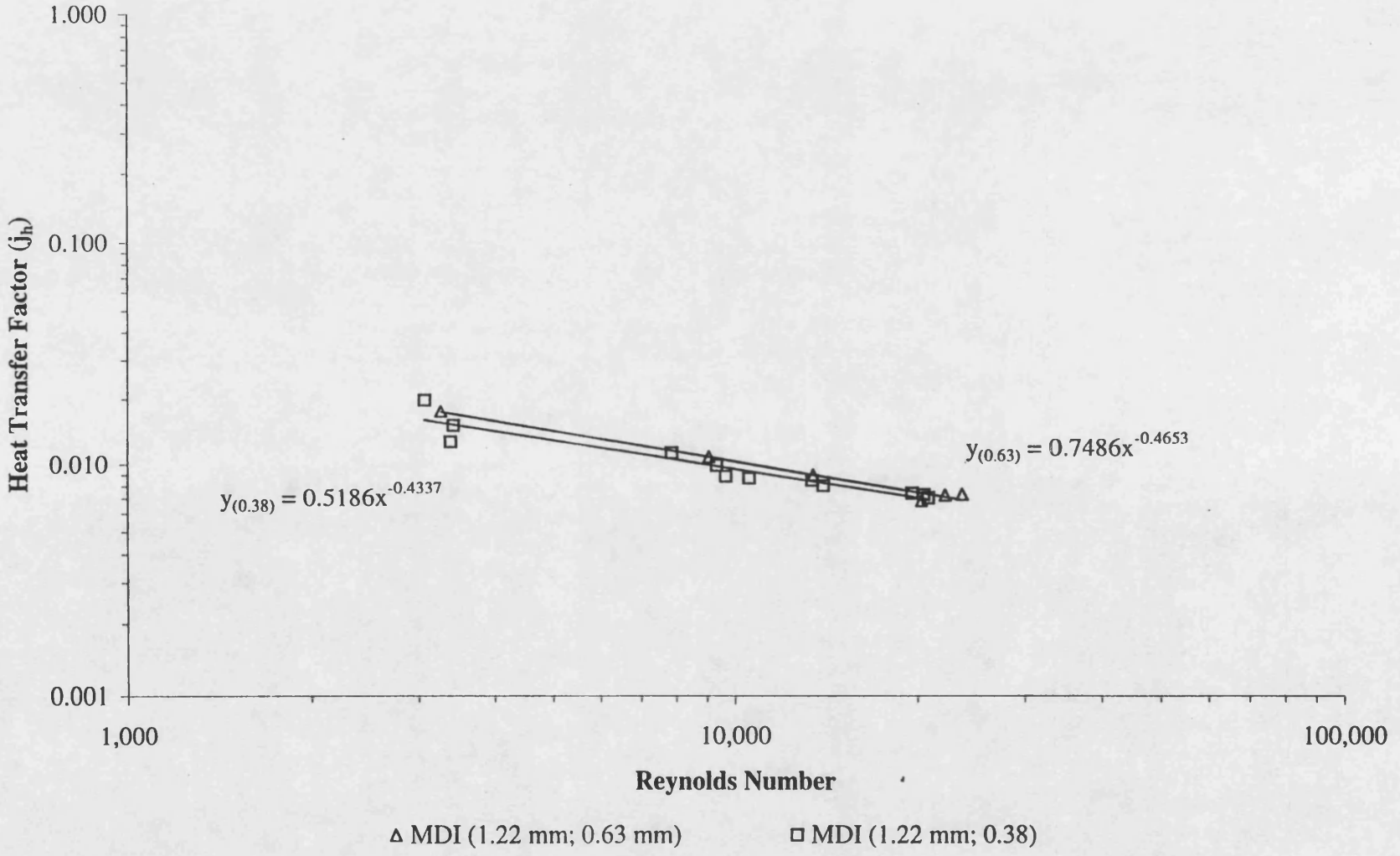

Figure 4.34 Variation in heat transfer factor with Reynolds number for MDI

4.3.6 Variation in heat transfer coefficient

Heat transfer coefficients are primarily functions of fluid properties, fluid velocity and flow regime. Variations in flow regime can have significant effects on the coefficient. Increases in turbulence arising from a greater velocity or greater complexity of flow channel generally result in an increase in the heat transfer coefficient.

In heat transfer equipment the reciprocal of U_O can be considered to be comprised of the sum the individual film heat transfer resistances and other resistances, both internal and external. The test section used as part of this study used electrically powered heating elements surrounding the tube. In this way contributions to overall resistance from external film resistances are irrelevant. Placing inserts into bare tubes has been shown to increase turbulence significantly. Therefore, an increase in internal heat transfer coefficient is expected. The variation in internal heat transfer coefficient with velocity and insert geometry is shown Figure 4.35.

MDI (1.22; 0.63) exhibited the greatest increase in heat transfer coefficient for a given velocity, followed by MDI (1.22; 0.38) and then LDI (1.22; 0.63). these results are to be expected as the higher the insert density and loop wire diameter the greater the turbulence which promotes greater heat transfer.

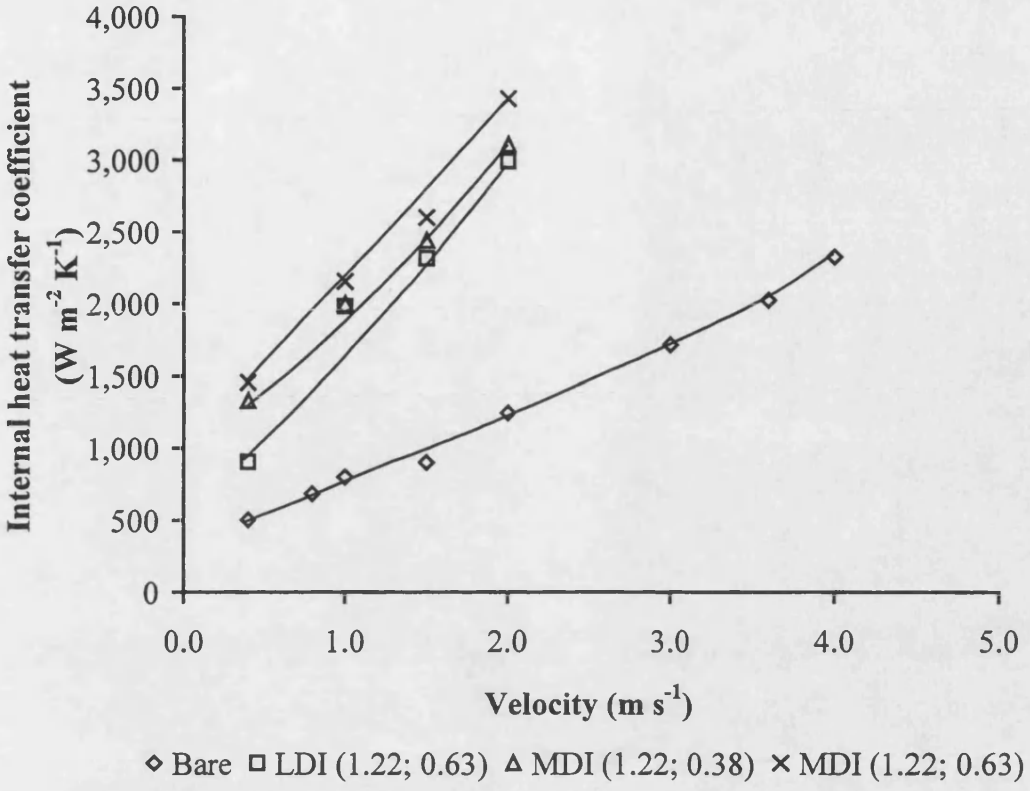

Figure 4.35 Variation in heat transfer coefficient for bare tubes and inserts

4.3.7 Selection of a HiTRAN® insert

The insert study has shown that under certain circumstances inserts can significantly reduce fouling rates compared with bare tubes. Generally, higher insert densities and higher loop wire diameters resulted in greater reductions in fouling rates. Additionally, the effect of variations in loop wire diameter became less apparent as insert densities were increased. Heat transfer coefficients were found to increase with both insert density and loop wire diameter. However, medium density inserts were found to be more effective at reducing fouling rates when compared with lower density inserts at the lower velocities (<1.5 m s^{-1}).

The aim of this project was to quantify the effects of HiTRAN® inserts on fouling from crude oil, to enable their confident implementation in shell and tube heat exchange equipment. In practice, exchangers would be operated on the basis of a desired outlet

temperature of one of the fluids, not on the basis of a desired tube surface temperature. By making use of the improvement in heat transfer coefficient experienced by tubes containing inserts an opportunity could be taken to reduce the linear velocity. This in turn would reduce the pressure drop. This study shows that for MDI similar fouling performance was achieved at significantly lower pressure drops using a lower (0.38 mm) loop wire diameter.

Consequently, the MDI (1.22, 0.38) could offer the plant designer and operator flexibility for a number of reasons, namely:

- its lower pressure drop compared with higher loop wire diameter (0.63 mm) at the same density would allow a slightly higher velocity to be used in an exchanger;

- its greater reduction in fouling rate compared with lower density inserts (VLDI and LDI) at low flow-rates would allows a greater range of velocities to be used. This is especially important during periods of low through put;

- its significantly higher heat transfer coefficient at any given velocity compared with bare tubes and tubes with LDI, means that the designer could optimise the design to achieve lower tube surface temperatures, maintain pressure drops, or a combination of both.

4.3.8 General observations

In general, the change in fouling resistance with time occurred at a constant rate from the beginning of the experiment to its conclusion. Therefore, linear fouling rates could be calculated easily from the experimental data. However, for a few runs the rate of change in the fouling resistance reduced as the experiment progressed, resulting in a falling rate type response.

Whether the fouling rate remained linear or falling rate appeared to be random and did not seem to correlate with particular experimental conditions. The test section design only permitted surface temperatures of up to 400 °C due to the construction method. In many cases experiments were curtailed therefore due to the surface temperature of the test section reaching the operating limit. It is not possible to predict whether the linear or falling rate fouling responses observed in this study would have become asymptotic given sufficient time of operation.

4.3.9 Comments

At the start of this research project one of the underlying concerns was the time available to conduct a suitable number of experimental runs to enable the development of a feasible model for predicting fouling rates in bare tubes and tubes with inserts. In previous studies, fouling runs in excess of 60 hours were not uncommon, resulting in experimental cycles of two weeks per run. These concerns were further compounded by the fragility of the heaters on the test sections, which if more experimental runs were to be completed than in the previous studies, would be more likely to break.

The alterations to the experimental rig described in section 3.5.1 improved the robustness of the test sections, such that no breakage due to handling during the dismantling, cleaning and re-assembly of the rig occurred. However, on two occasions individual heaters malfunctioned as a result of power surges to the heater elements whilst at their limit of operation. Regardless of the two heater failures it is believed that the current design is fit for purpose. However, subsequent design reviews should focus on extending the operating range of the test section and robustness still further, possibly by closer collaboration with the heater manufacturer (Watlow Ltd.).

4.4 Synopsis

This chapter has presented the results of the fouling experiments carried out as part of this research project. Experiments with bare tubes have shown that increases in velocity can either increase or decrease the initial fouling rate depending on the control of the overall rate mechanism. Increases in fouling rates were observed with velocity in situations where by mass transfer control was thought to be dominant. Conversely, under kinetic control fouling rates were seen to decrease with velocity.

Over the range of velocities studied (0.5 m s^{-1} to 4.0 m s^{-1}) the average overall apparent activation energy has been found to be 77.5 kJ $kmol^{-1}$, suggesting that the mechanism is predominantly reaction controlled. However, the apparent activation energy increased with increasing velocity, indicating strong mass transfer influences.

Experimental studies with inserts have found that under nominally identical operating conditions to bare tubes, fouling rates can either be increased or decreased by their presence, again depending on mass transfer or kinetic control of the mechanism. At relatively low velocities (~ 0.5 m s^{-1}) the presence of inserts was found to increase the fouling rate. At relatively high velocities (> 1.0 m s^{-1}) the opposite was observed, and the presence of inserts reduced fouling rates.

Studies with inserts have also revealed evidence of a critical insert density of 290 loops m^{-1}. Below this value variations in both density and loop wire diameter significantly affect the fouling rate. Conversely, above the critical loop density, increasing both density and wire loop diameter appear to have little effect.

5. Modelling hydrocarbon fouling

Altering the physical parameters of heat exchange equipment to optimise performance is often a balance between improving thermal and fouling performance and reducing hydraulic performance. Optimising exchanger performance using accurate thermal, hydraulic and fouling models increases the ability of plant designers and operators to deliver a solution that fits all criteria. Additionally, using accurate fouling models allows mitigation strategies to be assessed quickly without compromising operating plant or investing in extensive pilot scale trials.

The underlying principle in many predictive fouling models is that the fouling rate of the heat exchanger can be modelled in terms of a set of parameters such as temperature, Reynolds number, tube diameter, deposit properties, etc. This implies that there are no significant changes in these properties as the fluid progresses through the exchanger. As such, the results of calculations can be expected to be valid only for the particular position in the heat exchanger at which all these parameters are valid. Some form of averaging is necessary to obtain a value for the fouling resistance that can be applied over the length of the whole exchanger. The fluid composition and conditions encountered in the heat exchanger are the key criteria in determining the dominant fouling mechanism (e.g. scaling, particulate, chemical reaction, etc.) and the generalised mechanism of fouling can be summarised by the following sequence of events (Epstein (1983)):

1. initiation: where chemical reactions occur to form insoluble material,

2. transport: where the foulant particles, or molecules, are transported from the bulk fluid to the heat transfer surface;

3. attachment: where the foulant bonds to the heat transfer surface;

4. removal: where the attached foulant is removed and re-entrained to the bulk fluid;

5. ageing: where the attached deposit is altered and forms a stronger attachment to the heat transfer surface.

Fouling models ideally should incorporate all the above steps, and be able to predict the effect of altering one or more of the parameters such as surface temperature and velocity. In relatively simple systems such as styrene in kerosene (Crittenden, Hout and Alderman (1987)), this is possible, since the hydrocarbon fluid and foulant (formed by the polymerisation of the styrene monomer) have known and easily determined physical properties. In contrast however, the complexity of crude oil means that identifying a single component or mechanism responsible for fouling is not generally possible. The use of simple fouling systems (such as styrene in kerosene) enables effective models to be developed and verified against experimental data. The possibility then exists to adapt such simple models to predict fouling from more complex hydrocarbon fluids.

This chapter presents a historical review of the key fouling models contributing to the model developed as part of this research. The model used will then be fitted to the experimental data that was presented in chapter Four.

5.1 Fouling Models

Fouling occurs when the foulant accumulates on the heat transfer surface in sufficient quantity to affect measurably the performance of the heat exchanger. Early fouling models assume that once fouling reactions have taken place, and the fouling particles are in bulk solution, the overall fouling rate at time "t" ($R_{f(t)}^{\bullet}$) can be modelled as the difference between the deposition rate (ϕ_d) and the removal rate (ϕ_r) of the foulant (Kern and Seaton (1959)):

$$R^{\bullet}_{f(t)} = \phi_d - \phi_r \tag{5.1}$$

Once there is a zero net rate of accumulation of foulant on the surface, i.e. $\phi_d = \phi_r$, then the fouling resistance can be considered to have attained an asymptotic value. Fouling resistances at any time *"t"*, ($R_{f(t)}$) may be related to the asymptotic fouling resistance (R_f^{∞}) by the use of a time constant (β), as given by equation (2.4) (Kern *et al* (1959)):

$$R_{f(t)} = R_f^{\infty}\left(1 - e^{-\beta t}\right) \tag{2.4}$$

If the asymptotic fouling resistance and time constant are known, then equation (2.4) permits the prediction of fouling rate, and fouling resistance, as a function of time. However, equation (2.4) does not predict the effect that changes in velocity or surface temperature have on fouling rates or resistances.

A study on the effect that velocity has on fouling from sour gas oils showed that increased velocity resulted in reduced asymptotic fouling resistances. Consequently the fouling resistance at any given time was also reduced (Watkinson *et al* (1969)). The initial fouling rate ($R^{\bullet}_{f(0)}$) for this gas oil research was found to be related to T_w and G by an apparent activation energy (E_A) and a pre-exponential factor (A), in an Arrhenius type relationship, described by equation (2.7) (Watkinson *et al* (1970)):

$$R^{\bullet}_{f(0)} = A\frac{e^{\left(\frac{-E_A}{RT_w}\right)}}{G^{1.07}} \tag{2.7}$$

Using an Arrhenius type relationship in fouling models, as in equation (2.7), permits the effect of variations in surface temperature to be predicted. The inclusion of the mass flow term (G) in the denominator also permits study of variations in flow-rate to some

degree. Equation (2.7) predicts that an increase in G, whilst maintaining a constant surface temperature, would result in a decrease in initial fouling rate.

The results of this current study with Maya crude oil have demonstrated that fouling rates can in contrast, increase with increasing velocity, up to a maximum from which subsequent increases in velocity result in the anticipated decrease in fouling rate. Consequently, equation (2.7) is too simplistic to account for the complexity of the mechanism encountered with Maya crude oil.

Alterations in surface temperature and velocity can affect the physical properties of the fluid, which in turn can affect the fouling mechanism. Raising the fluid velocity increases mass transfer rates and reduces the size of the boundary layer film adjacent to the tube wall. Consequently, there is a reduction in the volume of fluid exposed to temperatures greater than the bulk temperature. The combination of increased mass transfer and reduced volume results in a decrease in the time that the fouling particle or precursor is exposed to the higher temperatures in the film (Nelson (1934)). However, the increase in mass transfer and reduction in volume of the boundary film also result in a reduction in the time taken for the fouling particle or precursor to reach the hotter heat transfer surface, possibly resulting in increased fouling rates.

The relationship between fouling rate and velocity is not simple and is the result of mass transfer and chemical kinetic effects. Based on film theory and chemical kinetics, a two step model encompassing mass transfer and chemical kinetics was developed by (Crittenden, Kolaczkowski and Hout (1987)). Mass transfer from the bulk fluid to the film can be represented by a mass flux of the foulant precursor (N_P), and is related to the concentration of the precursor in the bulk fluid (C_{Pb}) and at the interface (C_{Pi}) by the mass transfer coefficient (K_P), as given by equation (5.2) (Crittenden, Kolaczkowski and Hout (1987)):

$$N_P = K_P\left(C_{Pb} - C_{Pi}\right) \tag{5.2}$$

At steady state N_P is balanced by the rate of deposition. Therefore, N_P can be related to the concentration of the foulant precursor at the interface (C_{Pi}) by a reaction rate constant (k_R), as described by equation (5.3) (Crittenden, Kolaczkowski and Hout (1987)). In this equation, the rate is assumed to be first order with respect to the precursor concentration.

$$N_P = k_R C_{Pi} \tag{5.3}$$

N_P can be considered in terms of the growth in foulant deposit thickness (x_f), and characterised by the thermal conductivity of the deposit (k_f) and the density of the deposit (ρ_f). Consequently, the fouling rate at any given time ($R^{\bullet}_{f\,(t)}$) is given by equation (5.4) (Crittenden, Kolaczkowski and Hout (1987)):

$$R^{\bullet}_{f(t)} = \frac{d}{dt}\left(x_f / k_f\right) = \frac{1}{\rho_f k_f}\left\{\frac{C_{Pb}}{\frac{1}{K_P} + \frac{1}{k_R}}\right\} \tag{5.4}$$

The insoluble products of the fouling reactions may be removed back to the bulk fluid by convection or diffusion, if they are weakly attached to the tube surface. However, the two step model illustrated by equation (5.4), does not allow for the re-entrainment of the foulant particle back to the bulk fluid (Crittenden, Kolaczkowski and Hout (1987)).

The two step model (equation (5.4)) was extended to account for re-entrainment of the foulant particle. The three step model incorporates convection of mobile foulant particles back to the bulk fluid. Consequently the build up of the fouling layer can be related to the difference between N_P and the mass flux of foulant removed back to the

bulk fluid (N_f), as described by equation (5.5) (Crittenden, Kolaczkowski and Hout (1987)):

$$\frac{dx_f}{dt} = \frac{1}{\rho_f}\left(N_P - N_f\right) \tag{5.5}$$

The mass flux of the foulant away from the tube surface can be related to the concentration of the foulant at the interface (C_{fi}) and in the bulk fluid (C_{fb}), and by the mass transfer coefficient (K_f), as given by equation (5.6) (Crittenden, Kolaczkowski and Hout (1987)):

$$N_f = K_f\left(C_{fi} - C_{fb}\right) \tag{5.6}$$

Assuming that the concentration of the foulant in the bulk fluid is negligible, the net mass flux of deposition can be given by equation (5.7) (Crittenden, Kolaczkowski and Hout (1987)):

$$R^{\bullet}_{f(t)} = \frac{d}{dt}\left(x_f / k_f\right) = \frac{1}{\rho_f k_f}\left\{\frac{C_{Pb}}{\frac{1}{K_P} + \frac{1}{k_R}} - K_f C_{fi}\right\} \tag{5.7}$$

As deposits build up on the heat transfer surface they become subjected to shear forces exerted by the flowing fluid. Where deposits are weakly attached to the heat transfer surface, or where relatively high shear forces exist, a portion of the deposit may be removed from the surface by the bulk fluid. The rate of removal (in thermal resistance terms) of the deposit through shear action has been considered to be a function of the shear rate (τ), the local thickness of the foulant (x_f), the thermal conductivity of the foulant (k_f) and the deposit structure (ψ), as shown in equation (5.8) (Kern *et al* (1959)):

$$\phi_r = -\frac{\tau x_f}{\psi k_f} \tag{5.8}$$

Under clean condition, i.e. at time *t=0,* there is no deposit and therefore no shear removal term exists. The removal rate can be represented in terms of fouling resistance (R_f), as shown by equation (5.9) (Crittenden, Kolaczkowski and Hout (1987)):

$$\phi_r = -\frac{\tau}{\psi k_f} R_f \tag{5.9}$$

Combining equations (5.7) and (5.9) results in equation (5.10) for the net rate of fouling (Crittenden, Kolaczkowski and Hout (1987)):

$$R^{\bullet}_{f(t)} = \frac{1}{\rho_f k_f}\left\{\frac{C_{Pb}}{\frac{1}{K_P}+\frac{1}{k_R}} - K_f C_{fi}\right\} - \frac{\tau}{\psi k_f} R_f \tag{5.10}$$

This model predicts a complex dependency of fouling rate on the flow rate. Whether the fouling rate increases or decreases with flow rate depends on the relative balance between mass transfer and kinetic effects. However, at time t = 0, no foulant exists at the wall and therefore dissolution and convection back to the wall cannot occur (Epstein (1994)). Even so, when constructing a model for the initial fouling rate ($R^{\bullet}_{f(0)}$), all the sequential stages involved, such as transport and deposition on the surface must be taken in to account.

After any induction period that may have occurred, $R^{\bullet}_{f(0)}$ is governed by the transport of the foulant precursor to the heat transfer surface followed by conversion to a solid product which adheres to the surface (Epstein (1994)).

Based on work carried out by Crittenden, Hout and Alderman (1987) using 1% volume for volume ($^{v}/_{v}$) styrene in kerosene, an overall model has been proposed by Epstein to

relate $R_{f(0)}^{\bullet}$ to the density and thermal conductivity of the foulant (ρ_f and k_f respectively), deposition flux (ϕ) and a stoichiometric factor (m). This is described by equation (5.11) (Epstein (1994)):

$$R_{f(0)}^{\bullet} = \frac{m\phi}{k_f \rho_f} \tag{5.11}$$

The deposition flux (ϕ) may be considered, as before, to be the result of both mass transfer and kinetic mechanisms occurring in series. Mass transfer from the bulk fluid to the reaction surface of the fouling precursor can be considered to be a function of the bulk and surface concentrations (C_b and C_s respectively) and mass transfer coefficient (k_m), as shown by equation (5.12) (Epstein (1994)):

$$\phi = k_m\left(C_b - C_s\right) \tag{5.12}$$

Once at the surface, the reaction of foulant precursor to form a deposit can be related to the surface concentration (C_s) by the rate constant (k_r) and the order of the reaction (n), according to equation (5.13) (Epstein (1994)):

$$\phi = k_r C_s^n \tag{5.13}$$

Combining equations (5.12) and (5.13) yields an overall mass flux equation, equation (5.14) (Epstein (1994)):

$$\phi = \frac{C_b}{\frac{1}{k_m} + \frac{1}{k_r C_s^{n-1}}} \tag{5.14}$$

The mass transfer coefficient (k_m) can be related to the friction velocity (u_c) and Schmidt number (Sc) by a constant (k') assumed to be 11.8 in all cases (Epstein (1994)):

$$k_m = \frac{u_c}{k' Sc^{2/3}} \tag{5.15}$$

The friction velocity (u_c) can be related to the linear velocity (u_m) and the shear rate of the fluid, as expressed by the friction factor (j_f), according to equation (5.16) (Epstein (1994)):

$$u_c = u_m \sqrt{j_f} \tag{5.16}$$

The Schmidt number (Sc) is a function of viscosity (μ), density (ρ) and diffusivity (D_f), according to equation (5.17):

$$Sc = \frac{\mu}{\rho D_f} \tag{5.17}$$

Fouling is a complex phenomenon, but evident only when sufficient material accumulates on the heat transfer surface. For reasons stated before the estimation of a purely kinetic rate for the fouling reaction is difficult. This difficulty may be overcome however by considering the fouling process collectively using a kinetic plus attachment constant. The kinetic plus attachment constant (k_r) is related to the viscosity (μ), apparent activation energy (E_A), tube wall temperature (T_w), density (ρ) and friction velocity (u_c) of the fluid by the universal gas constant (R) and reactivity constant (k"), as shown by equation (5.18) (Epstein (1994)):

$$k_r = \frac{\mu e^{\frac{-E_A}{RT_w}}}{k'' \rho u_c^2} \tag{5.18}$$

The key equations of Epstein's model are (5.11) to (5.18), which have been successfully used to predicted fouling rates at alternate combinations of initial surface temperature and fluid velocities for a 1% ($^v/_v$) styrene in kerosene ideal fouling solution (Epstein

(1994)). The data were supplied by Crittenden from Hout's PhD thesis (Hout (1983)).At various constant surface temperatures the model successfully predicted the increase or decrease in fouling rates as velocity was increased. Further, at relatively high temperatures the model also successfully predicted the velocity beyond which subsequent increases in velocity reduced the fouling rate. The fouling model described by Epstein, will now be adapted to predict the experimental fouling rates from Maya crude oil in the hydrocarbon recycle rig. Before using the model developed by Epstein (1994) a number of physical properties and parameters need to be estimated; these are:

1. Schmidt number;
2. friction velocity;
3. mass flux of foulant;
4. mass and kinetic constants.

5.1.1 Schmidt number

It has been proposed earlier that crude oil fouling rates and asymptotic fouling resistances in heat transfer equipment are affected by the presence, or absence, of insoluble asphaltenes (Lambourn and Durrieu (1983); Eaton and Lux (1984); Dickakian and Seay (1988) and Asomaning and Watkinson (1997)).

Therefore, in the absence of suitable alternatives, the physical properties of asphaltenes are to be used in order to calculate a value of diffusivity that can be used in the calculation of the Schmidt number. The molar volumes (V_a) of asphaltenes are not quoted, and are therefore estimated from the molecular weight (MW_a) and specific gravity (SG_a), using equation (5.19) adapted from Hall and Yarborough (1971):

$$V_a = 1.561 \times 10^{-3} \left(\frac{MW_a}{SG_a^{0.69}} \right)^{1.15} \tag{5.19}$$

Using a molecular weight of 3,000 and a specific gravity of 1.1, the molar volume was found to be 14.43 m^3 $kmol^{-1}$. The diffusivity of the asphaltene (D_a) was then calculated using the association factor (ϕ_{solv}), molecular weight of the solvent (MW_{solv}), viscosity of the solvent (μ_{solv}), and the average film temperature (T_f), according to equation (5.20) (Coulson, Richardson, Skinner and Harker (1993)):

$$D_a = \frac{1.173 \times 10^{-16} \left(\phi_{solv} MW_{solv} \right)^{1/2} T_f}{\mu_{solv} V_a} \tag{5.20}$$

The average fluid film temperature (T_f) is taken to be the mean of the bulk and surface temperatures (T_b and T_w respectively):

$$T_f = \frac{\left(T_w + T_b \right)}{2} \tag{5.21}$$

Crude oil is an undefined solvent and is therefore considered to have an association factor of 1.0 (Coulson, Richardson, Skinner and Harker (1993)). Based on physical property data provided by BP Oil Ltd. and using the API 2B6.1 chart, the molecular weight of the crude was found to be approximately 400. This is shown in Appendix B.

The Schmidt number was then calculated at the combinations of initial surface temperature and linear velocity used in this study. The Schmidt number was found not to vary notably with velocity, but did vary with surface temperature as summarised in Table 5.1. It should be remembered that the bulk temperature was constant for all the experimental runs.

Table 5.1 Variation of calculated Schmidt number with initial clean surface temperature

Surface temperature (°C)	Schmidt number
250	198
265	112
270	92
280	63

These values are in general agreement with the Schmidt numbers found by Epstein (1994) for the fouling of a bare tube in the styrene in kerosene system.

5.1.2 Friction velocity

The friction velocity (u_c) was calculated from equation (5.16) at each of the flow rates and surface temperatures studied. Above 1.0 m s^{-1} for bare tubes using Maya crude, j_f was found to be equal to $0.0181e^{-0.000002Re}$ for Re > 10,000. The results of calculations using equation (5.16) are summarised in Table 5.2. Little variation in u_c with surface temperature arose.

Table 5.2 Calculated values of friction velocity for bare tubes

Velocity (m s^{-1})	
Linear	**Friction**
1.0	0.088
1.5	0.118
2.0	0.159
3.0	0.215
3.6	0.243
4.0	0.259

5.1.3 Mass flux

The fouling deposit was considered to comprise two main constituents, namely coke and free oil trapped in the porous structure formed by the coke. Analysis of the deposits showed that the coke content was approximately 1% of the total mass of the deposit, giving an oil to coke ratio ($X_{o/c}$) of 0.99.

The thermal conductivity of the coke (k_c), was assumed to be 0.11 W m^{-1} K^{-1} at all temperatures (Perry and Green (1984)). The thermal conductivity of the fluid trapped in the deposit (k_{lf}) was calculated using equation (3.3). The overall thermal conductivity of the foulant (k_f) was then calculated by using the weighted average of each of the constituents, as shown by equation (5.22):

$$k_f = \left(X_{o/c} k_{lf}\right) + \left(\left(1 - X_{o/c}\right) k_c\right) \tag{5.22}$$

The mass flux (ϕ) was then calculated at each temperature and flow-rate by rearranging equation (5.11) to yield equation (5.23):

$$\phi = \frac{R^{\bullet}_{f(0)} k_f \rho_f}{m} \tag{5.23}$$

The foulant particles are assumed to behave according to the laws of Brownian motion, therefore the stoichiometric factor (m) is assumed to be 1 at all combinations of velocity and initial surface temperature (Epstein (1994)).

5.1.4 Mass and kinetic coefficients

The mass transfer coefficient (k_m) was calculated using equation (5.15), following the calculation of Sc and u_c.

$$k_m = \frac{u_c}{k' Sc^{2/3}} \tag{5.15}$$

The kinetic plus attachment coefficients (k_r) were calculated using equation (5.18), at each combination of temperature and flow-rate.

$$k_r = \frac{\mu e^{\frac{-E_A}{RT_w}}}{k'' \rho u_c^2} \tag{5.18}$$

5.2 *Application of the fouling model*

The model described by Epstein (1994) has successfully described the fouling of a bare tube by the polymerisation of styrene in kerosene. In this ideal fouling system the mechanism and physical data for the foulant and precursor are relatively well known and documented. However, the complexity of crude oil means that a number of compounds may react to form insoluble products, depositing on the tube surface and causing fouling.

In this section the model proposed by Epstein (1994) will be applied to the experimental data obtained during the course of this study with Maya crude oil. Bare tube fouling experiments have been completed on the parallel flow rig at four different initial surface temperatures and a number of velocities. This combination of initial surface temperatures and flow-rates offers a suitable range of data points by which the model can be adapted and verified. Only data obtained at velocities above 1.0 m s^{-1} have been used to develop the model. This is to ensure that data in the laminar regime is not included.

The results of this study have found that the apparent activation energy (E_A) is dependent on velocity, hence on mass transfer (refer to figure 4.19). Therefore, selection of a single value for E_A to cover the range of bare tube velocities may not be appropriate. Furthermore, increases in fluid turbulence shift the control of the fouling process towards kinetic effects. This is more significant when the tube contains inserts

since an insert promotes greater turbulence at identical linear velocities. The model will be used to explore the effect that E_A has on the mechanism. The model is used in the following manner:

1. set an apparent activation energy
2. iteratively derive the reaction order;
3. calculate the bulk concentration of fouling precursors;
4. predict fouling rates and compare with experimental data

5.2.1 Apparent activation energy

This study has found that E_A increases with velocity ranging from 26 kJ $kmol^{-1}$ at 1.0 m s^{-1} to 149 kJ $kmol^{-1}$ at 4.0 m s^{-1}. This is most likely indicative of the mechanism shifting towards kinetic effects at higher velocities. As mentioned previously, it is unlikely that a single activation energy will be valid for bare tubes and tubes containing inserts. Therefore, in order to identify the combination of activation energy and reaction order that best suits both bare tubes and tubes with inserts over the range of velocities in this study, three trial uses of the model were conducted using the lowest, average and highest apparent activation energies. These values are summarised in Table 5.3:

Table 5.3 Activation energies used in applying the model to the Maya fouling results

	E_A (kJ $kmol^{-1}$)
Case 1	26
Case 2	77
Case 3	149

Using the model in this fashion will help to elucidate the effect that E_A has on the fouling rate.

5.2.2 Reaction order

The calculation of reaction order usually requires knowledge of the dependence of the rate of reaction on the concentration of reactants. However, in this case the concentration and mechanism of the reacting species are not known due to the large number of possibilities. Estimation of this order is further complicated by the dependence of the fouling rate on the mass transfer of the foulant or precursor to the reaction site. The polymerisation of styrene has a reaction order of 5/2, indicating a complex reaction mechanism. It is believed that fouling from crude oil is even more complex compared with styrene polymerisation. Therefore, it is not unreasonable to expect reaction orders of at least 5/2, if not higher, for the Maya crude oil.

5.2.3 Case 1

Initial conditions for Case 1 are summarised in Table 5.4:

Table 5.4 Initial conditions for Case 1

Parameter	Initial Value
E_A (kJ kmol^{-1})	26
n	2.5
k"	1

5.2.3.1 Bulk concentration

Estimating the concentration of fouling precursors in the bulk fluid can be difficult for a number of reasons. The greatest difficulty lies in the fact that a single compound may not responsible for fouling in hydrocarbon systems. Even so, an equation for the calculation of bulk concentration, based on initial reaction rate ($R_{f(0)}^{\bullet}$) and kinetic data

has been found by Rose, Epstein and Watkinson (1997) to agree well with their data using a whey protein solution:

$$C_b = \frac{k' R^{\bullet}_{f(0)} Sc^{2/3}}{u_c} + k'' \left(R^{\bullet}_{f(0)}\right)^{1/n} \left(\frac{\rho e^{\frac{E_A}{RT_w}}}{\mu} \right)^{1/n} u_c^{2/n} \qquad (5.24)$$

In hydrocarbon fouling an individual compound cannot be identified as being responsible for the fouling deposit. Therefore, calculating a "concentration" based on fouling rates using equation (5.24) above is deemed to predict a pseudo concentration of all the fouling species for the Maya crude. This pseudo concentration is likely to be a result of the weighted contributions of many individual compounds that take part in the overall fouling process.

Values for C_b and k" are unknown, but may be derived graphically by simplifying and rearranging equation (5.24).

$$\text{Let A} = \frac{k' R^{\bullet}_{f(0)} Sc^{2/3}}{u_c} \qquad (5.25)$$

$$\text{Let B} = \left(R^{\bullet}_{f(0)}\right)^{1/n} \left(\frac{\rho e^{\frac{E_A}{RT_w}}}{\mu} \right)^{1/n} u_c^{2/n}, \qquad (5.26)$$

Substituting equations (5.25) and (5.26) back in to equation (5.24), results in:

$$C_b = A + k'' B \qquad (5.27)$$

Now in the recycle flow loop used in the present research with Maya crude, the bulk concentration (C_b) could be considered to be constant, that is, not to vary with either prevailing fluid temperature or velocity. Therefore equation (5.27) may be rearranged to form a straight line. The results of equation (5.28) is shown in Figure 5.1.

$$A = -k'' B + C_b \tag{5.28}$$

Following graphical interpretation C_b was found to be 0.0001 kg m^{-3} and k" to be $6.00 \, x \, 10^{-7}$.

The values for C_b and k" were then incorporated into the model and the resulting predicted fouling rates were verified with those found experimentally. It was found that the data had a great deal of scatter, fitting a linear relationship poorly ($R^2 = 0.0150$). The poor comparison with the experimental data means that this particular method for finding C_b and k" is not appropriate.

Clearly a better method is required. In order to solve for the unknowns n and k" their values where iterated until an optimal solution was found. The process can be summarised by Figure 5.2.

The reaction order (n) and reactivity rate factor (k") used in equations (5.18) and (5.24) was varied in an iterative manner for each velocity and temperature studied, until the predicted value of the initial fouling rate ($R_{f(0)}$) was equal the value found experimentally. For case 1 the reaction order n was found to be 5/2, and the reactivity rate factor k" 15.5 for all surface temperatures used in this study.

Use of equation (5.24) relies on a number of initial fouling rates ($R_{f(0)}^{\bullet}$) over a range of different velocities and initial surface temperatures. However, values of C_b calculated from this equation can be related to the linear velocity and initial surface temperature in order to develop an equation for C_b independent of $R_{f(0)}^{\bullet}$.

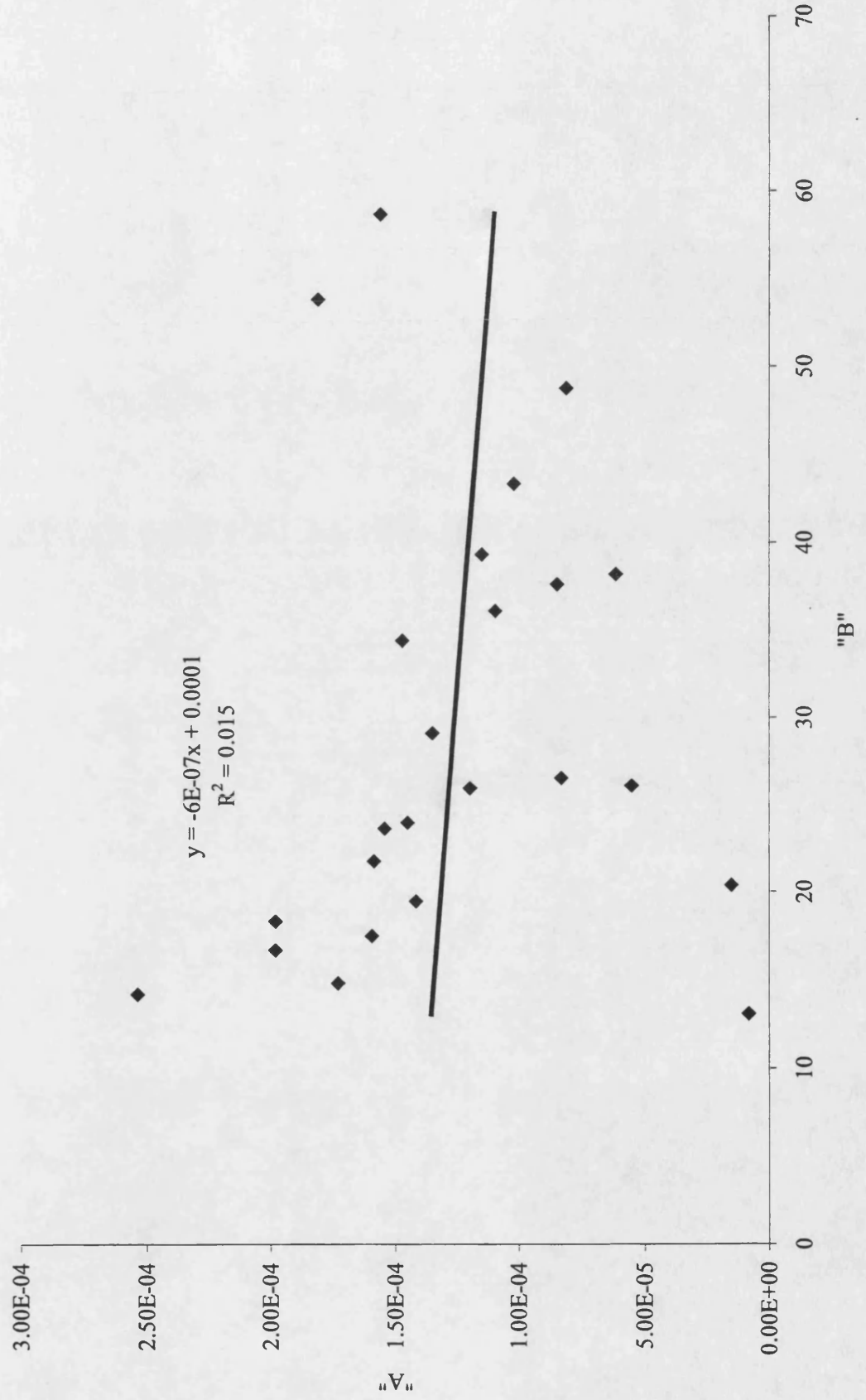

Figure 5.1 Case 1 graphical determination of bulk concentration and reactivity rate factor

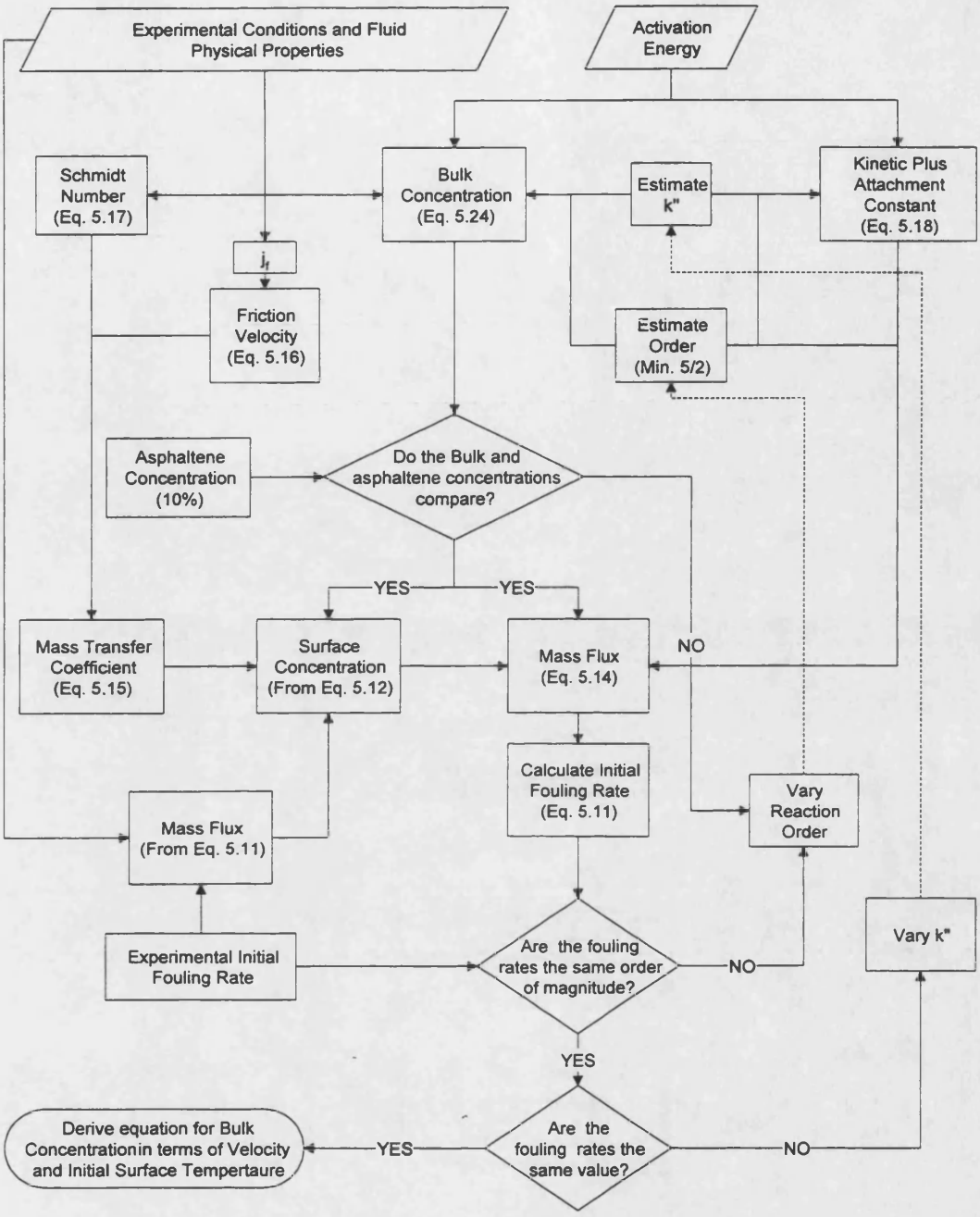

Figure 5.2 Flow chart showing iterative calculation procedure

Figure 5.3 shows the variation in bulk concentration (C_b) with velocity (u_m) at the four different initial surface temperatures used in this study. The best fit of the data was obtained by fitting 2nd order polynomial curves of the type $y = ax^2 + bx + c$. The resulting equations are summarised in Table 5.5.

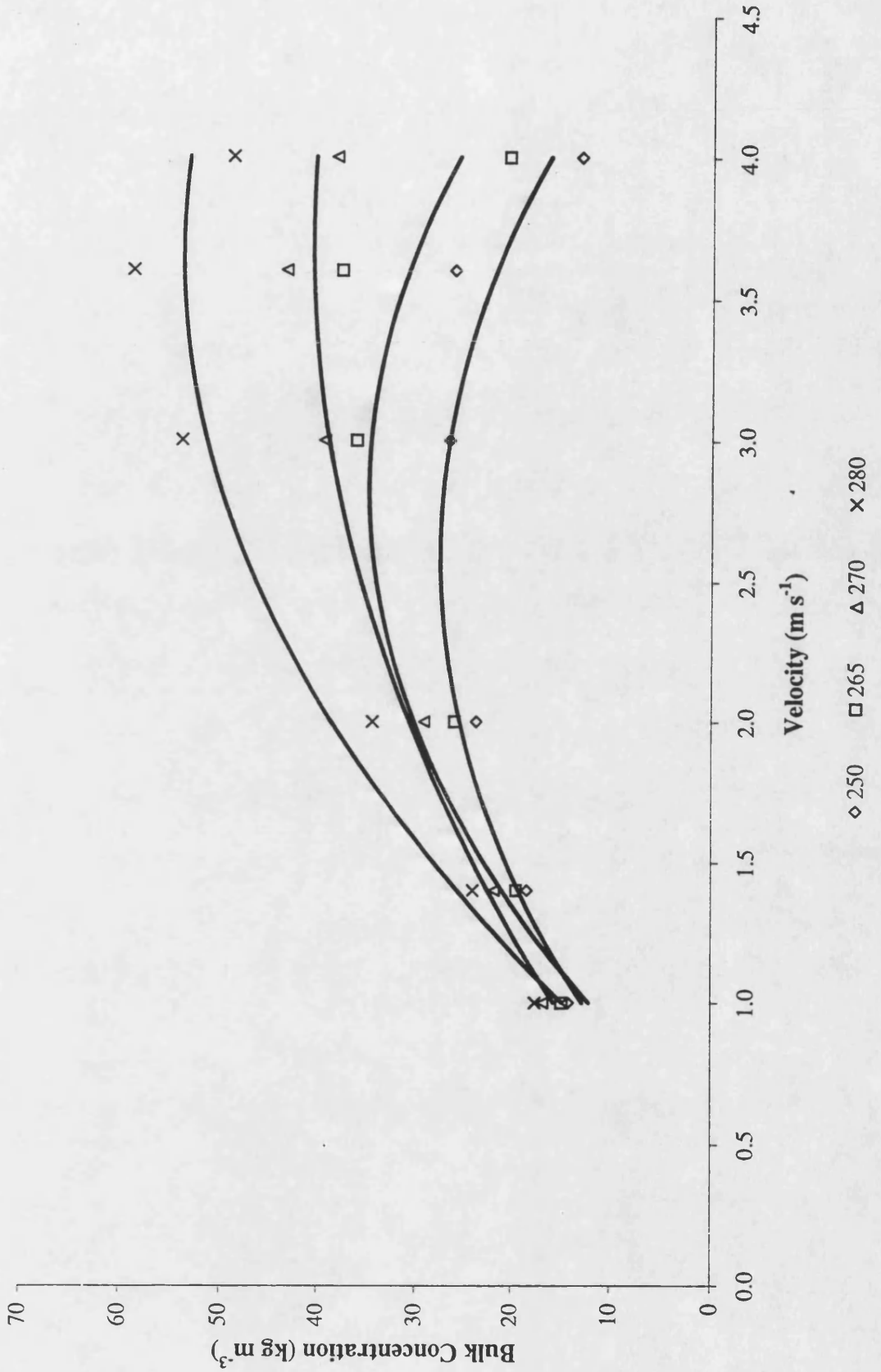

Figure 5.3 Case 1 calculated bulk concentration against velocity at different tube wall temperatures

Table 5.5 Equations Resulting from Figure 5.3

Clean Surface Temperature (°C)	Equation
250	$C_b = -5.772u_m^2 + 29.981u_m - 11.443$
265	$C_b = -6.775u_m^2 + 38.379u_m - 19.509$
270	$C_b = -3.407u_m^2 + 25.27u_m - 6.227$
280	$C_b = -5.526u_m^2 + 40.416u_m - 20.144$

The values of the constants a, b and c in the polynomial equations for each of the initial surface temperatures shown in Table 5.5 were then plotted against tube wall temperature (T_w), as shown in Figure 5.4.

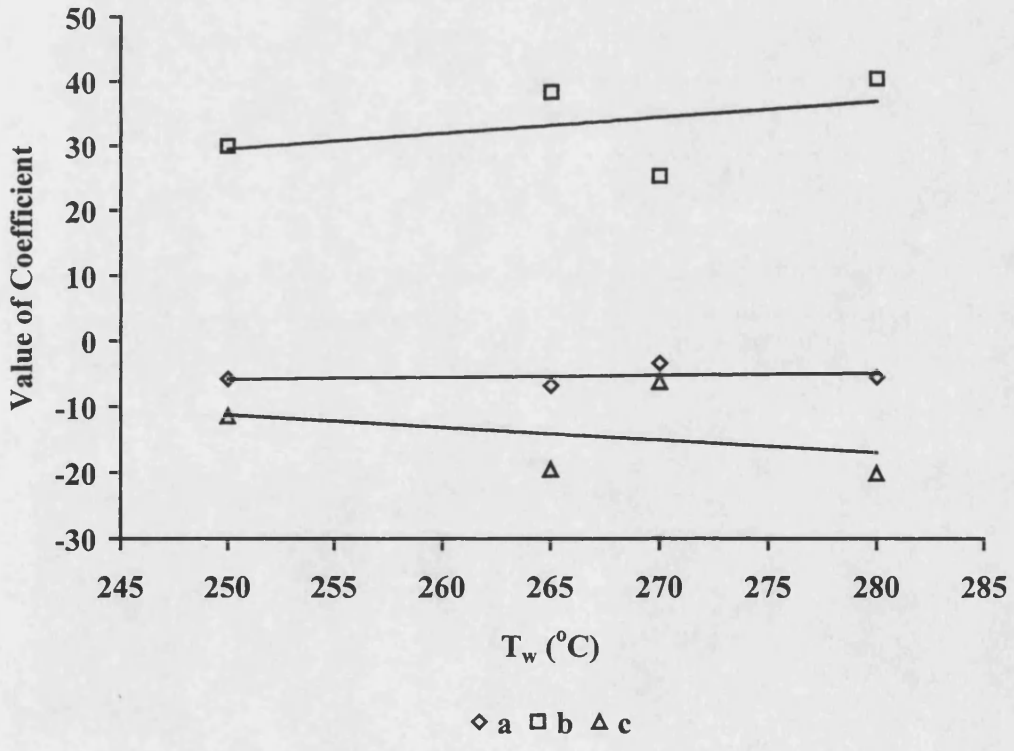

Figure 5.4 Case 1 variation in constants "a, b and c" with initial surface temperature

The variations of "a", "b" and "c" with surface temperature were then obtained and shown in Table 5.6.

Table 5.6 Equations resulting from Figure 5.4

Constant	Equation
a	$a = -0.028T_w - 13.0$
b	$b = 0.246T_w - 32.0$
c	$c = 0.192T_w - 36.9$

An overall equation for bulk concentration dependent on the velocity may then be given by combining the results of these plots, as illustrated by equation (5.30):

$$C_b = -(-0.028T_w - 13.0)u_m^2 + (0.246T_w - 32.0)u_m - (0.192T_w - 36.9) \quad (5.30)$$

5.2.3.2 Verifying the model with bare tube experimental data for Case 1

Predicted fouling rates in bare tubes were found to increase with increasing velocity up to a point, beyond which further increases in velocity resulted in a decrease in the fouling rate. This is in agreement with the experimental results. These comparisons are shown in Figure 5.5 to Figure 5.8. The reasonably successful prediction of the trend in fouling rates at velocities between 1.0 m s^{-1} and 4.0 m s^{-1} (Re ~8,500 - ~46,000) and initial surface temperatures of 250 °C, 265 °C, 270 °C and 280 °C is indicative of the suitability of the model for bare tubes over this range. Further, the reasonable success of this model also suggests that a low E_A of 26 kJ $kmol^{-1}$ and an order of 5/2 are appropriate to model fouling rates in bare tubes for Maya crude oil.

It has been suggested that asphaltenes are the principal compounds in involved in the formation of fouling deposits. The average asphaltene content has been reported to be approximately 10% at 15.6 °C (60 °F) (BP Amoco Data (1995)). In this first trial, the maximum bulk concentration of foulant or precursor was predicted to be 49 kg m^{-3},

which is approximately 6% of the bulk density (849 kg m^{-3}). This is reasonably close to the reported value of 10%.

At an initial surface temperature of 250 °C, the model predicts the maximum fouling rate to occur at approximately 2.0 m s^{-1}, as shown in Figure 5.5. This is in agreement with the experimental results. However, agreement between predicted and experimental results is relatively poor below 1.5 m s^{-1}.

At an initial surface temperature of 265 °C, the model predicts the maximum fouling rate again to occur at approximately 2.0 m s^{-1}, as shown in Figure 5.6. However, experimentation has found that the maximum fouling rate to occur at approximately 3.0 m s^{-1}. Generally, agreement between the predicted and experimental fouling rates was relatively poor over the range of velocities studied.

At an initial surface temperature of 270 °C the model predicts the maximum fouling rate to be at approximately 2.0 m s^{-1}, as shown in Figure 5.7. However, experimental results have shown that the maximum fouling rate occurs at 3.6 m s^{-1}. Agreement is somewhat better over the range studied compared with 250 °C and 265 °C.

At an initial surface temperature of 280 °C, the model predicts the maximum fouling rate to occur at approximately 3.0 m s^{-1}, as shown in Figure 5.8, which is in agreement with the experimental results. The predicted maximum fouling rate is below that found experimentally. However, reasonably good agreement is seen over the range of velocities used in the model.

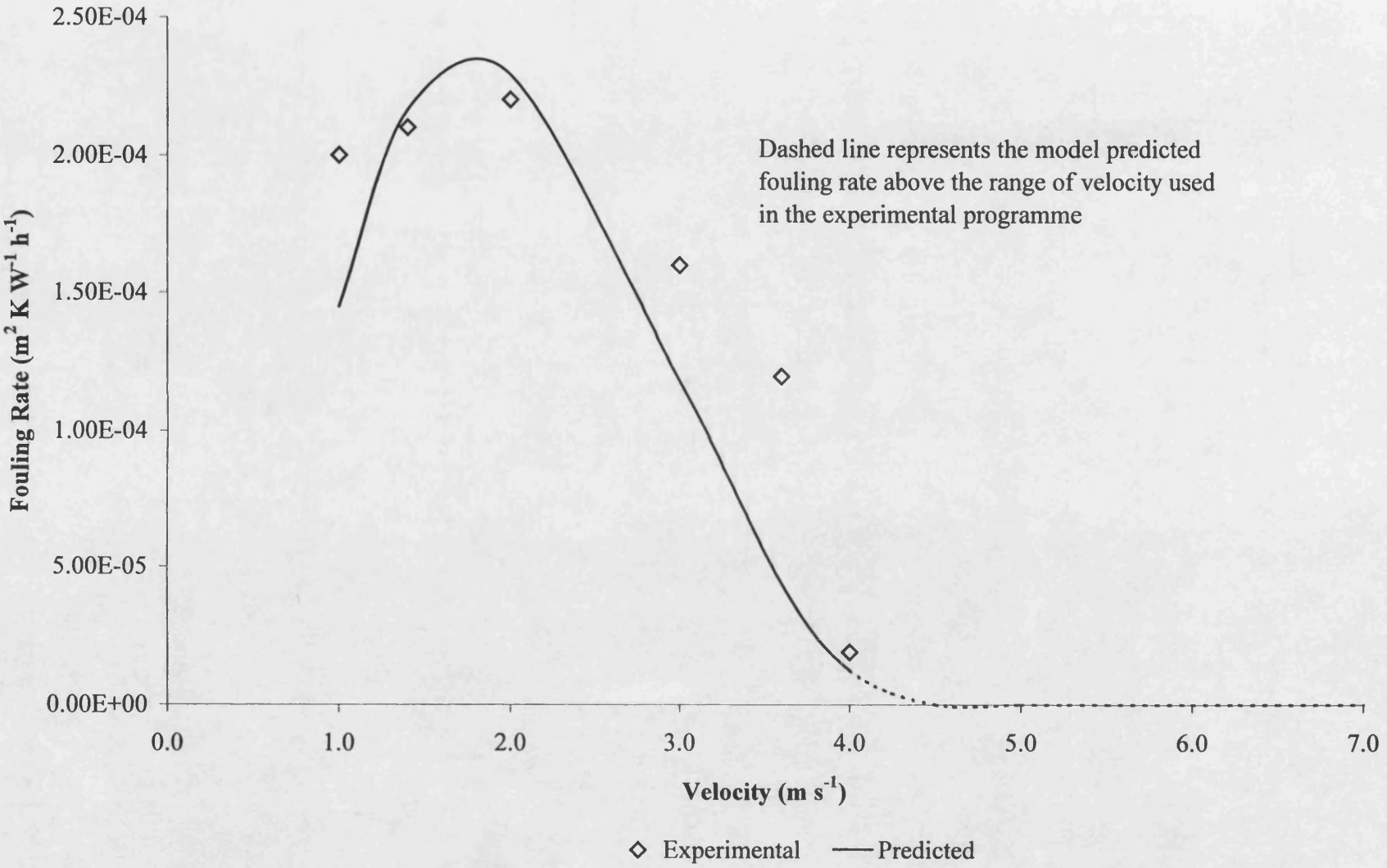

Figure 5.5 Experimental and predicted fouling rates in bare tubes at 250 °C for Case 1

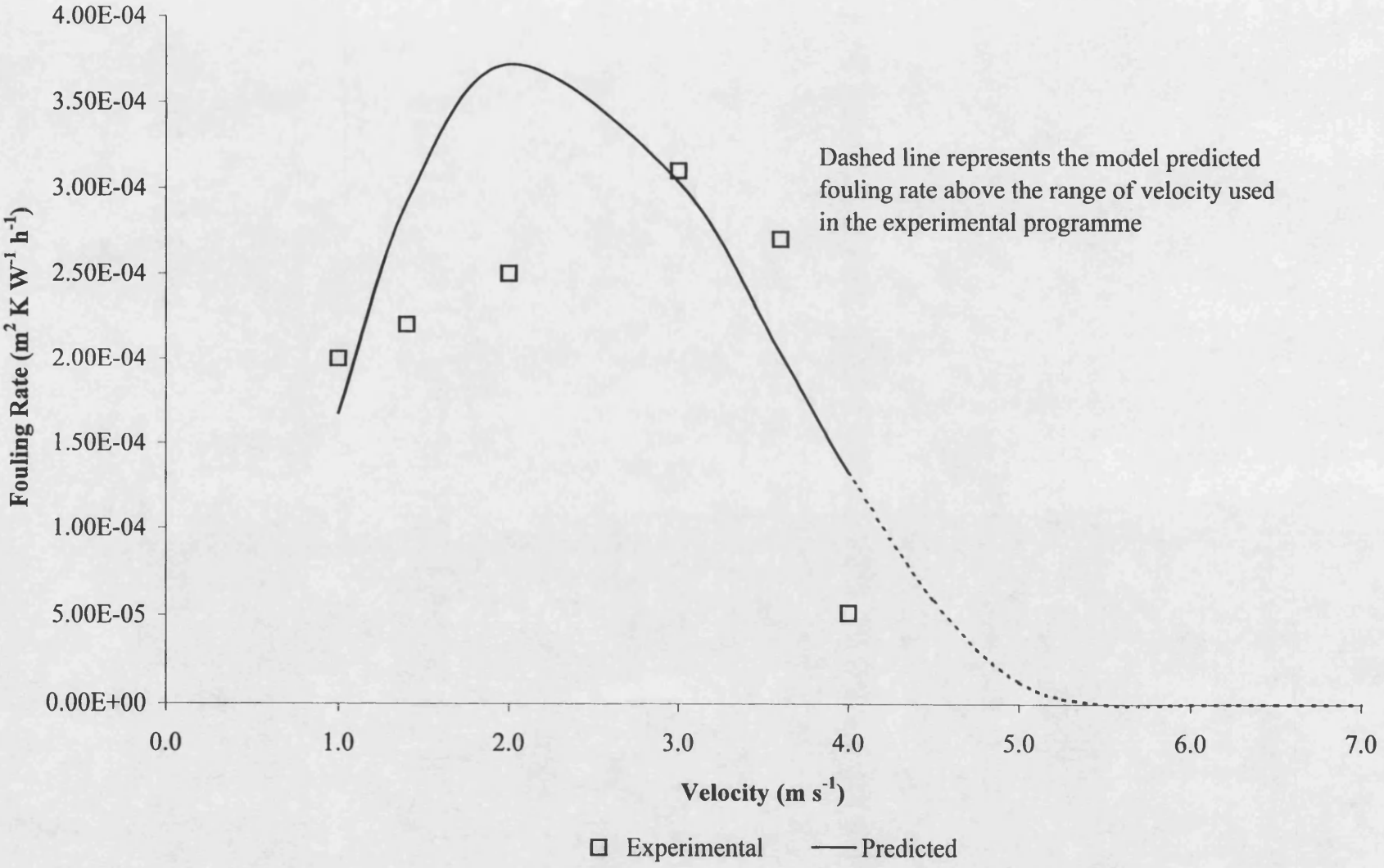

Figure 5.6 Experimental and predicted fouling rates in bare tubes at 265 °C for Case 1

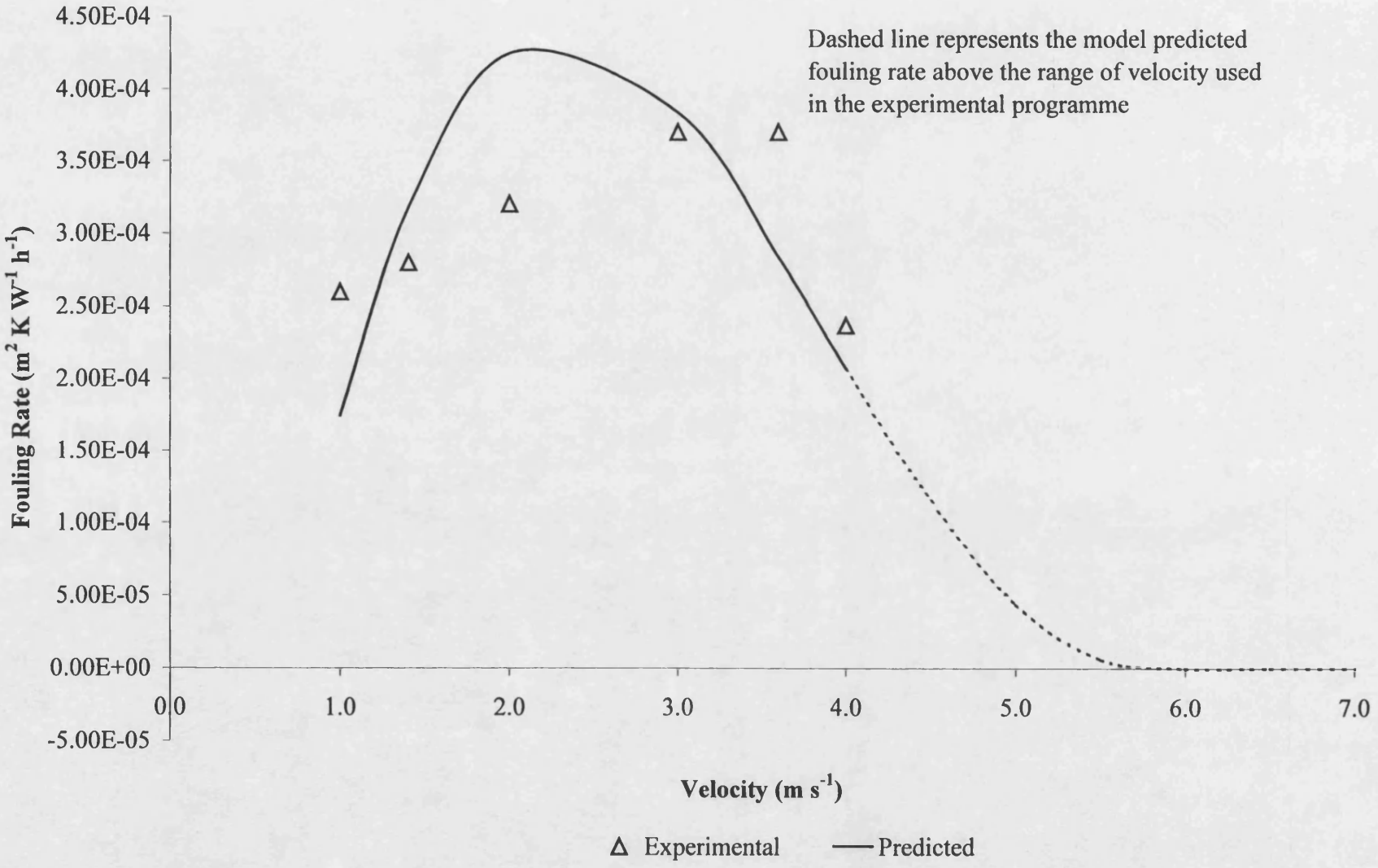

Figure 5.7 Experimental and predicted fouling rates in bare tubes at 270 °C for Case 1

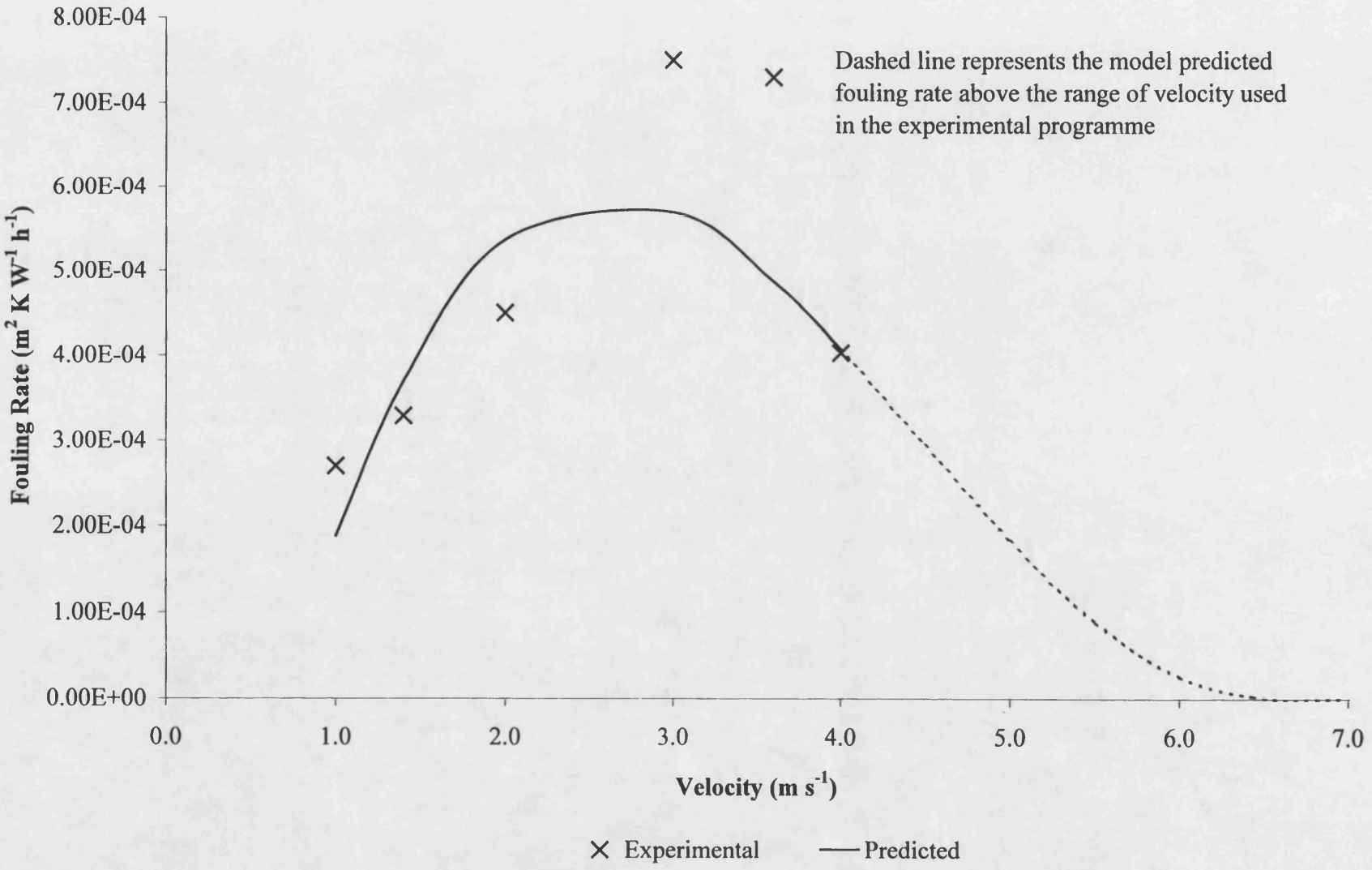

Figure 5.8 Experimental and predicted fouling rates in bare tubes at 280 °C for Case 1

5.2.3.3 *Applying the model to fouling rates with inserts for Case 1*

The model used to predict fouling rates with inserts is deemed to be identical to that used to predict fouling rates for bare tubes, with the exception of the substitution of the appropriate friction factor correlation for the insert, namely:

$$j_f = 2.5525\,\mathrm{Re}^{-0.3232} \qquad \text{For LDI (1.22; 0.63)} \qquad (4.14)$$

$$j_f = 5.9642\,\mathrm{Re}^{-0.4061} \qquad \text{For MDI (1.22; 0.38)} \qquad (4.15)$$

At all initial surface temperatures and insert geometries the model predicts fouling rates markedly below those found experimentally. The comparisons are shown in Figure 5.9 to Figure 5.11.

For two inserts LDI (1.22 0.63) and MDI (1.22, 0.38) at 250 °C the fouling rates predicted by the model do not agree at all well with the experimental data over the range of velocities studied, as shown in Figure 5.9 and Figure 5.10 respectively. At the initial surface temperature of 265 °C, poor agreement was once again noted between predicted fouling rates and those found experimentally, as illustrated by Figure 5.11.

The reason for this poor fit of data when inserts are used is most likely due to the apparent activation energy not being representative of the control of the mechanism when inserts are present. Inserts promote turbulence, increasing mass transfer to the tube surface. At constant initial surface temperatures increases in mass transfer shift control of the overall fouling process towards kinetic control. Consequently, an apparent activation energy below 40 kJ $kmol^{-1}$ may not best describe the mechanism when inserts are installed.

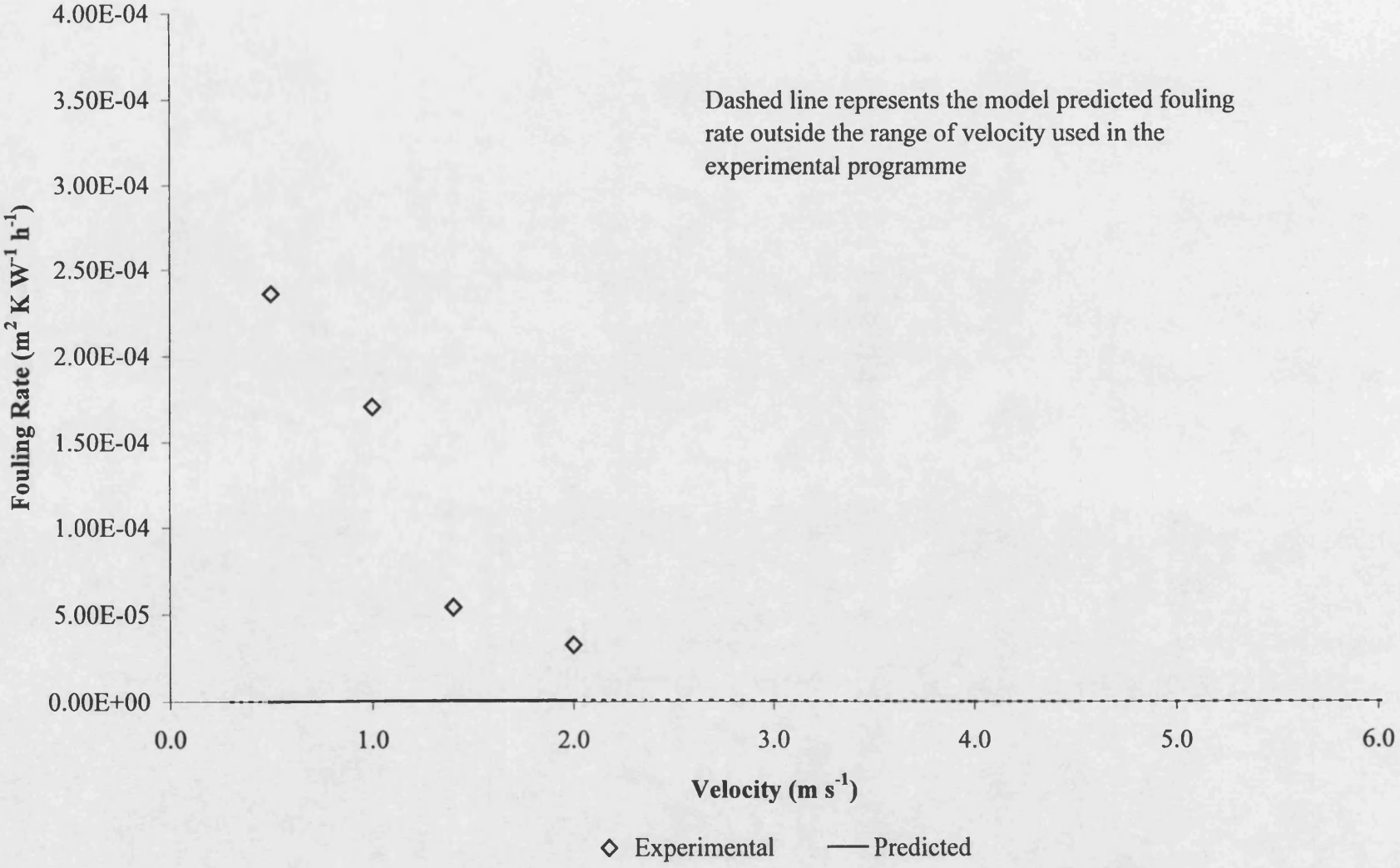

Figure 5.9 Experimental and predicted fouling rates with LDI (1.22; 0.63) at 250 °C for Case 1

Figure 5.10 Experimental and predicted fouling rates with MDI (1.22; 0.38) at 250 °C for Case 1

Figure 5.11 Experimental and predicted fouling rates with MDI (1.22; 0.38) at 265 °C for Case 1

5.2.4 Case 2

For Case 2 the initial conditions are as summarised in Table 5.7. Here the average activation energy and an initial reaction order of 5/2 are used.

Table 5.7 Initial conditions for Case 2

Parameter	Initial Value
E_A (kJ $kmol^{-1}$)	77
n	2.5
k"	1

5.2.4.1 Bulk concentration

As with Case 1, equations (5.25) and (5.26) were substituted back in to equation (5.24). The plot is shown in Figure 5.12. Following graphical interpretation C_b was found to be 0.0002 kg m^{-3} and k" to be 2.00×10^{-6}. The values for C_b and k" are found to be greater in comparison with those calculated using the lower E_A in Case 1.

Again the values calculated for C_b and k" derived using Figure 5.12 were incorporated into the model and the predicted fouling rates compared to the experimental data. It was found that a poor fit was still obtained, even though the data was a better fit to a linear relationship than for Case 1 ($R^2 = 0.0408$).

Hence again, in order to solve for the unknowns n and k" the values where iterated until a solution offering the best fit of the experimental data was found. The process used identical to that used in Case 1 and is summarised by Figure 5.2. For Case 2 the reaction order n was found to be 5, and reactivity rate factor k" 2.8 for all surface temperatures in this study.

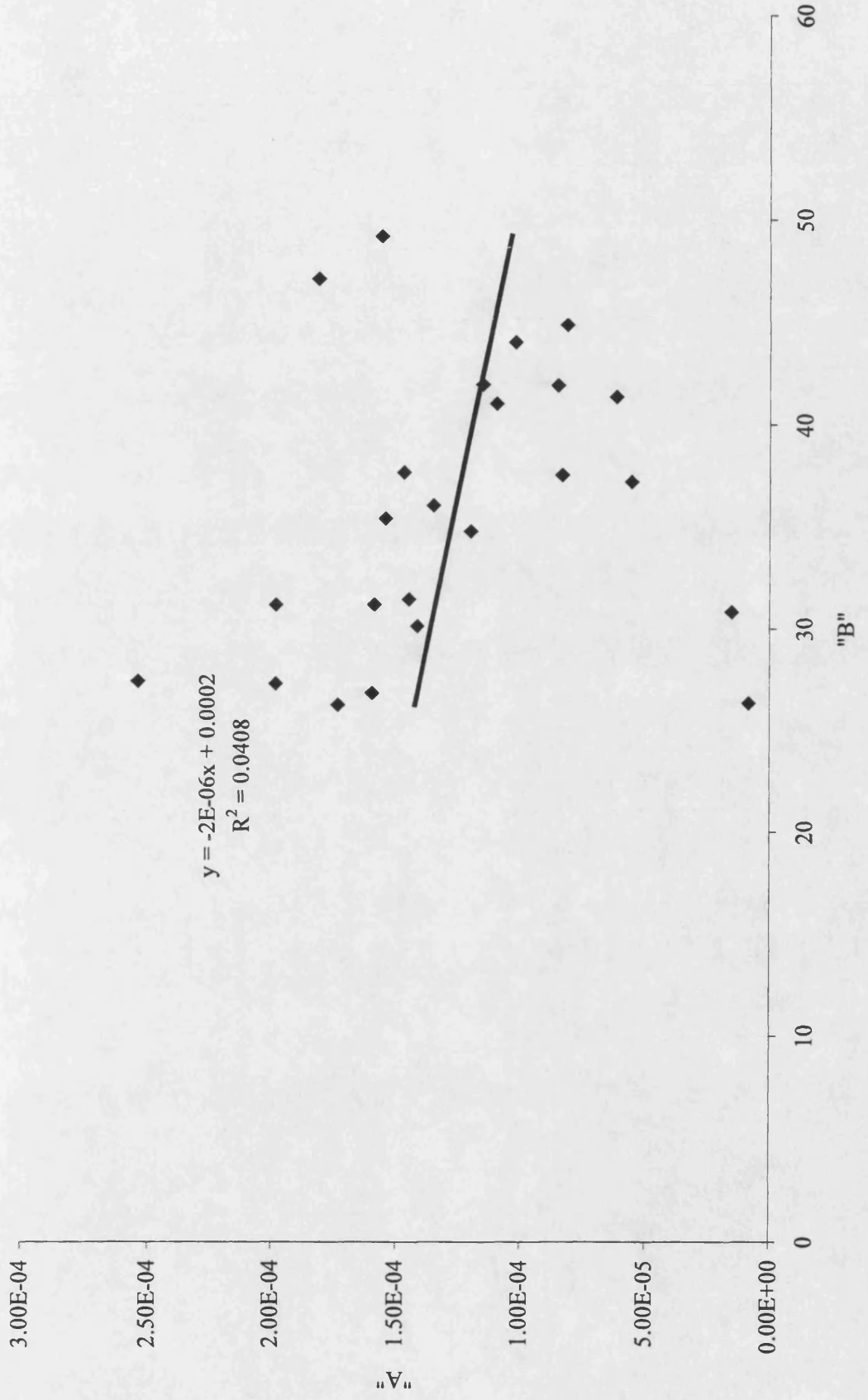

Figure 5.12 Case 2 graphical determination of bulk concentration and reactivity rate factor

Figure 5.13 shows the variation in bulk concentration (C_b) with velocity (u_m) at the four different initial surface temperatures used in this study. As before, a second order polynomial curve was fitted to the data. The resulting equations are summarised in Table 5.8:

Table 5.8 Equations Resulting from Figure 5.13

Clean Surface Temperature (°C)	Equation
250	$C_b = -4.837u_m^2 + 24.987u_m + 6.260$
265	$C_b = -4.720u_m^2 + 26.690u_m + 2.7848$
270	$C_b = -2.354u_m^2 + 16.905u_m + 12.359$
280	$C_b = -3.287u_m^2 + 23.352u_m + 5.774$

As before, the values of the constants a, b and c, shown in Table 5.8, were then plotted against tube wall temperature (T_w), as shown in Figure 5.14, leading to the linear equations given in Table 5.9.

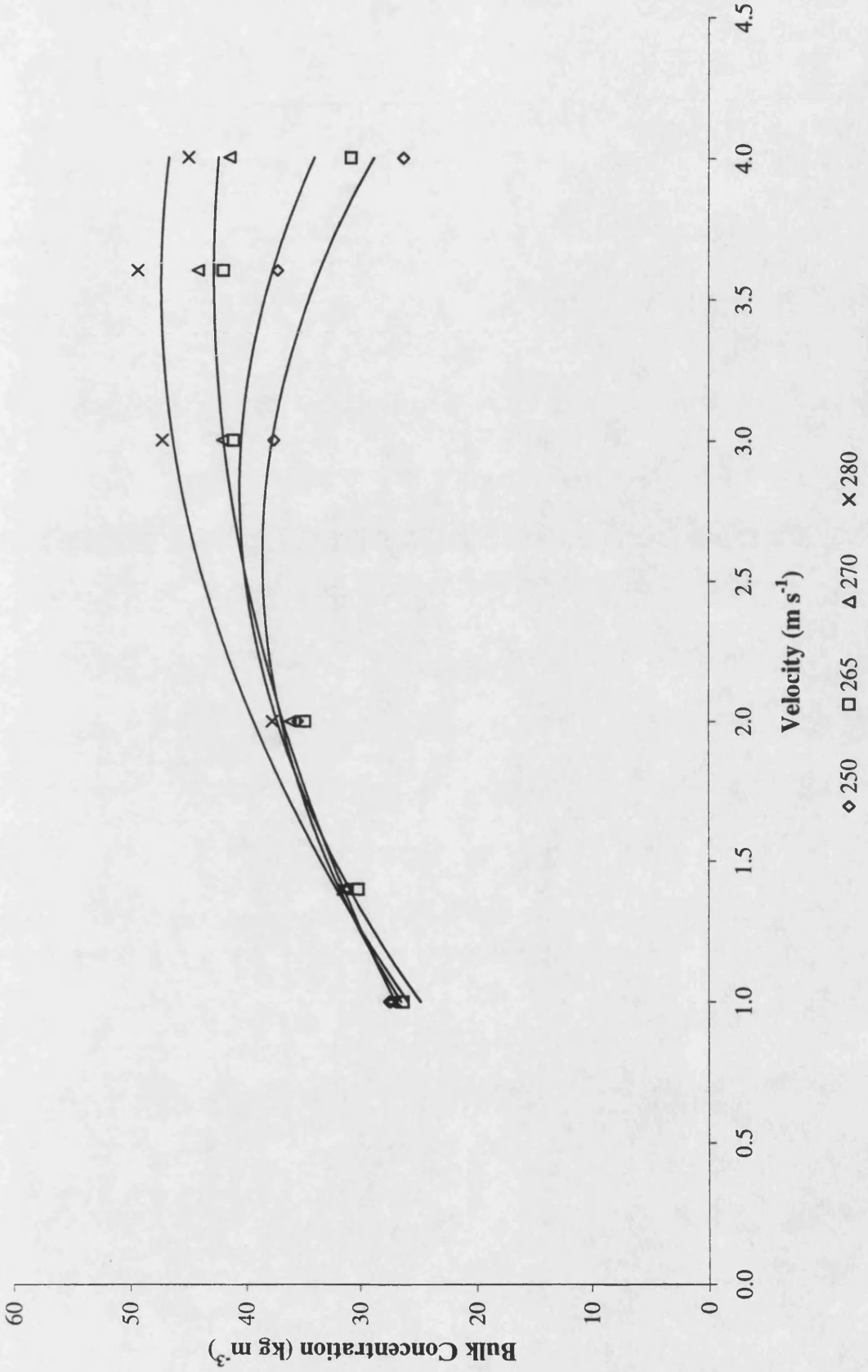

Figure 5.13 Case 2 calculated bulk concentration against velocity at different tube wall temperatures

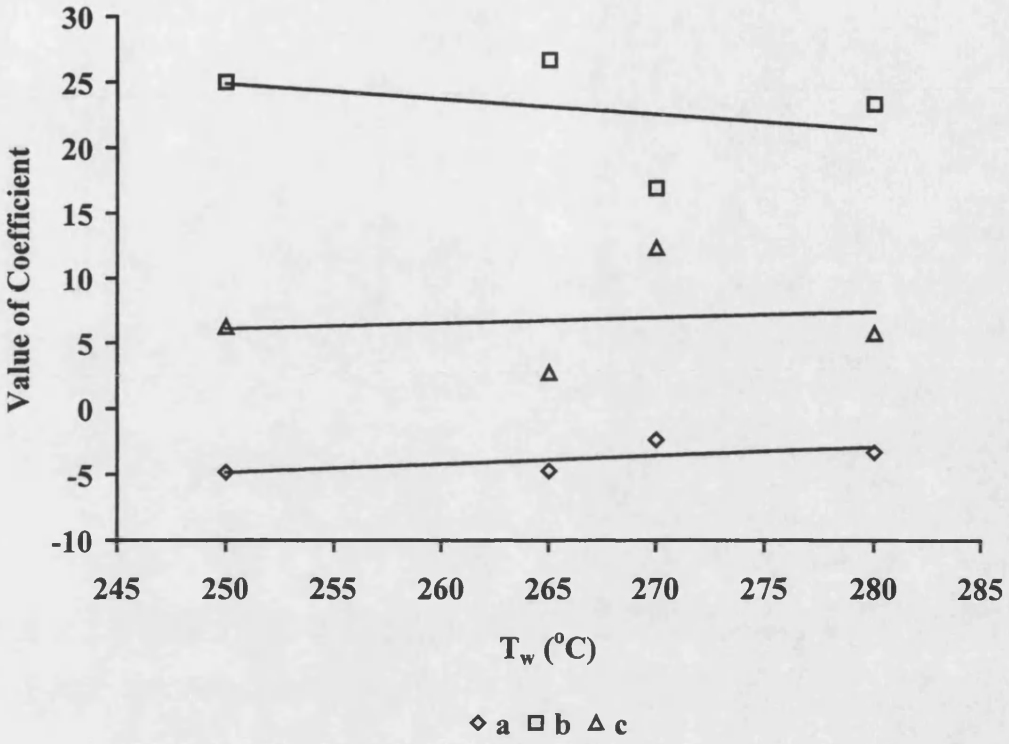

Figure 5.14 Case 2 variation in constants "a, b and c" with initial surface temperature

Table 5.9 Equations Resulting from Figure 5.14

Constant	Equation
a	$a = -0.064T_w + 21.08$
b	$b = 0.044T_w - 4.87$
c	$c = -0.120T_w + 54.6$

An equation for bulk concentration dependent on the velocity and surface temperature may be given by combining the results of these plots, as illustrated by equation (5.31):

$$C_b = -(-0.065T_w + 21.08)u_m^2 + (0.044T_w - 4.87)u_m + (-0.120T_w + 54.6) \quad (5.31)$$

5.2.4.2 *Verifying the model with bare tube experimental data for Case 2*

For all initial surface temperatures in bare tubes it was found that the model predicted a decrease in fouling rate with increasing velocity. The comparisons are shown in Figure 5.15 to Figure 5.18. This does not agree with the experimental results. The E_A and reaction order for Case 2 are greater than for Case 1. Higher values of E_A and n are representative of increased kinetic control and increased complexity of the reaction respectively. However, the experimental results demonstrate that the fouling reaction is controlled by both mass transfer and kinetic effects.

The maximum bulk concentration of foulant or precursor was predicted to be 29 kg m^{-3}, approximately 3% of the bulk density of the feed stock (849 kg m^{-3}). This is somewhat lower but within the assumed theoretical maximum of 10%. The maximum bulk concentration is lower for Case 2 (29 kg m^{-3}) than for Case 1 (49 kg m^{-3}).

At an initial surface temperature of 250 °C, the model predicts a reduction in fouling rate with increasing velocity, as shown in Figure 5.15. This does not agree with the experimental results. However, extending the velocity range below 1.0 m s^{-1} the model did predict that a maximum fouling rate would occur at approximately 0.025 m s^{-1}.

At an initial surface temperature of 265 °C, a reduction in fouling rate with velocity was predicted as above, and is illustrated by Figure 5.16. Again, the predictions do not agree with the experimental fouling rates. However, extending the range to velocities below 1.0 m s^{-1} the model predicts that a maximum fouling rate would occur at approximately 0.03 m s^{-1}. This is a higher predicted velocity than for 250°C.

At an initial surface temperature of 270°C the model predicts a reduction in fouling rate with velocity, as shown in Figure 5.17. This again is not in agreement with the experimental results. As with the previous temperatures, extending the range below

1.0 m s^{-1} it was found that the model would predict a maximum to occur at approximately 0.03 m s^{-1}, the same velocity as for 265°C.

At an initial surface temperature of 280 °C the model again shows the fouling rate decreasing with increasing velocity, as illustrated by Figure 5.18. However, the model does predict that a maximum fouling rate would occur at approximately 0.04 m s^{-1}.

The experimental results have found do show that the velocity at which a maximum fouling rate occurs is increased with increased initial surface temperature. Therefore, the model does at least correctly predict the effect that temperature has on the mechanism, albeit at velocities which are too low.

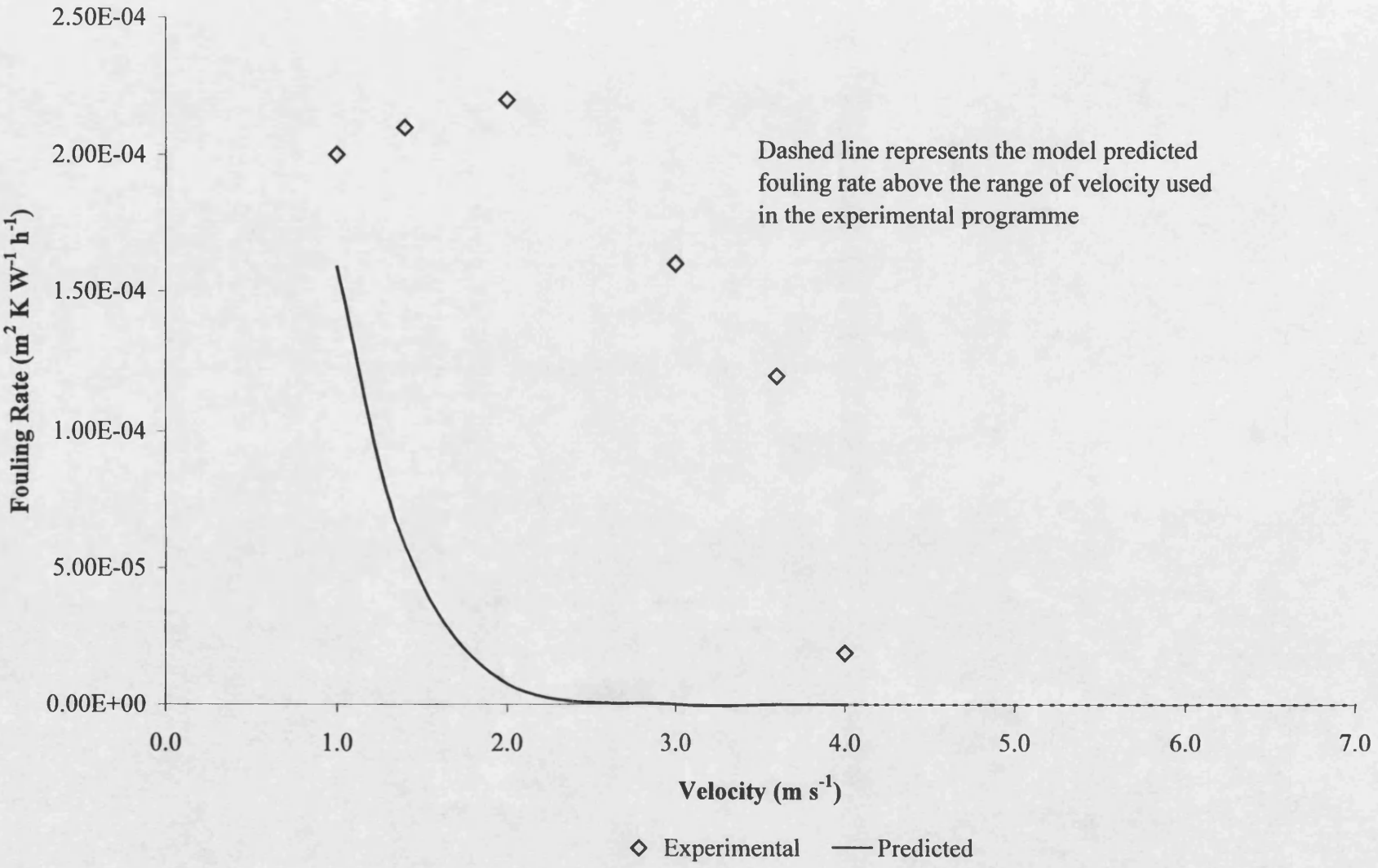

Figure 5.15 Experimental and predicted fouling rates in bare tubes at 250 °C for Case 2

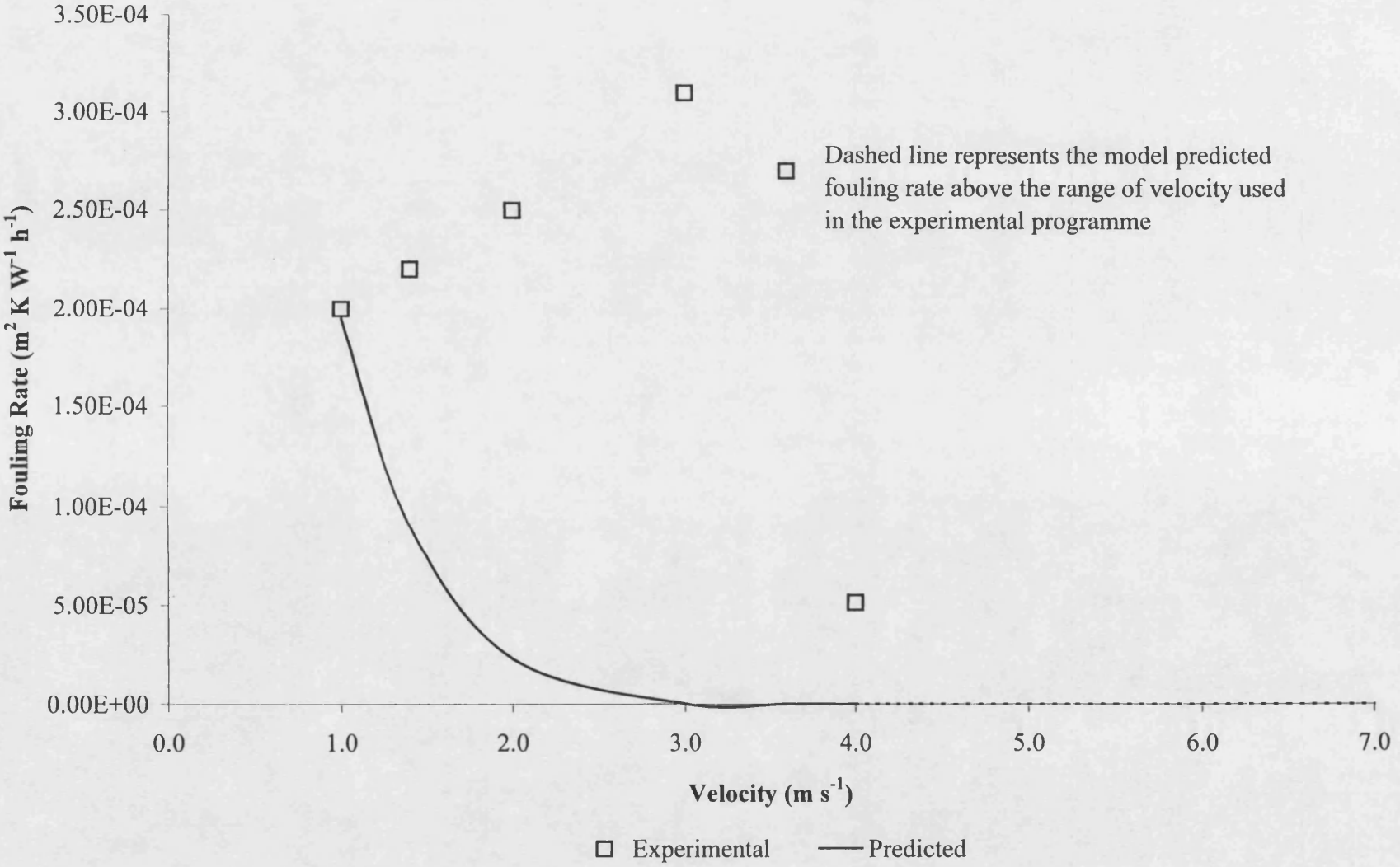

Figure 5.16 Experimental and predicted fouling rates in bare tubes at 265 °C for Case 2

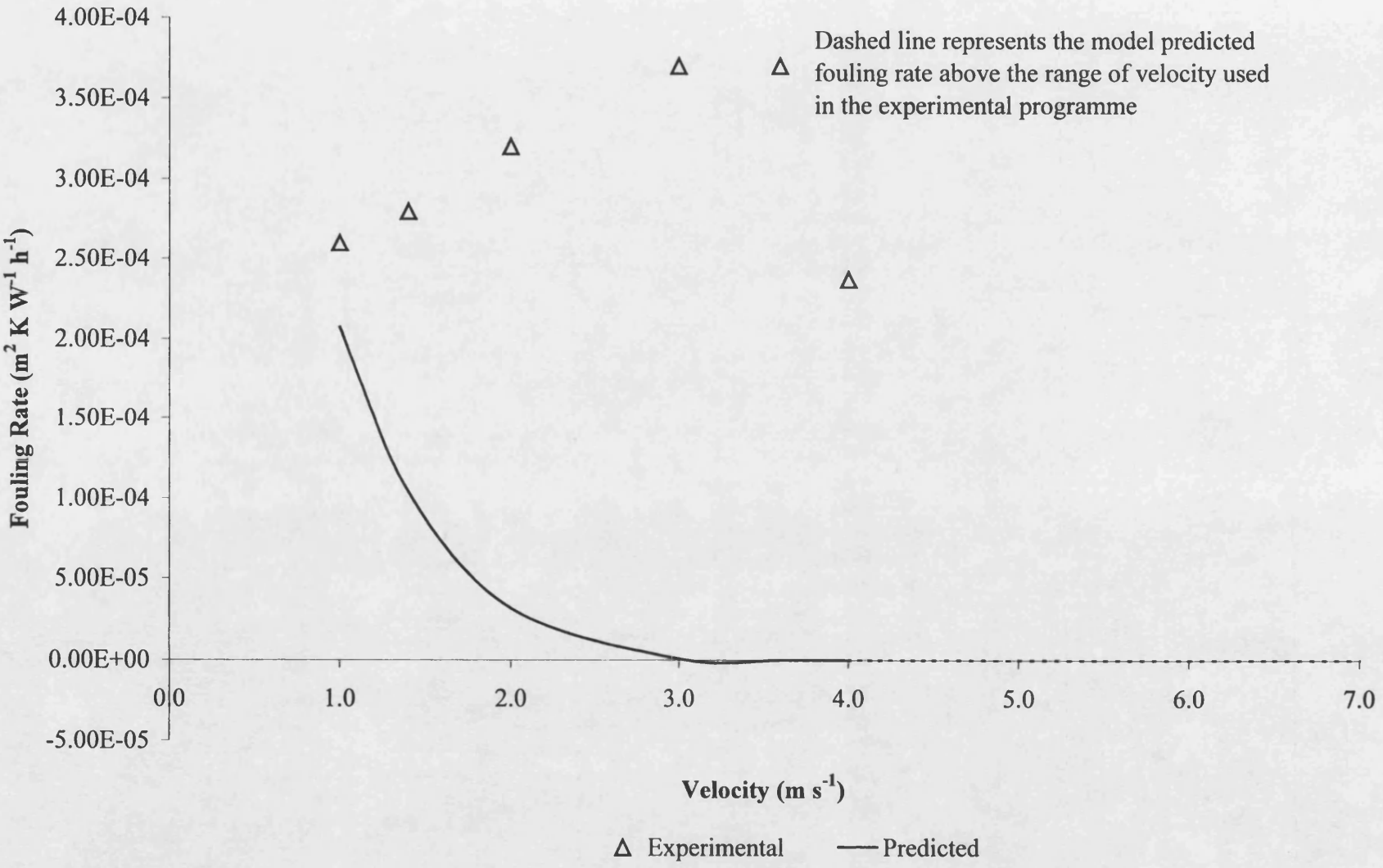

Figure 5.17 Experimental and predicted fouling rates in bare tubes at 270 °C for Case 2

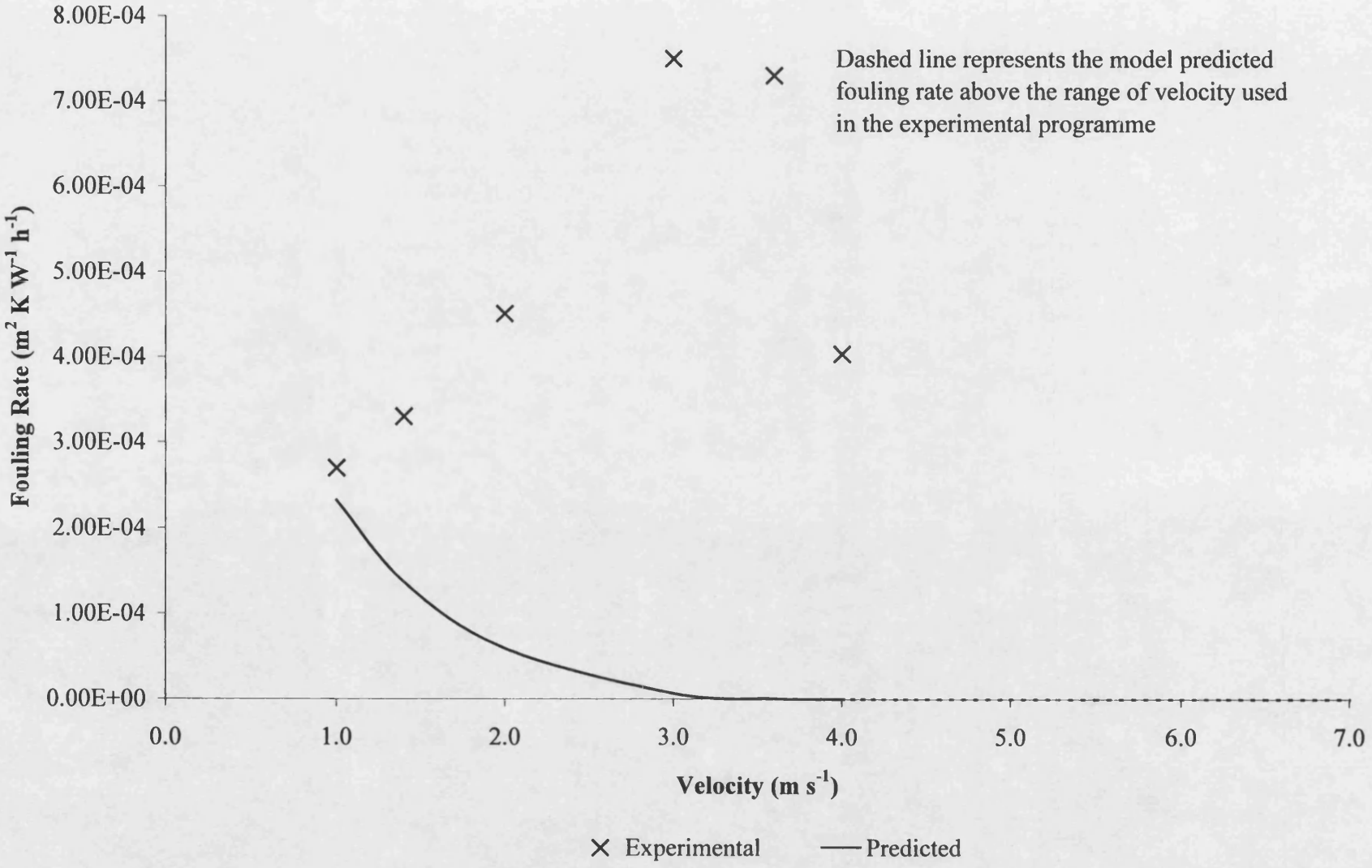

Figure 5.18 Experimental and predicted fouling rates in bare tubes at 280 °C for case 2

5.2.4.3 *Applying the model to fouling rates with inserts for Case 2*

As with Case 1, the model used to predict fouling rates with inserts was identical to that used to predict fouling rates for bare tubes, with the exception of the substitution of the appropriate friction factor equation for the insert, namely:

$$j_f = 2.5525\,\mathrm{Re}^{-0.3232} \qquad \text{For LDI (1.22; 0.63)} \qquad (4.14)$$

$$j_f = 5.9642\,\mathrm{Re}^{-0.4061} \qquad \text{For MDI (1.22; 0.38)} \qquad (4.15)$$

At all initial surface temperatures and insert geometries the model predicts a rapid reduction in fouling rate as velocity is increased. As the velocity is increased above 1.5 m s^{-1} the reduction in fouling rate is not as rapid, and the fouling rate tends to an asymptote.

For the inserts LDI (1.22 0.63) and MDI (1.22, 0.38) at 250 °C, the fouling rates predicted by the model agree fairly well with the experimental data over the range of velocities studied, as shown in Figure 5.19 and Figure 5.20 respectively. At the initial surface temperature of 265 °C the agreement becomes less good, as illustrated by Figure 5.21.

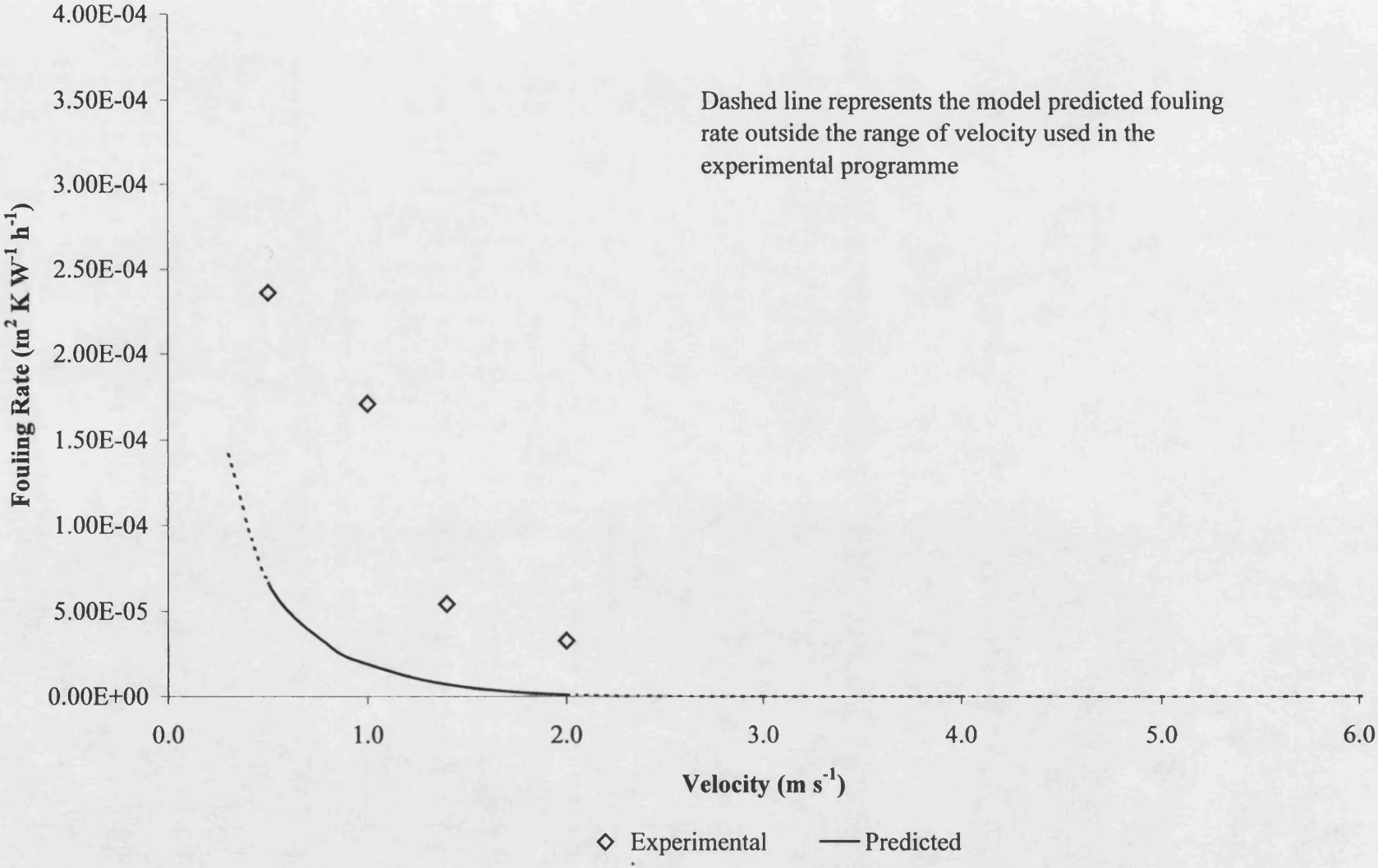

Figure 5.19 Experimental and predicted fouling rates with LDI (1.22; 0.63) at 250 °C for Case 2

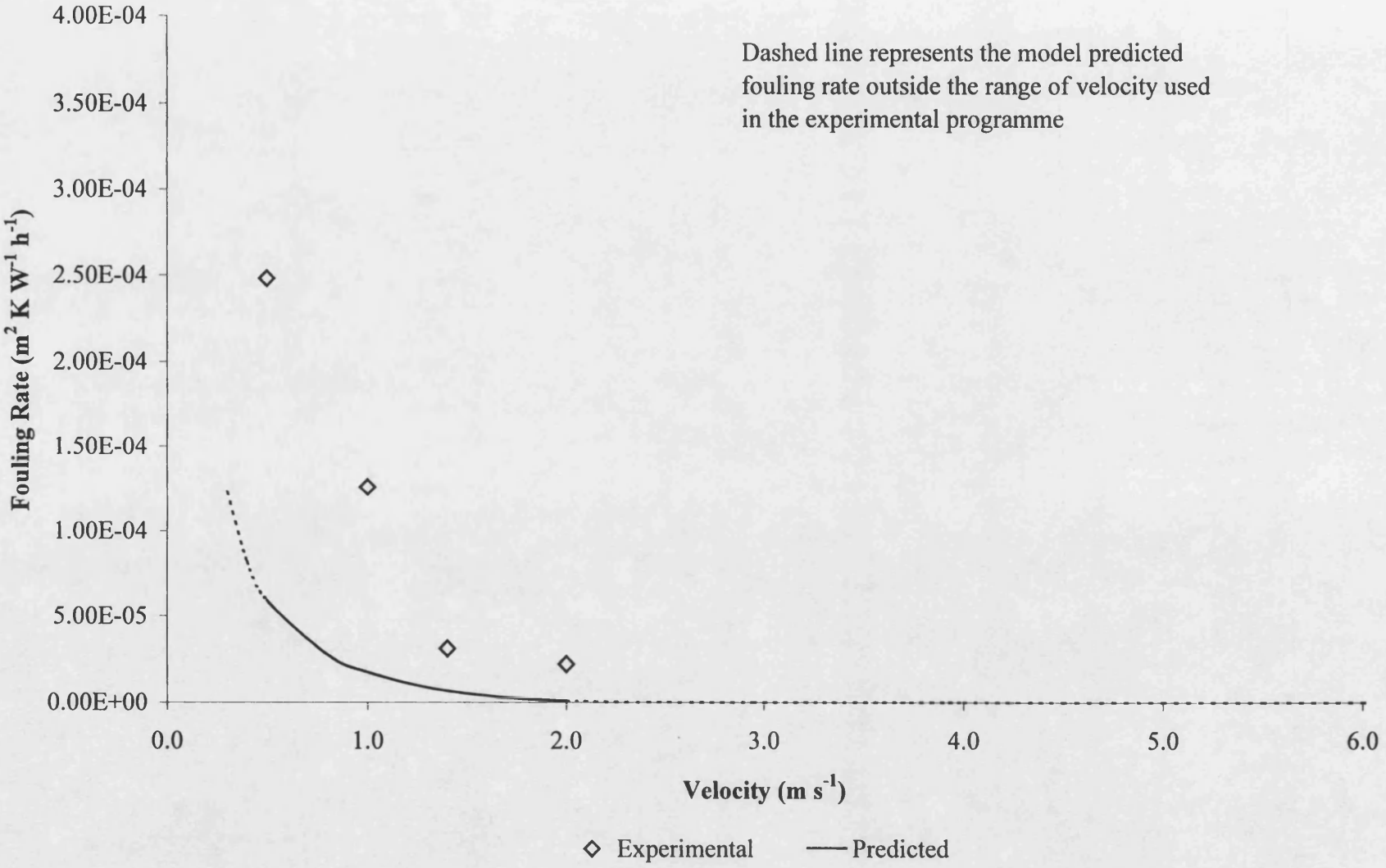

Figure 5.20 Experimental and predicted fouling rates with MDI (1.22; 0.38) at 250 °C for Case 2

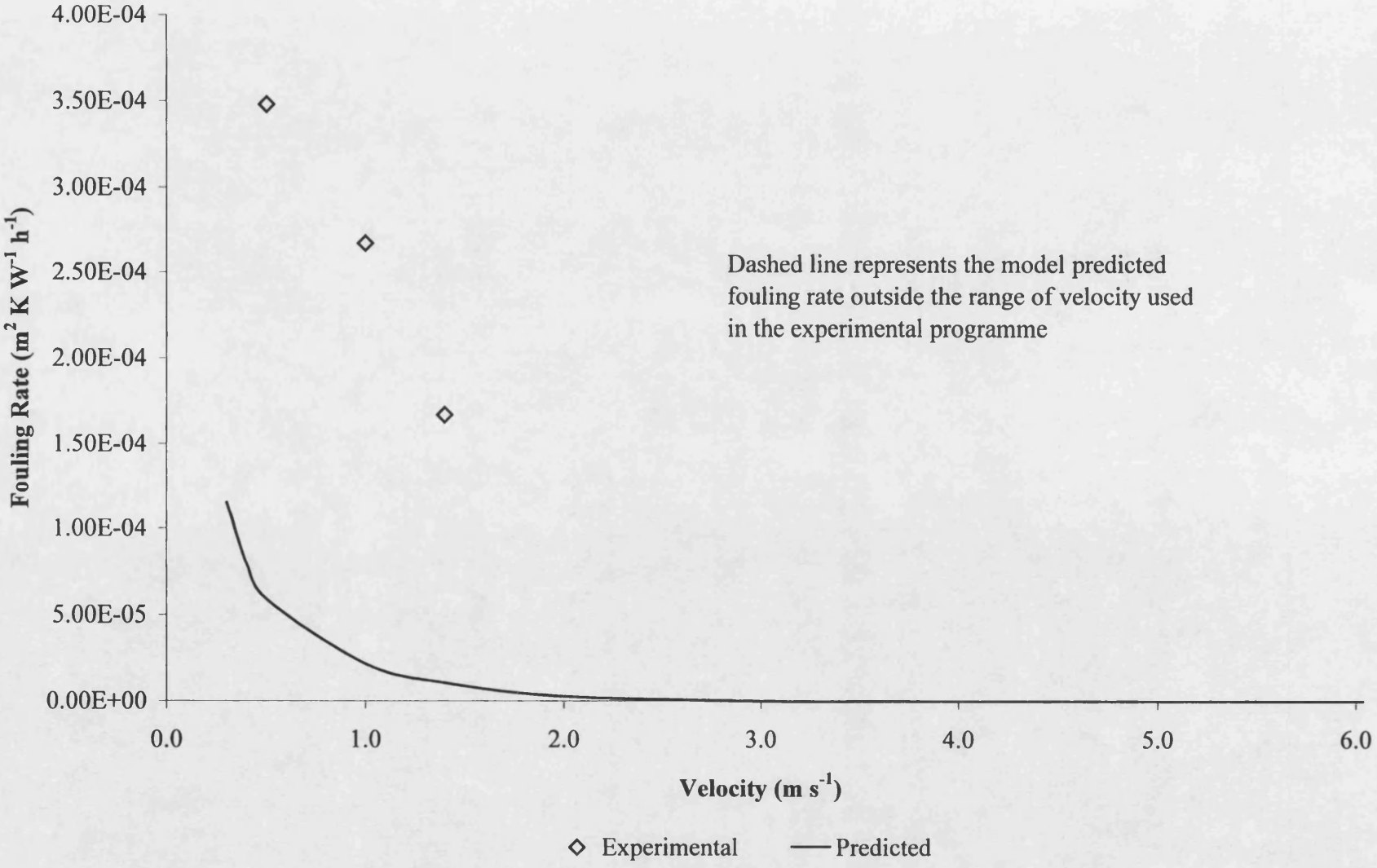

Figure 5.21 Experimental and predicted fouling rates with MDI (1.22; 0.38) at 265 °C for Case 2

5.2.5 Case 3

For Case 3 the initial conditions are as summarised in Table 5.10. In case three the highest value of activation energy was used.

Table 5.10 Initial conditions for Case 3

Parameter	Initial Value
E_A (kJ $kmol^{-1}$)	149
n	2.5
k"	1

5.2.5.1 Bulk concentration

As with previous cases, equations (5.25) and (5.26) were substituted back in to equation (5.24) and plotted in Figure 5.22. Following graphical interpretation C_b was found to be 0.0003 kg m^{-3} and k" to be 6.00 x 10^{-6}. These are higher values than those predicted using lower apparent activation energies.

Again the values calculated for C_b and k" were incorporated into the model and fouling rates calculated and compared with the experimental data. As for cases 1 and 2 the fouling rates predicted using C_b and k", were found to compare poorly with the experimental findings. Whilst it was found that a poor fit was obtained (R^2 = 0.0755) the degree of scatter was lower than compared to Case 1 and 2.

The reaction order n and reactivity rate constant k" were then found by iteration, until a solution was found. The process used identical to that used in Cases 1 and 2, and is summarised by Figure 5.2. For Case 3 n was found to be 10 and k" to be 1.58 for all surface temperatures in this study.

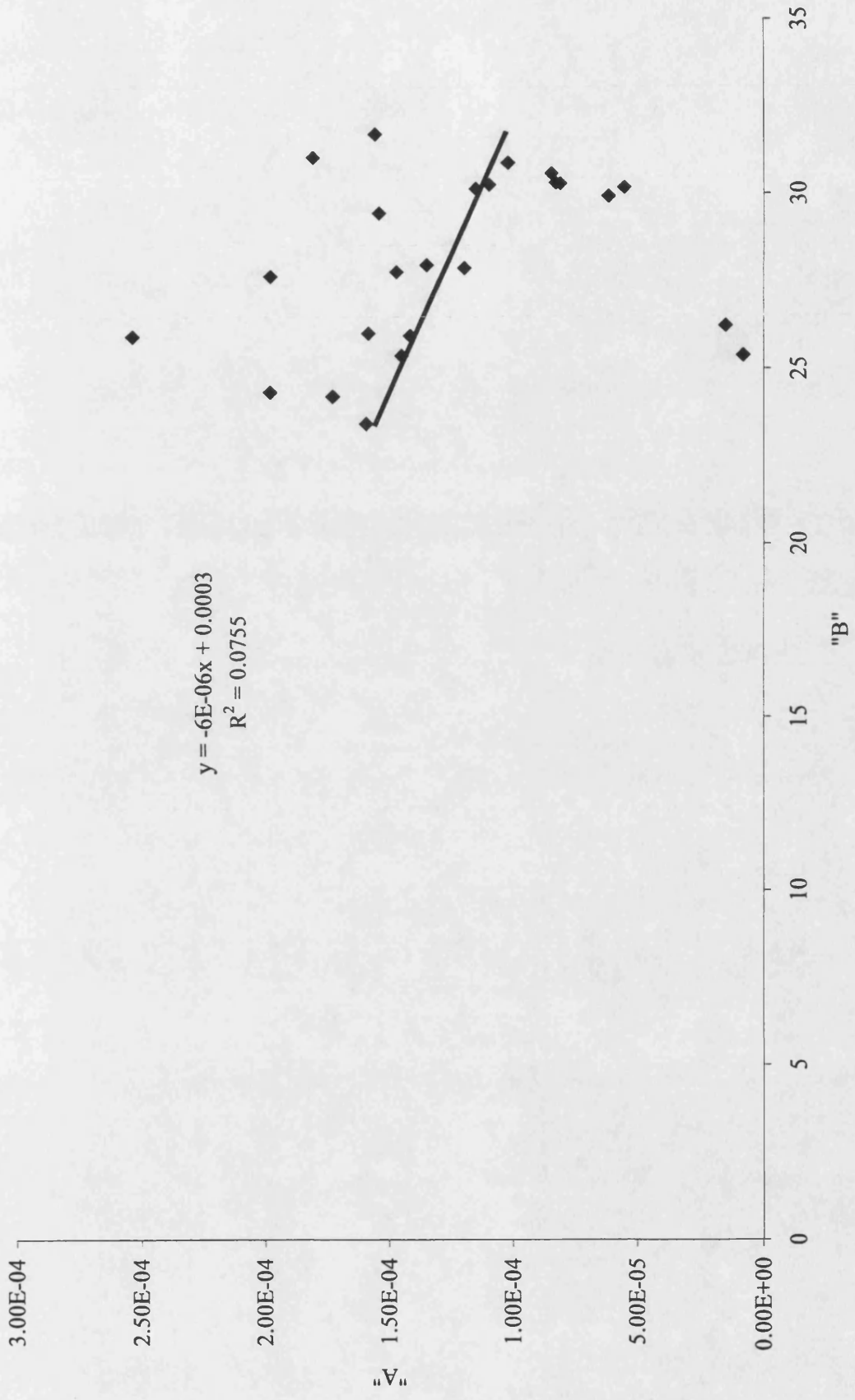

Figure 5.22 Case 3 graphical determination of bulk concentration and reactivity rate factor

Figure 5.23 shows the variation in bulk concentration (C_b) with velocity (u_m) at the four different initial surface temperatures used in this study. As before a second order polynomial curve was fitted to the data. The equations are summarised in Table 5.11.

Table 5.11 Equations Resulting from Figure 5.23

Clean Surface Temperature (°C)	Equation
250	$C_b = -2.129u_m^2 + 10.976u_m + 16.637$
265	$C_b = -1.936u_m^2 + 10.935u_m + 14.658$
270	$C_b = -0.966u_m^2 + 6.835u_m + 18.436$
280	$C_b = -1.275u_m^2 + 8.923u_m + 15.494$

The values of the constants a, b and c shown in Table 5.11 were then plotted against tube wall temperature (T_w), as shown in Figure 5.24. the linear plots of coefficient against initial surface temperature are shown in Table 5.12.

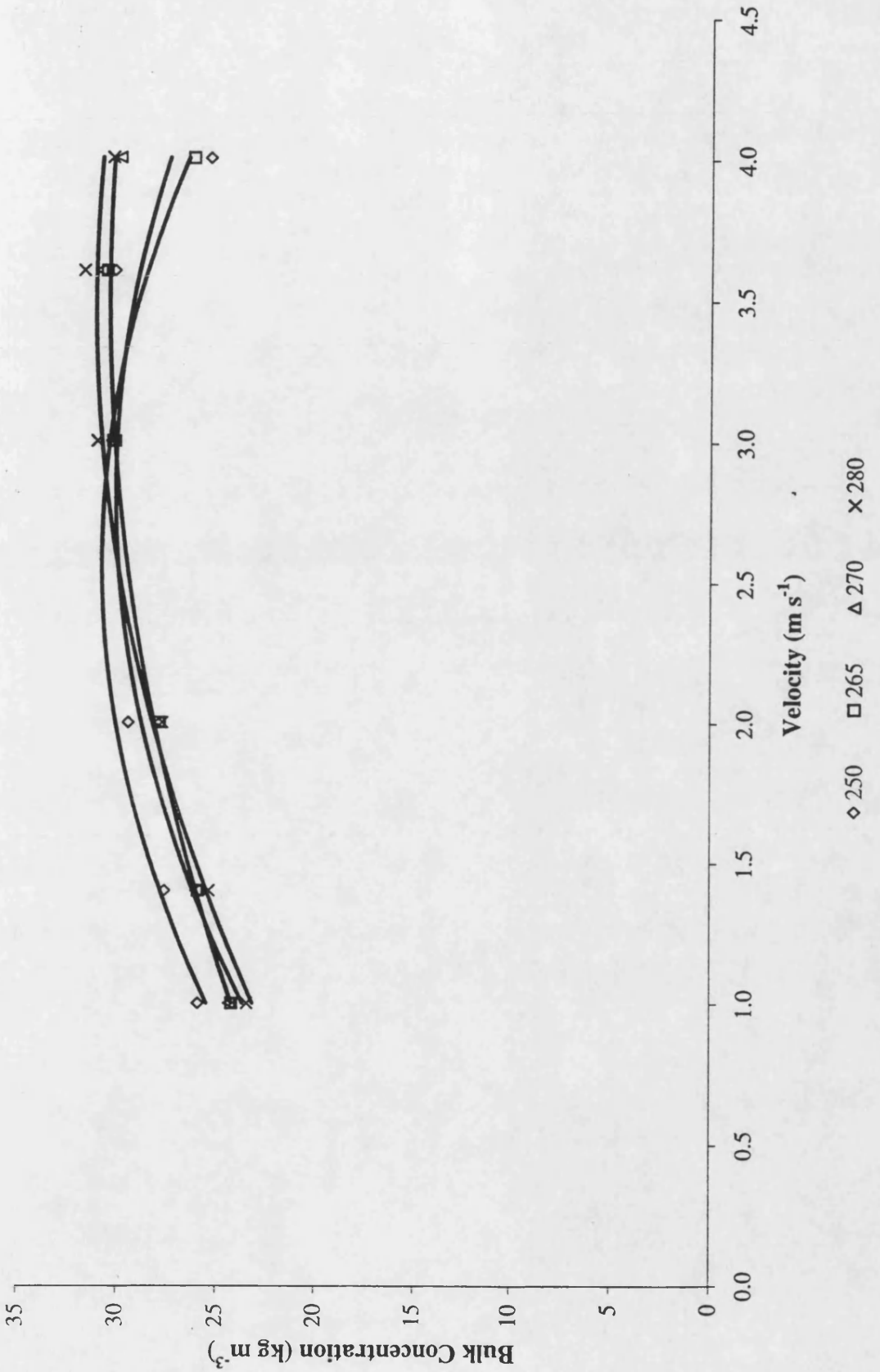

Figure 5.23 Case 3 calculated bulk concentration against velocity at different tube wall temperatures

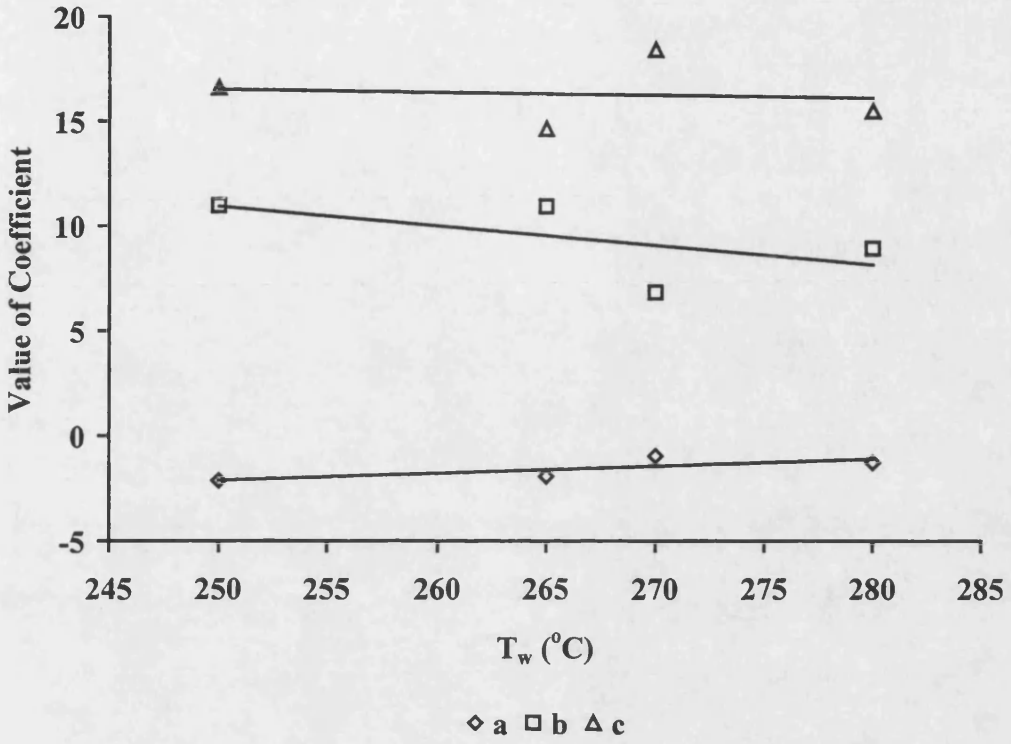

Figure 5.24 Case 3 variation in constants "a, b and c" with initial surface temperature

Table 5.12 Equations Resulting from Figure 5.24

Constant	Equation
a	$a = -0.038T_w + 10.59$
b	$b = -0.093T_w + 34.24$
c	$c = -0.015T_w + 20.17$

An equation for bulk concentration dependent on the velocity and surface temperature may be given by combining the results of these plots, as illustrated by equation (5.32):

$$C_b = -(-0.038T_w + 10.59)u_m^2 + (-0.093T_w + 34.24)u_m + (-0.015T_w + 20.17) \quad (5.32)$$

5.2.5.2 *Verifying the model with bare tube experimental data for Case 3*

For all initial surface temperatures with bare tubes it was found that the model predicted an increase in fouling rate with increasing velocity, except for an initial surface temperature of 250°C, where a maximum fouling rate was predicted to occur at 4.0 m s^{-1}. The predicted fouling rates were not in agreement with the experimental results. The comparisons are shown in Figure 5.25 to Figure 5.28.

The maximum bulk concentration of foulant or precursor was predicted to be 43 kg m^{-3}, approximately 6% of the bulk density (849 kg m^{-3}). The bulk concentration of foulant or precursor is therefore within the assumed theoretical maximum of 10%.

At an initial surface temperature of 250 °C, the model predicts a maximum fouling rate to occur at approximately 4.0 m s^{-1}, shown in Figure 5.25. Whilst the general trend is in agreement with the experimental results, the velocity at which the maximum occurs is double that found experimentally.

At higher initial surface temperatures of 265 °C, 270 °C and 280 °C the fouling rates increase with increasing velocity, as shown in Figure 5.26, Figure 5.27 and Figure 5.28 respectively.

For all initial surface temperatures the predicted fouling rates were greater than those found experimentally.

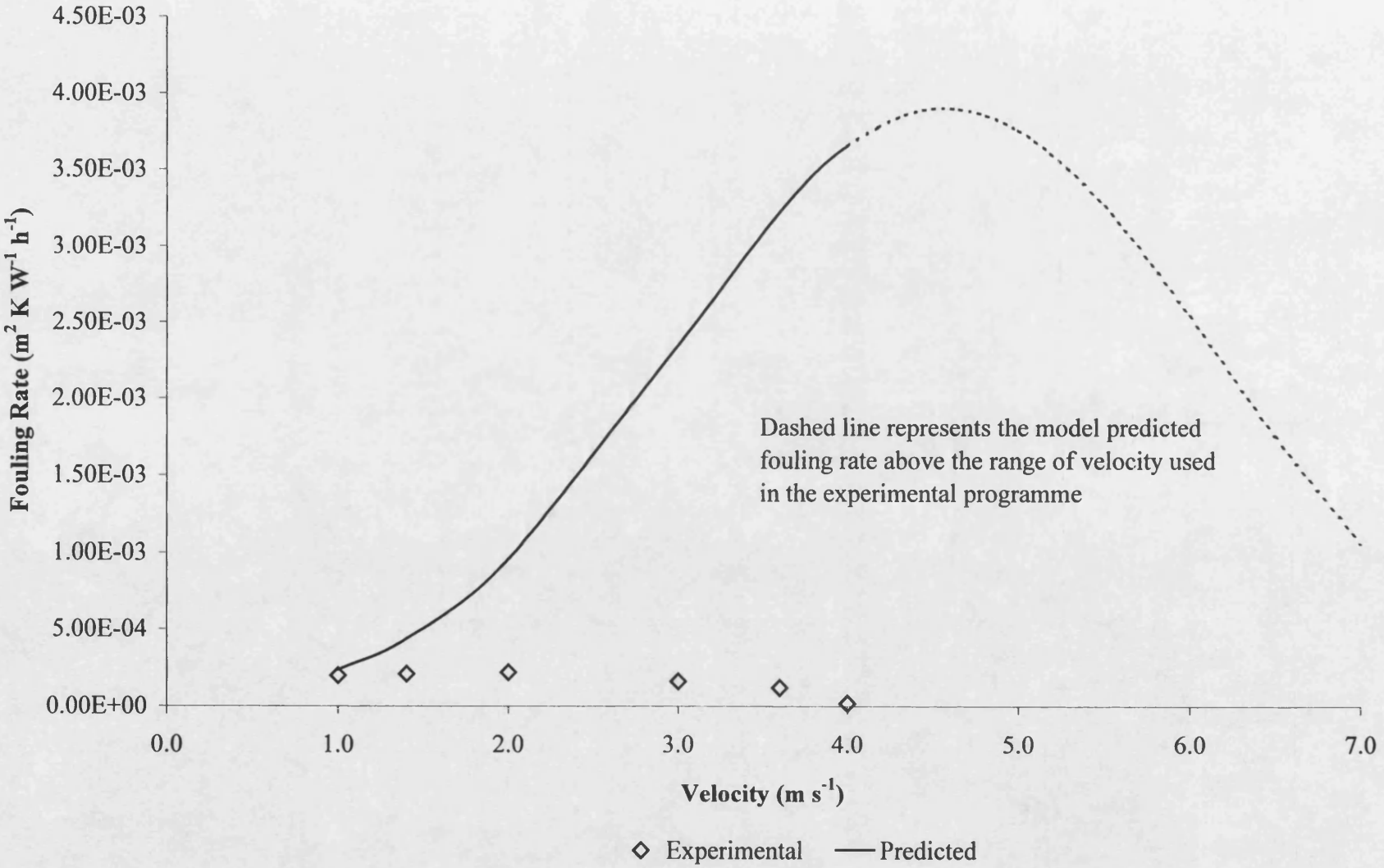

Figure 5.25 Experimental and predicted fouling rates in bare tubes at 250 °C for Case 3

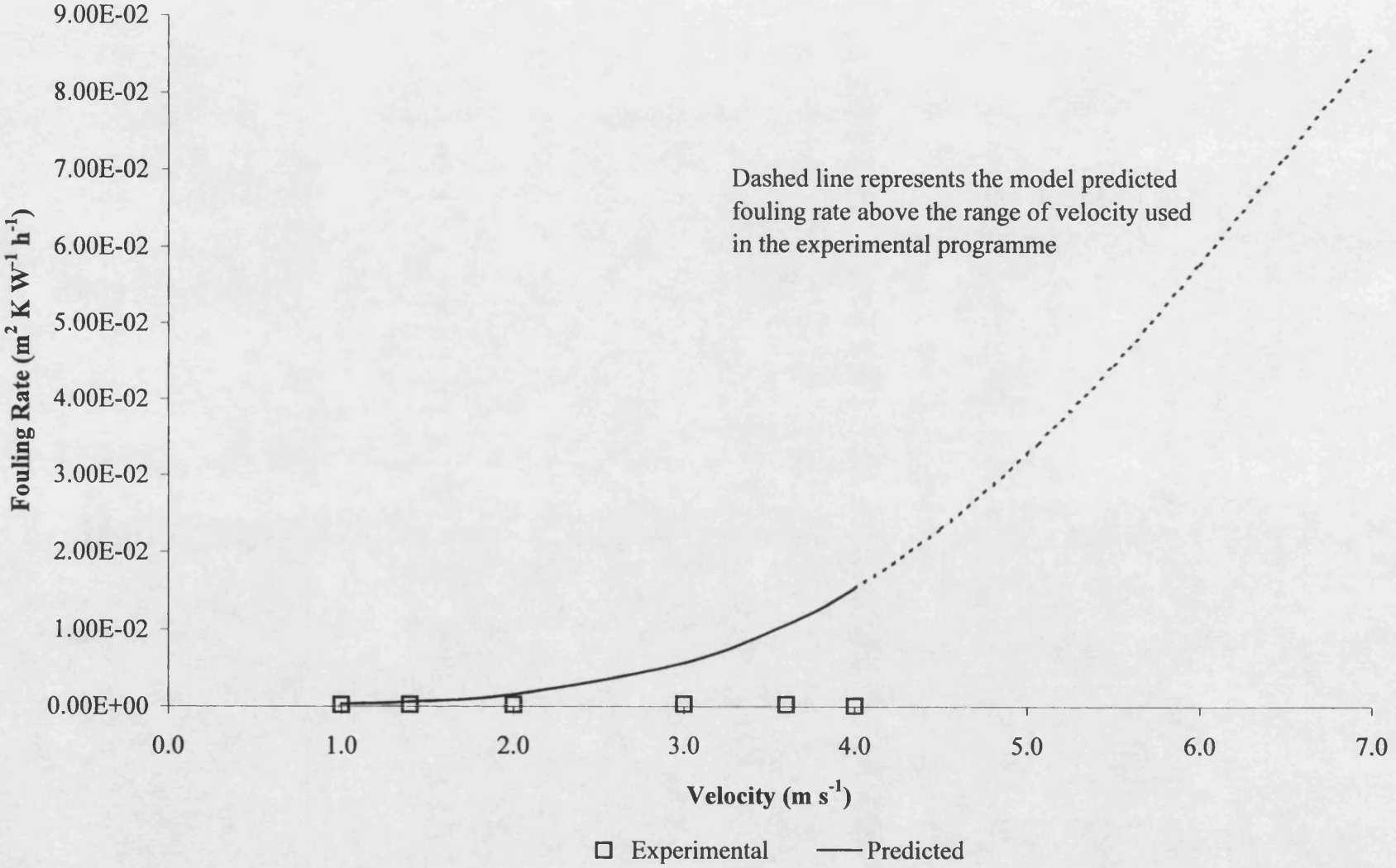

Figure 5.26 Experimental and predicted fouling rates in bare tubes at 265 °C for Case 3

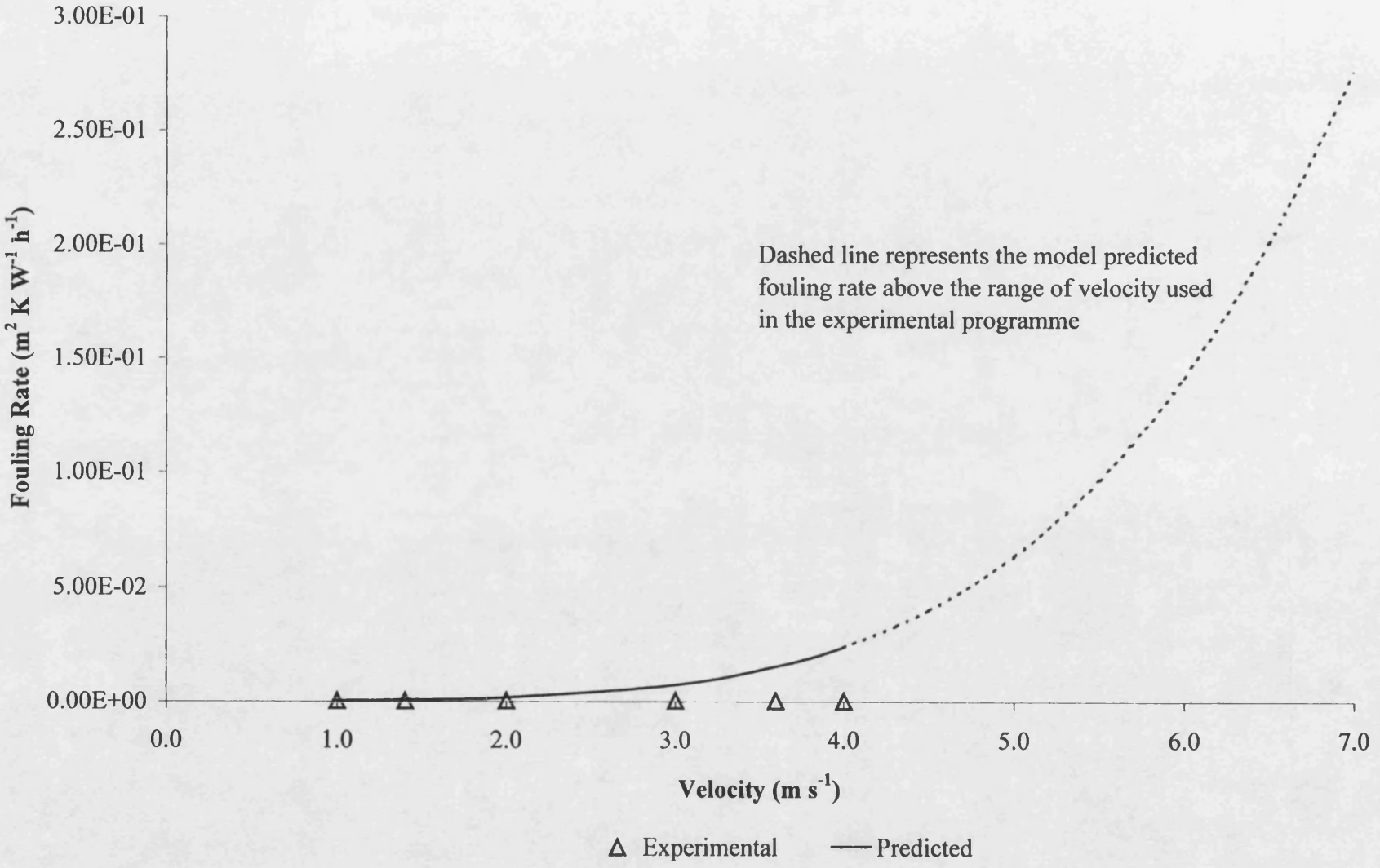

Figure 5.27 Experimental and predicted fouling rates in bare tubes at 270 °C for Case 3

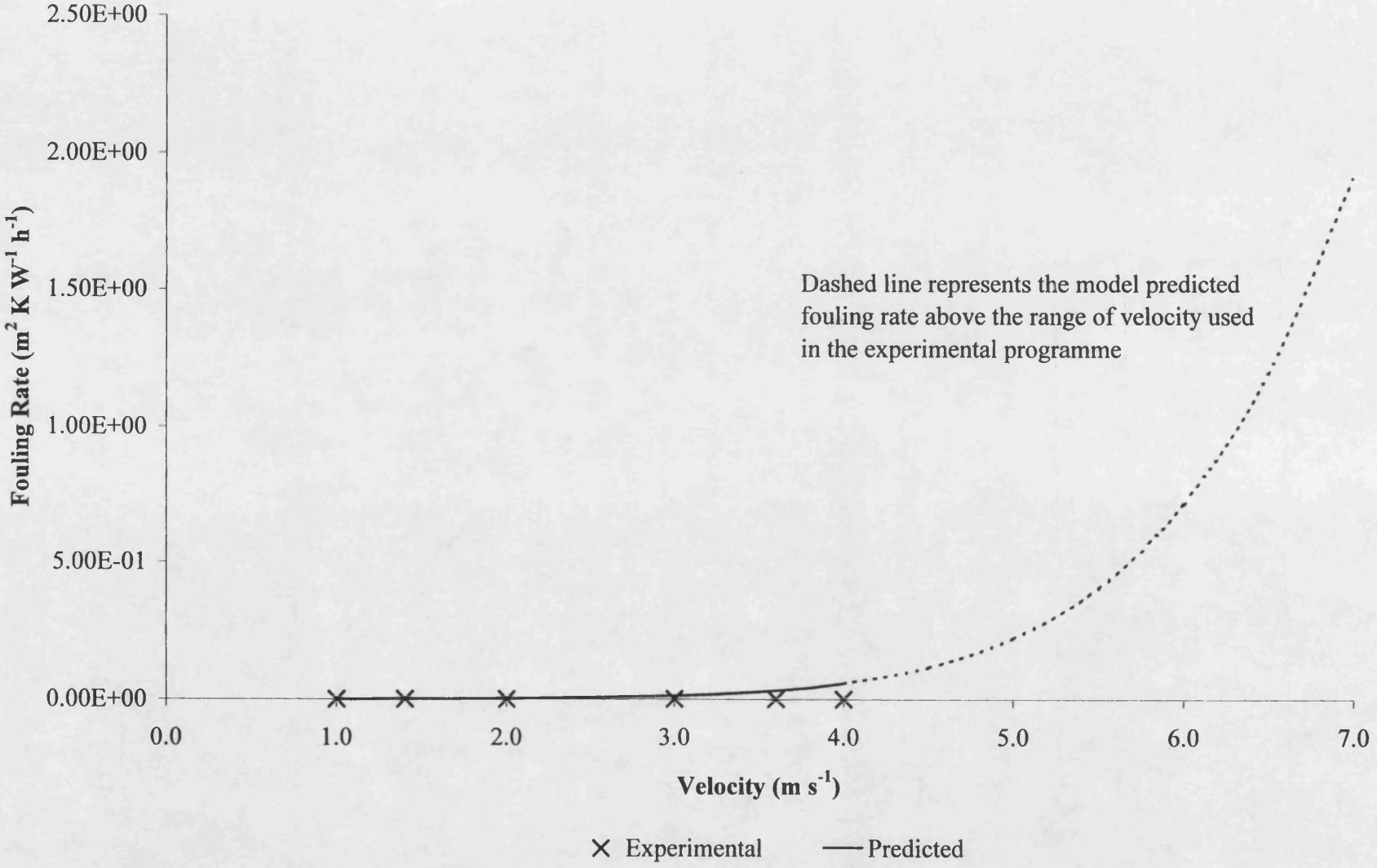

Figure 5.28 Experimental and predicted fouling rates in bare tubes at 280 °C for case 3

5.2.5.3 *Applying the model to fouling rates with inserts for Case 3*

The model for inserts used in Case 3 is identical to that used in the previous Cases (1 & 2). For all initial surface temperatures and insert geometries, the model predicts a rapid increase in fouling rate as the velocity is increased. the comparisons are shown in Figure 5.29 to Figure 5.31.

For the LDI (1.22 0.63) and MDI (1.22, 0.38) inserts at 250 °C, the fouling rates predicted by the model do not agree well with experimental data over the range of velocities studied, as shown in Figure 5.29 and Figure 5.30 respectively. At the higher surface temperature of 265 °C poor agreement was again noted between the predicted fouling rates and those found experimentally, as illustrated by Figure 5.31.

The figures do show that the predicted fouling rates with inserts do reach a maxima, although the velocities at which the maxima occur are much higher than those which could be found experimentally.

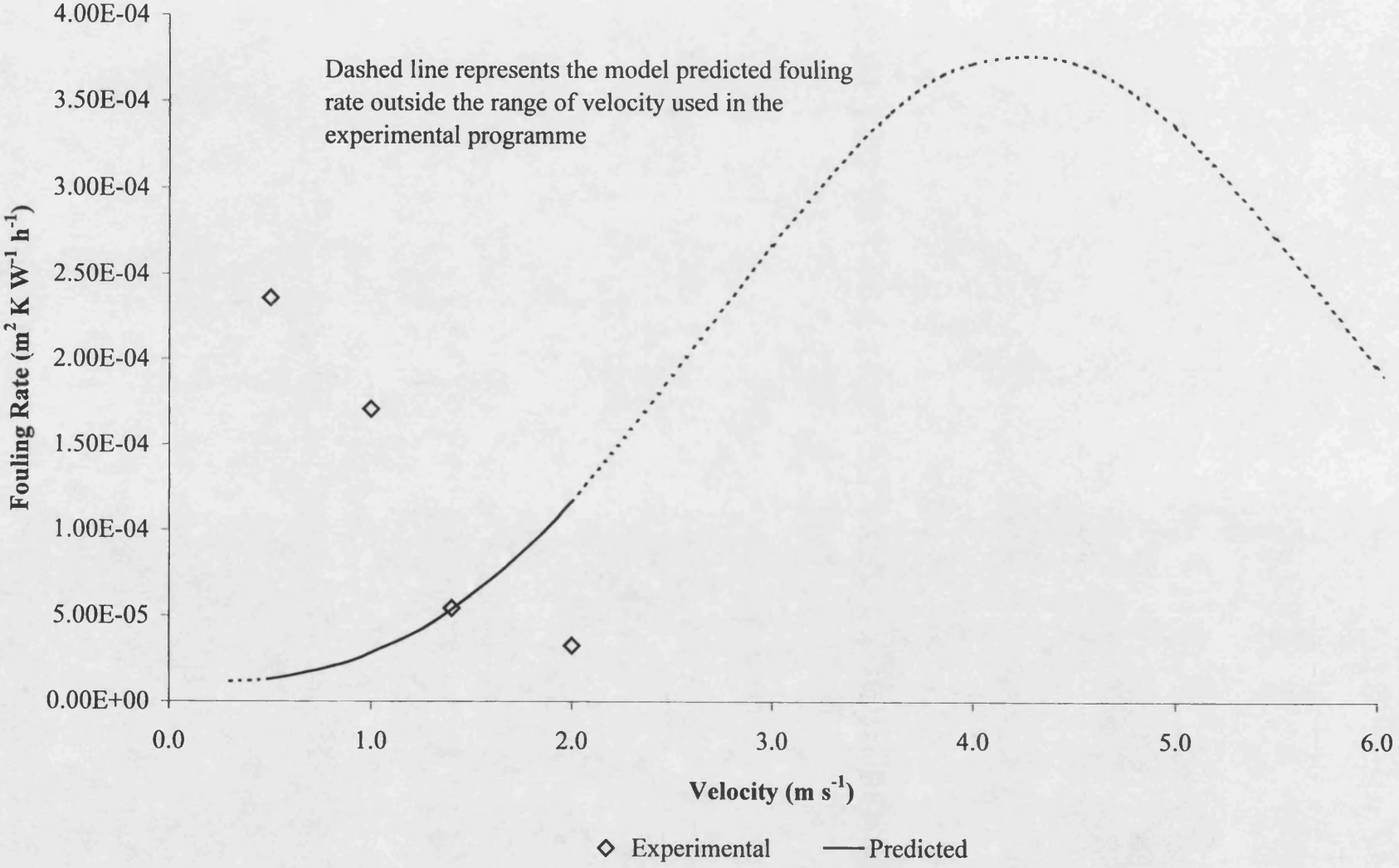

Figure 5.29 Experimental and predicted fouling rates with LDI (1.22; 0.63) at 250 °C for Case 3

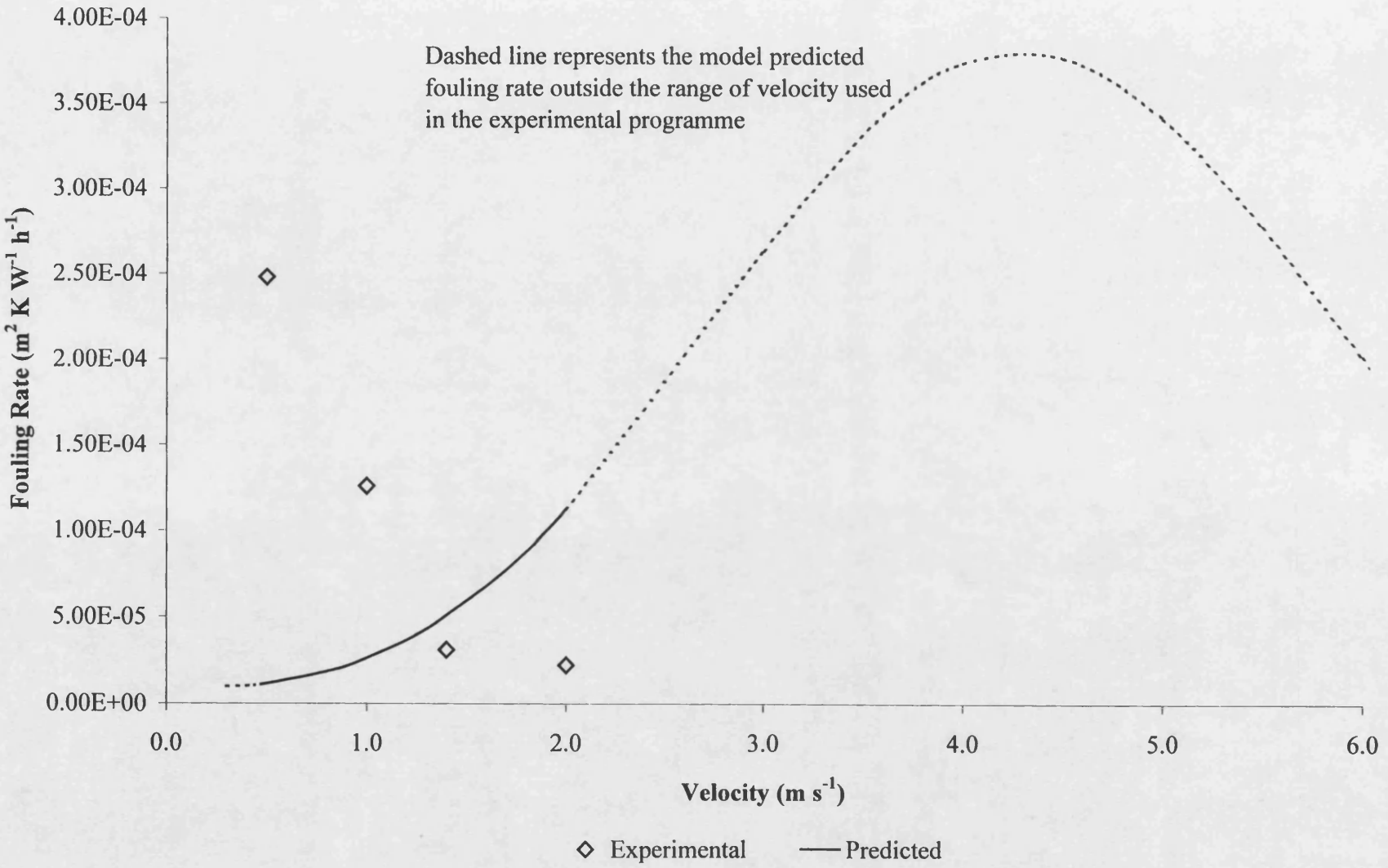

Figure 5.30 Experimental and predicted fouling rates with MDI (1.22; 0.38) at 250 °C for Case 3

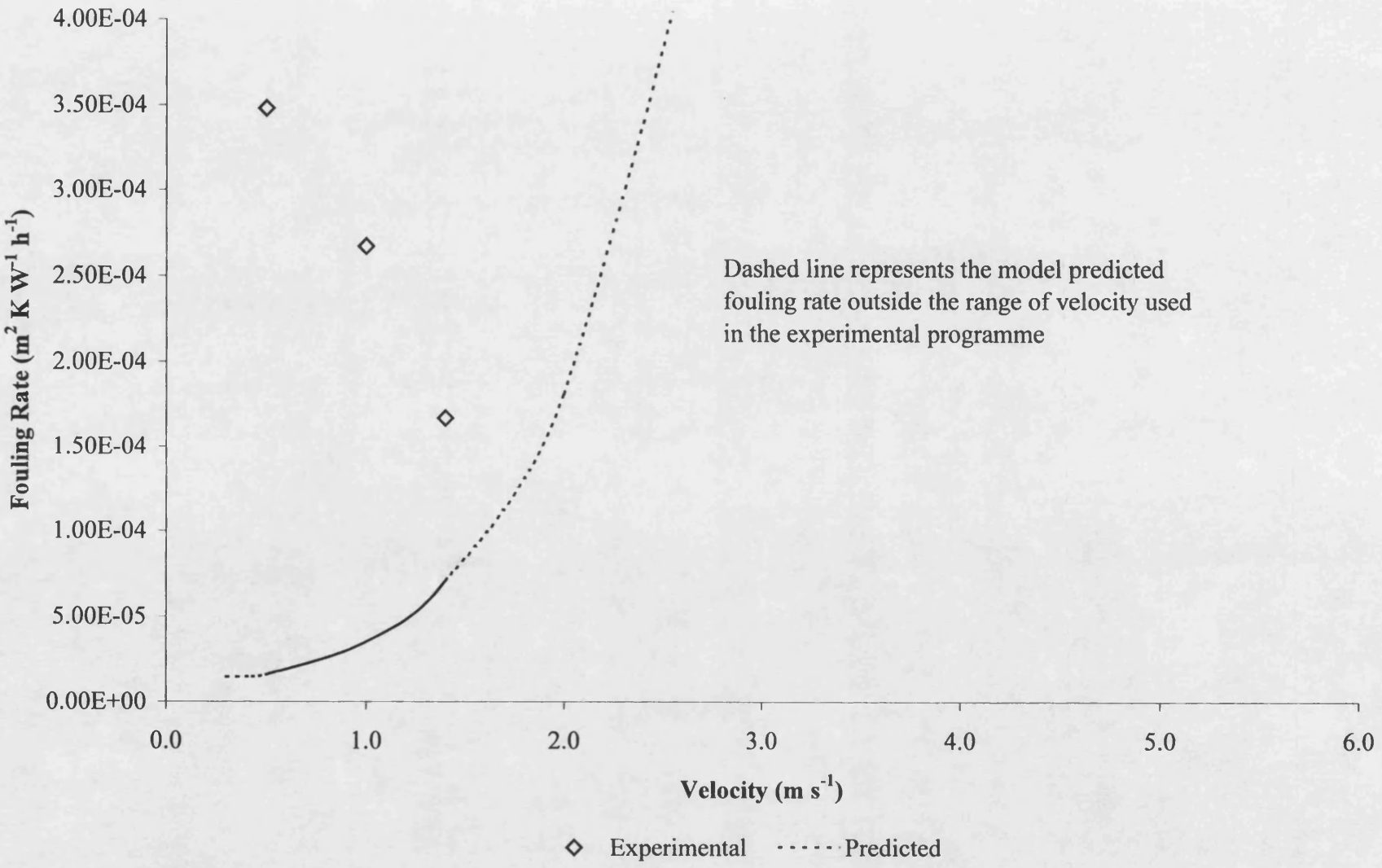

Figure 5.31 Experimental and predicted fouling rates with MDI (1.22; 0.38) at 265 °C for Case 3

5.3 Comparisons of Case 1, 2 and 3

It is clear from the preceding sections that the model is less than satisfactory in predicting all experimental data for bare tubes and for tubes fitted with inserts. Modelling fouling from complex hydrocarbons such as Maya crude oil requires a number of assumptions to be made due to a lack of knowledge. It is most likely that these assumptions strongly affect the accuracy of the model predictions. This study has found that velocity, hence turbulence, seems to have a marked effect on the apparent activation energy of the fouling reaction. Therefore, it is reasonable to assume that introducing a turbulence promoting device such as a HiTRAN® insert will also have an effect on E_A. The conditions for each Case are summarised in Table 5.13.

Table 5.13 Summary of Cases 1, 2 and 3

Case	E_A (kJ kmol-1)	Reaction Order	Reactivity Rate Factor (k")
1	26	5/2	15.50
2	77	5	2.80
3	149	10	1.58

In Case 1 the model provided a better fit with bare tubes than for tubes containing inserts. This may be explained by the fact that under bare tube conditions the reaction is more likely to be mass transfer controlled, which is typically characterised by low values of E_A. The reaction order indicates a complex reaction and is the same value as found for the polymerisation of styrene in kerosene (Epstein (1994)).

Conversely, the higher apparent activation energy in Case 2 was a better fit for tubes containing inserts than for bare tubes. As flow regimes become more turbulent, control of the overall reaction mechanism is shifted toward chemical kinetics. Reaction mechanisms controlled in this manner are likely to have E_A values above 40 kJ $kmol^{-1}$.

Case 3 poorly fitted the data for both bare tubes and tubes with inserts. This may be explained by the unsuitability of the value of E_A and / or the reaction order selected for this iteration.

This research has shown that mass transfer affects the apparent activation energy markedly. In Cases 2 and 3 the effects of temperature were more marked than in Case 1, where the E_A is appreciably lower. This could be indicative of the dependence of the overall fouling rate on kinetic effects at higher values of E_A. Until a value for the activation energy can be based purely on the intrinsic reaction kinetics, there will always be speculation as to its true value and what affect changes in velocity will have.

This Chapter has highlighted the complexity of fouling from hydrocarbons and the shortfalls that exist in the current understanding of the reaction mechanism. Acceptance of this model will depend on achieving a much better understanding of the effects of apparent activation energy, reaction order and reactivity rate factor.

5.4 Global error estimate

In calculating a value for the global experimental error for the model, the key experimental parameters must be identified. In this case the key parameters are those which are used to calculate the other inputs to the model are:

1. temperature;
2. velocity;
3. reaction order;
4. apparent activation energy.

The complexity of the mechanism has meant that the reaction order has been derived iteratively based on a set value of activation energy, as described in Chapter 4. It may be

assumed that the resultant reaction order will be compensate some of the error arising from the activation energy. Table 5.14 summarises the error estimates for the key parameters listed above:

Table 5.14 Summary of experimental errors of the key parameters

Parameter	Error (%)
Temperature	± 3.00
Apparent activation energy	± 5.30
Velocity	± 2.50

The error in the predicted fouling rate using this model by the parameters above is further compounded by the error that they induce in the remaining model inputs. These errors are summarised in Table 5.15 and Table 5.16:

Table 5.15 Summary of induced errors in calculated model inputs

Parameter	Error (%)
Density (ρ)	± 0.3
Film viscosity (μ_f)	± 15.52
Thermal conductivity of the Fluid or deposit (k)	± 1.26
Diffusivity (D_a)	± 21.77
Reynolds Number (Re)	± 20.96
Schmidt Number (Sc)	± 34.15
Friction Factor (j_f)	± 4.16
Critical velocity (u_c)	± 0.35
Critical Volume	± 7.00

Table 5.16 Summary of induced errors in calculated model inputs

Parameter	Error (%)
Mass Transfer Coefficient (k_m)	± 32.57
Reaction Rate Constant (k_R)	± 59.45
Bulk concentration (C_b)	± 0.50
Mass Flux (ϕ)	± 60.43

Accounting for all of these errors listed above, the resultant error in the initial fouling rate ($R_{f(0)}^{\bullet}$) is ± 59.93%. The magnitude of the error in $R_{f(0)}^{\bullet}$ (± 59.93%) would preclude the use of the model on the grounds of reliability. However, it must be noted that this model was derived by iteration, described in chapter 4, and tested at three arbitrarily chosen values of activation energies, namely 26 kJ $kmol^{-1}$, 77 kJ $kmol^{-1}$ and 149 kJ $kmol^{-1}$.

Excluding the errors resulting from the activation energy, the overall error in $R_{f(0)}^{\bullet}$ for bare tubes is reduced to ± 3.5%. However, where inserts are present the errors are substantially increased, in some cases to levels greater than the ± 59.93% suggested by the error calculation including the apparent activation energy.

This is most likely due to the change in the mechanism from mass transfer to chemical kinetics, and the consequent change in the apparent activation energy, as inserts are introduced. This emphasises the need to better understand the fouling mechanism, and where possible derive a true activation energy for the chemical reaction, independent of mass transfer effects.

5.5 Comments

The differences in experimental and predicted initial fouling rates may, in part, be due to the fact that the overall fouling mechanism is comprised of a number of component

mechanisms which are strongly dependent on the concentrations of a number of reacting species. The concentration term in the model strongly affects the predicted fouling rate. For example an error of 1% in the concentration results in a 10% difference in the calculated fouling rate. The bulk concentration calculated using u_m and T_w differs from the bulk concentration calculated using initial fouling rate data that was used in the iteration stage. Therefore, errors which may arise in the measurement of flow-rate or temperature will result in errors in the calculation of the bulk concentration. These errors, in turn, lead to errors in the predicted fouling rate.

The effect of errors of +1% in the values of the various parameters used in the model equations are summarised in Table 5.17 and Table 5.18, a negative resulting error depicts a reduction in the predicted fouling rate. It was found that the other parameters, such as those parameters used to calculate the asphaltene diffusivity (D_a) (MW_a, ϕ, SG_a and V_a) and bulk and film fluid density (ρ_b, ρ_f) had no apparent effect on the calculation of initial fouling rate.

Table 5.17 Summary of initial fouling rate calculation errors

Parameter	Resulting error in $R_{f(0)}^{\bullet}$ (%)
Thermal conductivity of oil in the deposit (k_{lf})	-10.00
Reaction order (n)	8.21
Apparent activation energy (E_A)	-6.26
Critical velocity (u_c)	-2.65
Bulk concentration (C_b)	2.00
Bulk temperature (T_b)	-1.46
Reactivity constant (k")	-1.00
Film viscosity (μ_f)	1.00

Table 5.18 Summary of initial fouling rate calculation errors

Parameter	Resulting error in $R_{f(0)}^{\bullet}$ (%)
Stoichiometric factor (m)	0.99
Foulant Thermal Conductivity (k_f)	-0.98
Tube wall temperature (T_w)	0.80
Bulk viscosity (μ_b)	-0.20
Velocity (u)	-0.15
Thermal conductivity of coke (k_c)	-0.01

Whilst the model does predict with reasonable accuracy the effect of changes in velocity and temperature on the trends for initial fouling rate, the results must be interpreted with caution. Until such times as a more accurate method for estimating the reaction order, pseudo concentration and apparent activation energy are developed, these parameters will be the weaknesses in any model relying on the concentration and reactivity of the fouling species.

5.6 Limitations of the model

The model presented in this chapter has been built using data from fouling experiments conducted using Maya crude only. The model predicts with reasonable accuracy the trends of changes in operating parameters such as surface temperature and flow-rate with this particular oil. However, fouling of heat exchange equipment is a practical problem present in almost all exchangers, regardless of the exchanger configuration, duty or fluid processed. Widespread acceptance of fouling models will only be achieved through the use of a model which allows one equation, or set of equations, to account for the variety of fluids, temperatures and flow rates found in industrial heat exchangers. However, to achieve this models derived from experimental data must be evaluated against industrial data.

The model developed in this thesis has been evaluated against data from laboratory experiments. The model has been used to predict with reasonable accuracy the trends caused by changes in operating conditions, together with insert presence and insert geometry. Maya crude oil has been used in the hydrocarbon fouling rig at surface temperatures and velocities ranging between 0.5 m s^{-1} to 4.0 m s^{-1} and 250 °C to 280 °C respectively. Without further experimental work outside of this range, no assessment can be made of the validity of the model. Further work is required to assess the validity of the model to industrial situations, different fluids, alternate temperatures and velocities.

6. Conclusions, recommendations and future work

6.1 Conclusions

This project was initiated to study the effects of HiTRAN® inserts on fouling rates, more specifically to:

1. quantify the benefits of HiTRAN® inserts, with regard to fouling prevention;
2. establish generic design data and a method for the confident implementation of HiTRAN® inserts.

A number of experiments have been conducted with Maya crude oil supplied by BP Oil Ltd., using the hydrocarbon fouling rig at the University of Bath. In addition to work conducted with HiTRAN® inserts, a number of experiments were completed with bare tubes. These provided a benchmark against which the effects of the inserts could be evaluated fairly. This chapter summarises the results of this fouling study, with particular emphasis being placed on the significance of the results with regard to the aims and objectives listed above.

Recommendations arising from the study are also presented in this chapter.

6.1.1 Bare tube fouling study

The bare tube fouling experiments were conducted using Maya crude at a pressure of 15 bar (to prevent nucleation). Initial surface temperatures of 250 °C, 265 °C, 270 °C and 280 °C and velocities between 0.5 m s^{-1} and 4.0 m s^{-1} were used. These ranges of initial surface temperature and velocity are within those found in industrial heat exchange equipment. Under the conditions tested the following conclusions can be drawn:

1. fouling rates are dependent on the relative balance of mass transfer and chemical kinetics;

2. altering the velocity in a bare tube can either increase or decrease the intial fouling rate, depending on whether the fouling rate is mass transfer or kinetically controlled;

3. increasing the velocity results in an increase in the apparent activation energy of the fouling process, indicating the influence of mass transfer;

4. fouling does not seem to occur at initial surface temperatures below 225 °C;

5. an increase in velocity increases the threshold fouling temperature. As the velocity is increased the mass transfer rate is also increased, requiring higher reaction rates before sufficient accumulation of fouling deposits on the heat transfer surface occurs;

6. extended periods of high velocity can result in the removal downstream of some of the fouling deposit.

6.1.2 Insert fouling study

Fouling studies have been conducted using Maya crude and a number of HiTRAN® inserts of varying density and wire diameter. Experiments were conducted at a pressure of 15 bar (to prevent nucleation). Initial surface temperatures of 250 °C, 265 °C and 270 °C and velocities between 0.5 m s^{-1} and 2.0 m s^{-1} were used. These ranges of initial surface temperature and velocity are within those found in industrial heat exchange equipment. The insert densities used in the study were 200 loops m^{-1} (very low density insert), 290 loops m^{-1} (low density insert) and 420 loops m^{-1} (medium density insert).

These densities are generally typical of those supplied to industry. Under the conditions tested the following conclusions can be drawn:

1. the increase in fluid turbulence caused by the presence of an insert in the tube can either increase or decrease the fouling rate, depending on the relative balance of mass transfer and chemical kinetics;

2. under nominally identical conditions increases in insert density up to approximately 290 loops m^{-1} (low density inserts), are found to reduce fouling rates beyond which further increases in insert density have no apparent benefit;

3. increases in loop wire diameter at densities of 290 loops m^{-1} and below are found to have a greater effect on reducing fouling rates;

4. a greater reduction in fouling is achieved for low velocities (>2.0 m s^{-1}) by increasing the loop wire diameter with densities of 290 loops m^{-1}, or below;

5. under nominally identical conditions increases in loop wire diameter at densities greater than 290 loops m^{-1} are found to have little additional effect on the reduction of fouling rates;

6. increases in insert density result in increased heat transfer coefficients;

7. increases in loop wire diameter at nominally identical insert densities result in increases in the heat transfer coefficient for the two wire diameters tested;

8. inserts result in greater pressure drops than bare tubes under nominally identical conditions;

9. increases in insert density result in greater pressure drops for otherwise identical conditions;

10. increases in wire loop diameter result in greater pressure drops for otherwise identical conditions and insert densities for the two wire diameters tested;

11. the use of intermittent inserts require careful consideration as the benefits of using inserts are rapidly lost once the fluid exits the insert matrix section; this is due to the reformation of the boundary layer;

6.1.3 Modelling

The model developed by Epstein (1994) to account for fouling from the 1% ($^{v}/_{v}$) styrene in kerosene ideal fouling solution used by Crittenden, Hout and Alderman (1987) has been adapted to try and predict the experimental fouling rates from Maya crude oil in the hydrocarbon recycle rig. The model is based on the transport of the foulant or precursor to the reaction site followed by reaction and attachment to the heat transfer surface. The range of activation energies found with the bare tube study ranged from 26 kJ $kmol^{-1}$ to 149 kJ $kmol^{-1}$, with an average of 77 kJ $kmol^{-1}$. These three different apparent activation energies have been used to model fouling from Maya crude oil. The following conclusions can be drawn:

1. model predicted reaction rates are strongly dependent on the unknown concentration of foulant or precursors;

2. accurate estimation of the foulant or precursor concentrations is essential to predict correctly the fouling rate;

3. in Case 1 (E_A = 26 kJ $kmol^{-1}$) the model predicts an increase in bare tube fouling rates as the velocity is increased up to a certain point, beyond which

the fouling rate decreases. This trend concurs with the experimental data. However, poor agreement was observed between predicted fouling rates and those for tubes containing inserts;

4. agreement between predicted fouling rates for tubes with inserts and experimental values was better for Case 2 (E_A = 77 kJ $kmol^{-1}$) than for Case 1. However, poor agreement was observed between predicted and experimental fouling rates for bare tubes, as the fouling rates were found to decrease with velocity over the range velocities used in the study;

5. in Case 3 (E_A = 149 kJ $kmol^{-1}$) the model predicted an increase in fouling rate with velocity for both bare tubes and tubes containing inserts. This does not agree with the experimental fouling rates for bare tubes and tubes with inserts;

6. the reaction order and kinetic plus attachment constant in the model were both found to increase with apparent activation energy;

7. using the appropriate combination of activation energy, reaction order and kinetic plus attachment constant the, proposed model is a good basis for modelling fouling from crude oil, but needs much more refinement;

8. the model can in principle be applied to assist the designer to identify the most beneficial scenarios for coping with fouling.

6.2 Recommendations for future work

As part of this study the experimental apparatus has been modified to extend its operating range. Process parameters such as initial surface temperature, velocity, insert presence and insert geometry have all been found to affect fouling rates. However,

further fundamental work is needed to understand more fully the fouling mechanism and how inserts interact with the fouling fluid to mitigate fouling.

This study has shown that increasing the loop wire diameter at otherwise identical conditions can result in reduced fouling. Further work is required to elucidate whether relatively low densities and "high" loop wire diameters or relatively high densities and "low" loop wire diameters offer the greatest benefits.

Further bare tube studies are required to derive the intrinsic activation energy for the fouling reaction such that it is independent of mass transfer effects. This will enable the fouling mechanism to be better understood and the model further refined. Further work exploring the relationship between fluid and critical insert parameters such as insert density and loop wire diameter is required to gain a better understanding of how the relative benefit of inserts is affected by different fluids and different operating conditions. Additionally, further development work on the model for use with inserts is required to improve its accuracy.

The model developed as part of this study is, at the moment, particular to Maya crude. The model therefore may not be used with confidence to predict the fouling rate with a different crude oil. Further experimental work on different crude oils therefore is required.

Fouling is a practical problem and the results and conclusions of this project must be interpreted for industrial situations that the hydrocarbon fouling rig has been set up to emulate. The model developed as part of this study needs to be validated against industrial data. Successful validation of the model against plant data will promote confidence in the fouling model, permitting designers and plant engineers to develop better strategies to counter the effects of fouling in heat exchangers.

6.3 *Application of the model to industrial situations*

Once model development and validation have been completed successfully, the model may be integrated into exchanger design programmes. This will allow the designer and plant engineer to optimise the best design for thermal, hydraulic or fouling performance as required by the purchaser.

Before placing an insert into heat exchange equipment, consideration must be given as to why the insert is being installed. A HiTRAN® insert may be used to intensify an existing exchanger that may or may not have a fouling problem, reduce fouling in an exchanger that does have the problem, or both. Careful consideration of all these points is required prior to the selection of an insert that will best suit the application. Generally the following must be considered:

1. the range of velocities that the exchanger will be subjected to: where large turndown ratios are expected, higher density and loop wire diameter inserts may be considered. This is due to the fact that they appear to mitigate fouling more effectively at lower velocities than low density low loop wire diameter inserts;

2. the function of the exchanger: where the exchanger is used to control the temperature of one of the streams, inserts can be used to reduce the approach temperatures, thereby increasing the efficiency of the exchanger;

3. why the insert is installed: if the service is clean, then fouling prevention will not be a factor, therefore a lower density and loop wire diameter can be considered.

By using tube wall temperature estimations common in most exchanger calculation packages, the model can be applied to predict fouling rates. Consequently the engineer

can quickly assess the impact of the revised design on the exchanger network and hence optimise the solution to achieve the initial objectives. Additionally, energy consumed by the provision of additional pressure drop may not be as great compared with the savings made by recovering more heat; these benefits must be assessed for each case.

7. References

Asomaning, S and Watkinson, AP (1997) *Deposit formation by asphaltene-rich heavy oil mixtures on heat transfer surfaces*, Engineering Foundation Conference on Understanding Heat Exchanger Fouling and its Mitigation, 11 - 16 May.

Bergeles, AE (1988) *Some Perspectives On Enhanced Heat Transfer - Second Generation Heat Transfer Technology*, Transactions Of The ASME, **110**, 1082 - 1096.

Bergeles, AE and Somerscales, EFC (1995) *The Effect Of Fouling On Enhanced Heat Transfer Equipment*, Journal Of Enhanced Heat Transfer, **2** (1 - 2), 157 - 166.

Bott, TR (1990) *Fouling Notebook*, Institution Of Chemical Engineers, Rugby.

Chenoweth, JM (1990) *Final Report Of The HTRI / TEMA Joint Committee To Review The Fouling Section Of The TEMA Standards*, Heat Transfer Engineering, **11** (1), 73 - 107.

Coulson, JM, Richardson, JF and Sinnott RK (1991) *Chemical Engineering Volume 6: An Introduction to Chemical Engineering Design*, Pergamon Press, London.

Coulson, JM, Richardson, JF, Blackhurst, JR and Harker, JH (1993) *Chemical Engineering Volume 1: Fluid Flow, Heat Transferand Mass Transfer*, 4th Ed., Pergamon Press, London.

Crittenden, BD (1988a) *Basic Science And Models Of Reaction Fouling*, In Fouling Science And Technology, Melo, LF, Bott, TR and Bernardo, CA eds., Kluwer Academic Publishers, Holland, 293 - 313.

Crittenden, BD (1988b) *Chemical Reaction Fouling Of Heat Exchangers*, In Fouling Science And Technology, Melo, LF, Bott, TR and Bernardo, CA eds., Kluwer Academic Publishers, Holland, 315 - 332.

Crittenden, BD and Khater, EMH (1984) *Fouling In A Hydrocarbon Vaporiser*, Institute Of Chemical Engineers Symposium Series, **86** (1), 401 - 414.

Crittenden, BD, Hout, SA and Alderman, NJ (1987) *Model Experiments Of Chemical Reaction Fouling*, Chemical Engineering Research Design, **65**, 165 - 170.

Crittenden, BD, Kolaczkowski, ST and Downey, IL (1992) *Fouling Of Crude Pre-heater Exchangers*, Transactions of The Institute Of Chemical Engineers, **70** (A), 547 - 557.

Crittenden, BD, Kolaczkowski, ST and Hout, SA (1987 *Modelling Hydrocarbon Fouling*, Chemical Engineering Research Design, **65**, 171 - 179.

Crittenden, BD, Kolaczkowski, ST and Phillips DZ (1997) *Chemical Reaction Fouling*, Engineering Foundation Conference on Understanding Heat Exchanger Fouling and its Mitigation, 11 - 16 May.

Crittenden, BD, Kolaczkowski, ST and Takemoto, T (1993) *Use Of In-Tube Inserts To Reduce Fouling*, 29th AIChE Heat Transfer Conference, Atlanta, 8th - 11th August.

Crittenden, BD, Kolaczkowski, ST, Takemoto, T and Gough, MJ (1993) *Use Of Wire Matrix Inserts To Control Hydrocarbon Fouling: Current Achievements And Future Prospects*, Proceedings Of The Tenth International Heat Transfer Conference, Industrial sessions, Institute Of Chemical Engineers, 213 - 218.

Dickakian, G and Seay, S (1988) *Asphaltene Precipitation Primary Crude Exchanger Fouling Mechanism*, Oil And Gas Journal, March, 47 - 50.

Eaton, P and Lux, R (1984) *Laboratory Fouling Test Apparatus For Hydrocarbon Feedstocks*, In Fouling In Heat Exchange Equipment, Suitor, JW and Pritchard, AM eds., ASME HTD-35, New York, 33 - 42.

Epstein, N (1981) *Fouling: Technical Aspects (Afterword To Fouling In Heat Exchangers)*, In Fouling Of Heat Transfer Equipment, Somerscales, EFC and Knudsen, JG eds., M^{C}Graw-Hill International Book Company, London, 31 - 53.

Epstein, N (1983) *Fouling Of Heat Exchangers*, In Heat Exchangers: Theory And Practice, Taborek, J, Hewitt, GF and Afgan, N eds., Hemisphere Publishing Corporation, London, 795 - 815.

Epstein, N (1988) *Particulate Fouling Of Heat Transfer Surfaces*, In Fouling Science And Technology, Melo, LF, Bott, TR and Bernardo, CA eds., Kluwer Academic Publishers, Holland, 143 - 164.

Epstein, N (1994) *A Model of the Initial Chemical Reaction Fouling Rate for Flow Within a Heated Tube, and its Verification*, In Heat Transfer 1994: Proceedings Of The Tenth International Heat Transfer Conference, Hewitt, GF ed., Institute Of Chemical Engineers, **4**, 225 - 229.

Fitzer, E, Mueller, K and Schaeffer, W (1971) The Chemistry of the Pyrolitic Conversion of Organic Compounds to Carbon, in Chemistry and the Physics of Carbon, Walker, P.J. (Jnr.) ed., Marcel Dekker, New York, 273 - 383.

Garrett-Price, BA (1985) *Fouling Of Heat Exchangers*, Noyes Publications, New Jersey.

Gough, MJ and Rogers, JV (1987) *Reduced Fouling By Enhanced Heat Transfer Using Wire Matrix Radial Mixing Elements*, The American Institute Of Chemical Engineers Symposium Series, **83** (257), 16 - 21.

Gough, MJ and Rogers, JV (1992) *The Theory, application and use of matrix tube elements (HiTRAN System) to control tube side fouling*, Eurotherm Seminar N° 23, Editions Europeennes Thermique & Industrie.

Gough, MJ and Terranova, A (1992) *Up Grading Thermal Performance And Reducing Fouling Of Tubular Heat Exchangers By The Use Of Tube Side Enhancement Technology*, Refining, LNG and Petrochem Asia, Singapore, 1st - 4th December.

Hall, KR and Yarborough, L (1971) *New, Simple Correlation for Predicting Critical Volume*, Chemical Engineering, **1**, 76 - 77.

Houser, G and Sommer, K (1990) Basic aspects on plant cleaning in the food industry, Process Engineering in the Food Industry, Field, RW and Howell, JA eds., Elsiver, Oxford.

Hout, SA (1983) *Chemical Reaction Fouling*, PhD, University of Bath.

Jones, AG and Balster, WJ (1995) *Surface fouling in aviation fuel: short vs long-term isothermal tests*, Energy and Fuels, **9** (4), 610 - 615.

Jones, AG, Balster, WJ and Anderson, SD (1992) *Formation of Insolubles in Jet Fuels: Effects of Oxygen*, Symposium Series on the Structure of jet Fuels III, ACS, San Francisco, April, 393 - 402.

Jones, AG, Balster, WJ and Post, ME (1995) *Degradation of a Jet A fuel in a single-pass heat exchanger*, Journal of Engineering for Gas Turbines and Power, January, **117**, 125 - 131.

Kern, DQ (1950) *Process Heat Transfer*, McGraw Hill, New York.

Kern, DQ and Seaton, RE (1959) *A Theoretical Analysis Of Thermal Fouling*, British Chemical Engineering, **4** (5), 258 - 269.

Lambourn, GA and Durrieu, M (1983) *Fouling In Crude Oil Preheat Trains*, In Heat Exchangers: Theory And Practice, Taborek, J, Hewitt, GF and Afgan, N eds., Hemisphere Publishing Corporation, London, 841 - 852.

M^{c}Mullan, AS, Gough, MJ, Gibbard, I and Polley, GT (1995) *Case Studies Of Refinery Fouling Reduction*, Engineering Foundation Conference on Fouling Mitigation Of Industrial Heat Exchangers, 18th - 23rd June 1995.

Müller-Steinhagen, H and Jamialahmadi, M (1997) *Mitigation of scale formation in bauxite refineries*, Engineering Foundation Conference on Understanding Heat Exchanger Fouling and its Mitigation, 11 - 16 May.

Müller-Steinhagen, H and Zhao, Q (1997) *Investigation of Low Fouling Surface Alloys Made by Ion Implantation Technology*, Chemical Engineering Science, **52** (19), 3321 - 3332.

Nelson, WL (1934) *Fouling Of Heat Exchangers*, Refiner And Natural Gas Manger, **13** (7), 271 - 276.

Oliver, DR and Adlington RWJ (1988) *Heat Transfer Enhancement In Round Tubes Using Wire Matrix Turbulators: Newtonian And Non-Newtonian Fluids*, Chemical Engineering Research Design, **66**, 555 - 565.

Panchal, CB, Halpern, Y, Kuru, WC and Miller, G (1997) *Mechanisms of Iron Sulphide Formation in Refining Processes*, Engineering Foundation Conference on Understanding Heat Exchanger Fouling and its Mitigation, 11 - 16 May.

Paterson, WR and Fryer, PJ (1988) *A Reaction Engineering Approach To The Analysis Of Fouling*, Chemical Engineering Science, **43** (7), 1714 - 1717.

Perry, RH and Green D (1984) *Perry's Chemical Engineers' Handbook*, 5th Ed, McGraw-Hill Book Company, London.

Polley, GT and Gibbard, I (1995) *The Application Of HiTRAN Inserts In Sulofane Solvent Extraction Plants*, The Energy Efficiency Office / Instute Of Petroleum Meeting 4th October 1995.

Polley, GT, Nasr, J, and Terranova, A (1994) *Determinatrion and application of benefits of heat transfer enhancement*, Transactions of The Institute Of Chemical Engineers, **72** (A), 616 - 620.

Pritchard, AM (1988) *The Economics Of Fouling*, In Fouling Science And Technology, Melo, LF, Bott, TR and Bernardo, CA eds., Kluwer Academic Publishers, Holland, 3 - 14.

Rebello, WJ, Richlen, SL and Childs, F (1988) *Cost Of Heat Exchanger Fouling In US Industries*, Report EGG - M - 39187.

Rose, I, Epstein, N and Watkinson, AP (1997) *The Effect of Velocity on the Initial Fouling Rate of Whey Protein Solutions at Elevated Wall and Low Bulk Temperatures*, Engineering Foundation Conference on Understanding Heat Exchanger Fouling and its Mitigation, 11 - 16 May.

Shalhi, AM (1993) *The Use Of HiTRAN® Inserts To Enhance Heat Transfer And Control Fouling From Hydrocarbons*, PhD, University of Bath.

Smith, JD (1969) *Fuel for the supersonic transport - effects of deposits on hea transfer to aviation fuels*, Industrial Engineering Chemistry Production Research And Development, **8**, 299 - 308.

Takemoto, T (1993) *Use Of HiTRAN® Inserts To Reduce Fouling From Crude Oils*, PhD, University of Bath.

Taylor, WF (1974) *Deposit Formation From Deoxygenated Hydrocarbons. 1. General Features*, Industrial Engineering Chemistry Production Research And Development, **13** (1), 133 - 138.

Taylor, WF (1976) *Deposit Formation From Deoxygenated Hydrocarbons. 2. Effects Of Trace Sulphur Compounds*, Industrial Engineering Chemistry Production Research And Development, **15** (1), 64 - 68.

Taylor, WF and Frankenfeld, JW (1978) *Deposit Formation From Deoxygenated Hydrocarbons. 3. Effects Of Trace Nitrogen And Oxygen Compounds*, Industrial Engineering Chemistry Production Research And Development, **17** (1), 86 - 90.

Taylor, WF and Wallace TJ (1968) *Kinetics Of Deposit Formation From Hydrocarbons*, Industrial Engineering Chemistry Production Research And Development, **7** (3), 198 - 202.

Thome, JR (1992) *Heat Transfer Augmentation In The Hydrocarbon Processing Industries*, American Institute Of Chemical Engineers Symposium Series, **88** (288), 220 - 224.

Van Nostrand, WL, Leach, SH and Haluska, JL (1981) *Economic Penalties Associated With The Fouling Of Refinery Heat Transfer*, In Fouling Of Heat Transfer Equipment, Somerscales, EFC and Knudsen, JG eds. M^{C}Graw-Hill International Book Company, London, 619 - 643.

Varnos, A, Marteney, PJ and Knight, BA (1981) *Determination Of Coking Rates In Jet Fuel*, In Fouling Of Heat Transfer Equipment, Somerscales, EFC and Knudsen, JG eds., M^{C}Graw-Hill International Book Company, London, 489 - 499.

Watkinson, AP (1988) *Critical Review Of Organic Fluid Fouling: Final Report*, Argonne National Laboratory, Report N^{o} ANL / CNSV - TM - 208.

Watkinson, AP (1990) *Fouling Of Augmented Heat Transfer Tubes*, Heat Transfer Engineering, **11** (3), 57 - 65.

Watkinson, AP (1991) *Interaction Of Enhancement And Fouling*, ASME HTD-164, New York, 1 - 7.

Watkinson, AP and Epstein, N (1969) *Gas Oil Fouling In A Sensible Heat Exchanger*, Chemical Engineering Progress Symposium Series, **65** (92), 84 - 90.

Watkinson, AP and Epstein, N (1970) *Proceedings of the 4th international heat transfer conference Paris*, **1**, Paper HE1.6, Elsevier, Amsterdam.

Weiland, JH, M^{c}Cay, RC and Barnes, JE (1949) *Rates Of Fouling And Cleaning Of Unfired Heat Exchange Equipment*, Transactions Of The ASME, **71**, 849 - 853.

Wilson, DI and Vassiliadis, VS (1997) *Mitigation of refinery fouling by management of cleaning*, Engineering Foundation Conference on Understanding Heat Exchanger Fouling and its Mitigation, 11 - 16 May.

Wilson, DI and Watkinson, AP (1995) *Model Experiments Of Autoxidation Reaction Fouling: Part I: Mechanisms*, Transactions of The Institute Of Chemical Engineers, **73** (A), 59 - 65.

Wilson, DI and Watkinson, AP (1996) *A study of autoxidation reaction in heat exchangers*, The Canadian Journal of Chemical Engineers, **74**, April, 236 - 245.

Wilson, DI and Watkinson, AP (1997) *Chemical reaction fouling: a review*, Experimental Thermal and Fluid Science, **14**, 361 - 374.

Wilson, DI, Lai, RC and Watkinson, AP (1995) *Model Experiments Of Autoxidation Reaction Fouling: Part II: Effect Of Flow Parameters And Antioxidants*, Transactions of The Institute Of Chemical Engineers, **73** (A), 69 - 77.

Zarbarnick, S (1993) *Chemical kinetic modelling of jet fuel autoxidation and antioxidant chemistry*, Industrial Engineering Chemistry Production Research And Development, **32** (6), 1012 - 1017.

8. Further Reading

Albright, LF (1988) *Coke From Small Diameter Tubes Analysed*, Oil And Gas Journal, August, 44 - 48.

Arici, ME, Asan, H and Ayhan, T (1994) *Enhancement Of Turbulent Flow Heat Transfer In Tubes By Means Of Wire Coil Inserts*, Transactions Of ASME (Petroleum Division), **64** (1), 113 - 117.

Bott, TR (1988) *General Fouling Problems*, In Fouling Science And Technology, Melo, LF, Bott, TR and Bernardo, CA eds., Kluwer Academic Publishers, Holland, 3 - 14.

Butler, RC, M^{c}Curdy, WN and Linden, NJ (1949) *Fouling Rates And Cleaning Methods In Refinery Heat Exchangers*, Transactions Of The ASME, **71**, 843 - 847.

Crittenden, BD and Alderman, NJ (1988) *Negative Fouling Resistances: The Effect Of Surface Roughness*, Chemical Engineering Science, **43**, (4), 829 - 838.

Crittenden, BD and Kolaczkowski, ST (1979) *Energy Savings Through The Accurate Prediction Of Heat Transfer Fouling Resistances*, In Energy For Industry, O'Callaghan, PW, Pergamon Press, Oxford, 257 - 266.

Geisbrecht, RA and Daubert TE (1976) *Hydrocarbon Partial Oxidation*, Industrial Engineering Chemistry Production Research And Development, **15** (2), 86 - 90.

Jones, AG and Balster, WJ (1994) *Formation of insolubles in a Jet A Fuel: temperature effects*, Preprints of the American Chemical Society Petroleum Division, **39** (1), 78 - 81.

Kirpov, VA (1991) *Classification Of Current Methods For Intensifying Heat Transfer With Forced Flow (And No Phase Transitions)*, Theoretical Foundations Of Chemical Engineering, **25** (1), 121 - 124.

Leach, SH and Factor, SA (1981) *Monitoring Fouling In Refinery And Petrochemical Plant Heat Exchange Equipment*, In Fouling In Heat Exchange Equipment, Chenoweth, JM and Impagliazzo, M eds., ASME HTD-17, New York, 39 - 43.

Melo, LF and Pinheiro, J de D RS (1984) *Laboratory Fouling Test Apparatus For Hydrocarbon Feedstocks*, In Fouling In Heat Exchange Equipment, Suitor, JW and Pritchard, AM eds., ASME HTD-35, New York, 33 - 42.

Nazmeev, YG, Konakhin, AM, Kumirov, BA and Shinkevich, OP (1994), *An Experimental Study Of Heat Transfer Under Laminar Flow Conditions In Tubes With Spiral Wound Inserts*, Thermal Engineering, **41** (11), 898 - 901.

Nelson, WL (1958) *Petroleum Refinery Engineering*, 4th ed., M°Graw - Hill, New York, 546 - 550.

Oufer, L and Knudsen, JG (1993) *Modelling Chemical Reaction Fouling Under Sub-Cooled Boiling Conditions*, American Institute Of Chemical Engineers symposium Series, **89** (295), 308 - 313.

Schrier, PJR and Freyer, PJ (1995) *heat Exchanger Fouling: A model of the Scaleup of Laboratory Data*, Chemical Engineering Science, **50**, (8), 1311 - 1321.

Thackery, PA (1980) *The Cost Of Fouling In Heat Exchange Plant*, Effluent And Water Treatment Journal, March.

Appendices

A. Test section data

A.1 Development of the Wilson plot

The use of the Wilson plot enables the resistance to heat transfer from the contact between the heat source and the inside wall of the test section (R_w) to be derived graphically. This can be achieved by plotting the reciprocal of the overall heat transfer coefficient (U_O^{-1}) against variation in mean linear velocity to the power -0.8 ($u_m^{-0.8}$). For a constant heat flux, a straight-line relationship should be obtained. Below is the development of the equation allowing the comparison of U_O with u_m.

In order to develop a relationship between U_O and u_m, a series equations can be combined to result in the required relationship. The comparison between U_O and u_m is primarily based on the equation relating Nusselts number (Nu), Reynolds number (Re) and Prandtls number (Pr), as illustrated by equation (A.1):

$$Nu = 0.023\mathrm{Re}^{0.8}\mathrm{Pr}^{0.4} \qquad \text{(A.1)}$$

The Nusselt number is a function of internal heat transfer coefficient (h_i), internal diameter of the flow annulus (d_i) and the thermal conductivity of the fluid (k), as illustrated by equation (A.2):

$$Nu = \frac{h_i d_i}{k} \qquad \text{(A.2)}$$

Reynolds number is a function of the mean linear velocity (u_m), internal diameter of the flow annulus (d_i), the density of the fluid (ρ) and the viscosity of the fluid (μ), as illustrated by equation (A.3):

$$\mathrm{Re} = \frac{u_m d_i \rho}{\mu} \qquad \text{(A.3)}$$

Prandtls number is a function of the specific heat capacity of the fluid (C_P), the viscosity of the fluid (μ), and the thermal conductivity of the fluid (k), as illustrated by equation (A.4):

$$\mathrm{Pr} = \frac{Cp\mu}{k} \tag{A.4}$$

Substituting equations (A.2), (A.3) and (A.4) into (A.1), and assuming constant physical properties, we can isolate h_i. Simplifying the resulting equation results in equation (A.5):

$$h_i = cu_m^{0.8} \tag{A.5}$$

The overall heat transfer coefficient (U_O) can be described as the reciprocal of the sum of individual resistances. The individual resistances are comprised of the corresponding film resistances, calculated from the heat transfer coefficients (h_i and h_o) and fouling resistances (R_{fi} and R_{fO}), for inside and outside the tube (denoted by subscript i and o respectively), as illustrated by equation (A.6):

$$\frac{1}{U_o} = \frac{1}{h_i}\frac{d_i}{d_o} + R_{fi} + \frac{1}{h_o} + R_{fo} + R_w \tag{A.6}$$

Heat is provided externally by electrically heat elements to the test fluid in the test sections used in hydrocarbon fouling rig at the University of Bath. Therefore, there are film resistances, such as h_o or R_o, on the external surface of the tube. To ensure that no fouling occurred on the inside of the tube a non-fouling high temperature heat transfer fluid was used (Santotherm SP 50). Combining equations (A.5) and (A.6) and simplifying, equation (A.7) results:

$$\frac{1}{\mathrm{U_O}} = c\frac{1}{\mathrm{u_m^{0.8}}} + R_w \tag{A.7}$$

Which is in the form $y = mx + c$, which therefore yields a straight line. In this plot the gradient *"m"* is a function of the fluid while the intercept *"c"* is representative of R_w.

A.2 SURFACE ROUGHNESS

The tube used in the test section has been subjected to a surface roughness test using a Talysurf machine. The results of this test are shown in Figure A2 1, below.

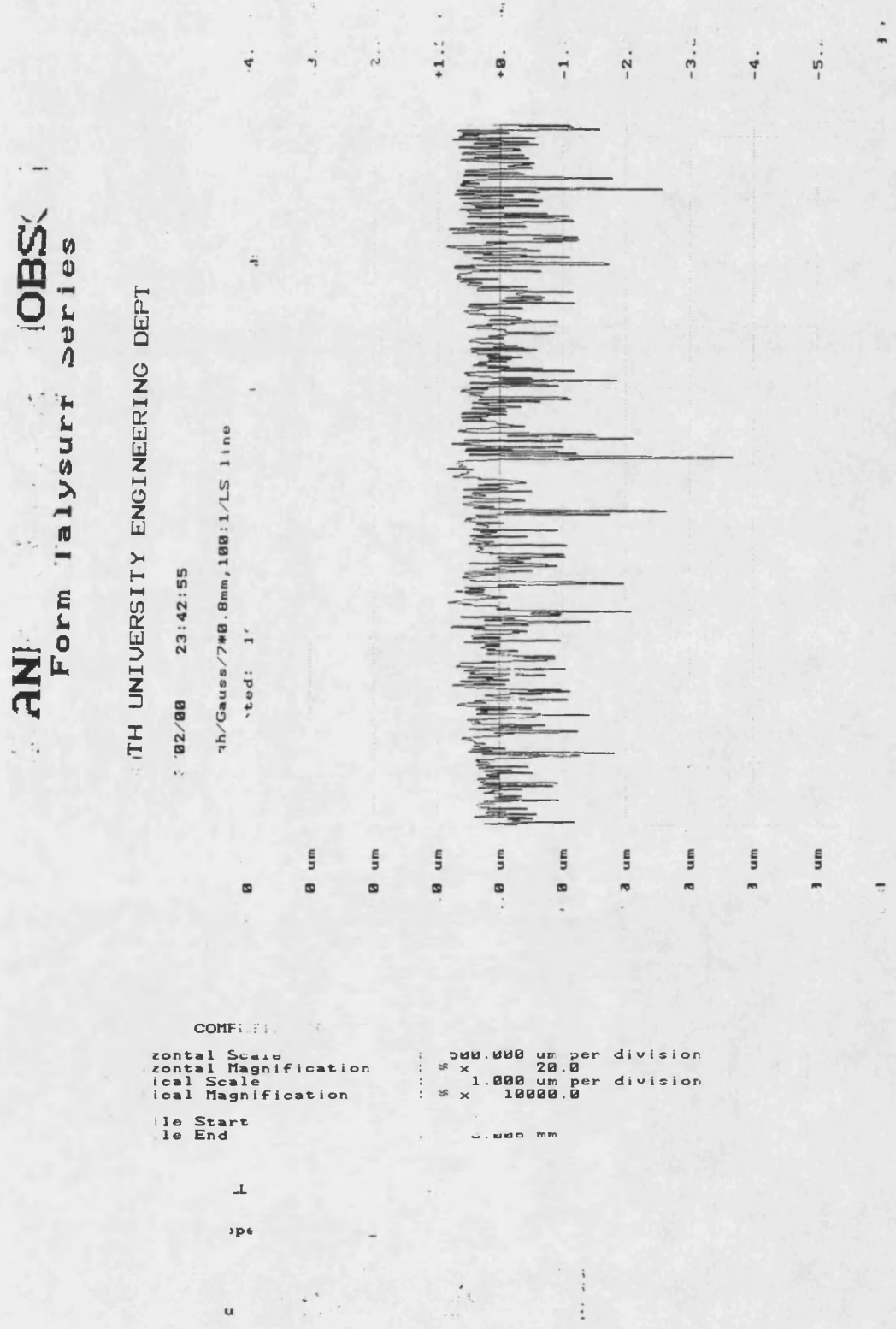

Figure A2 1 – Results of surface roughness test

B. Characterisation of Maya crude

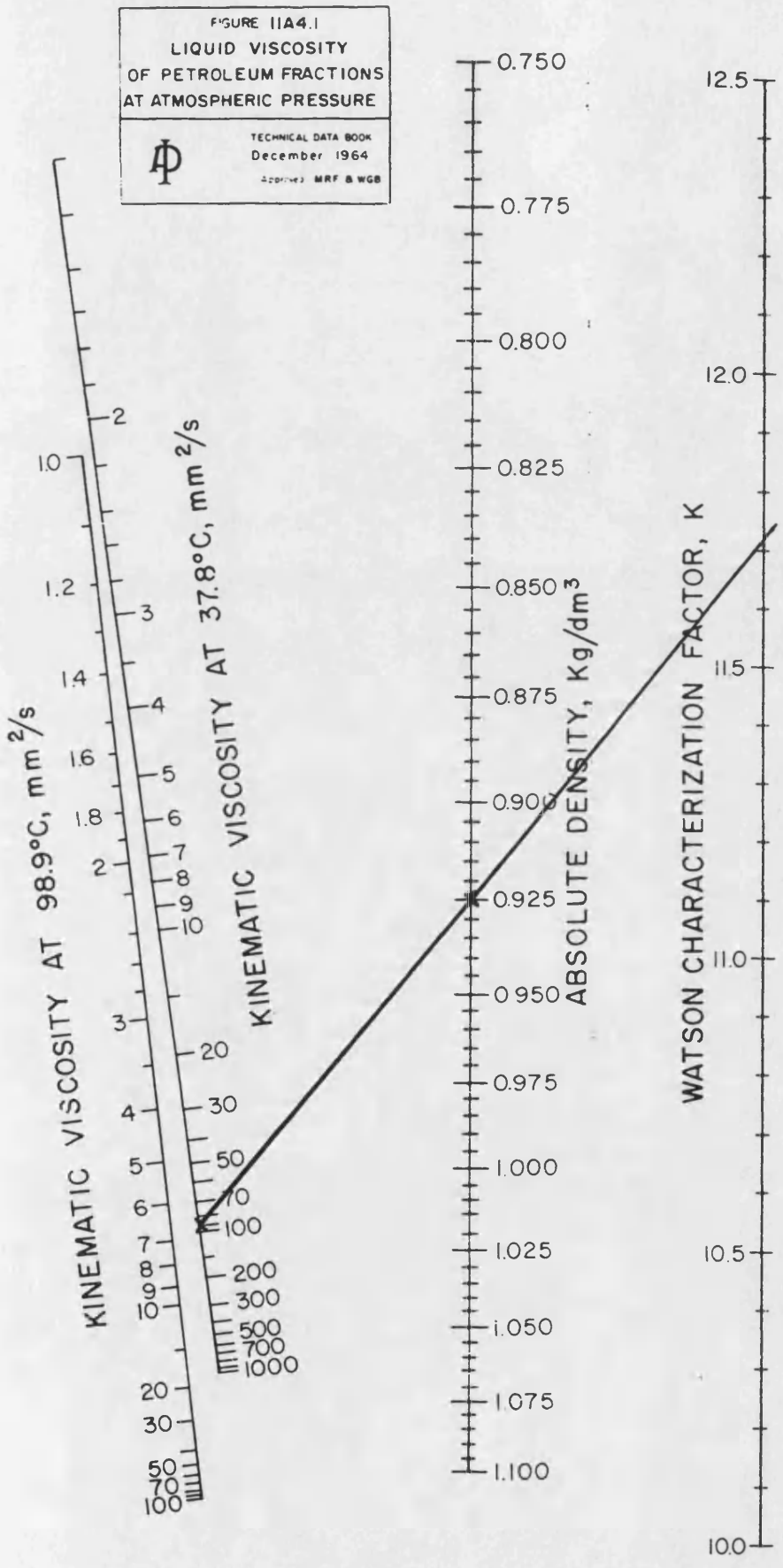

Figure B.1 API Figure 11A4.1 - "Watson K" value for Maya crude

PROCEDURE 7D2.2

ISOBARIC HEAT CAPACITY OF PETROLEUM FRACTION LIQUIDS

Discussion

The isobaric heat capacity of a liquid petroleum fraction may be estimated using this procedure. This method is suitable for both desk and digital computer calculations. The equations are:

for $T_r \leq 0.85$,

$$C_p = A_1 + A_2 T + A_3 T^2 \qquad \text{(7D2.2-1)}$$

Where:

C_p = isobaric heat capacity for liquid petroleum fraction in kJ/kg C.

$A_1 = -4.90383 + (0.099319 + 0.104281 \text{ rel den})\,\text{K} + \left(\frac{4.81407 - 0.194833\,\text{K}}{\text{rel den}}\right)$

$A_2 = (7.53624 + 6.214610\,\text{K})\left(1.12172 - \frac{0.27634}{\text{rel den}}\right)(10^{-4})$.

$A_3 = -(1.35652 + 1.11863\,\text{K})\left(2.9027 - \frac{0.70958}{\text{rel den}}\right)(10^{-7})$.

T_r = reduced temperature, T/T_{pc}.

T = temperature, in degrees Kelvin.

T_{pc} = pseudocritical temperature, in degrees Kelvin.

K = Watson characterization factor.

rel den = relative density, 15 C/15 C.

for $T_r > 0.85$,

$$C_p = B_1 + B_2 T + B_3 T^2 - \frac{R}{M}\left(\frac{\dot{C}_p^{\,0} - \dot{C}_p}{R}\right)$$

Where:

$B_1 = -1.492343 + 0.124432\,\text{K} + B_4\left(1.23519 - \frac{1.04025}{\text{rel den}}\right)$.

$B_2 = -\left[2.20412 - (1.16993 - 0.04177\,\text{K})\,\text{K} + B_4\left(4.54307 - \frac{3.82042}{\text{rel den}}\right)\right](10^{-3})$.

$B_3 = (2.29876 + 0.119917\,B_4)(10^{-6})$.

$B_4 = \left[\left(\frac{12.8}{\text{K}} - 1.0\right)\left(1.0 - \frac{10.0}{\text{K}}\right)(\text{rel den} - 0.885)(\text{rel den} - 0.70)(10^{-4})\right]^2$

for $10 < \text{K} < 12.8$ with $0.70 < \text{rel den} < 0.885$.

$B_4 = 0.0$ for all other cases.

R = gas constant = 8.3140 kJ/k-mole K.

M = molecular weight.

Procedure

Step 1: Using the available inspection data for the fraction, determine the characterization factor with the methods of Chap. 2.

Step 2: Calculate the pseudocritical temperature using the methods in Chap. 4.

Step 3: Calculate the reduced temperature. If the reduced temperature is greater than 0.85, proceed to Step 5.

Step 4: Use equation (7D2.2-1) to calculate the desired heat capacity.

Step 5: Calculate the pseudocritical pressure for the petroleum fraction using the methods of Chap. 4.

Step 6: Use the methods of Chap. 2 to determine the molecular weight and acentric factor for the fraction.

Step 7: Calculate the heat capacity pressure effect term $\left(\frac{\dot{C}_p^{\,0} - \dot{C}_p}{R}\right)$ using Procedure 7D1.1.

Step 8: Use equation (7D2.2-2) to calculate the desired heat capacity.

Figure B.2 API Figure 7D2.2 - Specific heat capacity equation for Maya Crude

COMMENTS ON FIGURE 12A3.1

Purpose

Figure 12A3.1 allows estimation of thermal conductivity at low pressures as a function of temperature for undefined liquid hydrocarbon mixtures. For pressures above 3450 kilopascals, correct the value from this figure by using Figure 12A4.1.

Limitations

This figure is an oversimplification, inasmuch as molecular type and weight have not been correlated. Accordingly, Procedure 12A2.1 should be used in preference for mixtures for which the composition is known.

Reliability

Average errors of 10 percent can be expected from Figure 12A3.1, with maximum errors of 40 percent.

Special Comments

Figure 12A3.1 is expressed analytically by equation (12A3.1-1), which may be used alternatively as:

$$k = 0.1337 - (1.420 \times 10^{-4})T \qquad \text{(12A3.1-1)}$$

Where:

k = thermal conductivity, in watts per meter-kelvin.
T = temperature, in kelvins.

Literature Sources

This figure is the best representation of data from the following sources: 21, 36, 41, 84, 95.

Figure B.3 API Figure 12A3.1 - Thermal conductivity equation for Maya crude

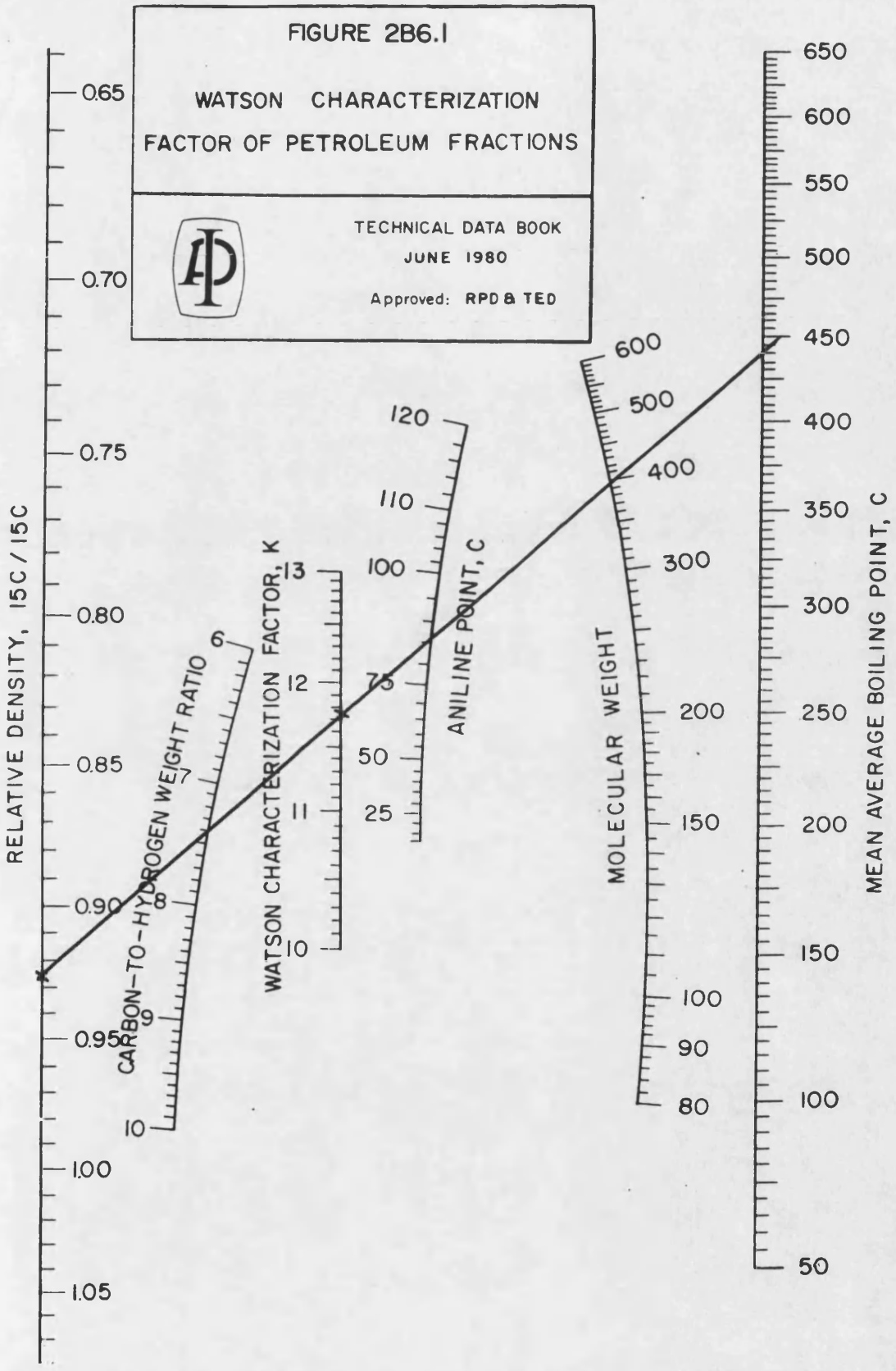

Figure B.4 API Figure 2B6.1 - Molecular weight for Maya crude

Table B.1 Variation in viscosity with temperature for Maya crude

Temperature (°C)	Viscosity (cSt)
40	84.30
50	57.10
60	40.35

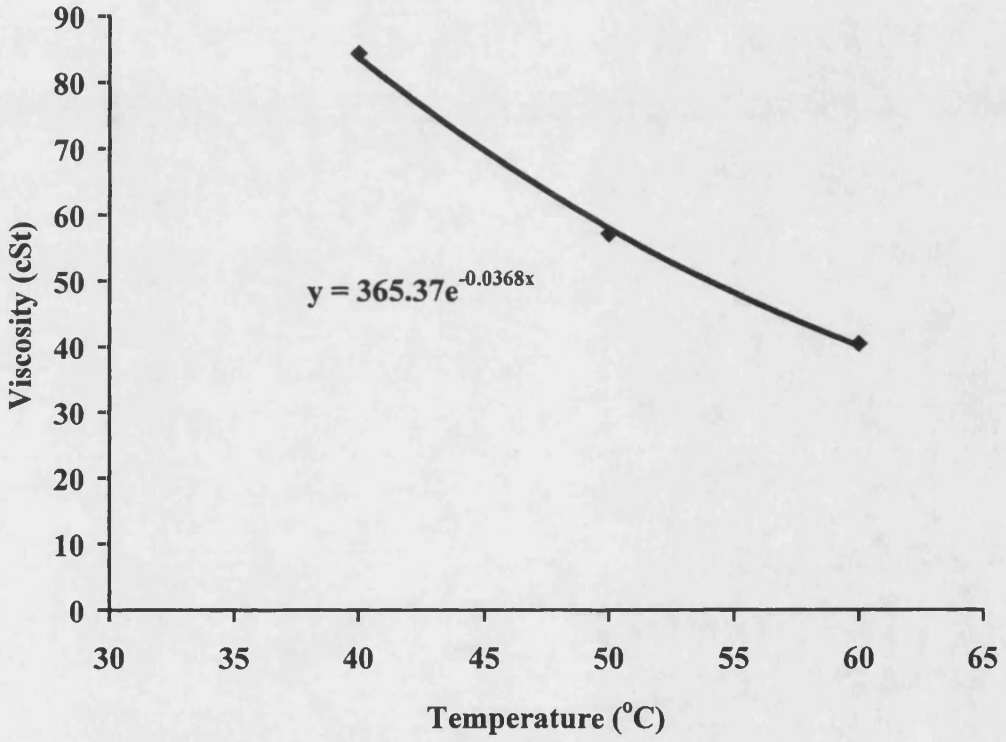

Figure B.5 Chart illustrating the variation in viscosity with temperature

Table B.2 Variation in density with temperature for Maya crude

Temperature (°C)	Density (kg m^{-3})
15	925
100	880
150	850
200	820

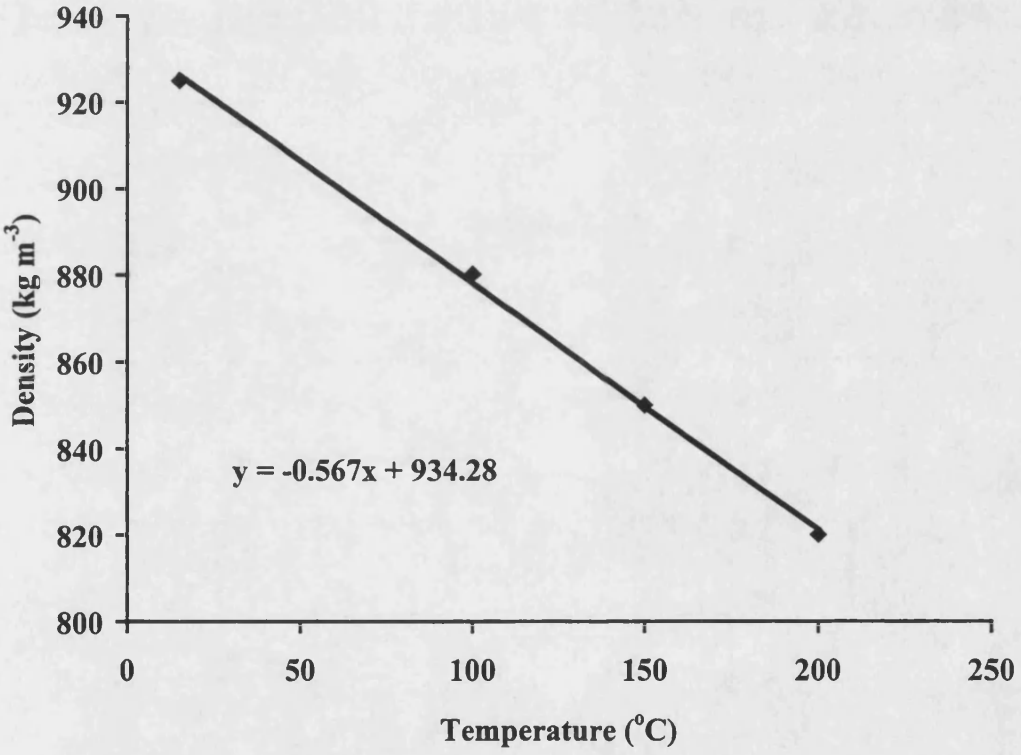

Figure B.6 Chart illustrating the variation in viscosity with temperature

Gas chromatograph data

The Maya crude was subjected to GC-MS analysis under the conditions summarised in Table B.3 to Table B.6. The printed out graphs of the analysis are shown in Figure B.7 to Figure B.10.

Table B.3 GC-MS analysis conditions

Dilution	0.4ml in 1.5ml CS2
1 microliter injection split ratio	80:1
Inlet head pressure	8 psi
Column	BP624, 25m, 1.2 μ film
Column initial	40 °C / 10 min
Ramp	5 °C / min to 240 °C for 30min
System PE Autosystem with Q-Mass	910 MS
Filament delay	3 min
Lens1 voltage	50.12
Lens2 voltage	70.00
Starting mass	50
Ending mass	556
Points per AMU	10
Peak width	1
Mass defect	0
Multiplier voltage	1400
Gain	6
Run time	70 mins
Threshold	5
Baseline	23
Integration time	0.20 ms

Table B.4 GC-MS resolution values

	Resolution DAC Values	Resolution Mass	Sensitivity
1	230	18	22
2	455	50	23
3	590	69	26
4	942	131	32
5	1307	219	40
6	1511	264	44
7	1739	314	50
8	2194	414	60
9	2538	502	73
10	2975	614	89

Table B.5 GC-MS specification table

Mass	Range	Reference	Intensity	Ratio	Status
50	1-2%	69	403	0.64	Low
69	100-100%	69	62885	100.00	Pass
131	26-50%	69	22936	36.47	Pass
219	40-70%	69	31701	50.41	Pass
264	8-18%	69	9185	14.61	Pass
314	0-4%	69	456	0.73	Pass
414	1.5-4%	69	1968	3.13	Pass
502	1.5-4%	69	1956	3.11	Pass
614	0.1-1%	69	395	0.63	Pass

Table B.6 Summary of peaks identified

Peak number	Compound	SI	Scan	Retention time (min)
1	Hexane	90	4	3.13
2	Heptane	91	20.5	6.58
3	Toluene	92	559	12.66
4	Octane	88	612	13.57
5	p-Xilene	87	904	18.54
6	Nonane	87	933	19.09
7	Decane	86	1186	23.44
8	Undecane	87	1406	27.23
9	Dodecane	87	1600	30.58
10	Tridecane	90	1780	33.75
11	Pentadecane	81	2108	39.41
12	Hexadecane	90	2254	41.98
13	Heptadecane	89	2393	44.44
14	Octadecane	82	2523	46.75
15	Nonadecane	80	2647	48.97
16	Eicosane	83	2668	51.16
17	Heneicosane	83	2911	53.80
18	Docosane	80	3090	57.16
19	Tricosane	78	3317	61.46

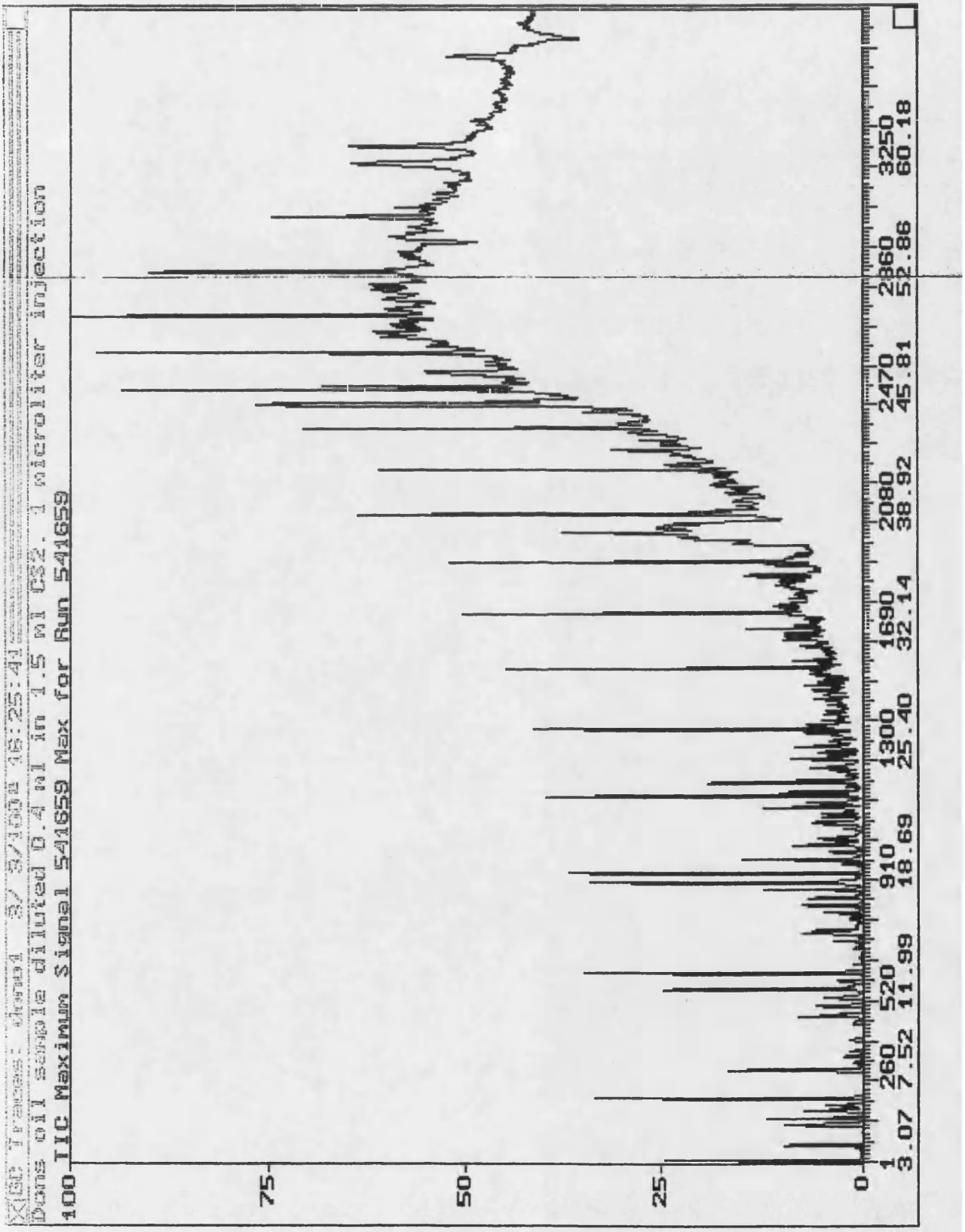

Figure B.7 Gas chromatograph of Maya crude - Complete

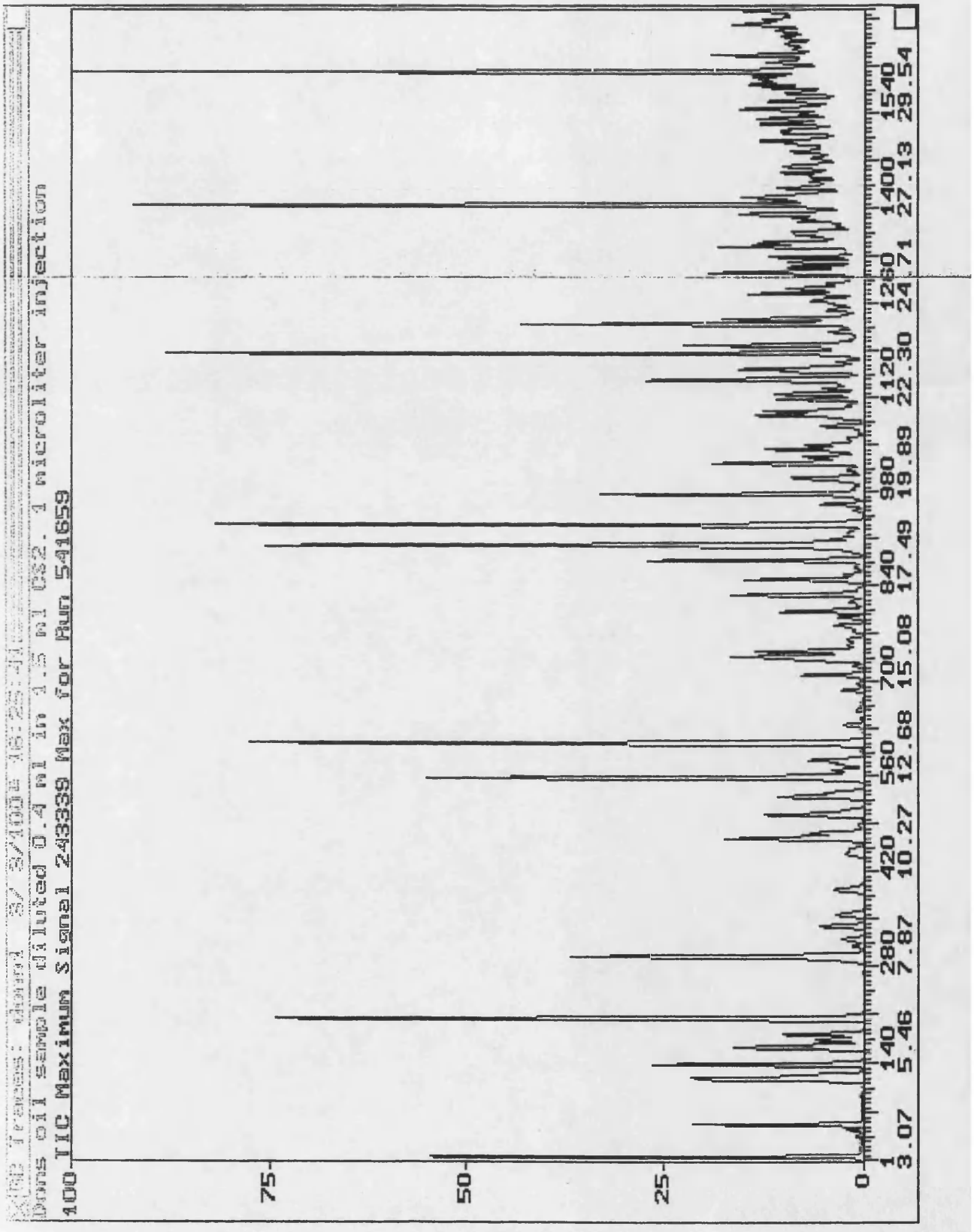

Figure B.8 Gas chromatograph of Maya crude – Resolution DAC 0 to 1869

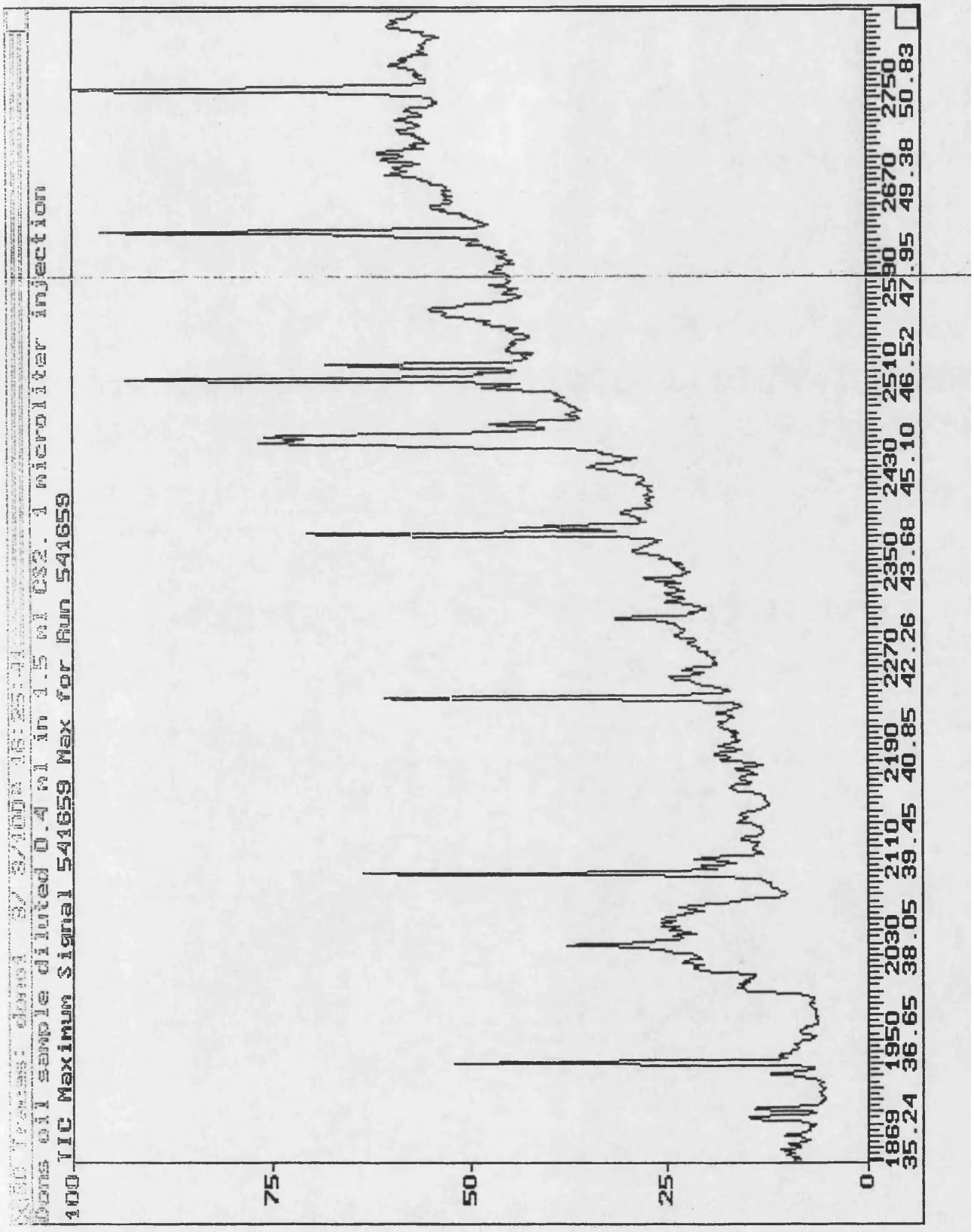

Figure B.9 Gas chromatograph of Maya crude - Resolution DAC 1540 to 2828

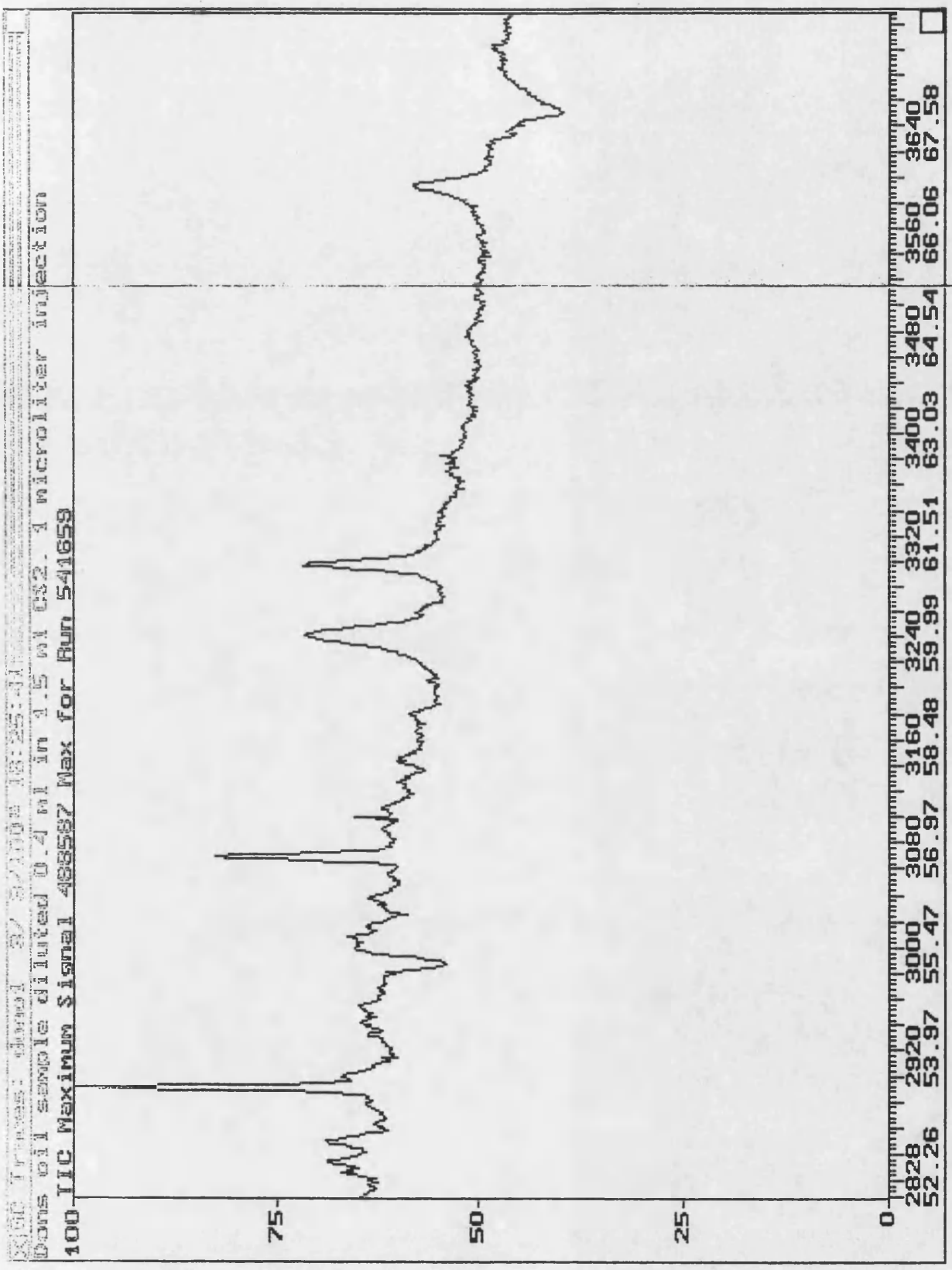

Figure B.10 Gas chromatograph of Maya crude - Resolution DAC 2828 to 3800

C. Disc Holders